ALI RAZA

INVESTIGATION OF DYNAMIC CHARACTERISTICS AND VIBRATION CONTROL OF ADDITIVELY MANUFACTURED COMPOSITE STRUCTURES USING PIEZOELECTRIC ACTUATORS

DOCTORAL DISSERTATION

Kaunas
2025

KAUNAS UNIVERSITY OF TECHNOLOGY

ALI RAZA

INVESTIGATION OF DYNAMIC CHARACTERISTICS AND VIBRATION CONTROL OF ADDITIVELY MANUFACTURED COMPOSITE STRUCTURES USING PIEZOELECTRIC ACTUATORS

Doctoral dissertation
Technological Sciences, Mechanical Engineering (T 009)

2025, Kaunas

The doctoral dissertation has been prepared at the Department of Production Engineering of the Faculty of Mechanical Engineering and Design of Kaunas University of Technology in 2021-2025. The research has been sponsored by the Research Council of Lithuania.

The doctoral right has been granted to Kaunas University of Technology together with Vytautas Magnus University.

Research supervisor:
Assoc. Prof. Dr. Rūta RIMAŠAUSKIENĖ (Kaunas University of Technology, Technological Sciences, Mechanical Engineering, T 009).

Edited by: English language editor Daiva Birutė Zavistanavičienė (KTU Centre of Foreign Languages), Lithuanian language editor Virginija Stankevičienė (KTU Centre of Foreign Languages).

The public defence of the dissertation will be held on 29 August 2025, at 10 am in a public meeting of the Dissertation Defence Board of the Mechanical Engineering science field at the Rectorate Hall of Kaunas University of Technology.

Address: K. Donelaičio 73-402, LT-44249 Kaunas, Lithuania.
Phone: (+370) 608 28 527; e-mail: doktorantura@ktu.lt

The doctoral dissertation was sent out on 29 July, 2025.
The dissertation is available on http://ktu.edu and at the Libraries of Kaunas University of Technology (Gedimino 50, LT-44239 Kaunas, Lithuania) and Vytautas Magnus University (K. Donelaičio 52, LT-44244, Kaunas, Lithuania).

KAUNO TECHNOLOGIJOS UNIVERSITETAS

ALI RAZA

DINAMINIŲ CHARAKTERISTIKŲ IR VIRPESIŲ VALDYMO ADITYVIAI PAGAMINTOSE KOMPOZITINĖSE STRUKTŪROSE NAUDOJANT PJEZOELEKTRINIUS VYKDIKLIUS TYRIMAS

Daktaro disertacija
Technologijos mokslai, mechanikos inžinerija (T 009)

2025, Kaunas

Disertacija rengta 2021–2025 metais Kauno technologijos universiteto Mechanikos inžinerijos ir dizaino fakultete, Gamybos inžinerijos katedroje. Mokslinius tyrimus rėmė Lietuvos mokslo taryba.

Doktorantūros teisė Kauno technologijos universitetui suteikta kartu su Vytauto Didžiojo universitetu.

Mokslinis vadovas:
doc. dr. Rūta RIMAŠAUSKIENĖ (Kauno technologijos universitetas, technologijos mokslai, mechanikos inžinerija, T 009).

Redagavo: anglų kalbos redaktorė Daiva Birutė Zavistanavičienė (KTU Užsienio kalbų centras), lietuvių kalbos redaktorė Virginija Stankevičienė (KTU Užsienio kalbų centras).

Mechanikos inžinerijos mokslo krypties disertacijos gynimo taryba:
prof. dr. Regita BENDIKIENĖ (Kauno technologijos universitetas, technologijos mokslai, mechanikos inžinerija, T 009) – **pirmininkė**;
prof. dr. Saulius BASKUTIS (Kauno technologijos universitetas, technologijos mokslai, mechanikos inžinerija, T 009);
doc. dr. Michal K. BUDZIK (Orhuso universitetas, Danija, technologijos mokslai, mechanikos inžinerija, T 009);
prof. dr. Giedrius JANUŠAS (Kauno technologijos universitetas, technologijos mokslai, mechanikos inžinerija, T 009);
doc. dr. Pawel KUDELA (Lenkijos mokslų akademijos Skysčių srauto mašinų institutas, Lenkija, technologijos mokslai, mechanikos inžinerija, T 009).

Disertacija bus ginama viešame Mechanikos inžinerijos mokslo krypties disertacijos gynimo tarybos posėdyje 2025 m. rugpjūčio 29 d. 10 val. Kauno technologijos universiteto Rektorato salėje.

Adresas: K. Donelaičio g. 73-402, LT-44249 Kaunas, Lithuania.
Tel. (+370) 608 28 527; el. paštas: doktorantura@ktu.lt

Disertacija išsiųsta 2025 m. liepos 29 d.
Su disertacija galima susipažinti interneto svetainėje http://ktu.edu, Kauno technologijos universiteto bibliotekoje (Gedimino g. 50, LT-44239 Kaunas, Lietuva) ir Vytauto Didžiojo universiteto bibliotekoje (K. Donelaičio g. 52, LT-44244, Kaunas, Lietuva).

CONTENT

LIST OF TABLES

LIST OF FIGURES

LIST OF ABBREVIATIONS

MFC	Macro fiber composite
PZT	Lead zirconium titanate
AM	Additively manufactured
FDM	Fused deposition modeling
OLAVC	Open-loop active vibration control
AVC	Active vibration control
PLA	Poly lactic acid
PLA-SCF	PLA reinforced with short carbon fibers
PLA-CCF	PLA reinforced with continuous carbon fibers
PLA-CGF	PLA reinforced with continuous glass fibers
LDS	Laser displacement sensor
BM	Bending mode
ADC	Analog to digital converter
R	Reduction factor
W_u	Uncontrolled amplitude
W_c	Controlled amplitude
PLAP	Polylactic acid polymer
FRA	Frequency response analysis
FEM	Finite element modeling
THz	Terahertz
Amp	Amplitude
Freq	Frequency

1. INTRODUCTION

Structures start vibrating when subjected to dynamic loading circumstances such as the external environment, machine vibrations, noise, and human activities, making vibration control in structural dynamics one of the most concerning issues in the research community [1]. These vibrations can significantly compromise structural integrity, leading to premature fatigue and eventual failure. Therefore, it is necessary to mitigate these vibrations or keep them within an acceptable limit to minimise the risk of structural failure [2, 3]. It is important to note that thin-walled composite beam structures have a considerable number of engineering applications. Structures such as helicopter and aircraft blades, robotic arms [4] and wind turbine blades structures demonstrate the geometry of thin-walled beams. However, aeroelastic flutter is a challenging issue concerned with these kinds of structures and needs to be minimised or eliminated [5]. Recently, structures are manufactured using various types of composite materials to obtain high specific stiffness as well as specific strength. On the other hand, vibration suppression has emerged as a crucial issue for the operational performance of the system due to the flexible properties of the composite structures [6,7].

Several vibration suppression technologies, including active control (which comprises both open-loop and closed-loop approaches), as well as semi-active, passive, and hybrid control methods, have been implemented recently to enhance system integrity. A passive control scheme includes incorporating various damping materials or devices (e.g. mass, spring and damper), producing the control counter force in reaction to external disturbances and does not need any external electrical source for operation. However, other schemes generally require actuators, sensors and controllers to function. These can provide control counter forces to the system based on the real time data but need external electrical sources to activate these devices [8]. It is important to highlight that active control schemes are increasingly used in numerous engineering fields due to the easy market accessibility of a range of smart materials, particularly piezoelectric [9,10]. Piezoelectric materials are often used for energy harvesting [11], monitoring structural integrity [12], and vibration suppression applications [13], due to their effective electromechanical capabilities, substantial blocking force, excellent stiffness, and prompt response [14]. Piezoelectric materials such as lead zirconium titanate (PZT), are commonly employed in numerous industrial applications due to their excellent stiffness and ability to generate high actuation force. Additionally, they may be implemented as sensors and actuators, attributed to direct piezoelectric and converse phenomena respectively. However, they have some constraints, such as brittle behaviour, inadequate flexibility, and limited capability to adapt curved surfaces, which have adverse effects on the stability and efficiency of piezoelectric materials [2]. The polyvinylidene fluoride is an alternative piezoelectric material, that is relatively more flexible than PZT but generates less actuation force.

These restrictions have encouraged researchers to work on alternative techniques for the development of advanced piezoelectric materials. To address the limitations of piezoelectric material for practical applications, extensive research has been conducted on the incorporation of piezoceramic fibers into polymeric matrix [15,

16]. NASA invented macro fiber composites (MFCs) in 1999 to address the above-mentioned limitations, the rectangular piezoceramic fibers had been incorporated into polymer matrix and sandwiched between the protective and electrode layers [12, 13, 17–19]. Smart Material began commercializing this invention as NASA's licensed manufacturer and supplier in 2002 [20].

In this study, the MFC patches have been employed as actuators to suppress vibration amplitudes in additively manufactured (AM) poly lactic acid (PLA) and PLA-based composite structures, such as PLA reinforced with short carbon fibers (PLA-SCF), continuous carbon fibers (PLA-CCF), and continuous glass fibers (PLA-CGF).

The creation of complicated structures with intricate geometries has been modified by 3D printing, which is also referred to as additive manufacturing technology [21]. Compared to traditional subtractive manufacturing techniques, additive manufacturing techniques create components through a layer-by-layer addition of material, some of which may be melted or cured. The key benefits of these include their ability to fabricate components with complicated geometries and allow reduction of material waste. Fused deposition modelling (FDM) is one of the additive manufacturing technologies that has received a lot of attention from the industrial and academic sectors [22, 23]. 3D printers utilizing FDM, fabricate items by depositing filaments made of thermoplastic polymers that have been heated up to their melting point and extruded through nozzle [24]. This methodology makes it possible to design various structures with a variety of configurable features, making it the right choice for several engineering applications [25]. Concerning the mechanical properties of 3D printed specimens, it should be noted that the mechanical characteristics of AM components are affected not only by the thermoplastic material but also by the printing settings such as layer height, layer orientations, filling density, temperature, and printing speed [26–28]. To maximize the performance and utility of AM structures in applications including vibration, resonance, and dynamic loading, it is essential to understand these factors [29].

In this research, for the first time, AM structures made of PLA and PLA composites such as PLA-SCF, PLA-CCF and PLA-CGF have been investigated to explore the impact of different layer orientations (0°-0° and 0°-90°) on their dynamic characteristics and vibration suppression. Moreover, the study demonstrates the influence of layer orientations and AM structures on vibration amplitude suppression to identify effective combination providing the maximum vibration suppression with the application of MFC actuator.

1.1. Aim of the Doctoral Dissertation

To investigate the dynamic characteristics of kinematically excited, additively manufactured (AM) structures and develop an effective vibration control methodology by integrating macro fiber composite (MFC) actuators to suppress vibration amplitudes. To achieve this aim, the following objectives were pursued:

1. To analyse the dynamic properties of AM poly lactic acid (PLA) and PLA-based composite structures, including PLA reinforced with short carbon fibers (PLA-

SCF), continuous carbon fibers (PLA-CCF), and continuous glass fibers (PLA-CGF), considering both unidirectional (0°-0°) and cross-ply (0°-90°) orientations.
2. To assess vibration amplitude suppression in kinematically excited AM structures made of PLA, PLA-SCF, PLA-CCF, and PLA-CGF with two distinct orientations (0°-0° and 0°-90°) by applying a vibration control methodology using MFC actuators, identifying the orientation and structure exhibiting the maximum vibration suppression at their relevant first resonance frequencies.
3. To investigate the influence of the signal phase, ranging from 0° to 360°, applied to the MFC actuators on the vibration amplitude of the AM structures and determine the phase that provides the maximum vibration suppression for each structure.
4. To create numerical models of the AM structures and develop a numerical simulation approach to evaluate their dynamic characteristics and vibration control using MFC actuators, while comparing the results with experimental data.

1.2. Research Methods and Techniques

The research involved the AM of beam structures, experimental investigations, numerical simulations, and theoretical analysis to obtain the expected results. PLA and PLA-SCF beam structures were fabricated using an Original Prusa i3 MK3S & MK3S+ 3D printer manufactured by Prusa Research, Czech Republic. The creation of PLA-CCF and PLA-CGF composite beam structures was carried out using a MeCreator-2 3D printer, produced by Geeetech, China, with a modified printing head. The Polytec 3D laser vibrometer (PSV-W-500), manufactured by Polytech GmbH, Germany, was used to evaluate modal characteristics, including natural frequencies, bending mode shapes, and amplitude spectrum. The laser displacement sensor (LK-G82) from Keyence Corporation, Japan, was utilised to measure the controlled and uncontrolled vibration amplitudes in kinematically excited beam structures. The non-destructive C-scanning of beam structures was performed to identify internal defects using the THz spectrometer (TPSTM Spectra 300 THz Pulsed Imaging and Spectroscopy from TeraView). The numerical investigation was performed using Abaqus CAE 2024 software. Most of the experimental work was performed at the Faculty of Mechanical Engineering and Design and Institute of Mechatronics, Kaunas University of Technology, while C-scanning spectroscopy and the numerical simulation study were carried out at the Institute of Fluid-Flow Machinery, Polish Academy of Sciences, Gdansk, Poland.

1.3. Scientific Novelty

1. The dynamic characteristics of additively manufactured (AM) PLA and PLA composite structures were investigated with a particular focus on the influence of different layer orientations (0°-0° and 0°-90°) on the natural bending mode frequencies, amplitude spectrum, and overall dynamic behaviour of these structures.
2. A vibration control methodology using MFC actuators has been developed to suppress vibration amplitudes in AM structures with 0°-0° and 0°-90°

orientations, identifying the most effective layer orientation and structure for vibration suppression.
3. A finite element based numerical simulation approach has been developed to study dynamic characteristics and vibration suppression using MFC actuators in AM structures.

1.4. Practical Value of the Work

1. The vibration control technique can be applied to additively manufactured composite structures fabricated from various materials and orientations to identify the most effective combination for suppressing vibration amplitudes.
2. The vibration control methodology can be implemented in microfabrication processes and medical robotic arms to effectively reduce small vibrations where precise movement is crucial. By minimising vibrations, the system's reliability is improved ensuring high accuracy during critical tasks.
3. The developed numerical simulation method can be employed to investigate the dynamic behaviour and vibration suppression of structures made from different materials and layer orientations before fabricating the actual additively manufactured structure with the suitable material and layer orientation for effective performance, thus saving both manufacturing costs and time.

1.5. Statements for the Defense

1. Dynamic characteristics of additively manufactured (AM) structures are significantly influenced by both the layer orientation and the type of reinforced fibers.
2. In AM structures, the layer orientation and reinforced fibers are crucial factors in vibration suppression. This appropriate combination facilitates selecting the AM structure with maximum vibration suppression.
3. The developed numerical simulation approach captures the dynamic characteristics and vibration suppression trends in AM structures effectively, as validated by the consistency between the numerical and experimental results.

1.6. Publications on Research Findings

The scientific experimental and numerical findings from this research have been published in international journals indexed in the Clarivate Analytics Web of Science database. Three scientific articles have been published in Quartile 1 (Q1) journals and one in Quartile 2 (Q2) journal. Additionally, these findings have been presented at six international conferences.

[A1]: **Raza, Ali**; Rimašauskienė, Rūta; Jūrėnas, Vytautas; Mahato, Swarup. Experimental investigation of vibration amplitude control in additive manufactured PLA and PLA composite structures with MFC actuator // Engineering structures. London: Elsevier. ISSN 0141-0296. eISSN 1873-7323. 2023, vol. 294, art. no. 116802, p. 1-13. DOI: 10.1016/j.engstruct.2023.116802. **[Q1]**

[A2]: **Raza, Ali;** Rimašauskienė, Rūta; Jūrėnas, Vytautas; Rimašauskas, Marius. An experimental study on the dynamic properties of 3D-printed structures with different

layer orientations // Journal of Vibration Engineering & Technologies: Springer Nature. ISSN 2523-3920. eISSN 2523-3939. 2024, vol. 12, p. 321-334. DOI: 10.1007/s42417-024-01417-w. **[Q2]**

[A3]: **Raza, Ali;** Rimašauskienė, Rūta; Jūrėnas, Vytautas; Kuncius, Tomas. Enhancing vibration control in kinematically excited additively manufactured continuous fiber composite structures with distinct orientations // Engineering structures. London: Elsevier. ISSN 0141-0296. eISSN 1873-7323. 2024, vol. 321, art. no. 118933, p. 1-15. DOI: 10.1016/j.engstruct.2024.118933. **[Q1]**

[A4]: **Raza, Ali;** Mieloszyk, Magdalena; Rimašauskienė, Rūta; Jūrėnas, Vytautas. Dynamic analysis and vibration control of additively manufactured thin-walled polylactic acid polymer (PLAP) and PLAP composite beam structures: numerical investigation and experimental validation // Materials. Basel: MDPI. ISSN 1996-1944. 2024, vol. 17, iss. 22, art. no. 5478, p. 1-26. DOI: 10.3390/ma17225478**. [Q1]**

1.7. Author's Contribution

The contributions of the author and co-authors in the scientific publications have been outlined in Table 1.

Table 1. Contributions of the author and co-authors in the scientific publications

Publications	Contributions	Author and co-authors
Article [A1]	Conceptualization	Rūta Rimašauskienė
	Methodology	Ali Raza, Vytautas Jūrėnas
	Investigation	Ali Raza, Vytautas Jūrėnas
	Validation	Ali Raza
	Software	Ali Raza
	Writing – original draft	Ali Raza
	Writing – review & editing	Rūta Rimašauskienė, Vytautas Jūrėnas
	Formal analysis	Ali Raza, Swarup Mahato
	Revisions of the manuscript as per reviewers' comments	Ali Raza
Article [A2]	Conceptualization	Ali Raza, Vytautas Jūrėnas
	Methodology	Ali Raza, Vytautas Jūrėnas
	Investigation	Ali Raza, Rūta Rimašauskienė
	Validation	Ali Raza
	Software	Ali Raza
	Writing – original draft	Ali Raza
	Writing – review & editing	Rūta Rimašauskienė
	Formal analysis	Ali Raza, Marius Rimašauskas
	Revisions of the manuscript as per reviewers' comments	Ali Raza
Article [A3]	Conceptualization	Ali Raza, Rūta Rimašauskienė
	Methodology	Ali Raza, Vytautas Jūrėnas
	Investigation	Ali Raza, Rūta Rimašauskienė
	Validation	Ali Raza
	Software	Ali Raza
	Writing – original draft	Ali Raza

	Writing – review & editing	Rūta Rimašauskienė
	Formal analysis	Ali Raza, Tomas Kuncius
	Revisions of the manuscript as per reviewers' comments	Ali Raza
Article [A4]	Conceptualization	Ali Raza, Magdalena Mieloszyk, Rūta Rimašauskienė
	Methodology	Ali Raza
	Investigation	Ali Raza, Magdalena Mieloszyk, Rūta Rimašauskienė, Vytautas Jūrėnas
	Data curation	Ali Raza
	Validation	Ali Raza
	Software	Ali Raza, Magdalena Mieloszyk
	Writing – original draft	Ali Raza
	Writing – review & editing	Magdalena Mieloszyk, Rūta Rimašauskienė, Vytautas Jūrėnas
	Revisions of the manuscript as per reviewers' comments	Ali Raza

2. LITERATURE ANALYSIS

In recent times, vibration control in structural dynamics has been one of the most concerning issues in the research community. The structure starts vibrating when subjected to dynamic loading circumstances such as the external environment, machine vibrations, noise, and human activities. The structure is harmed by mechanical vibrations, which create premature fatigue and subsequently the structure collapses. Therefore, it is critical to maintain vibration in structures within the permissible limit to reduce the risk of failure [2, 3, 30]. Composite structures are extensively utilised in many engineering fields due to their exceptional properties, such as significant stiffness, low density, and high strength-to-weight ratio.

However, low-frequency resonance occurrences have a detrimental effect on these structures and raise significant concerns about structural integrity. These aspects inspire researchers to examine the vibration amplitude suppression approaches [31]. Several vibration control technologies, including active control (AC) which comprises, both open loop and closed loop control approaches as well as semi-active control (SAC), passive control (PC), and hybrid control (HC), have been introduced in recent years to ensure system safety. A PC control system often consists of numerous materials and devices that provide a control force depending on the system's motion, whereas sensors and the control system are frequently used in AC, SAC, and HC. The PC technique is frequently implemented due to its low cost and ease of installation. [8, 32]. It is also worth mentioning that active control approaches are becoming popular in scientific fields due to the availability of a variety of smart materials, such as piezoelectric type, shape memory alloys and others in the market [9,10]. Piezoelectric materials, including traditional piezoelectric patches such as PZT and advanced piezoelectric patches like MFC, are extensively used in various engineering applications due to their rapid response and high efficiency. Both can be employed as actuators and sensors. However, PZT patches have some limitations, such as low structural flexibility due to their brittle nature, while MFC patches provide significant structural flexibility due to their composite design, making them more versatile and adaptable for real-life engineering applications.

Extensive experimental and numerical investigations have been conducted by researchers to mitigate vibrations in various structures through the application of piezoelectric actuators, as discussed below in this section.

Wani et al. [33] conducted a comprehensive review of various control methodologies, including active, passive, and hybrid control, for effectively controlling vibrations in structures. The adoption of a specific control technique is influenced by the complexity of the structural system. Furthermore, it was reported that more than one type of technique may be implemented to control vibrations effectively. Dafang et al. [34] conducted an experimental study on a flexible beam to examine the control of vibrations with piezoelectric patches. The independent modal space control technique was applied to specifically control and investigate the first three modes of the beam. A comparison between the vibration responses of the flexible beam before and after applying the control approach revealed a significant

vibration suppression. Furthermore, a numerical simulation was performed to simulate the first three modes, and the results from the simulation and experiment were quite comparable. The findings indicate that the proposed control method is quite effective in suppressing vibrations. Xie et al. [35] investigated the dampening of active vibration in a lattice grid beam by utilising piezoelectric material as an actuator. They employed a novel approach by utilising the fractional-order proportional-derivative (PD) approach to mitigate vibrations. Furthermore, the researchers conducted simulations involving the beam under diverse dynamic loads. These dynamic loads comprise of harmonic excitation, step excitation, and initial disturbance scenarios. The findings demonstrate that the applied control approach exhibited a significant and rapid decrease in vibration amplitudes in comparison to the conventional integer-order PD control approach. Mayer et al. [36] worked on active, passive, adaptive, and integrated vibration control techniques and compared their respective design challenges and advantages. The study employed a design arrangement to demonstrate different ways of implementing a vibration control system, as well as the integration of various vibration control approaches. Rezaei et al. [37] investigated the possibility of embedding a piezoelectric layer within a tuned mass damper system (TMDS) to achieve both power harvesting (PH) and vibration reduction concurrently. The investigation revealed that the TMDS proved effective in both vibration suppression within the host structure and enabling PH. Consequently, the investigation concludes that TMDS represents a potential approach for achieving both vibration suppression and PH. Przybylski et al. [38] did theoretical and experimental studies on nonlinear flexural vibration of uniform aluminum beams that were symmetrically integrated with smart piezoelectric actuators on their top and bottom sides. Theoretical and experimental findings prove that piezoelectric actuators play a significant role in suppressing vibrations across various applications.

Miao et al. [39] investigated the suppression of vibrations in the cantilever beam using MFCs as actuators and a sensor. Two MFC patches were used for AVC in the cantilever beam, and the third was used as a sensor. The AVC for the first two modes of vibration was executed using the PD control and fuzzy control algorithms. The results confirm that vibrations in the first two modes are significantly suppressed, and this scheme can be implemented in different industrial applications to control vibrations. Rimasauskiene et al. [7] conducted an experimental study to observe the influence of active and passive control schemes on the vibration control of a composite structure by using MFC patch. The findings show that active and passive control schemes efficiently suppress vibrations of the beam structure. Gawryluk et al. [40] conducted an extensive study of various algorithms to suppress vibrations in the composite beam, and an MFC patch (MFC-8528 P1 type) was integrated with the beam. Simulation and experimental studies were carried out to suppress vibrations in the beam structure. The results of the simulation and the experiment confirm that the vibration amplitude can be significantly reduced by applying these control algorithms. Zippo et al. [41] reported an experimental investigation on the AVC of a honeycomb carbon fiber sandwich composite plate bonded with MFCs as actuator and sensor. The first four modes were effectively controlled using a control algorithm. The control

algorithm was found reliable and effective in suppressing the vibration amplitude in linear and nonlinear systems. It was concluded that more tests are needed to investigate the non-linear behaviour of the system and the electromechanical interconnection between different components. Lee et al. [42] investigated a unique dual control approach to mitigate unwanted oscillations in bistable composites structure. The approach includes two MFCs and one Positive Position Feedback (PPF) controller. This technique entails applying a certain voltage to a single MFC to suppress one of the potential wells and push the structure towards a stable position. This is achieved by using a PPF controller to mitigate the resulting single-well vibrations in the structure through the second MFC. Both mathematical and experimental methods have been employed to demonstrate the effectiveness of the dual control approach in reducing the vibration amplitude under various oscillation scenarios. Hao et al. [43] conducted a study on the intra-well as well as inter-well vibrations of an asymmetric bi-stable rectangular-shaped laminate structure with a cross-ply configuration stimulated by a MFC (d33 type). According to the findings, it is easier to achieve the snap-through response in laminate structure when excited by pulsating impulse voltages rather than constant (static) voltages. In addition, snap-through response can be enhanced by varying the frequency as well as amplitude of the supplied voltage to MFC within a specific range. The supplied voltage applies an external force to the system, thereby altering its characteristics such as stiffness, damping, and others. Li et al. [44] utilised an active vibration control (AVC) approach to suppress vibration in a flexible beam. Two MFCs (P2 type) were integrated with the flexible beam; one as an actuator and the second as a sensor. The numerical simulation and experiment were performed on beam structure applying both linear quadratic regulator (LQR) and fuzzy control algorithm under diverse external dynamic conditions. The findings confirm that the LQR control approach is more effective in reducing vibration in beam structures than the fuzzy control. Lu et al. [45] employed an adaptive feedback loop to suppress the vibration amplitude at low frequencies in a sandwich structure composite. A modified analytical model is presented that incorporates the impacts of MFC patches to investigate the vibration properties of the sandwich structure. Numerical simulations and experiments were carried out to validate the accuracy of the modified analytical model. The adaptive feedback loop scheme was employed analytically as well as experimentally, and the findings confirm that vibrations in sandwich structure can be suppressed effectively by applying this scheme.

Wang et al. [46] reported a numerical approach to develop a geometric nonlinear fiber-reinforced thin-walled composite beam integrated with piezo-composite actuators to create a smart structure for the aircraft wing. The simple negative velocity feedback approach was applied, and it was shown that the damping performance can be improved, and the total cost of the system can also be decreased by selecting the suitable size and position of the piezo actuator. Chai et al. [47] reported the numerical simulation and theoretical investigation on the aero-thermoelastic behaviour of the laminated structure. Two MFC patches were integrated with the structure; one as a sensor to measure strain and the other creates a control force to suppress vibrations in

the structure. The findings confirm that MFC patch effectively reduces the vibration amplitude in the structure. Li et al. [3] presented a comprehensive numerical study on the AVC of a piezoelectric plate integrated with a piezoelectric patch, aiming to suppress vibrations. The velocity feedback approach was applied on the plate to observe the significant effect of AVC on the plate. The findings from the study reveal that a substantial vibration suppression is achieved. Mitura et al. [48] developed FEM for a beam structure composed of glass-epoxy with multi layers using the Abaqus platform. The purpose was to mitigate undesired vibrations through the application of embedded MFC actuators (M8528-P1). The PPF control was employed to manage vibration, and a dedicated subroutine was developed to incorporate PPF within the Abaqus platform. The study involved a comparison of the beam structure's behaviours with and without the implementation of the PPF controller. Subsequently, the numerical simulations associated with the efficacy of the PPF controller were validated through experimental verification. Kamel et al. [49] developed a dynamic model of a carbon composite-based cantilever beam in ANSYS using FEM to control vibrations. Frequency analysis of the dynamic model was conducted in ANSYS, considering four distinct scenarios. The state space model (SSM) of the smart beam for each scenario was created in the MATALB using the results obtained from ANSYS. Subsequently, a Proportional-Integral-Derivative (PID) controller was developed using the SSM derived from the first scenario in the MATLAB and confirmed against the other three scenarios. To enhance the performance of the system, three additional smart controllers based on fuzzy logic were studied. The findings reveal that fuzzy-based controllers contributed a significant role in the vibration control of the beam system.

After conducting an in-depth review of the existing literature, it has been identified that the current investigation addresses a scientific gap by exploring how distinct layer orientations, such as 0°-0° and 0°-90°, in AM structures influence their dynamic characteristics. These structures are made from PLA, PLA-SCF, PLA-CCF, and PLA-CGF. Moreover, this pioneering study also investigates vibration suppression in these structures with the application of MFC actuators, identifying the layer orientation and AM structure that play a significant role in effective vibration suppression.

3. REVIEW OF THE PUBLISHED ARTICLES[1]

This chapter consists of a summary of the findings of the published articles.

3.1. Article [A1]: Experimental investigation of vibration amplitude control in additive manufactured PLA and PLA composite structures with MFC actuator [57]

This sub-section references a scientific article published in 'Engineering Structures' (Elsevier, 2023, Vol. 294). It addresses the first, second, and third objectives of the dissertation. To date, this article has received a total of 9 citations.

In this article, a quantitative comparative study is presented on the use of macro fiber composite (MFC) as an actuator across various materials, especially AM fiber-reinforced composites in the field of vibration control. The MFC (M8507-P2) actuator has been utilized to control vibrations in AM beam structures with a 0°-0° layer orientation, made from polylactic acid (PLA) and PLA composites. The PLA composites include PLA with short carbon fibers (PLA-SCF composite) and PLA with continuous carbon fibers (PLA-CCF composite). The primary objectives of this study are to determine the dynamic properties (natural frequencies and bending mode shapes), assess vibration suppression with an impact of MFC in AM structures, and identify the structure in which the MFC is most effective at limiting vibration amplitudes.

The beams were manufactured individually using FDM technology with PLA, PLA-SCF and PLA-CCF. The PLA and PLA-SCF specimens were fabricated using an Original Prusa i3 MK 3S & MK3S+ 3D printer. While the creation of a PLA-CCF composite specimen was performed using a modified MeCreator-2 3D printer. The fabrication process of specimens has been presented in Fig. 1.

The vibration control system consists of a beam structure (parameters 120 mm × 20 mm × 1.35 mm), and an MFC (M8507-P2) as actuator (active size 85 mm × 7 mm × 0.3 mm with an overall size 100 mm × 10 mm × 0.3 mm) produced by Smart Materials [20]. An electrodynamic shaker (DDR-11077) made by the German company VEB Robotron-Messelektronik "Otto Schon" Dresden, was used to individually introduce vibrations from the clamped side of the beam structure. The MFC actuator was bonded with epoxy to the surface, 5 mm from the clamped side of the beam. The schematic view of the beam structure with the MFC patch is presented in Fig. 2. The overall experimental arrangement presented in Fig. 3 was used to obtain vibration amplitude at the free end (one point) of each beam structure.

The Polytec 3D laser vibrometer (PSV-W-500) manufactured by Polytech GmbH, Germany, shown in Fig. 4, was used to measure natural frequencies, bending mode shapes, and the amplitudes of bending modes. This experimental setup consists of three scanning heads (for 3D vibration measurement), voltage amplifier (F10A) made by FLC electronics, Sweden, and data management system (PSV-500-3D-HV).

[1]This chapter references the author's work published in WoS journals [56–59].

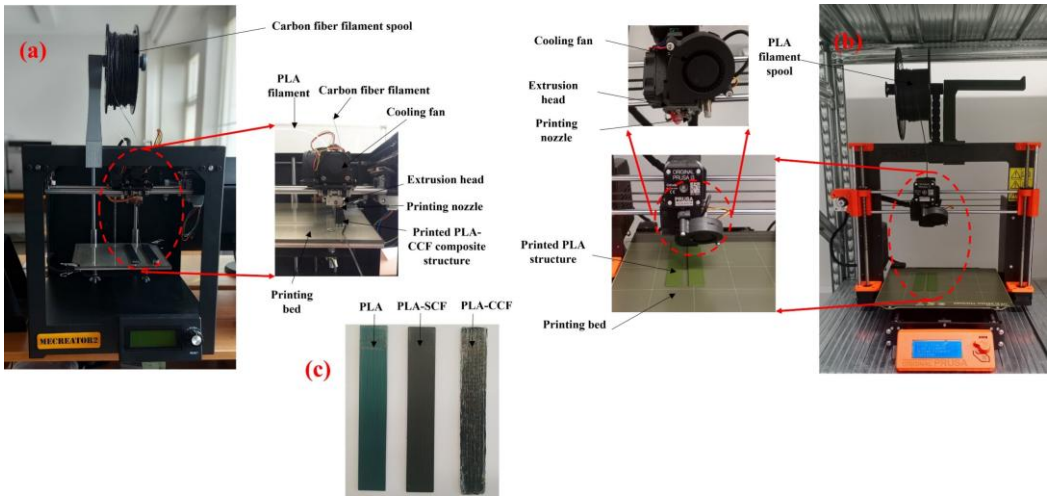

Fig. 1. Fabrication of beam structures: a) preparation of PLA-CCF structures; b) preparation of PLA and PLA-SCF structures; c) PLA, PLA-SCF and PLA-CCF samples

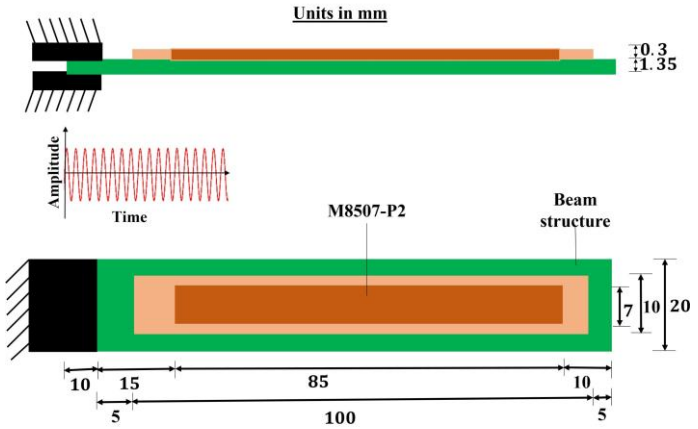

Fig. 2. Schematic view of the beam structure with the bonded MFC

The first stage of the experimental investigation was focused on determining the natural frequencies and bending mode (BM) shapes of structures made of PLA, PLA-SCF, and PLA-CCF individually. Vibrations were introduced in each structure, caused by the MFC actuator (M8507-P2) to determine the natural frequencies and mode shapes.

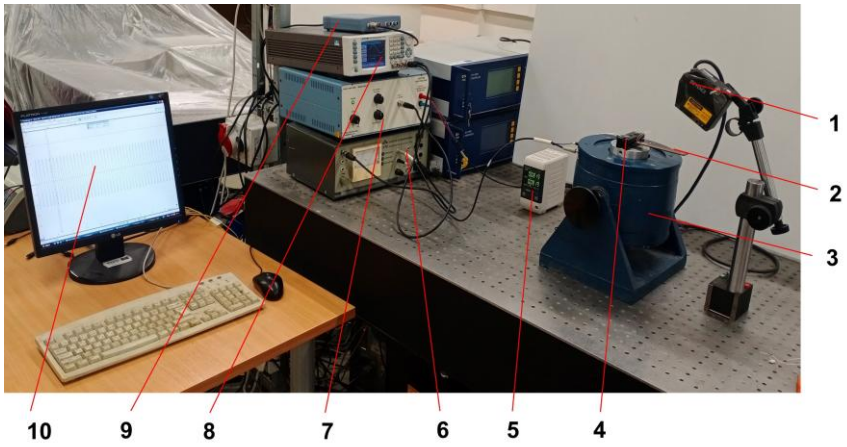

Fig. 3. Experimental Setup: 1 – laser displacement sensor (LK-G82); 2 – beam with MFC actuator; 3 – electrodynamic shaker (DDR-11077); 4 – clamper; 5 – laser displacement sensor controller LK-G3001PV; 6 – voltage amplifier (LV-103); 7 – voltage amplifier (EPA-104); 8 – function generator WW5064; 9 – analogue/digital signal converter (ADC) Pico-Scope- 3424; 10 – computer

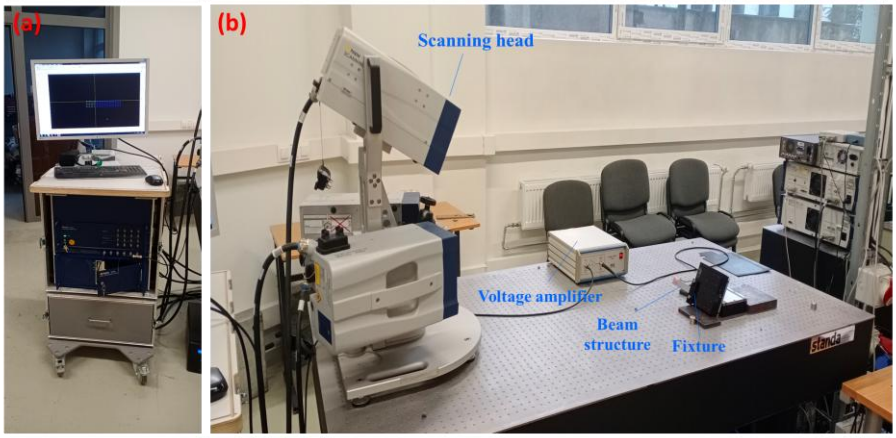

Fig. 4. Polytec 3D laser vibrometer (PSV-500): a) data management system (control unit); b) three scanning heads for 3D vibration measurement

The natural frequencies and respective amplitudes of the first four bending modes are listed in Table 2. It is reported in Table 2 that the vibration amplitudes are significantly reduced from first to fourth BM. The highest vibration amplitudes are found at the first natural frequencies, which are 9.295 µm at 30 Hz for PLA, 6.831 µm at 40.5 Hz for PLA-SCF, and 4.139 µm at 60 Hz for PLA-CCF. The lowest vibration amplitudes are obtained at the fourth natural frequencies of PLA, PLA-SCF, and PLA-CCF structures, which are 0.129 µm, 0.049 µm, and 0.022 µm at 1207.5 Hz, 1546 Hz, and 2192 Hz, respectively. The average spectrum of each structure is shown

in Fig. 5. The inset portion in Fig. 5 presents the maximum vibration amplitude values of PLA, PLA-SCF, and PLA-CCF at the corresponding first natural frequency.

It can be concluded from the above experimental results as well as from the literature study that the highest vibration amplitude consistently occurs at the first natural frequency and has a dominant impact on the overall vibration response [7]. Therefore, it was decided that only the first bending mode of each beam structure should be investigated as it is the dominant mode (with the largest amplitude) and offers the most potential for reducing vibration amplitudes.

Table 2. Natural frequency and corresponding amplitudes for PLA, PLA-SCF, and PLA-CCF beam structures

Bending Mode	PLA		PLA-SCF		PLA-CCF	
	Freq (Hz)	Amp (μm)	Freq (Hz)	Amp (μm)	Freq (Hz)	Amp (μm)
1st	30	9.295	40.5	6.831	60	4.139
2nd	215	3.602	280.5	1.911	410	1.131
3rd	626.5	0.349	802	0.136	1153	0.110
4th	1207.5	0.129	1546	0.049	2192	0.022

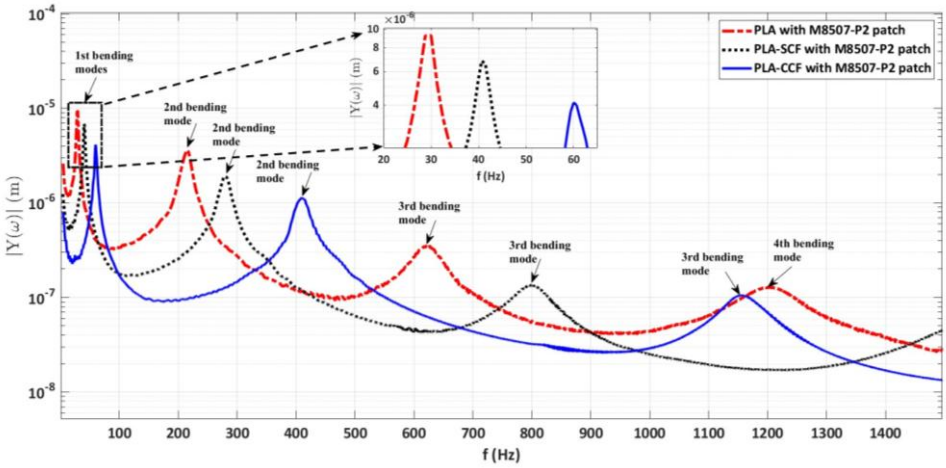

Fig. 5. Amplitude spectrum of the beam structure, made of PLA, PLA-SCF and PLA-CCF with MFC patch

In the second phase, structures made of PLA, PLA-SCF, and PLA-CCF were individually excited at their respective first resonant frequencies (30 Hz, 40.5 Hz and 60 Hz) using an electrodynamic shaker with harmonic signal of 0.16 V to obtain the uncontrolled displacement response. The maximum peak to peak displacement values were observed as ±400 μm, ±370 μm and ±210 μm for PLA, PLA-SCF and PLA-CCF

structures, respectively. An open-loop AVC approach with incremental domain searching was employed to determine the optimal phase and control voltage for maximum vibration amplitude reduction. The stable phase domains for PLA, PLA-SCF and PLA-CCF ranged from approximately 330° to 90°, 310° to 70° and 290° to 50° respectively. However, beyond these phase ranges, the vibration amplitude exhibited an increase rather than a decrease. The influence of phase change on the vibration amplitude has been depicted in Fig. 6. PLA exhibited the maximum reduction at a phase of 29° phase with control voltage of 22.4 V, while PLA-SCF demonstrated the optimal results at a phase of 10° with a control voltage of 13.92 Similarly, for PLA-CCF the maximum reduction was obtained at a phase of 351° with a control voltage of 10.52 V. These optimizations (optimal phase with control voltage) produced peak-to-peak vibration amplitudes for PLA, PLA-SCF, and PLA-CCF, ranging from +5.5 µm to -4.5 µm, +3.2 µm to -2.9 µm, and +1.7 µm to -1.7 µm, respectively, as shown in Fig. 7. to Fig. 9.

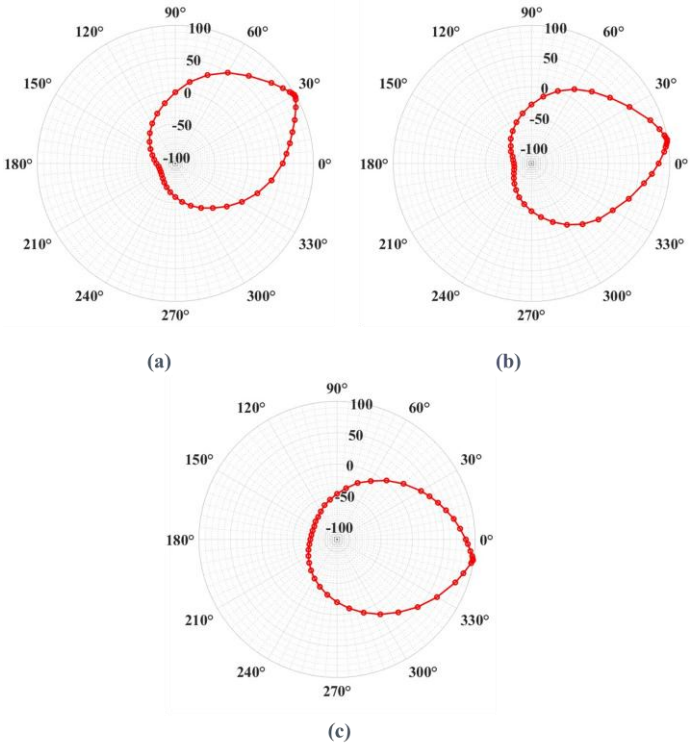

Fig. 6. Phase influence on amplitude reduction for: a) PLA; b) PLA-SCF; c) PLA-CCF

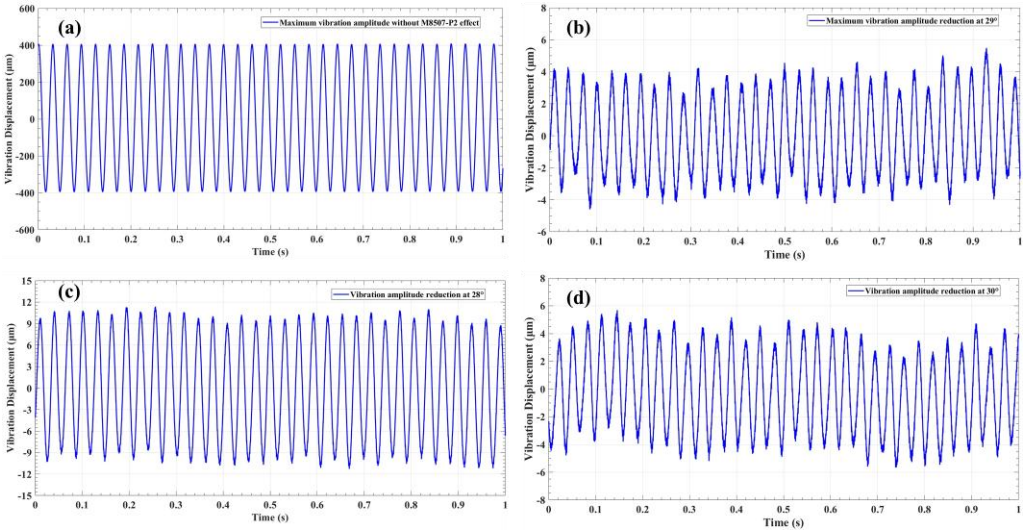

Fig. 7. Vibration amplitude in beam structure made of PLA: a) vibration amplitude without effect of MFC actuator; b) vibration amplitude with effect of MFC actuator at 29°; c) vibration amplitude with effect of MFC actuator at 28°; d) vibration amplitude with effect of MFC actuator at 30°

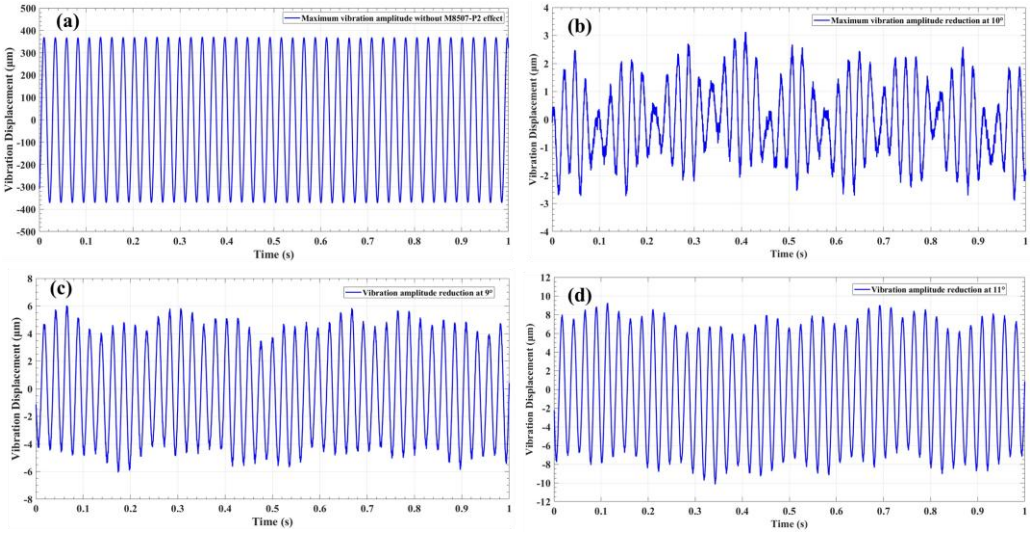

Fig. 8. Vibration amplitude in beam structure made of PLA-SCF: a) vibration amplitude without effect of MFC actuator; b) vibration amplitude with effect of MFC actuator at 10°; c) vibration amplitude with effect of MFC actuator at 9°; d) vibration amplitude with effect of MFC actuator at 11°

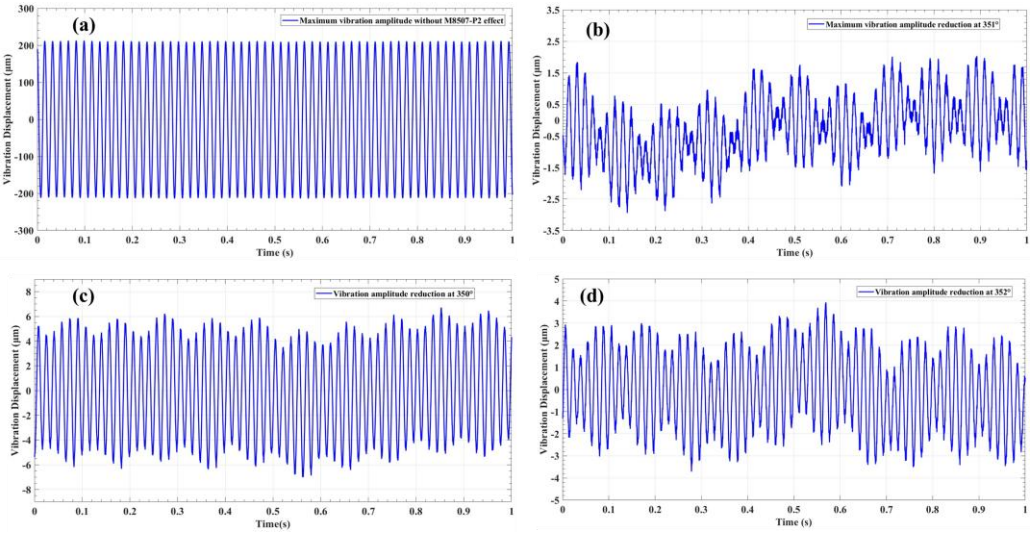

Fig. 9. Vibration amplitude in beam made of PLA-CCF: a) vibration amplitude without effect of MFC actuator; b) vibration amplitude with effect of M8507-P2 at 351°; c) vibration amplitude with effect of MFC actuator at 350°; d) vibration amplitude with effect of MFC actuator at 352°

The considerable vibration reductions of more than 80 times, 110 times and 120 times were observed in PLA, PLA-SCF and PLA-CCF, respectively. The maximum vibration amplitude reduction was observed in PLA-CCF, followed by PLA-SCF and PLA, respectively, in a controlled environment.

3.2. Article [A2]: An experimental study on the dynamic properties of 3D-printed structures with different layer orientations [56]

This sub-section references a scientific article published in 'Journal of Vibration Engineering & Technologies' (Springer Nature, 2024, Vol. 12). It addresses the first objective of the dissertation. To date, this article has received a total of 2 citations.

After a detailed examination of the available literature, it was concluded that most researchers have only investigated the impact of 3D printing process settings on the mechanical response of various structures. Consequently, it is necessary to examine the impact of printing settings on dynamic characteristics (natural frequencies, bending mode shapes, decrement coefficient, damping and deformation) of structures. In the current study, beam structures made of PLA, PLA-SCF, and PLA-CCF (dimensions: 120 mm × 20 mm × 1.35 mm) are created using FDM with two distinct layer orientations (0°-0° and 0°-90°). The impact of these orientations on the dynamic characteristics of the structures is investigated through various experiments.

The fabrication of PLA and PLA-SCF samples was carried out using an Original Prusa 3D printer (Model: MK3S and i3 MK3S+), while the PLA-CCF and PLA-CGF

specimens were fabricated using a customized MeCreator-2 3D printer. The fabrication process is depicted in Fig. 10.

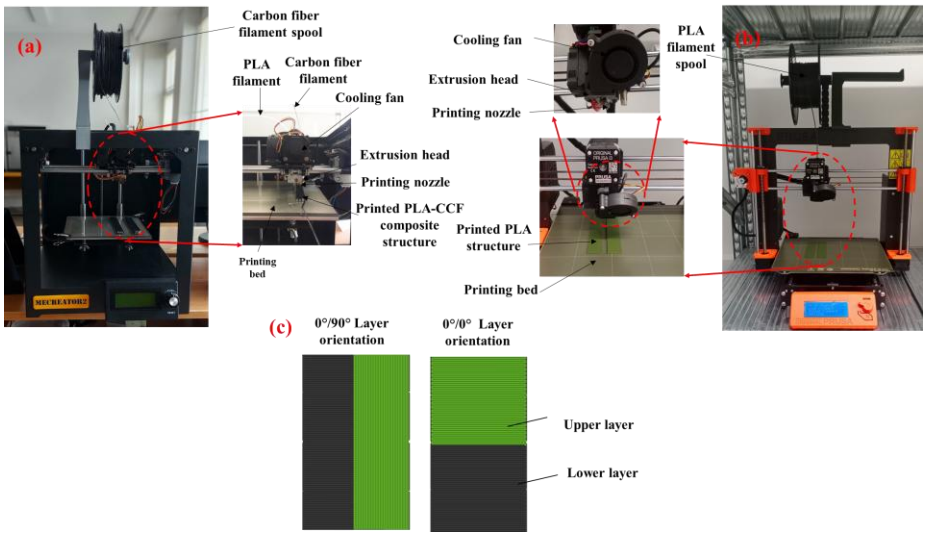

Fig. 10. Fabrication process of beam structures: a) fabrication of PLA-CCF and PLA-CGF; b) fabrication of PLA and PLA-SCF; c) 0°- 0° and 0°-90° layer orientations

To assess the deformation in beam structures with 0°-0° and 0°-90° layer orientations, the experimental setup shown in Fig. 11 was used. The beam structure was fixed at one end, and various point mass loads were applied to the free end of each structure, as presented in Fig. 12. The deformation in each structure was measured using a laser displacement sensor (LK-G82).

To determine the logarithmic decrement coefficient, a new experimental approach, as depicted in Fig. 13, has been employed. The arrangement was especially created for observing the exponential damped response in each structure caused by an electrodynamic shaker (DDR-11077), manufactured by VEB Robotron-Messelektronik Otto Schon, German and the response was measured at the one point from free end by a laser displacement sensor (LK-G82) made by Keyence Corporation, Japan. The structure was fixed from one side and vibrations in the structure were introduced by electrodynamic shaker from fixed side as indicated schematically in Fig. 14.

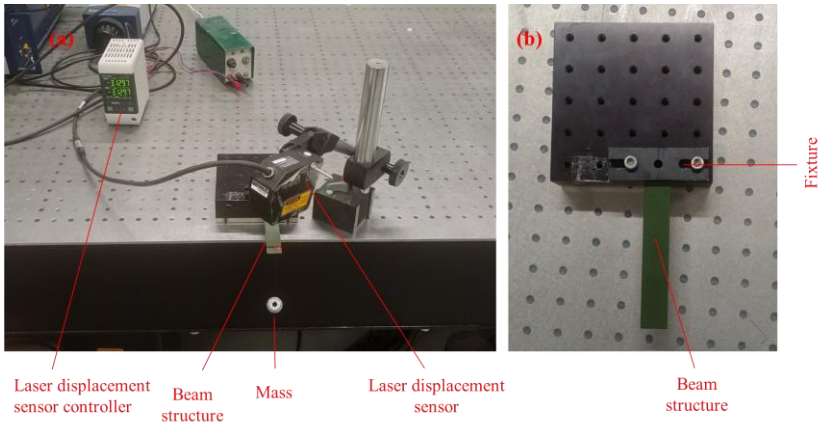

Fig. 11. Deformation measurement in beam structures: a) experimental setup; b) fixation of beam structure

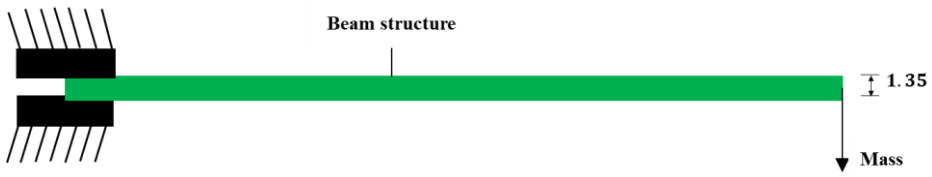

Fig. 12. Schematic of beam structure with point mass at free end

The burst signal of 50mV amplitude as input was provided to the electromagnetic shaker by the function -arbitrary waveform generator (33220A) built in Agilent, Malaysia. The decrement coefficient in each structure has been calculated using the following expression [50].

$$\delta = ln\left(\frac{U_n}{U_{n+m}}\right)/m, \tag{3.1}$$

where U_n is the amplitude at time t_n; U_{n+m} is the amplitude at time t_{n+m}; m is the number of cycles.

Moreover, modal analysis testing was performed to obtain the natural frequencies, mode shapes, and corresponding vibration amplitudes of each structure, as shown in Fig. 4. The MFC (M8507-P2) actuator was integrated into the beam structure at a point 5 mm from the fixed end. Vibrations in each beam were generated using an MFC patch by applying a 100 V chirp signal. A Polytec 3D laser vibrometer (PSV-500, GmbH, Germany) was used to measure observations at a single point on the free end of the structure.

Moreover, an impact test was conducted to estimate the first natural frequencies of the structures. The beam structure was fixed in a fixture, and vibrations were induced by impacting the free end of the structure with a relatively small object, as

shown in Fig. 15. The excitation response of each structure was measured using a laser displacement sensor (LK-G82).

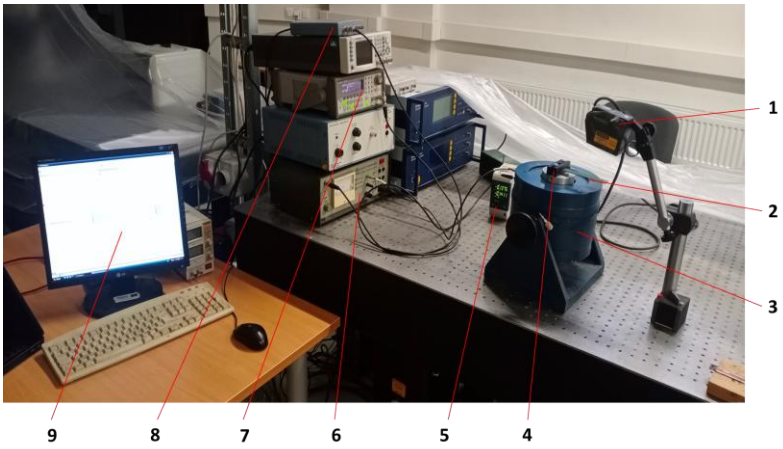

Fig. 13. Logarithmic decrement coefficient measurement setup: 1 – laser displacement sensor (LK-G82); 2 – beam structure; 3 – electrodynamic shaker (DDR-11077); 4 – fixture; 5 – laser displacement sensor controller (LK-G3001PV); 6 –voltage amplifier (LV-103); 7 – function generator (33220A); 8 – analogue/digital signal converter Pico-Scope; 9 – computer

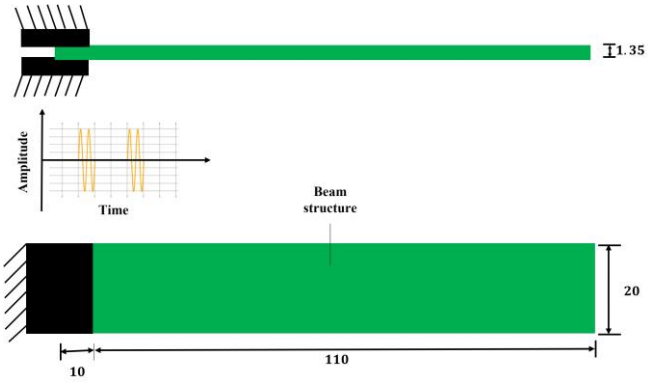

Fig. 14. Schematic view of vibration in beam structure by electromagnetic shaker

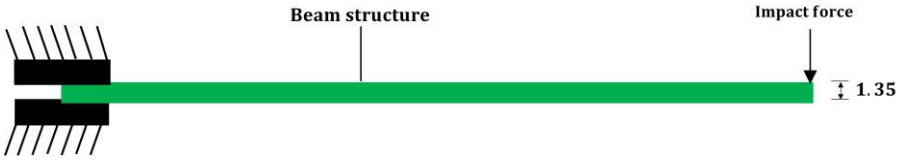

Fig. 15. Schematic view of impact force at free end of beam structure

The deformation in structures increases linearly with an increasing point mass load, as shown in Fig. 16. The maximum deformation is observed in PLA-CGF structure with 0°-90° layer orientation, 6.69 mm, and the minimum deformation is found in PLA-CCF structure with 0°-0° layer orientation, 0.78 mm under a mass of 8 g. The deformations in beam structures with 0°-90° layer orientation have been found more compared to their corresponding structures with 0°-0° orientation.

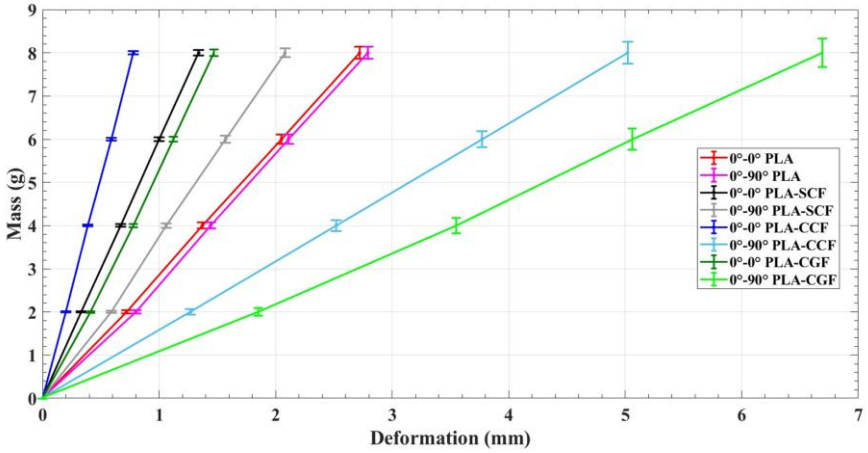

Fig. 16. Deformation in beam structures under varying masses

The resistance to deformation under a mass load in a structure is generally described as its stiffness. The experimental results indicate that with a layer orientation of 0°-0°, the stiffness increases from PLA to PLA-SCF to PLA-CGF and finally to PLA-CCF, while with a 0°-90° layer orientation, it increases from PLA-CGF to PLA-CCF to PLA and then PLA-SCF.

The decrement coefficient of each structure was determined by taking the first five successive peak amplitudes i.e., U_n to U_{n+4} (4 cycles), as represented in Fig. 17(a). The vibrating periodic amplitudes of beam structures were recorded by a laser displacement sensor, as depicted in Figs. 17(b) through 17(i).

For the 0°-0° layer orientation, the decrement coefficient values for PLA, PLA-SCF and PLA-CCF, PLA-CGF as calculated by Eq. (3.1), were 0.043,0.081,0.214 and 0.063 respectively. The vibration amplitude damping effect was observed maximum in PLA-CCF followed by PLA-SCF, PLA-CGF and finally PLA structures.

In contrast, for the 0°-90° layer orientation, the decrement coefficients for PLA, PLA-SCF, PLA-CCF, and PLA-CGF were 0.041, 0.052, 0.040, and 0.038, respectively. Consequently, PLA-SCF exhibited the maximum amplitude damping effect, while PLA and PLA-CCF showed similar amplitude damping effects, and PLA-CGF demonstrated the minimum. The findings reveal that 0°-0° structures demonstrate greater damping properties compared to their corresponding 0°-90° beam structures.

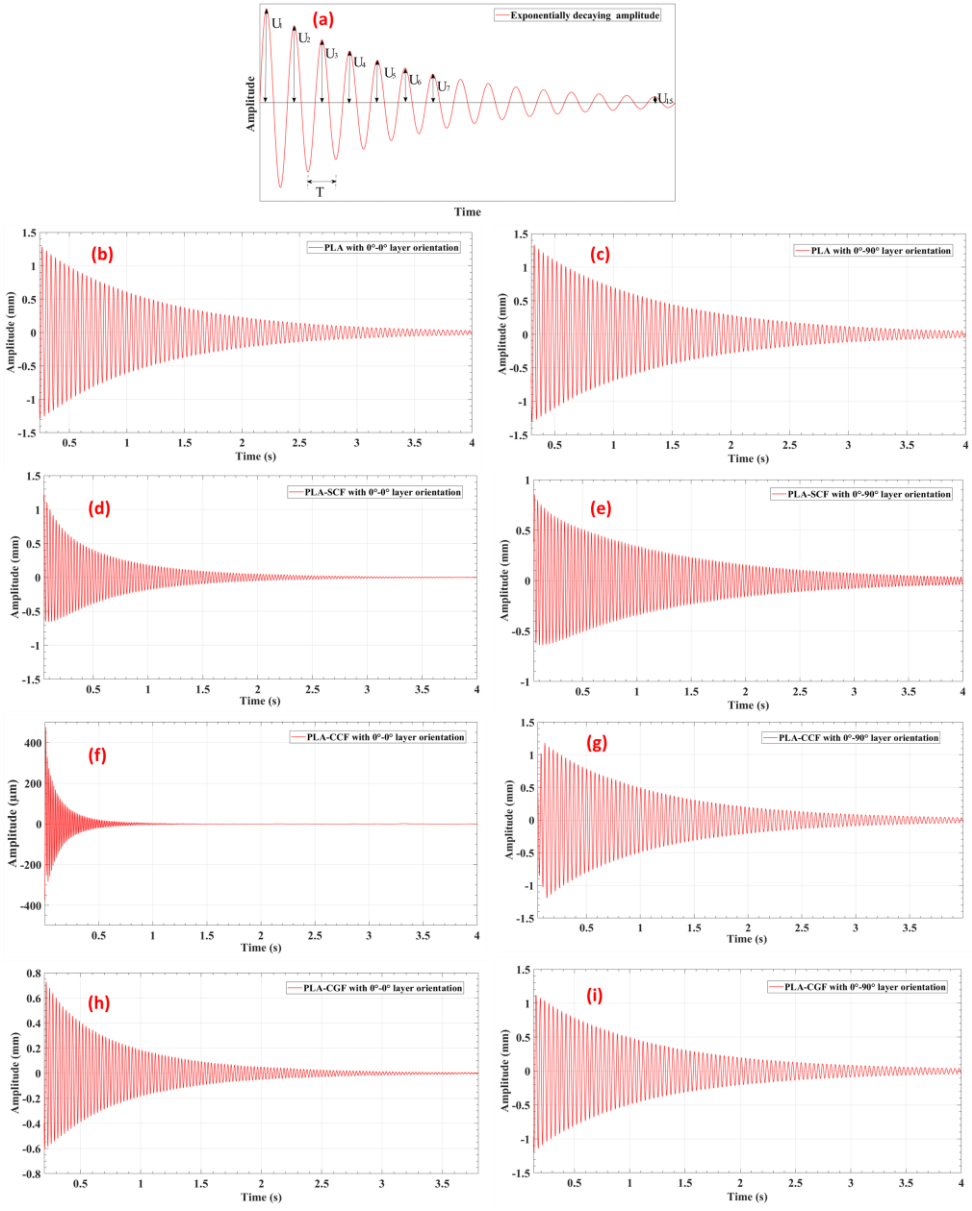

Fig. 17. Amplitude damping of PLA, PLA-SCF, PLA-CCF and PLA-CGF beam structures: a) exponentially decaying amplitude trend; b) 0°-0° PLA; c) 0°-90° PLA; d) 0°-0 PLA-SCF; e) 0°-90° PLA-SCF; f) 0°-0° PLA-CCF; g) 0°-90° PLA-CCF; h) 0°-0° PLA-CGF; i) 0°-90° PLA-CGF

Moreover, the first four natural frequencies of the bending modes are summarised in Table 4. The results reveal that the natural frequencies of beam structures with 0°-0° layer orientation are comparatively higher than the respective

structures with 0°-90° layer orientation. The mechanical characteristics of the material, such as its mass and stiffness, assess its natural frequencies according to Eq. (3.2) [51–53].

$$f = \frac{\sqrt{k/m}}{2\pi}, \tag{3.2}$$

where k represents stiffness; m represents mass; f represents natural frequency.

According to the modal testing findings, within 0°-0° oriented structures, the frequency increases progressively from PLA to PLA-SCF to PLA-CGF, with PLA-CCF exhibiting the maximum frequency. For 0°-90° oriented structures, it increases from PLA-CGF to PLA-CCF to PLA and finally to PLA-SCF.

Table 4 presents the vibration amplitudes of the structures at their respective frequencies. The findings indicate that the vibration amplitude is highest at the first natural frequency and lowest at the fourth natural frequency.

Finally, the estimation of the first natural frequency of each beam structure, without MFC patch (only actual beam) was performed. Applying an impact force to the free end of the beam structure caused vibrations, which were then monitored using a laser displacement sensor (LK-G82). The average value of each structure is reported in Table 3.

Table 3. Natural frequencies of beam structures by impact test

Beam structure	Frequency of 0°-0° oriented structures (Hz)	Frequency of 0°-90° oriented structures (Hz)
PLA	26.54	25.95
PLA-SCF	39.31	30.62
PLA-CCF	58.87	25.65
PLA-CGF	46.61	20.27

The impact responses of structures made from various materials depend on several aspects, such as material properties (both the matrix and reinforcing elements), structure layout, the number of layers in structures, and the impact force [54].

Thus, the findings demonstrate that specimens with 0°-0° layout have substantially higher first natural frequency than 0°-90° layout specimens.

Table 4. Natural frequencies and corresponding amplitudes of beam structures

Bending Modes	PLA				PLA-SCF				PLA-CCF				PLA-CGF			
	0°-0° layer orientations		0°-90° layer orientations		0°-0° layer orientations		0°-90° layer orientations		0°-0° layer orientations		0°-90° layer orientations		0°-0° layer orientations		0°-90° layer orientations	
	Freq (Hz)	Amp (μm)	Freq (Hz)	Amp (μm)	Freq (Hz)	Amp (μm)	Freq (Hz)	Amp (μm)	Freq (Hz)	Amp (μm)	Freq (Hz)	Amp (μm)	Freq (Hz)	Amp (μm)	Freq (Hz)	Amp (μm)
1st	30.0	9.295	27.5	10.924	40.5	6.831	28.8	9.733	60.0	4.139	26.6	10.110	47.7	4.400	21.3	9.260
2nd	215.0	3.602	207.5	3.753	280.5	1.911	221.3	3.437	410.0	1.131	203.1	3.375	315.6	1.450	165.0	3.330
3rd	626.3	0.349	603.8	0.330	802.3	0.136	635.0	0.327	1153.1	0.110	592.2	0.255	895.3	0.120	480.0	0.250
4th	1207.5	0.129	1157.5	0.152	1545.8	0.049	1193.8	0.111	2190.0	0.022	1114.1	0.121	1707.0	0.050	918.0	0.100

3.3. Article [A3]: Enhancing vibration control in kinematically excited additively manufactured continuous fiber composite structures with distinct orientations [58]

This part of the dissertation references a scientific article published in 'Engineering Structures' (Elsevier, 2024, Vol. 321). It addresses the first, second, and third objectives of the dissertation. To date, this paper has received a total of 1 citation.

In this sub-section, after conducting an in-depth review of the existing literature, it has been identified that the current study offers a novel contribution by exploring how AM composite structures with two distinct layer orientations, 0°-0° and 0°-90°, influence dynamic characteristics and vibration suppression, with the application of MFC (M8507-P2). These composite structures were made from PLA-CCF and PLA reinforced with continuous glass fibers (PLA-CGF). The primary aim of the study is to identify a distinct layer orientation that contributes a significant role in vibration suppression.

Moreover, this section also examines the dynamic characteristics and vibration suppression of PLA and PLA-SCF with 0°-0° and 0°-90° orientations. The dynamic characteristics and vibration suppression of PLA and PLA-SCF with 0°-0° orientations have been published in the article [A1]; however, the findings related to 0°-90° orientations were not previously published and are now included in this sub-section. Adding this information is crucial for a comparative investigation of the influence of distinct layer orientations on the dynamic characteristics and vibration suppression of PLA, PLA-SCF, PLA-CCF, and PLA-CGF beam structures.

Composite specimens reinforced with continuous carbon fiber and glass fiber were produced using the MeCreator-2 3D printer with a modified printing head. The printing method employed is based on Co-Extrusion with Towpreg technology. In other words, the modified printing head has two input channels: one for PLA thermoplastic matrix and another for impregnated continuous carbon fiber or glass fiber. The authors have exhaustively examined the impregnation process for continuous fiber [55]. The fabrication process of composite structures is depicted in Fig. 18, whereas schematic description of fabrication process with modified printing head is illustrated in Fig. 19. While the fabrication process of PLA and PLA-SCF has been illustrated in Fig. 10.

The experimental design shown in Fig. 3, was utilised to observe and examine the vibration suppression in composite structures. The system comprises a composite structure with dimensions of 120 mm × 20 mm × 1.35 mm, integrated with an MFC (M8507-P2) made by Smart Material [20]. The MFC actuator was integrated with epoxy, 5 mm from the fixed edge of the composite structure, as illustrated in Fig. 2.

The OLAVC approach has been used to measure vibration suppression; the experimental approach layout is schematically depicted in Fig. 20. Vibrations were introduced into each composite structure from the fixed edge side using an 'Electrodynamic Shaker (DDR-11077)', with the input signal supplied through a function generator (WW5064). Vibration amplitudes were monitored and measured

4 mm from the free end of each beam, with the impact of the MFC patch assessed using a Laser Displacement Sensor (LDS).

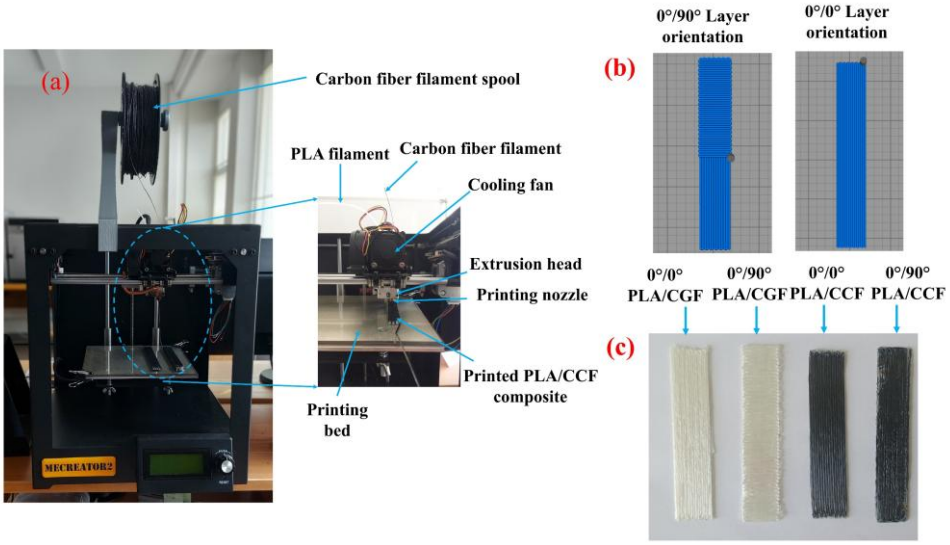

Fig. 18. Fabrication scheme of composite structures: a) preparation process of composite structures; b) depiction of 0°-0° and 0°-90° layer patterns; c) 3D printed composite structures

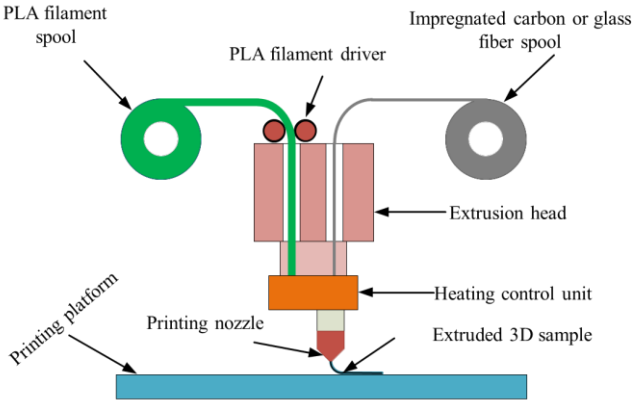

Fig. 19. Schematic description of fabrication process with modified printing head

The voltage signal with the optimal phase was supplied to the MFC through the function generator (WW5064) to achieve maximum reduction in amplitude. The LDS (LK-G82) captured the deformation in the composite beam and transferred signal to the LDS control unit (LK-GD500) for processing. This data in analogue format was further processed through a Pico-Scope 3424 device, which functioned as analog to digital converter (ADC). The data was then analysed using Pico-Scope 6 software.

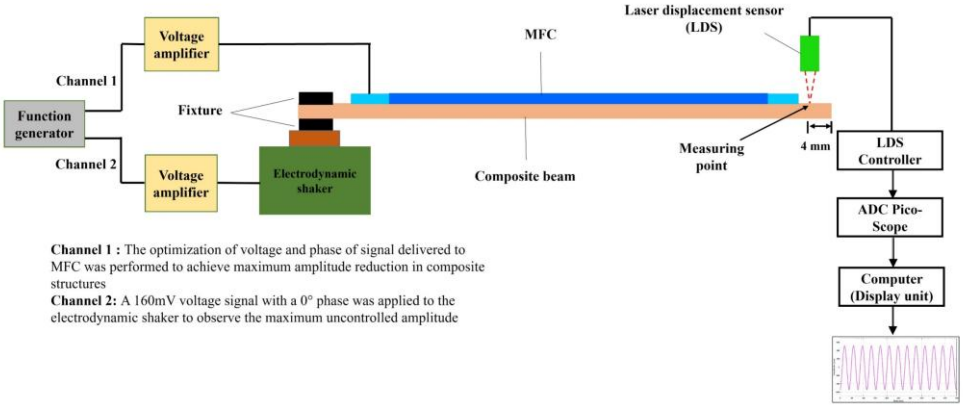

Fig. 20. Scheme of the layout of the experimental approach

The experimental design depicted in Fig. 4 was utilised to ascertain the inherent frequencies, bending mode shapes, and amplitude spectra for each beam. The composite structures started vibration when a chirp signal of 100 V was supplied to the MFC actuator. To examine the responses at the free end, a Polytec 3D laser vibrometer (PSV-W-500) was used.

To assess the deformation in PLA-CCF and PLA-CGF composite structures, the experimental design illustrated in Fig. 11, was utilised. Both structures were composed of 0°-0° and 0°-90° layer orientations. The deformation assessment in each structure was carried out by fixing one side and subjecting the free end to various static concentrated masses. The response in each composite structure was examined using an LDS (LK-G82). Moreover, the deformations in PLA and PLA-SCF with 0°-0° and 0°-90° layer orientations were also determined employing the same methodology. The deformations in all configurations have been reported in Fig. 16. Fig. 16 shows that the deformation in 0°-90° beam structures is higher compared to the corresponding 0°-0° beam structures.

The structures with minimal deformation are generally associated with enhanced stiffness [10]. Moreover, the findings highlight that the PLA-CCF structure with 0°-0° layers exhibit the highest stiffness, while the PLA-CGF structures with 0°-90° layers demonstrate the lowest stiffness.

In the second phase of the experimentation, modal analysis was conducted to evaluate the inherent frequencies of the first four bending modes, along with their corresponding bending mode (BM) shapes and amplitude spectra, for PLA-CCF and PLA-CGF composite structures with 0°-0° and 0°-90° layer orientations. Vibrations were induced in each structure using an integrated MFC (M8507-P2). The integrated MFC patch was stimulated with a chirp signal of 100 V, generated by a function generator, it is an integral part of the 3D laser vibrometer. The inherent frequencies, along with their corresponding amplitude have been provided in Table 3.4.

The highest vibration amplitude for each composite structure is observed at the first frequency and the lowest amplitude at the fourth frequency (see Table 5). Furthermore, Fig. 21 illustrates the amplitude spectra of PLA-CCF and PLA-CGF with 0°-0° and 0°-90° layer arrangements.

Table 5. Inherent frequencies and corresponding amplitudes for PLA-CCF and PLA-CGF composite structures

Bending modes	**0°-0° PLA-CCF**		**0°-90° PLA-CCF**		**0°-0° PLA-CGF**		**0°-90° PLA-CGF**	
	Freq (Hz)	Amp (μm)	Freq (Hz)	Amp (μm)	Freq (Hz)	Amp (μm)	Freq (Hz)	Amp (μm)
1st	60	4.14	26.6	10.11	47.7	4.40	21.3	9.26
2nd	410	1.13	203	3.38	315.6	1.45	165	3.33
3rd	1153	0.11	592	0.26	895.3	0.12	480	0.25
4th	2190	0.02	1114	0.12	1707	0.05	918	0.10

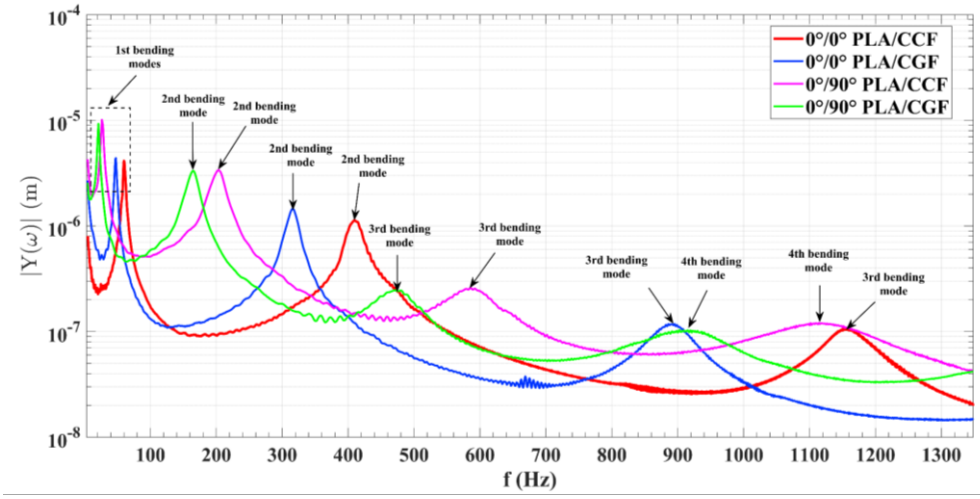

Fig. 21. Amplitude spectra of PLA-CCF and PLA-CGF with 0°-0° and 0°-90° orientations

For PLA and PLA-SCF with 0°-0° and 0°-90° layer arrangements, the maximum amplitude occurs at the first frequency, and the lowest at the fourth, as reported in Table 4. Additionally, the amplitude spectra of PLA and PLA-SCF are presented in the article [A2]. The results reveal that 0°-0° beam structures consistently exhibit higher frequencies compared to their corresponding 0°-90° structures.

Based on the reported experimental findings and the literature study, it can be deduced that the first BM always exhibits the maximum vibration amplitude and dominance in the entire vibrational behaviour [7, 53, 56]. Thus, this article focuses on further investigating the reduction in vibration amplitude at the first BM due to its dominance.

To investigate the uncontrolled vibration amplitude behavior, each composite structure was stimulated at first resonant frequency using electrodynamic shaker. The maximum uncontrolled vibration amplitudes for 0°-0° PLA-CCF, 0°-90° PLA-CCF, 0°-0° PLA-CGF and 0°-90° PLA-CGF exhibited a range approximately from +210 μm to -212μm at 60 Hz, +514 μm to -545μm at 26.6 Hz, +244 μm to -242 μm at 47.7 Hz and +785 μm to -810 μm, respectively.

In the case of 0°-0° PLA and 0°-0° PLA-SCF beam structures, the uncontrolled vibration amplitudes were observed as approximately ±400 μm at 30 Hz and ±370 μm at 40.5 Hz, respectively (published data in the article [A1]). For 0°-90° PLA and 0°-90° PLA-SCF, the uncontrolled vibration amplitudes were identified as approximately ±526 μm at 27.5 Hz and +492 μm to -503 μm at 28.8 Hz, respectively.

To achieve vibration amplitude reduction in each beam structure, a voltage signal was introduced to MFC, generating a counter force that decreases the vibration amplitude. As the voltage amplitude increased, the MFC produced more force, as specified by the manufacturer [20]. However, this approach does not yield optimal control applicable to both amplitude and phase regulation. Accurate tuning of both the control voltage amplitude and phase is imperative for achieving maximum reduction in vibration amplitude.

For a comparative analysis, vibration amplitude reduction can be quantified using the Eq. (3.3):

$$R = \left(\frac{W_u - W_c}{W_u}\right) \times 100\%, \tag{3.3}$$

where R, W_u, W_c correspond to the reduction factor, uncontrolled amplitude, and controlled amplitude in the time series. Using the OLAVC methodology with incremental parameter tuning, optimal control voltage and phase settings were determined to achieve maximum amplitude reduction. The control voltage along with phase for 0°-0° PLA-CCF, 0°-90° PLA-CCF, 0°-0° PLA-CGF and 0°-90° PLA-CGF were determined as follows:10.52 V with 351° phase,29.4 V with 45°phase, 17.68 V with 4° phase and 43 V with 79° phase.

For 0°-0° PLA and 0°-0° PLA-SCF, the control voltages with optimal phases were determined as 22.4 V with a 29° phase and 13.92 V with a 10° phase, respectively (reported in the article [A1]). While in 0°-90° PLA and 0°-90° PLA-SCF, the settings were determined as 30.1 V with 37° phase and 27 V with 32° phase, respectively.

An interesting insight derived from this investigation is that the vibration amplitude of the dynamic system only decreases when voltage phase exists within the specific range. The stable phase range for 0°-0° PLA-CCF and 0°-90° PLA-CCF spans from 290° to 50° (comprising both intervals 290° to 360° and 0° to 50°) and 350° to 100° (encompassing both intervals 350° to 360° and 0° to 100°), respectively, as illustrated in Figs. 22 (a) and 22 (b).

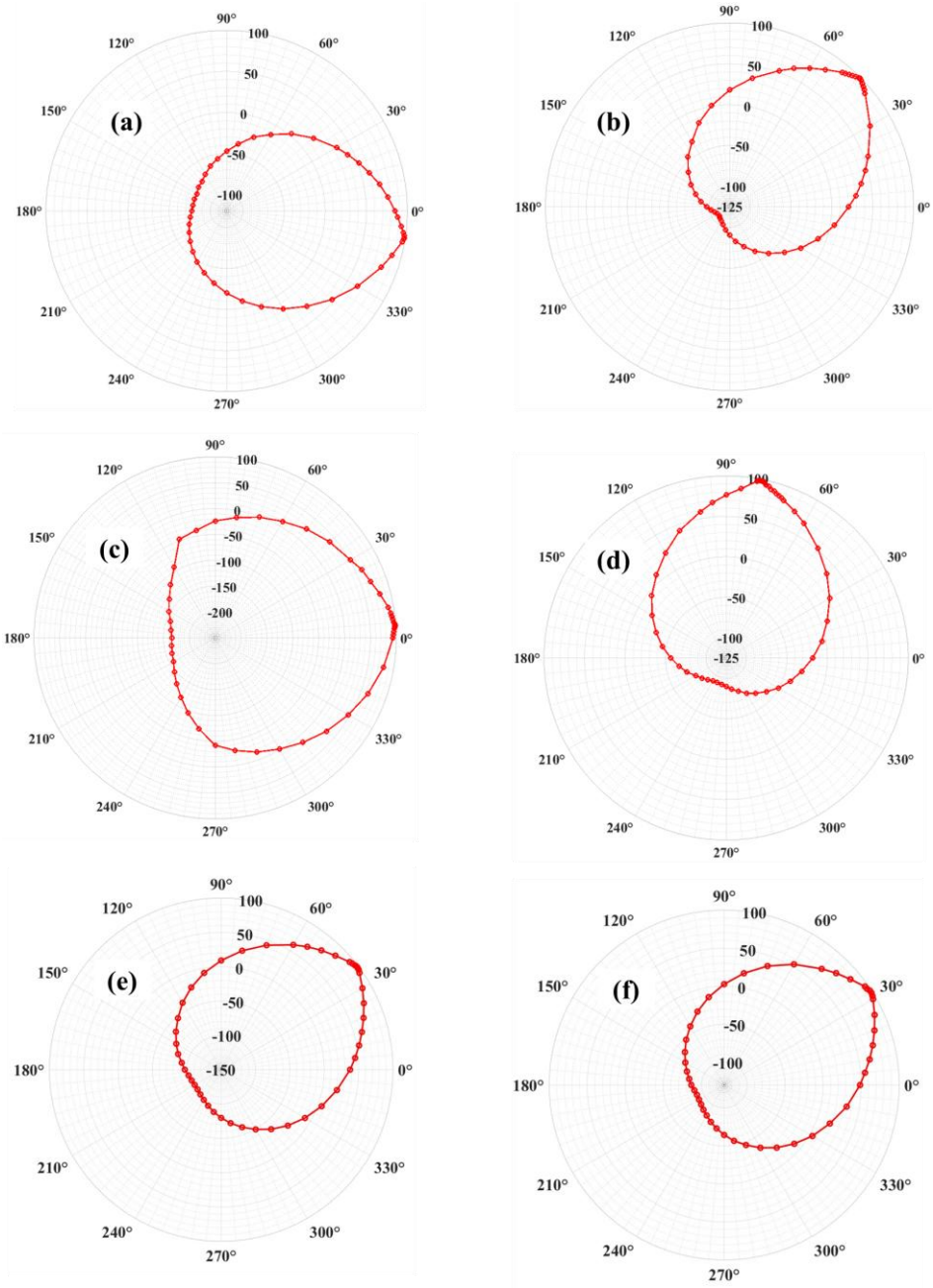

Fig. 22. Influence of phase change on the vibration amplitude: a) 0°-0° PLA-CCF; b) 0°-90° PLA-CCF; c) 0°-0° PLA-CGF; d) 0°-90° PLA-CGF; e) 0°-90° PLA; f) 0°-90° PLA-SCF

Within this stable range, the W_c value remains lower compared to W_u, yielding a positive R value indicative of a decrease in vibration magnitude. For 0°-0° PLA-CGF and 0°-90° PLA-CGF, the stable phase region spans approximately 300° to 70° (encompassing both intervals 300° to 360° and 0° to 70°) and 15° to 135°, respectively, as depicted in Figs. 22 (c) and 22 (d).

For 0°-0° PLA and 0°-0° PLA-SCF, the stable phase ranges approximately from 330° to 90° and from 310° to 70°, respectively (reported in article [A1]). In the case of 0°-90° PLA and 0°-90° PLA-SCF, the stable phase spans approximately from 335° to 95° and from 330° to 90°, respectively, as presented in Figs. 22 (e) and 22 (f).

These optimisations (optimal phase with control voltage) resulted in amplitude reduction of more than 120 times,80 times,90 times and 75 times for 0°-0° PLA-CCF, 0°-90° PLA-CCF, 0°-0° PLA-CGF and 0°-90° PLA-CGF respectively, as presented in Figs. 23 – 26. Similarly, reductions of more than 80, 70, 110, and 95 times were observed for 0°-0° PLA, 0°-90° PLA, 0°-0° PLA-SCF, and 0°-90° PLA-SCF, respectively. Fig. 27 and Fig. 28, illustrate the results for 0°-90° PLA and 0°-90° PLA-SCF, while the results for 0°-0° PLA and 0°-0° PLA-SCF are shown in Fig. 7 and Fig. 8. A summary of the vibration suppression analysis for the beam structures is provided in Table 6.

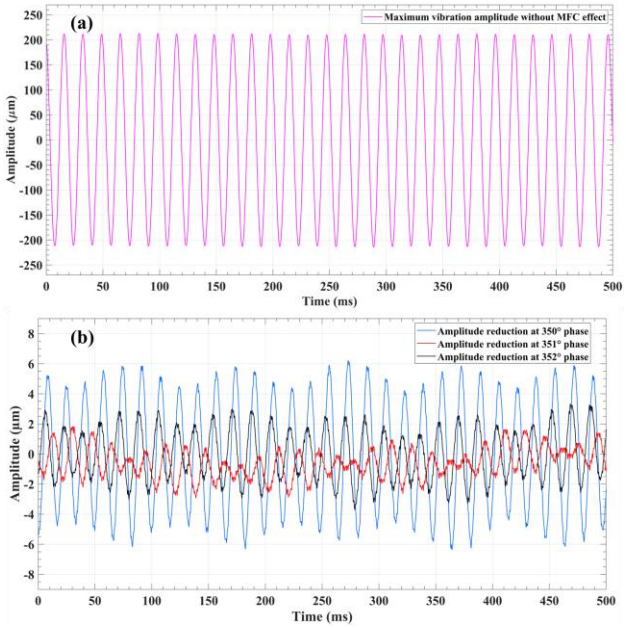

Fig. 23. Vibration amplitude behaviour in composite structure comprising 0°-0° PLA-CCF: a) uncontrolled vibration amplitude; b) controlled vibration amplitude at 350°, 351° and 352°

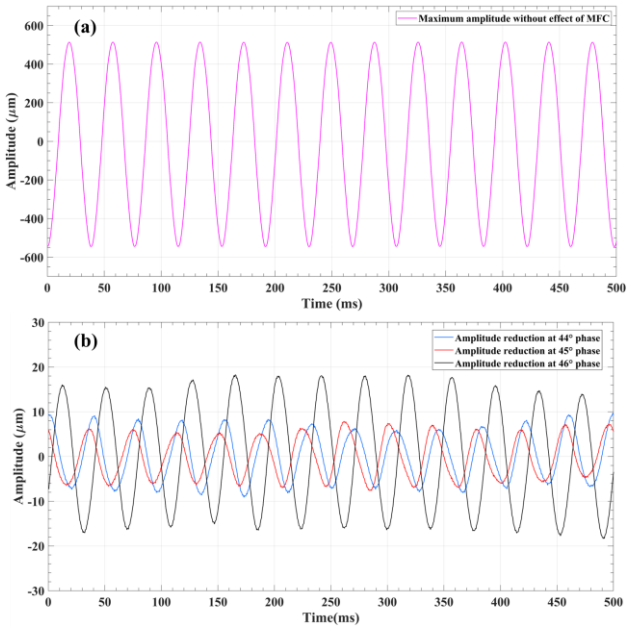

Fig. 24. Vibration amplitude behaviour in composite structure comprising 0°-90° PLA-CCF: a) uncontrolled vibration amplitude; b) controlled vibration amplitude at 44°, 45° and 46°

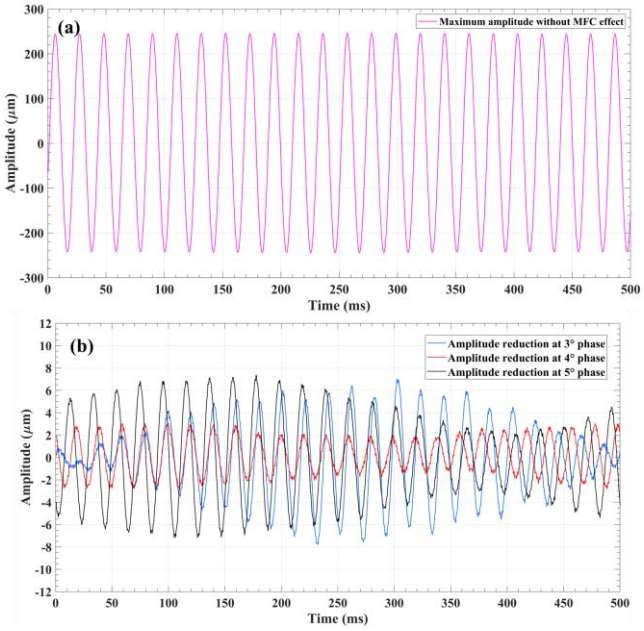

Fig. 25. Vibration amplitude behaviour in composite structure comprising 0°-0° PLA-CGF: a) uncontrolled vibration amplitude; b) controlled vibration amplitude at 3°, 4° and 5°

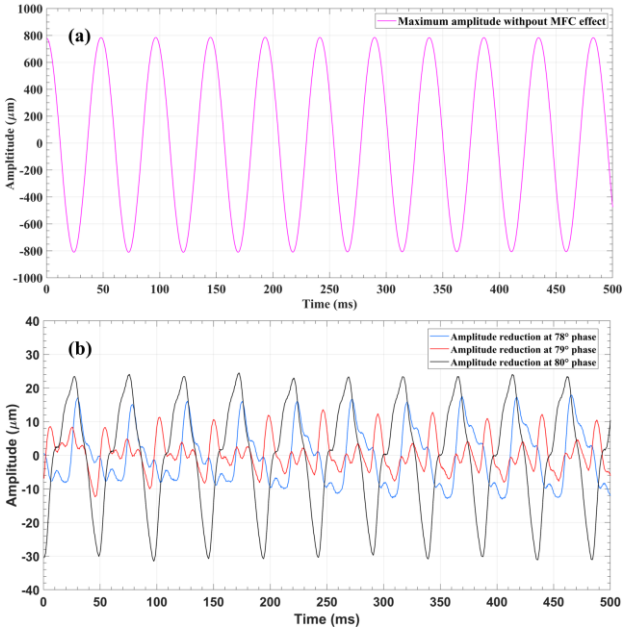

Fig. 26. Vibration amplitude behaviour in composite structure comprising 0°-90° PLA-CGF: a) uncontrolled vibration amplitude; b) controlled vibration amplitude at 78°, 79° and 80°

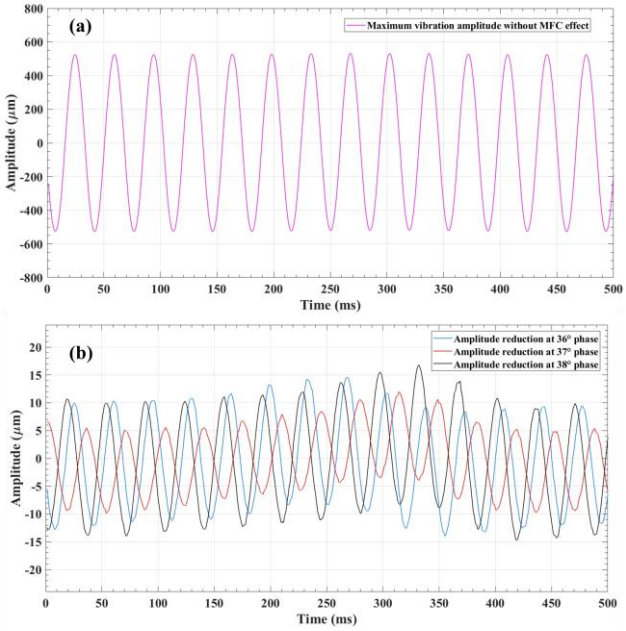

Fig. 27. Vibration amplitude behaviour in 0°-90° PLA: a) uncontrolled vibration amplitude; b) controlled vibration amplitude at 36°, 37° and 38°

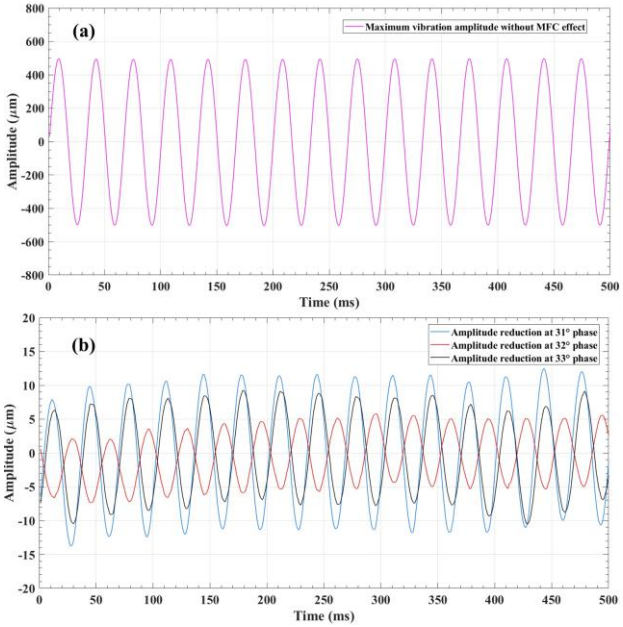

Fig. 28. Vibration amplitude behaviour in 0°-90° PLA-SCF: a) uncontrolled vibration amplitude; b) controlled vibration amplitude at 31°, 32° and 33°

Table 6. Vibration suppression analysis in composite structures

Beam structures	**A_1= Uncontrolled peak-to-peak amplitude (μm)**	**Voltage and phase for maximum suppression**	**A_2= Controlled peak-to-peak amplitude (μm)**	**Reduction factor= A_1 / A_2**
0°-0° PLA	+400 to -400	22.4 V with 29° phase	+5.5 to -4.5	> 80 times
0°-90° PLA	+526 to -525	30.1 V with 37° phase	+7.8 to -6.4	> 70 times
0°-0° PLA-SCF	+370 to - 370	13.92 V with 10° phase	+3.2 to -2.9	> 110 times
0°-90° PLA-SCF	+492 to -503	27 V with 32° phase	+4.5 to -5.8	> 95 times
0°-0° PLA-CCF	+210 to -212	10.52 V with 351° phase	+1.7 to -1.7	> 120 times
0°-90° PLA-CCF	+514 to -545	29.4 V with 45° phase	+6.15 to -6.4	> 80 times
0°-0° PLA-CGF	+244 to -242	17.68 V with 4° phase	+2.9 to -2.4	> 90 times
0°-90° PLA-CGF	+785 to -810	43 V with 79° phase	+8.5 to -12.2	> 75 times

The results indicated that beam structures with 0°-0° layer orientations demonstrated higher vibration reduction with lower control voltage compared to their corresponding 0°-90° structures.

3.4. Article [A4]: Dynamic analysis and vibration control of additively manufactured thin-walled polylactic acid polymer (PLAP) and PLAP composite beam structures: numerical investigation and experimental validation [59]

This sub-section refers to a scientific article published in 'Materials' (MDPI, 2024, Vol. 17). It addresses the fourth objective of the dissertation.

This numerical study aims to validate the previously published experimental investigations [57]. Prior research extensively explored the dynamic characteristics of kinematically excited AM beam structures, including modal characterization, frequency-dependent amplitude spectra, and vibration control influenced by MFC (M8507-P2). The beam structures were fabricated using polylactic acid polymer (PLAP), short carbon fiber reinforced in PLAP (PLAP-SCF), and continuous carbon fiber reinforced in PLAP (PLAP-CCF) with 0°-0° layer orientations, and their fabrication process has been thoroughly discussed in a published experimental work [57].

In this numerical simulation study, the 0°-0° oriented PLAP, PLAP-SCF and PLAP-CCF beam structures were modeled to investigate the dynamic characteristics such as modal characterisation assessment and frequency response analysis (FRA), with the aim of vibration suppression in beam structures integrated with MFCs by implementing OLAVC. The numerical results were thoroughly compared and validated with the previously published experimental results [57].

Additionally, similar investigations were comprehensively conducted on other beam structures, such as 0°-0° PLAP-CGF, 0°-90° PLAP, 0°-90° PLAP-SCF, 0°-90° PLAP-CCF, and 0°-90° PLAP-CGF. However, these structures have not been examined and discussed in the article [59]. It is crucial to include a comparative analysis of the 0°-0° and 0°-90° configurations to evaluate their dynamic characteristics and vibration suppression. Therefore, these additional structures are examined and discussed in this sub-section.

The finite element modeling (FEM) of laminated beam structures (length: 110 mm; width: 20 mm; thickness: 1.35 mm) with MFC patches was performed in the Abaqus CAE 2024 software. The overall effective dimensions of both numerical models and AM beam structures were considered similar. However, the actual length of the AM beam was 120 mm, as a 10 mm portion of the beam was placed in the support to firmly fix the beam on one side. Thus, the effective length of AM beams during the experiments was 110 mm.

Firstly, the PLAP and PLAP-SCF laminated beams with [0°-0°] layer sequences were individually modeled as continuum solid shells (CSS8). The layup-ply approach was adopted to describe the layer arrangement, as presented in Fig. 29 (a). A similar approach was used for beam structures with [0°-90°] layer sequences. Conversely, the PLAP-CCF and PLAP-CGF beam composites with [0°-0°] fiber layer sequences, with an ~18% volume fraction of fibers (consistent with real AM beam structures), were modeled as continuum solid shells (CSS8), as illustrated in Fig. 29 (b). Furthermore, the same approach was used for PLAP-CCF and PLAP-CGF beam composites with

[0°-90°] fiber layer sequences, which had a ~17% volume fraction of fibers, as illustrated in Fig. 29 (c).

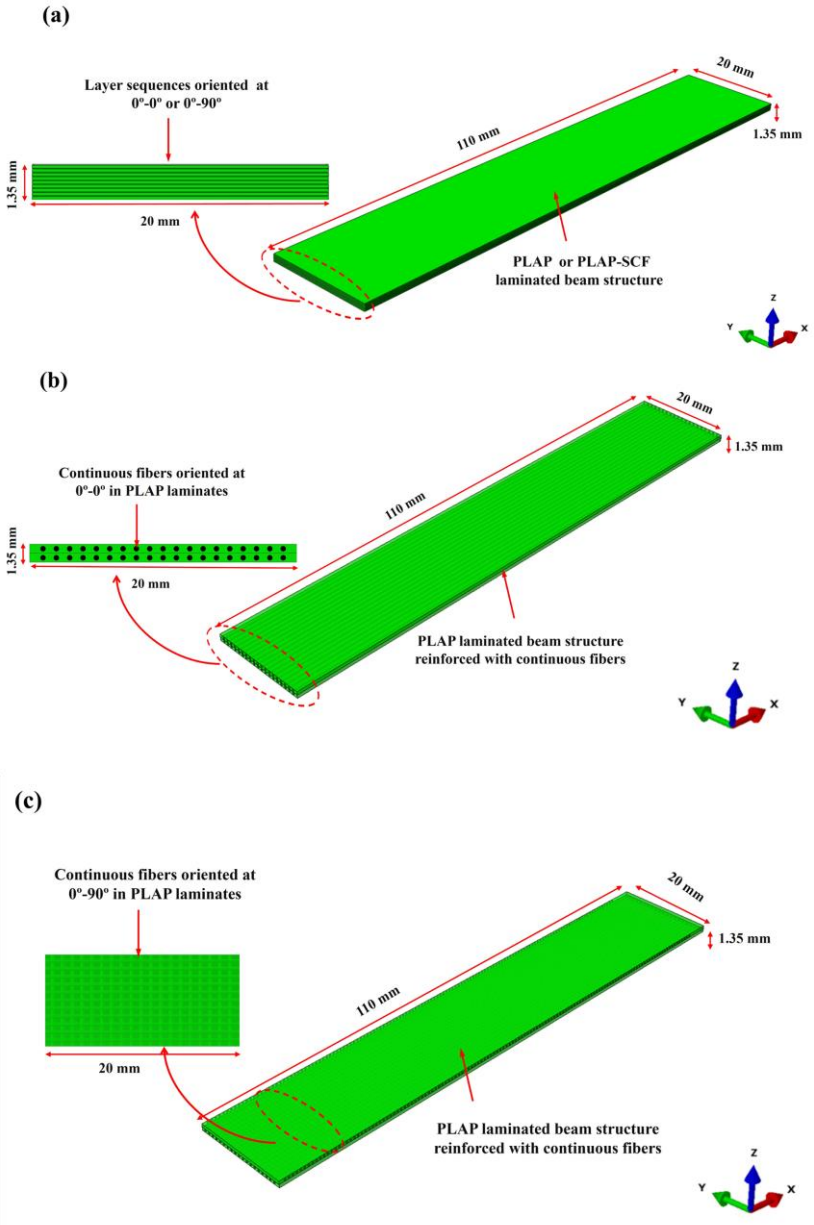

Fig. 29. FEM of laminated beam structures: a) PLAP and PLAP-SCF oriented at 0º-0º or 0º-90º; b) PLAP-CCF and PLAP-CGF oriented at 0º-0º; c) PLAP-CCF and PLAP-CGF oriented at 0º-90º

Subsequently, the FEM of integrated MFC (M8507-P2) was performed using piezoelectric solid elements (C3D20RE). The active part of the MFC (length: 85 mm; width: 7 mm; thickness: 0.3 mm) was simplified as a homogeneous material rather than an intricate design. The active portion of the MFC was affixed to each beam structure, 15 mm from the fixed end. The Tie constraint was implemented to ensure interaction between the surfaces of the beam and the MFC. After numerically modeling the geometry, hexahedral (hex) meshing with refinement was performed on the MFC and each beam structure resulting in no additional significant changes in the computed natural frequencies. Further on, mechanical boundary conditions involved fixing one side of the beam, with nodes restricted to displace in the X, Y, and Z direction, as depicted in Fig. 30 (a). On the other hand, a sinusoidal force was employed to kinematically excite the beam. However, due to limitations of the Abaqus, it was not possible to apply the excitation force through the fixed side as it was carried out in the experiments exhibited in Fig. 30 (b). The electrical boundary conditions, such as a sinusoidal signal (U_{MFC}), were applied from the upper side of the MFC, while the bottom side was grounded (0 V).

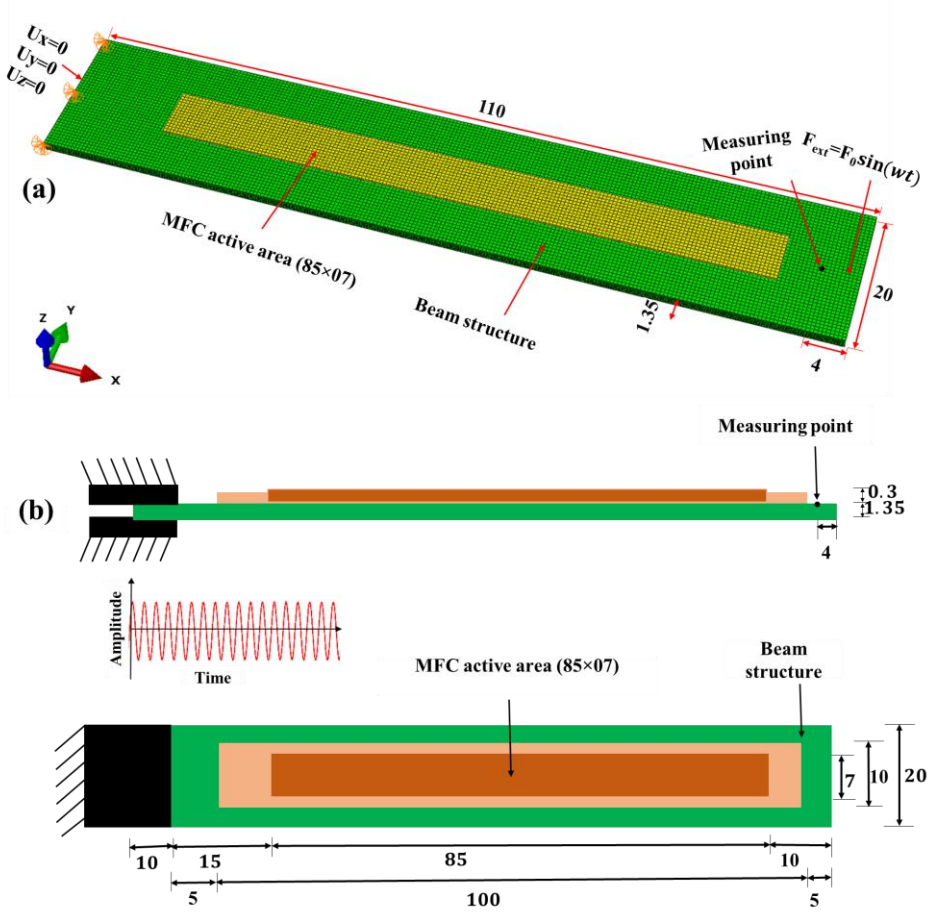

Fig. 30. Beam structures integrated with MFC illustrating boundary conditions : a) FEM model; b) schematic view of experimental sample

The Lanczos methodology has been employed to compute the modal natural frequencies and corresponding mode shapes of beam structures without applying external forces.

FRA finds out the response of the structure subjected to harmonic force over a spectrum of frequencies. The frequency-dependent dynamic response (amplitude spectrum) of each beam was assessed across a frequency spectrum.

Afterwards, vibration suppression in each beam was thoroughly studied and compared with the published experimental data [57] addressing the limitations of the numerical simulation.

The numerical and experimental natural frequencies of the bending modes of 0°-0° oriented beam structures are presented in Table 7, with the percentage error between the values shown in Fig. 31. The first natural frequencies of the 0°-0° oriented numerical models were found to be 30.45 Hz for PLAP, 39.95 Hz for PLAP-SCF, 60.50 Hz for PLAP-CCF and 45.03 Hz for PLAP-CGF. These numerical values closely align with the experimental frequencies of 30.00 Hz, 40.50 Hz, 60.00 Hz and 47.70 Hz respectively, resulting in differences of only 1.50%, 1.35%, 0.83% and 5.59% for PLAP, PLAP-SCF, PLAP-CCF and PLAP-CGF respectively. The second, third and fourth natural frequencies of the numerical models deviate within 10% of the experimental values.

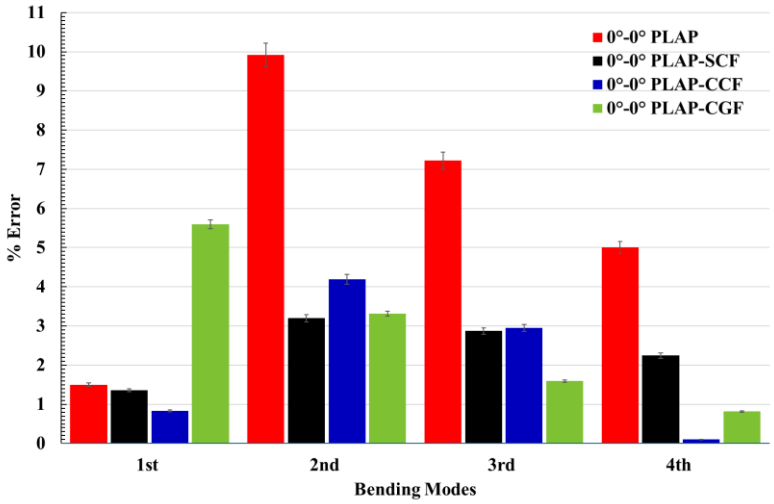

Fig. 31. Percentage error in experimental and numerical bending mode frequencies for 0°-0° beam structures

The numerical and experimental natural frequencies of the bending modes of 0°-90° oriented beam structures are presented in Table 8, and the percentage error between the values is shown in Fig. 32. For the 0°-90° oriented numerical models, the first natural frequencies are 28.63 Hz for PLAP, 29.47 Hz for PLAP-SCF, 27.89 Hz for PLAP-CCF, and 22.27 Hz for PLAP-CGF, closely aligning with the experimental values of 27.50 Hz, 28.80 Hz, 26.60 Hz, and 21.30 Hz, respectively. These correspond

to differences of 4.10%, 2.32%, 4.84%, and 4.55%, respectively. The second, third, and fourth natural frequencies of the numerical models deviate by approximately up to 16% from the experimental values.

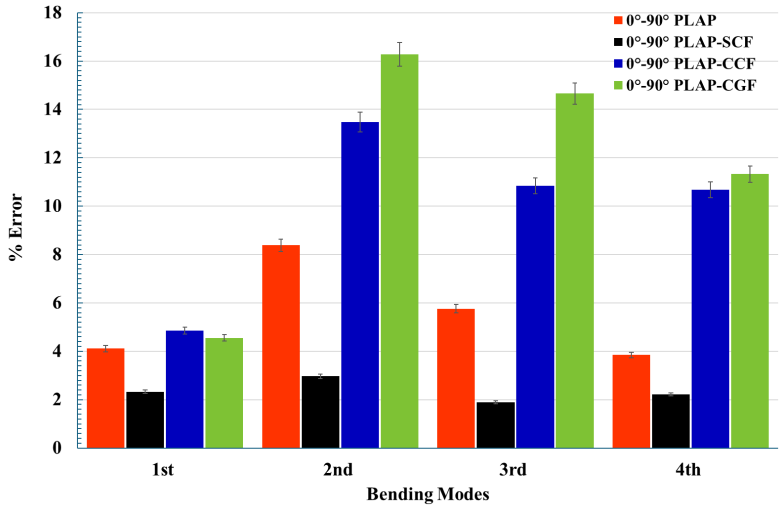

Fig. 32. Percentage error in experimental and numerical bending mode frequencies for 0°-90° beam structures

Several factors could contribute to discrepancies between the modal frequencies of the FEM and actual AM beam models. Firstly, the geometry of the AM beam could differ slightly from the idealised numerical model used in Abaqus. This difference might be due to internal irregularities such as defects that are not perfectly considered in the numerical model. Secondly, defining boundary conditions in the numerical model with simple assumptions could lead to inconsistencies with experimental results. For instance, in the numerical simulation, the beam structure is firmly fixed at one end, while in real condition (experiments) there is a possibility that the beam was not firmly fixed leading to a lack of consistency with the numerical model.

The frequency-dependent dynamic response of the actual AM beam structures was measured by fixing one side of each beam structure in a fixture and applying a 100 V excitation signal to the MFC patch. The amplitude spectrum of each beam structure, illustrating the variation in vibration amplitudes with changing frequencies, was measured by a 3D laser vibrometer (PSV-W-500) manufactured by 'Polytec GmbH, Germany'. Notably, the amplitude spectrum revealed (Fig. 33 and Fig. 34) that vibration amplitudes peaked at the first natural frequencies of the bending mode and decreased towards the fourth natural frequencies in both numerical and experimental scenarios. Although there was a considerable difference in the absolute values of vibration amplitudes between numerical and experimental data, a consistent trend of amplitude variation over the frequencies was observed in both sets of results.

Table 7. Natural frequencies of 0°-0°-oriented beam structures with MFC: experiments and numerical simulation results

Bending Modes	0°-0° PLAP		0°-0° PLAP-SCF		0°-0° PLAP-CCF		0°-0° PLAP-CGF	
	Experiment	Numerical	Experiment	Numerical	Experiment	Numerical	Experiment	Numerical
	Hz							
1st	30.00	30.45	40.50	39.95	60.00	60.50	47.70	45.03
2nd	215.00	236.33	280.50	289.47	410.00	392.83	315.60	305.15
3rd	626.50	671.73	802.00	825.02	1153.00	1119.00	895.30	881.02
4th	1207.50	1268.00	1546.00	1580.70	2192.00	2189.70	1707.00	1720.90

Table 8. Natural frequencies of 0°-90°-oriented beam structures with MFC: experiments and numerical simulation results

Bending Modes	0°-90° PLAP		0°-90° PLAP-SCF		0°-90° PLAP-CCF		0°-90° PLAP-CGF	
	Experiment	Numerical	Experiment	Numerical	Experiment	Numerical	Experiment	Numerical
	Hz							
1st	27.50	28.63	28.80	29.47	26.60	27.89	21.30	22.27
2nd	207.50	224.89	221.30	227.86	203.00	230.37	165.00	191.87
3rd	603.80	638.55	635.00	647.00	592.00	656.15	480.00	550.38
4th	1157.50	1202.00	1193.80	1220.30	1114.00	1233.00	918.00	1022.00

Despite the discrepancy in the vibration amplitude values between the two datasets, there was consistency in the overall behaviour of vibration amplitudes as frequency varied.

For the 0°-0° oriented numerical results, the vibration amplitudes at the first natural frequency were observed to be the highest as follow: 7.0870 μm at 30.45 Hz for PLAP, 3.9240 μm at 40.00 Hz for PLAP-SCF, 1.8980 μm at 60.5 Hz for PLAP-CCF and 3.1702 μm at 45.03 Hz for PLAP-CGF. The corresponding experimental vibration amplitudes at the first natural frequency were determined: 9.295 μm at 30 Hz for PLAP, 6.831 μm at 40.5 Hz for PLAP-SCF, 4.139 μm at 60.0 Hz for PLAP-CCF and 4.400 μm at 47.7 Hz for PLAP-CGF.

In the 0°-90° oriented numerical results, the highest vibration amplitudes at the first natural frequency were detected as follow: 7.9860 μm at 28.63 Hz for PLAP, 7.1110 μm at 29.47 Hz for PLAP-SCF, 8.0267 μm at 27.89 Hz for PLAP-CCF and 12.2230 μm at 22.27 Hz for PLAP-CGF. The corresponding experimental vibration amplitudes at the first natural frequency were determined: 10.9240 μm at 27.5 Hz for PLAP, 9.7330 μm at 28.8 Hz for PLAP-SCF, 10.1100 μm at 26.6 Hz for PLAP-CCF and 9.2600 μm at 21.3 Hz for PLAP-CGF.

For both numerical and experimental scenarios, the fourth natural frequencies exhibited the lowest vibration amplitudes, and the results followed the same trend, as presented in Fig. 33 and Fig. 34.

Overall, the numerical approach captures the dynamic behaviour of each AM beam structure effectively, as evidenced by the consistency between numerical and experimental results. However, the observed differences in absolute amplitude values may be attributed to the limitations in boundary conditions: in experimental case, the excitation force was provided by the MFC patch, while in numerical case, the force was provided at the free-end side of each beam structure.

Ultimately, the analysis of vibration amplitude suppression was thoroughly performed on numerically modeled beam structures, with the results compared and validated against experimental data. The numerical models of PLAP, PLAP-SCF, PLAP-CCF and PLAP-CGF with 0°-0° and the 0°-90° orientations were externally excited at their respective first resonant frequencies.

The 0°-0° oriented numerical models reveal uncontrolled vibration amplitudes of +435 μm to -408 μm, ±395 μm, +220 μm to -224 μm and +252 μm to -251 μm, respectively. In the experimental case, uncontrolled vibration amplitudes were, ±400 μm, ±370 μm, ±210 μm and +242 μm to -240 μm, respectively. These uncontrolled amplitudes are depicted in Figs. 35(a) to 35(d).

For 0°-90° oriented numerical models, uncontrolled vibration amplitudes were found as +548 μm to -540 μm, +515 μm to -510 μm, +555 μm to -540 μm and +820 μm to -815 μm, for PLAP, PLAP-SCF, PLAP-CCF and PLAP-CGF respectively. The corresponding experimental uncontrolled amplitudes were +526 μm to -525 μm, +492 μm to -503 μm, +514 μm to -545 μm and +785 μm to -810 μm. Both numerical and uncontrolled amplitudes are depicted in Figs. 36(a) to 36(d).

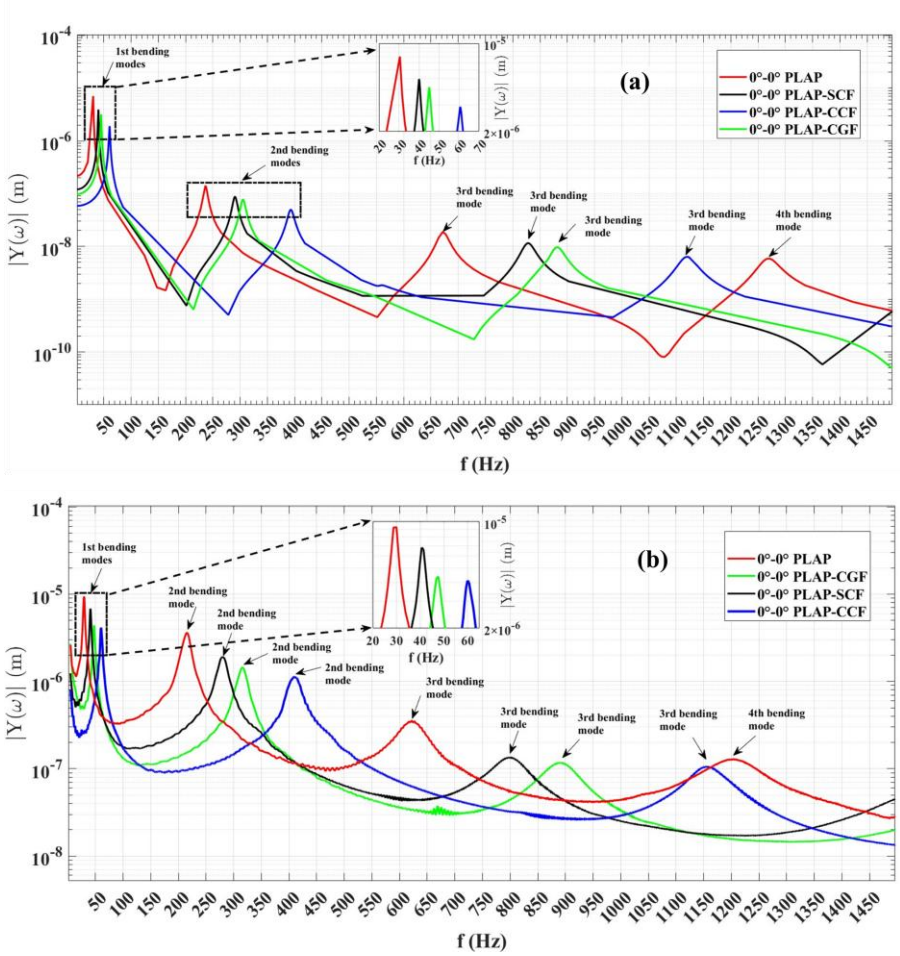

Fig. 33. Frequency-dependent amplitude spectrum of 0°-0° oriented beam structures: a) numerical data; b) experimental data

After applying a counterforce with the MFC, the controlled vibration amplitudes for the 0°-0° oriented numerical models of PLAP, PLAP-SCF, PLAP-CCF and PLAP-CGF were approximately ±19 μm, ±16 μm, and ±13 μm, ±14.3 μm respectively. Experimentally, the controlled vibration amplitudes were observed to be around ±5 μm, ±3 μm, ±1.7 μm and +2.9 μm to -2.4 μm for the respective models. Both numerical and experimental results exhibited the same trend of decreasing amplitude from PLAP to PLAP-SCF, PLAP-CGF and finally to PLAP-CCF, as illustrated in Figs. 35(a) to 35(d).

For the 0°-90° oriented numerical models of PLAP, PLAP-SCF, PLAP-CCF and PLAP-CGF, the controlled vibration amplitudes were about +21.5 μm to -21.7 μm, +19.9 μm to -20.4 μm, +23.3 μm to -21.5 μm and +25.5 μm to -24.7 μm respectively. Experimentally, the controlled vibration amplitudes were found as approximately +7.8 μm to -6.4 μm, +4.5 μm to -5.8 μm, +6.15 μm to -6.4 μm and

+8.5 µm to -12.2 µm for the respective models. Both numerical and experimental results exhibited the same trend of decreasing amplitude from PLAP-CGF to PLAP-CCF, PLAP and ultimately PLAP-SCF, as illustrated in Figs. 36(a) to 36(d).

The overall findings from numerical and experimental analyses reveal that the 0°-0° oriented beam structures exhibited higher vibration suppression compared to the corresponding beam structures with 0°-90° orientations.

The disparity in controlled vibration amplitudes between the numerical and experimental results is influenced by the inherent limitations of the numerical models, which do not fully capture the complexities of real experimental conditions.

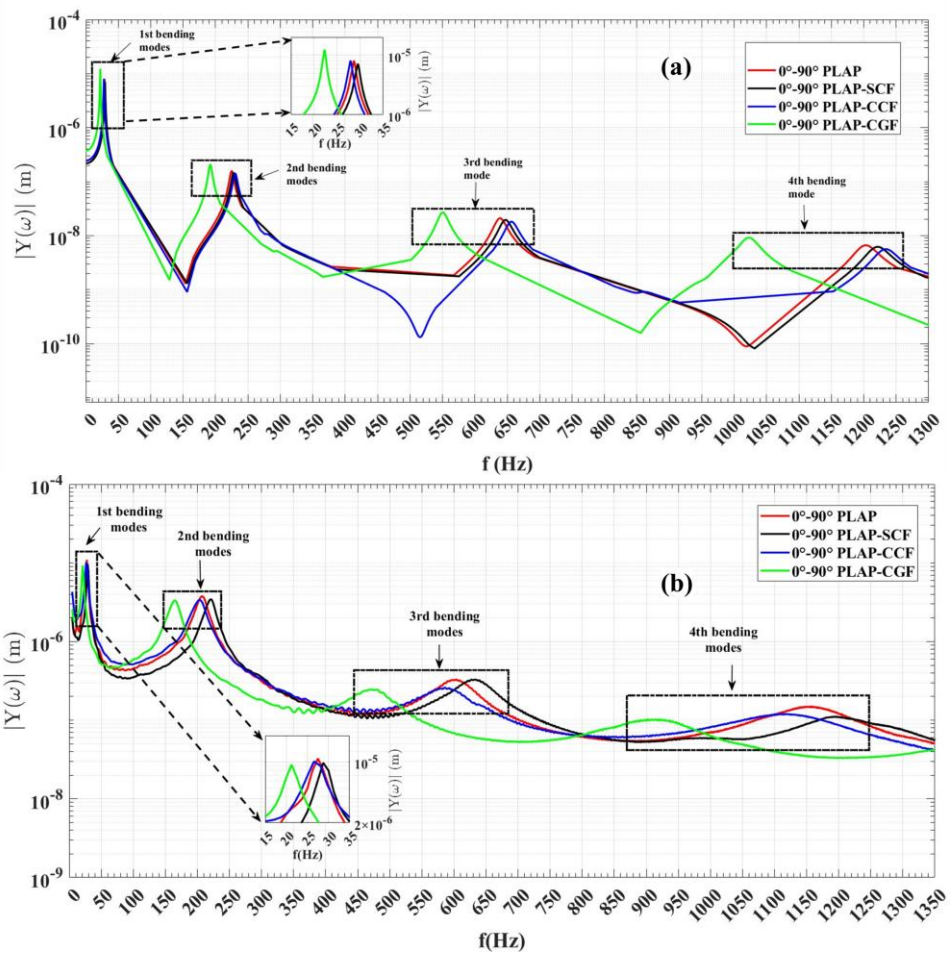

Fig. 34. Frequency-dependent amplitude spectrum of 0°-90° oriented beam structures: a) numerical data; b) experimental data

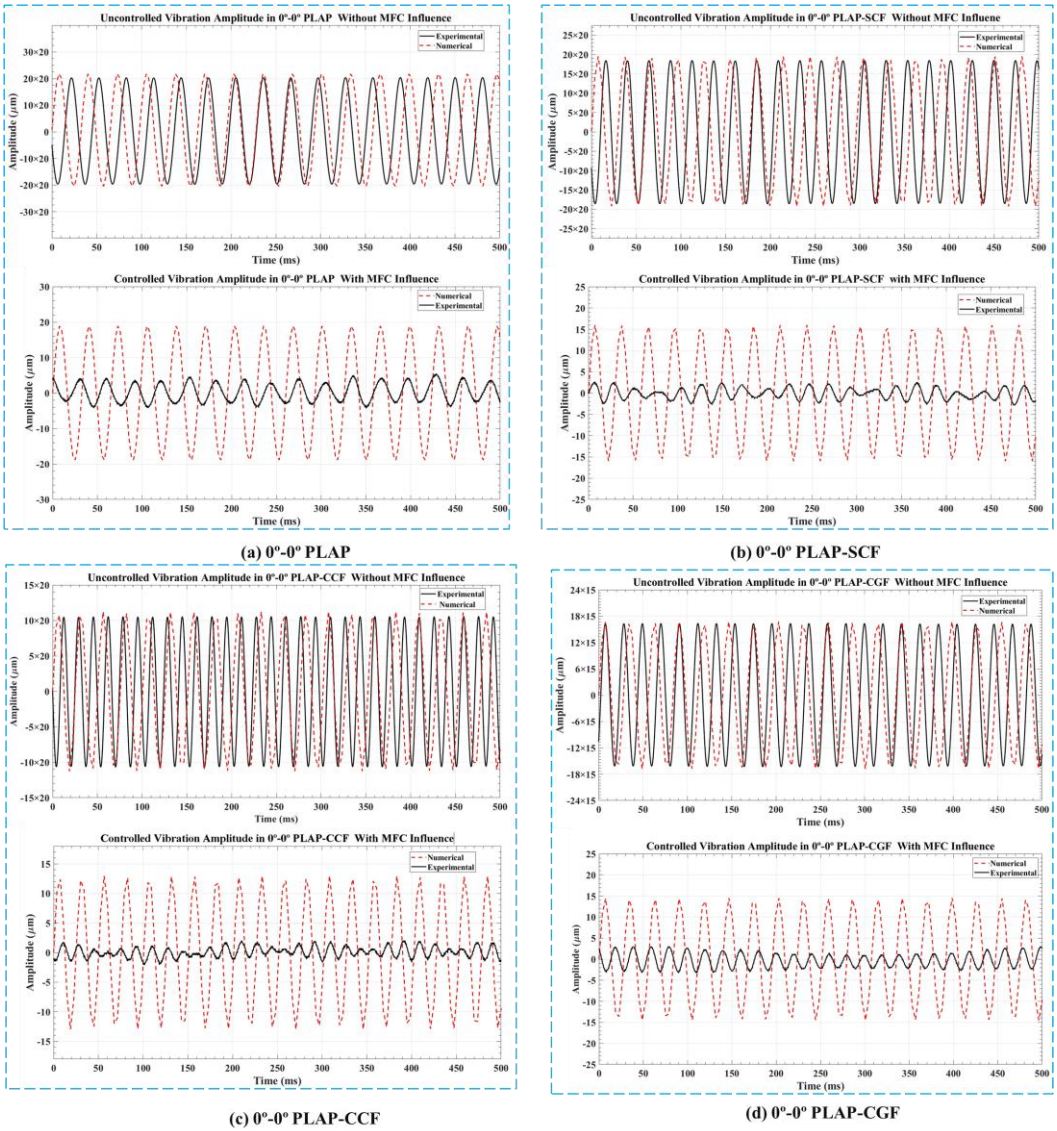

Fig. 35. Uncontrolled and controlled vibration amplitude in 0°-0° oriented beam structures

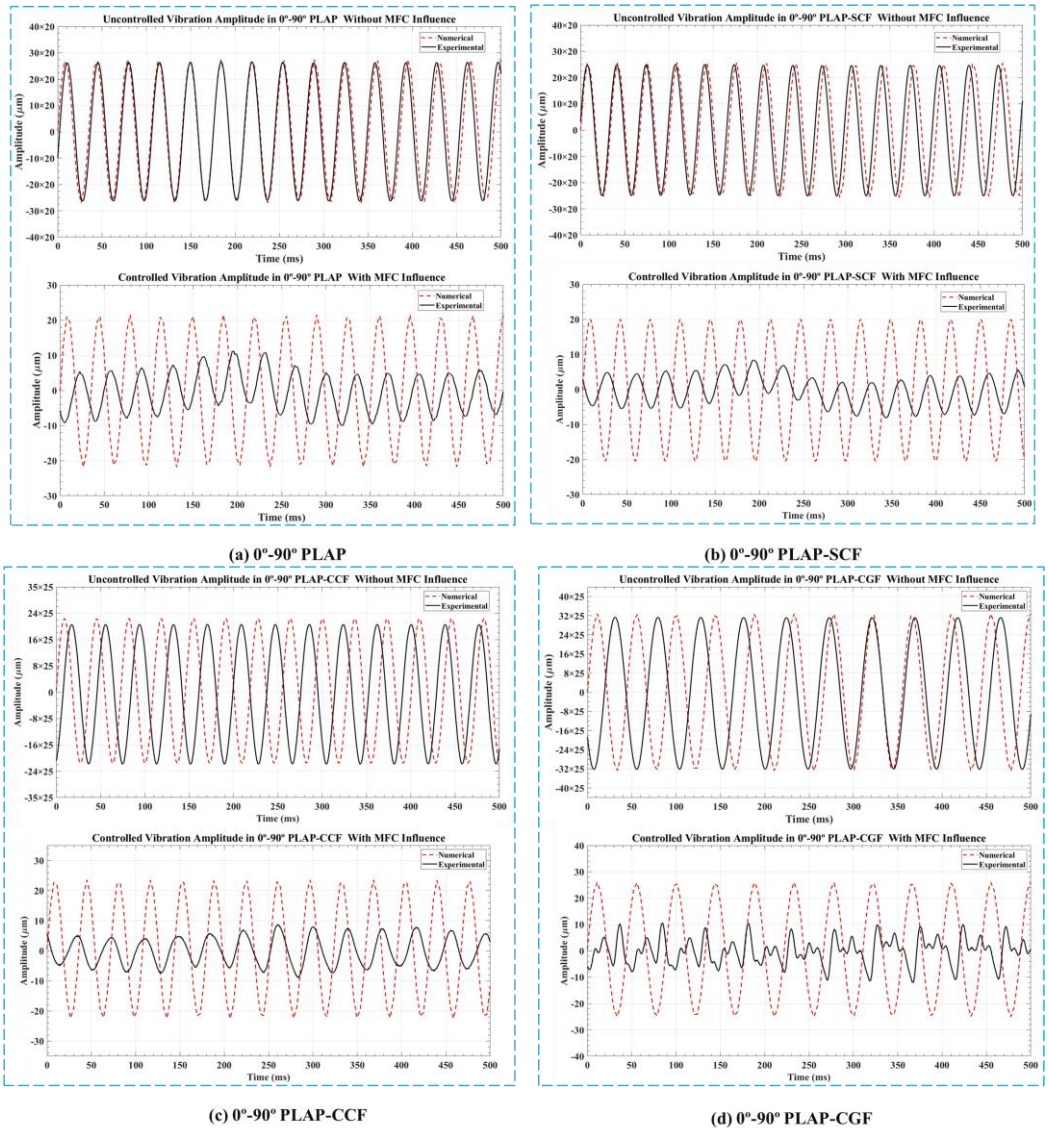

Fig. 36. Uncontrolled and controlled vibration amplitude in 0°-90° oriented beam structures

Numerical simulations typically rely on generalised assumptions and may not properly account for material imperfections such as voids, porosity, or any irregularities present in the actual model. Additionally, environmental factors and intricate damping characteristics resulting from the fixture used to secure one side of the beam during experiments are not fully considered in the numerical simulation.

4. CONCLUSIONS

1. The dynamics characteristics of additive manufactured (AM) structures were carried out and the following key findings were achieved:

- AM structures with a 0°-0° orientation exhibited higher natural bending mode frequencies than those with the corresponding 0°-90° orientation. In 0°-0° case, the layers are aligned in the same direction, which increases stiffness, resulting in higher natural frequencies. In contrast, in the 0°-90° case, the layers are perpendicular to each other, which decreases stiffness and increases flexibility, leading to lower natural frequencies. For the 0°-0° oriented structures, the first natural bending mode frequencies for PLA, PLA-SCF, PLA-CCF, and PLA-CGF were 30.0 Hz, 40.5 Hz, 60.0 Hz, and 47.7 Hz, respectively. In comparison, the corresponding values for the 0°-90° oriented structures were 27.5 Hz, 28.8 Hz, 26.6 Hz, and 21.3 Hz.
- Decrement coefficient values for AM structures with a 0°-0° orientation were higher than those with corresponding 0°-90°, indicating greater damping. For the 0°-0° orientation, the coefficient values for PLA, PLA-SCF, PLA-CCF, and PLA-CGF were 0.043, 0.081, 0.214, and 0.063, respectively, with PLA-CCF exhibiting the highest damping and PLA the lowest. In the 0°-90°, the corresponding coefficient values were 0.041, 0.052, 0.040, and 0.038, respectively, with PLA-SCF exhibiting the maximum damping effect, while PLA-CGF had the lowest.

2. Vibration suppression was thoroughly compared and examined in kinematically excited AM structures made of PLA, PLA-SCF, PLA-CCF, and PLA-CGF, with 0°-0° and 0°-90° orientations using MFC (M8507-P2) actuators. The following key findings were obtained:

- The MFC actuator was found to be more efficient in containing the vibration amplitude of stiffer AM structures. Vibration suppression was higher in the 0°-0° oriented structures compared to the corresponding 0°-90° structures. For the 0°-0° orientation, significant vibration reductions of over 80 times for PLA, 110 times for PLA-SCF, 120 times for PLA-CCF, and 90 times for PLA-CGF were observed. In 0°-90° orientation, significant vibration reductions of over 70 times for PLA, 95 times for PLA-SCF, 80 times for PLA-CCF, and 75 times for PLA-CGF were identified.

3. The phases (ranging from 0° to 360°) of a signal provided to the MFC actuators significantly influence the vibration amplitude of kinematically excited AM structures.

- During the fine-tuning of phases for PLA, PLA-SCF, PLA-CCF and PLA-CGF with 0°-0° and 0°-90° orientations, specific phase ranges were noticed where the uncontrolled vibration amplitude decreased, while outside these ranges, amplitude increased. In the 0°–0° orientation, the MFC actuator covers a wider phase interval of up to 130° for vibration amplitude reduction, while in the 0°–90° orientation, the MFC covers a phase interval of up to 120°. For 0°-0° oriented structures, the specific phase ranges were 330° to 90° for PLA, 310° to 70° for PLA-SCF, 290° to 50° for PLA-CCF, and 300° to 70° for PLA-CGF. The phases

yielding maximum vibration reduction were 29° for PLA, 10° for PLA-SCF, 351° for PLA-CCF and 4° for PLA-CCG. In 0°-90°, the specific phase ranges were 335° to 95° for PLA, 330° to 90° for PLA-SCF, 350° to 100° for PLA-CCF, and 15° to 135° for PLA-CGF with maximum reduction observed at 37° for PLA, 32° for PLA-SCF, 45° for PLA-CCF and 79° for PLA-CCG.

4. Numerical models of PLA, PLA-SCF, PLA-CCF and PLA-CGF AM structures with 0°-0° and 0°-90° layer orientations were created using Abaqus 2024 software. Simulations were performed to investigate their dynamic characteristics and vibration suppression using MFC actuators, comparing the results with experimental data.

– The developed numerical approach captures the dynamic characteristics of actual AM structures effectively, demonstrating a close alignment with experimental data. In the modal analysis, the first natural bending mode frequencies of the 0°-0° and 0°-90° oriented numerical models closely aligned with the experimental values, with differences of only approximately 5%. The higher natural bending mode frequencies (second, third, and fourth) deviated by approximately 10% and 16% from the experimental values for the 0°-0° and 0°-90° oriented structures, respectively.
– In vibration control analysis, the controlled peak-to-peak vibration amplitudes for 0°-0° numerical models including PLA, PLA-SCF, PLA-CCF and PLA-CGF were approximately ±19 μm, ±16 μm, and ±13 μm, ±14.3 μm respectively, while the corresponding experimental values were around ±5 μm, ±3 μm, ±1.7 μm and +2.9 μm to -2.4 μm, respectively. Both numerical and experimental results exhibited the same trend of decreasing vibration amplitude from PLA to PLA-SCF, PLA-CGF and finally to PLA-CCF. In 0°-90° numerical models, the controlled vibration amplitudes were approximately +21.5 μm to -21.7 μm for PLA, +19.9 μm to -20.4 μm for PLA-SCF, +23.3 μm to -21.5 μm for PLA-CCF and +25.5 μm to -24.7 μm for PLA-CGF, while experimental values ranged from +7.8 μm to -6.4 μm, +4.5 μm to -5.8 μm, +6.15 μm to -6.4 μm and +8.5 μm to -12.2 μm respectively. Both sets exhibited the same trend of decreasing amplitude from PLA-CGF to PLA-CCF, PLA and ultimately PLA-SCF.

5. SANTRAUKA

Struktūros pradeda vibruoti veikiamos tokių dinaminių apkrovų kaip išorinė aplinka, įrenginių virpesiai, triukšmas ir žmonių veikla, todėl virpesių valdymas konstrukcinėje dinamikoje yra viena iš aktualiausių bendruomenės mokslinių tyrimų problemų [1]. Šie virpesiai gali labai pakenkti struktūros vientisumui, sukelti ankstyvą susidėvėjimą ir galiausiai suirimą. Todėl, siekiant sumažinti struktūros suirimo riziką, būtina šiuos virpesius sušvelninti arba juos išlaikyti tarp tam tikrų ribų [2,3]. Paminėtina, kad plonasienės kompozitinės pluoštų struktūros turi nemažai inžinerinių pritaikymų. Plonasienių pluoštų geometriją atspindi tokios struktūros kaip sraigtasparnių mentės, lėktuvų mentės, robotų rankos [4] ir sparnų turbinų mentės. Tačiau su tokiomis struktūromis susijęs virpesys yra sudėtinga problema, kurią reikia sumažinti arba pašalinti [5]. Pastaruoju metu struktūros gaminamos naudojant įvairių rūšių kompozitines medžiagas, kad būtų pasiektas didelis savitasis standumas ir savitasis stipris. Kita vertus, dėl lanksčių kompozitinių struktūrų savybių, virpesių slopinimas tapo itin svarbiu sistemos eksploatavimo savybių veiksniu [6,7].

Siekiant padidinti sistemos vientisumą, pastaruoju metu įdiegtos kelios virpesių slopinimo technologijos, įskaitant aktyvųjį valdymą (kuris apima tiek atvirojo, tiek uždarojo ciklo metodus), taip pat pusiau aktyvius, pasyvius ir hibridinius valdymo metodus. Pasyvioji valdymo schema apima įvairias slopinimo medžiagas ar įtaisus (pavyzdžiui, masę, spyruoklę ir amortizatorių), kurie sukuria valdymo priešpriešinę jėgą reaguodami į išorinius trikdžius ir kuriems veikti nereikia jokio išorinio elektros šaltinio. Tačiau kitoms schemoms veikti paprastai reikalingi aktyvatoriai, jutikliai ir valdikliai. Jie gali suteikti sistemai valdymo priešpriešines jėgas, remdamiesi realaus laiko duomenimis, tačiau šiems įtaisams įjungti reikia išorinių elektros šaltinių [8]. Svarbu paminėti, kad aktyvaus valdymo schemos vis dažniau naudojamos daugelyje inžinerijos sričių, nes rinkoje lengvai gaunamos įvairios pažangios medžiagos, ypač pjezoelektrinės [9,10]. Pjezoelektrinės medžiagos dažnai naudojamos energijai sukaupti [11], struktūriniam vientisumui stebėti [12] taip pat virpesių slopinimo programoms [13] dėl veiksmingų elektromechaninių savybių, didelės blokavimo jėgos, puikaus standumo ir greito atsako [14]. Pjezoelektrinės medžiagos, pavyzdžiui, švino cirkonio titanatas (PZT), dėl puikaus standumo ir gebėjimo generuoti didelę suveikimo jėgą, paprastai naudojamos daugelyje pramonės sričių. Be to, jos gali būti naudojamos kaip jutikliai ir vykdikliai, atitinkamai dėl tiesioginio ir atvirkštinio pjezoelektrinio efekto. Tačiau jos turi tam tikrų apribojimų, pavyzdžiui, yra trapios, nepakankamai lanksčios ir ribotai prisitaiko prie lenktų paviršių, o tai turi neigiamą įtaką pjezoelektrinių medžiagų stabilumui ir efektyvumui [2]. Polivinilidenfluoridas yra alternatyvi pjezoelektrinė medžiaga, santykinai lankstesnė nei PZT, tačiau sukuria mažesnę veikimo jėgą.

Šie apribojimai paskatino mokslininkus ieškoti alternatyvių pažangių pjezoelektrinių medžiagų. Siekiant išspręsti pjezoelektrinių medžiagų apribojimus praktiniam pritaikymui, atlikta daug tyrimų, susijusių su pjezokeraminių pluoštų įterpimu į polimerinę matricą [15,16]. NASA 1999 m. išrado makropluoštinius kompozitus (MFC), kad išspręstų anksčiau minėtus apribojimus. Stačiakampiai pjezokeraminiai pluoštai buvo įkomponuoti į polimerinę matricą ir įterpti tarp

apsauginio ir elektrodinio sluoksnių [12,13,17–19]. 2002 m. „Smart Material“ pradėjo komercializuoti šį išradimą kaip NASA licencijuotasis gamintojas ir tiekėjas [20].

Šiame tyrime MFC elementai buvo panaudoti kaip vykdikliai virpesių amplitudėms slopinti adityviai pagamintose PLA ir PLA pagrindu sukurtose kompozitinėse struktūrose, įskaitant PLA-SCF, PLA-CCF ir PLA-CGF.

Sudėtingų struktūrų su įmantria geometrija kūrimas buvo modifikuotas 3D spausdinimu, kuris dar vadinamas adityviąja gamybos technologija [21]. Palyginti su tradicinėmis subtraktyviosios gamybos technologijomis, adityviosios gamybos technologijomis komponentai kuriami sluoksnis po sluoksnio pridedant medžiagą, kurios dalis gali būti išlydyta arba sukietinta. Pagrindiniai jų pranašumai – galimybė gaminti sudėtingos geometrijos komponentus ir sumažinti medžiagų atliekų kiekį. Lydžios masės formavimas (FDM) yra viena iš adityviosios gamybos technologijų, sulaukusi didelio pramonės ir akademinio sektoriaus dėmesio [22,23]. 3D spausdintuvai naudodami FDM metodą, gaminius gamina išpurškdami termoplastinius polimerus ant darbo zonos per antgalį [24]. Ši metodika leidžia projektuoti įvairias konfigūruojamas struktūras, tad ji yra pageidautinas variantas įvairioms inžinerinėms reikmėms [25]. Kalbant apie 3D spausdinamų bandinių mechanines savybes, reikėtų paminėti, kad AM komponentų mechaninėms savybėms įtakos turi ne tik termoplastinė medžiaga, bet ir spausdinimo parametrai, pavyzdžiui, sluoksnių aukštis, sluoksnių orientacija, užpildymo tankis, temperatūra ir spausdinimo greitis [26–28]. Norint maksimaliai padidinti AM struktūrų efektyvumą ir naudingumą, įskaitant virpesius, rezonansą ir dinaminę apkrovą, būtina suprasti šiuos veiksnius [29].

Šiame tyrime pirmą kartą buvo tiriamos AM struktūros, pagamintos iš PLA ir PLA kompozitų, tokių kaip PLA-SCF, PLA-CCF ir PLA-CGF, siekiant ištirti skirtingų sluoksnių orientacijų (0–0 º ir 0–90 º) įtaką jų dinaminėms charakteristikoms ir virpesių slopinimui. Be to, tyrime parodytos sluoksnių orientacijos ir AM struktūrų įtaka virpesių amplitudėms slopinti, siekiant nustatyti optimalų derinį, kuris pasižymi didžiausiu virpesių slopinimu taikant MFC vykdiklį.

5.1. Daktaro disertacijos tikslas

Ištirti kinematiškai sužadintų, adityviuoju būdu pagamintų AM struktūrų dinamines charakteristikas ir sukurti efektyvią virpesių slopinimo metodiką integruojant makropluošto kompozito (MFC) vykdiklius, siekiant sumažinti vibracijų amplitudes. Šiam tikslui pasiekti buvo iškelti šie **uždaviniai**:

1. išanalizuoti dinamines polilaktido (PLA) ir PLA pagrindu sukurtų kompozitinių struktūrų, įskaitant PLA, sustiprintą trumpais anglies pluoštais (PLA-SCF), ištisiniais anglies pluoštais (PLA-CCF) ir ištisiniais stiklo pluoštais (PLA-CGF), savybes, atsižvelgiant į vienkryptę (0–0 º) ir skersinę (0–90 º) sluoksnių orientacijas;
2. įvertinti virpesių amplitudės slopinimą kinematiškai sužadintose AM struktūrose, pagamintose iš PLA, PLA-SCF, PLA-CCF ir PLA-CGF su dviem skirtingomis sluoksnių orientacijomis (0–0 º ir 0–90 º), taikant veiksmingą virpesių slopinimo metodiką naudojant MFC vykdiklius, nustatant orientaciją ir struktūrą, pasižyminčią didžiausiu virpesių slopinimu atitinkamuose pirmuosiuose rezonanso dažniuose;

3. ištirti signalo fazės nuo 0 º iki 360 º veikiančius MFC vykdiklius, įtaką AM struktūrų virpesių amplitudei ir nustatyti fazę, kuri užtikrina didžiausią kiekvienos konstrukcijos virpesių slopinimą;
4. sukurti skaitinius AM struktūrų modelius ir skaitinio modeliavimo metodą, kad būtų galima įvertinti jų dinamines charakteristikas ir virpesių valdymą naudojant MFC vykdiklius, lyginant rezultatus su eksperimentiniais duomenimis.

5.2. Tyrimo metodai ir būdai

Tyrimas apėmė pluošto struktūrų AM eksperimentinius tyrimus, skaitinį modeliavimą ir teorinę analizę, kad būtų gauti laukiami rezultatai. PLA ir PLA-SCF pluoštų struktūros buvo pagamintos naudojant originalų „Prusa i3“ MK3S ir MK3S+ 3D spausdintuvą, pagamintą „Prusa Research“ (Čekija). PLA-CCF ir PLA-CGF kompozitinių pluoštų struktūros buvo kuriamos naudojant 3D spausdintuvą „MeCreator-2“, pagamintą „Geeetech“ (Kinija) su modifikuota spausdinimo galvute. Modalinėms charakteristikoms, įskaitant savuosius dažnius, lenkimo virpesių formas ir amplitudės spektrus, įvertinti naudotas „Polytec 3D“ lazerinis vibrometras (PSV-W-500), pagamintas „Polytech GmbH“ (Vokietija). Lazerinis poslinkio jutiklis (LK-G82), pagamintas „Keyence Corporation“ „Japonija“, buvo naudojamas kinematiškai sužadintų struktūrų valdomų ir nevaldomų virpesių amplitudėms matuoti. Vidiniams defektams nustatyti atliktas neardomasis pluoštų struktūrų C-skenavimas naudojant THz spektrometrą (angl. *TPSTM Spectra 300 THz Pulsed Imaging and Spectroscopy from TeraView*). Skaitinis tyrimas atliktas naudojant „Abaqus CAE 2024“ programinę įrangą. Didžioji dalis eksperimentinių darbų atlikta Kauno technologijos universiteto Mechanikos inžinerijos ir dizaino fakultete ir Mechatronikos institute, o C-skenavimo spektroskopija ir skaitinio modeliavimo tyrimas – Lenkijos mokslų akademijos Skysčių srauto mašinų institute, Gdanske, Lenkijoje.

5.3. Mokslinis naujumas

1. Nustatytos adityviuoju būdu pagamintų PLA ir PLA kompozitų struktūrų dinaminės charakteristikos, daugiausia dėmesio skiriant skirtingų sluoksnių orientacijų (0–0 º ir 0–90 º) įtakai šių struktūrų natūraliems lenkimo virpesių dažniams, amplitudės spektrui ir bendrai dinaminei būsenai.
2. Sukurta veiksminga virpesių slopinimo metodika naudojant MFC vykdiklius, skirta valdyti virpesius 0–0 º ir 0–90 º orientacijos adityviuoju būdu pagamintose struktūrose, nustatant veiksmingiausią sluoksnių orientaciją ir struktūrą virpesiams slopinti.
3.Sukurtas skaitinio modeliavimo metodas, skirtas tirti dinaminėms charakteristikoms ir virpesių slopinimui naudojant MFC vykdiklius adityviai pagamintose struktūrose .

5.4. Praktinė darbo vertė

1. Virpesių valdymo metodas gali būti taikomas iš įvairių medžiagų ir sluoksnių orientacijų pagamintoms adityviai gaminamoms kompozitinėms struktūroms siekiant nustatyti efektyviausią derinį virpesių amplitudėms slopinti.
2. Virpesių valdymo metodika gali būti įdiegta mikrogamybos procesuose ir medicininėse robotų rankose, siekiant veiksmingai mažinti nedidelius virpesius, kai

labai svarbus tikslus judėjimas. Sumažinus virpesius iki minimumo, pagerinamas sistemos patikimumas ir užtikrinamas aukštas tikslumas atliekant svarbias užduotis.
3. Sukurtas skaitinio modeliavimo metodas gali būti taikomas tiriant iš skirtingų medžiagų ir sluoksnių orientacijų pagamintų struktūrų dinaminę elgseną ir virpesių slopinimą prieš adityviuoju būdu gaminant realią struktūrą, kurios efektyviam veikimui užtikrinti būtų parinkta tinkama medžiaga ir sluoksnių orientacija, taip taupant gamybos sąnaudas ir laiką.

5.5. Teiginiai gynimui

1. Dinaminėms adityviuoju būdu pagamintų (AM) konstrukcijų savybėms didelę įtaką daro tiek sluoksnių orientacija, tiek armuojančių pluoštų tipas.
2. AM konstrukcijose sluoksnių orientacija ir armuojantys pluoštai yra lemiami veiksniai slopinant virpesius. Tinkamai parinktas derinys palengvina AM konstrukcijos kūrimą, kuris maksimaliai slopina vibracijas.
3. Sukurtas skaitmeninio modeliavimo metodas veiksmingai atspindi AM konstrukcijų dinamines charakteristikas ir virpesių slopinimo tendencijas, tai patvirtina skaitmeninių ir eksperimentinių rezultatų suderinamumas.

5.6. Mokslinių tyrimų rezultatų publikacijos

Šio tyrimo moksliniai eksperimentiniai ir skaitiniai rezultatai buvo paskelbti tarptautiniuose žurnaluose, indeksuotuose „Clarivate Analytics Web of Science“ duomenų bazėje. Trys moksliniai straipsniai publikuoti 1 kvartilio (Q1) žurnaluose ir vienas – 2 kvartilio (Q2) žurnale. Be to, šie rezultatai buvo pristatyti šešiose tarptautinėse konferencijose.

5.7. Publikuotų straipsnių apžvalga[1]

Šį skyrių sudaro paskelbtų straipsnių išvadų santrauka.

5.7.1. Straipsnis [A1]. Eksperimentinis virpesių amplitudės valdymo tyrimas adityviuoju būdu pagamintose PLA ir PLA kompozitinėse struktūrose naudojant MFC vykdiklį [57]

Šiame poskyryje pateikiamos nuorodos į mokslinį straipsnį, paskelbtą žurnale „Engineering Structures“ (Elsevier, 2023, Vol. 294). Jame nagrinėjami pirmasis, antrasis ir trečiasis disertacijos tikslai. Iki šiol šis straipsnis iš viso cituotas 9 kartus. Straipsnyje pateikiamas kiekybinis lyginamasis makropluošto kompozito (MFC), kaip vykdiklio naudojimo įvairiose medžiagose, ypač AM pluoštu armuotų kompozitų, tyrimas virpesių valdymo srityje. MFC (M8507-P2) vykdiklis buvo panaudotas virpesiams valdyti AM pluoštų struktūrose su 0–0 º sluoksnių orientacija, pagamintose iš polilacto rūgšties (PLA) ir PLA kompozitų. PLA kompozitai apima PLA su trumpais anglies pluoštais (PLA-SCF kompozitas) ir PLA su ištisiniais anglies pluoštais (PLA-CCF kompozitas). Pagrindiniai šio tyrimo tikslai – nustatyti dinamines savybes (savuosius dažnius ir lenkimo virpesių formas), įvertinti virpesių slopinimą AM struktūrose naudojant MFC ir nustatyti struktūrą, kurioje MFC efektyviausiai riboja virpesių amplitudes.

Pluoštai buvo gaminami atskirai, naudojant FDM technologiją su PLA, PLA-SCF ir PLA-CCF. PLA ir PLA-SCF bandiniai buvo pagaminti naudojant originalų „Prusa i3“ MK 3S ir MK3S+ 3D spausdintuvą. O PLA-CCF kompozito bandinys buvo sukurtas naudojant modifikuotą „MeCreator-2“ 3D spausdintuvą.

Virpesių valdymo sistemą sudaro pluoštų struktūra (parametrai 120 mm x 20 mm x 1,35 mm) ir MFC (M8507-P2) kaip vykdiklis (aktyvusis dydis 85 mm x 7 mm x 0,3 mm, bendras dydis 100 mm x 10 mm x 0,3 mm). Elektrodinaminis virpintuvas (DDR-11077) buvo naudojamas individualiai įvesti virpesius iš prispaustosios pluoštų struktūros pusės. MFC vykdiklis buvo priklijuotas epoksidine medžiaga prie paviršiaus, 5 mm atstumu nuo pluoštų prispaustosios pusės. Kiekvienos pluoštų struktūros laisvajame gale (viename taške) virpesių amplitudei gauti buvo naudojama 1 pav. pateikta bendra eksperimentinė schema.

„Polytec 3D“ lazeriniu vibrometru (PSV-W-500) buvo matuojami savieji dažniai, lenkimo virpesių formos ir lenkimo virpesių amplitudės.

Pirmajame eksperimentinio tyrimo etape daugiausia dėmesio skirta atskirai iš PLA, PLA-SCF ir PLA-CCF pagamintų struktūrų saviesiems dažniams ir lenkimo virpesių formoms nustatyti.

Nustatyta, kad virpesių amplitudės gerokai sumažėja nuo pirmojo iki ketvirtojo lenkimo virpesių. Didžiausios virpesių amplitudės nustatytos prie pirmųjų savųjų dažnių: esant 30 Hz PLA atvejui jos yra 9,295 μm; esant 40,5 Hz PLA-SCF – 6,831 μm; esant 60 Hz PLA-CCF atvejui – 4,139 μm. Mažiausios virpesių amplitudės

[1]Šiame skyriuje pateikiamos nuorodos į autoriaus darbą, paskelbtą WoS žurnaluose [56–59].

gaunamos esant PLA, PLA-SCF ir PLA-CCF struktūrų ketvirtiesiems saviesiems dažniams – 0,129 μm, 0,049 μm ir 0,022 μm, atitinkamai 1207,5 Hz, 1546 Hz ir 2192 Hz.

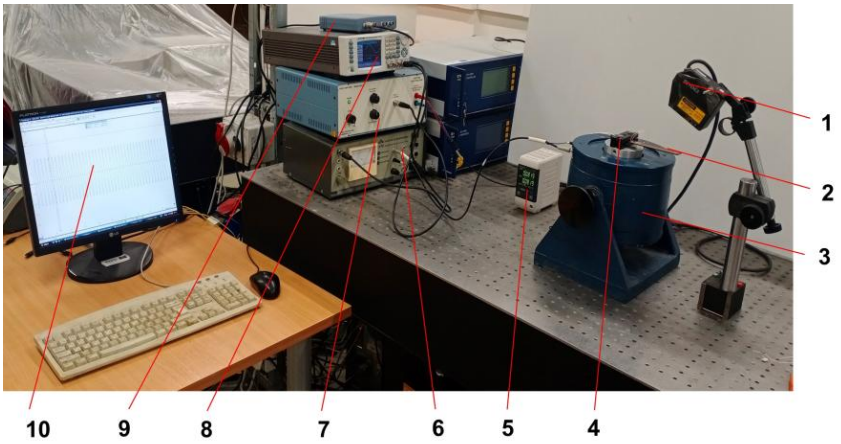

1 pav. Eksperimentinis stendas: 1 – lazerinis poslinkio jutiklis (LK-G82); 2 – bandinys su MFC vykdikliu; 3 – elektrodinaminis virpintuvas (DDR-11077); 4 – spaustuvas; 5 – lazerinio poslinkio jutiklio valdiklis LK-G3001PV; 6 – įtampos stiprintuvas (LV-103); 7 – įtampos stiprintuvas (EPA-104); 8 – funkcijų generatorius WW5064; 9 – analoginio / skaitmeninio signalų keitiklis (ADC) „Pico-Scope-3424“; 10 – kompiuteris

Iš minėtų eksperimentinių rezultatų ir mokslinės literatūros tyrimų galima daryti išvadą, kad didžiausia virpesių amplitudė nuosekliai pasireiškia ties pirmuoju savuoju dažniu ir turi dominuojančią įtaką bendram virpesių atsakui. Todėl buvo nuspręsta tirti tik pirmuosius kiekvienos pluoštų struktūros lenkimo virpesius, nes tai dominuojantys virpesiai (su didžiausia amplitude) ir turi didžiausią virpesių amplitudžių mažinimo potencialą.

Antrajame etape iš PLA, PLA-SCF ir PLA-CCF pagamintos struktūros buvo atskirai žadinamos atitinkamais pirmaisiais rezonansiniais dažniais (30 Hz, 40,5 Hz ir 60 Hz) naudojant elektrodinaminį virpintuvą su 0,16 V harmoniniu signalu, kad būtų gautas nevaldomo poslinkio atsakas. Nustatytos didžiausios PLA, PLA-SCF ir PLA-CCF struktūrų poslinkio nuo piko iki piko vertės atitinkamai ±400 μm, ±370 μm ir ±210 μm. Siekiant nustatyti optimalią fazę ir valdymo įtampą maksimaliam virpesių amplitudės sumažinimui, taikytas atviro kontūro aktyviojo virpesių valdymo metodas su inkrementine domeno paieška. Atlikus šiuos optimizavimus (optimali fazė ir valdymo įtampa), PLA, PLA-SCF ir PLA-CCF virpesių amplitudės nuo maksimumo iki maksimumo svyravo atitinkamai nuo +5,5 μm iki –4,5 μm, nuo +3,2 μm iki –2,9 μm ir nuo +1,7 μm iki –1,7 μm. Dėl to PLA, PLA-SCF ir PLA-CCF virpesiai

sumažėjo daugiau kaip 80, 110 ir 120 kartų. Didžiausias virpesių amplitudės sumažėjimas nustatytas PLA-CCF, po to PLA-SCF ir galiausiai PLA.

5.7.2. Straipsnis [A2]. Eksperimentinis 3D spausdintų struktūrų su skirtingomis sluoksnių orientacijomis dinaminių savybių tyrimas [56]

Šiame poskyryje pateikiamos nuorodos į mokslinį straipsnį, paskelbtą žurnale „Journal of Vibration Engineering & Technologies“ (Springer Nature, 2024, Vol. 12). Jame nagrinėjamas pirmasis disertacijos tikslas. Iki šiol šis straipsnis iš viso cituotas 2 kartus.

Išsamiai išnagrinėjus turimą literatūrą padaryta išvada, kad dauguma mokslininkų tyrė tik 3D spausdinimo proceso nustatymų poveikį įvairių struktūrų mechaniniam atsakui. Todėl būtina ištirti spausdinimo nustatymų įtaką struktūrų dinaminėms charakteristikoms (saviesiems dažniams, lenkimo virpesių formoms, dekremento (mažėjimo) koeficientui, slopinimui ir deformacijoms). Šiame tyrime iš PLA, PLA-SCF ir PLA-CCF pagamintos pluoštų struktūros (matmenys: 120 mm x 20 mm x 1,35 mm) sukurtos naudojant FDM su dviem skirtingomis sluoksnių orientacijomis (0–0 º ir 0–90 º). Šių orientacijų įtaka dinaminėms struktūrų savybėms tirta įvairiais eksperimentais.

PLA ir PLA-SCF bandiniai buvo gaminami naudojant originalų „Prusa“ 3D spausdintuvą (modelis: MK3S ir i3 MK3S+), o PLA-CCF ir PLA-CGF bandiniai pagaminti naudojant specialiai pritaikytą „MeCreator-2“ 3D spausdintuvą.

Kiekvienos struktūros deformacija buvo matuojama naudojant „Keyence Corporation“ (Japonija) pagamintą lazerinį poslinkio jutiklį (LK-G82). Logaritminiam deformacijos koeficientui nustatyti taikytas naujas eksperimentinis metodas pavaizduotas 2 paveiksle.

Išdėstymas buvo specialiai sukurtas kiekvienos struktūros eksponentiniam slopinamajam atsakui, kurį sukelia elektrodinaminis virpintuvas (DDR-11077), stebėti, o atsakas buvo matuojamas viename taške nuo laisvojo galo lazeriniu poslinkio jutikliu (LK-G82). Be to, siekiant nustatyti kiekvienos struktūros savuosius dažnius, virpesių formas ir atitinkamas virpesių amplitudes, buvo atlikti modalinės analizės bandymai.

Struktūrų deformacija didėja tiesiškai, didėjant taškinei masės apkrovai. Didžiausia deformacija nustatyta PLA-CGF struktūroje su 0–90 º sluoksnių orientacija – 6,69 mm, o mažiausia – PLA-CCF struktūroje su 0–0 º sluoksnių orientacija – 0,78 mm, veikiant 8 g taškinei masės apkrovai. 0–90 º sluoksnių orientacijos pluoštų struktūrose nustatytos didesnės deformacijos, palyginti su atitinkamomis 0–0 º orientacijos struktūromis. Struktūros atsparumas deformacijoms veikiant masės apkrovai paprastai įvardijamas kaip jos standumas. Eksperimentų rezultatai rodo, kad esant 0–0 º sluoksnių orientacijai standumas didėja nuo PLA iki PLA-SCF, nuo PLA-CGF iki PLA-CGF ir galiausiai iki PLA-CCF, o esant 0º–90º sluoksnių orientacijai – nuo PLA-CGF iki PLA-CCF, nuo PLA-CCF iki PLA ir galiausiai iki PLA-SCF.

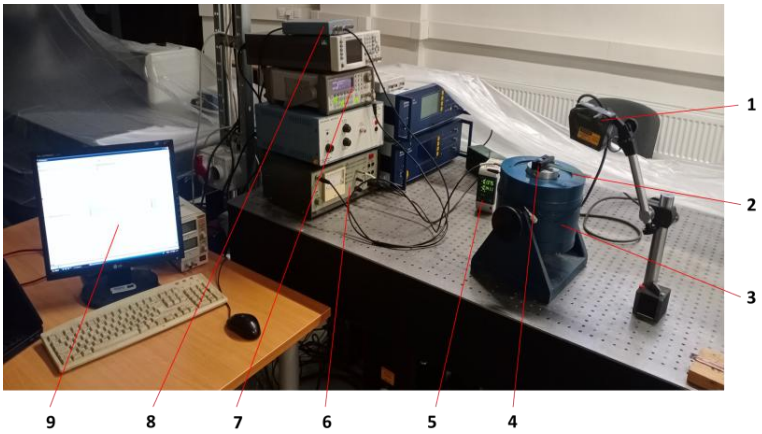

2 pav. Logaritminio dekremento koeficiento matavimo stendas: 1 – lazerinis poslinkio jutiklis (LK-G82); 2 – bandinys; 3 – elektrodinaminis virpintuvas (DDR-11077); 4 – tvirtinimo įtaisas; 5 – lazerinio poslinkio jutiklio valdiklis (LK-G3001PV); 6 – įtampos stiprintuvas (LV-103); 7 – funkcijų generatorius (33220A); 8 – analoginio / skaitmeninio signalo keitiklis „Pico-Scope "3424; 9 – kompiuteris

Esant 0–0 º sluoksnių orientacijai nustatyta, kad PLA, PLA-SCF ir PLA-CCF, PLA-CGF dekremento koeficiento vertės yra atitinkamai 0,043; 0,081; 0,214 ir 0,063. Didžiausias virpesių amplitudės slopinimo efektas nustatytas PLA-CCF, po to PLA-SCF, PLA-CGF ir galiausiai PLA struktūrose.

Priešingai, esant 0–90 º sluoksnių orientacijai, PLA, PLA-SCF, PLA-CCF ir PLA-CGF dekremento koeficientai buvo atitinkamai 0,041; 0,052; 0,040 ir 0,038. Todėl PLA-SCF pasižymėjo didžiausiu amplitudės slopinimo poveikiu, PLA ir PLA-CCF – panašiu amplitudės slopinimo poveikiu, o PLA-CGF – mažiausiu. Rezultatai atskleidžia, kad 0–0 º sijų struktūros pasižymi didesnėmis slopinimo savybėmis, palyginti su atitinkamomis 0–90 º pluoštų struktūromis.

Be to, atlikus modalinę (virpesių formų) analizę, nustatyti pirmieji keturi lenkimo virpesių savieji dažniai. Tai rodo, kad pluoštų struktūrų su 0–0 º sluoksnių orientacija savieji dažniai yra palyginti didesni nei atitinkamų struktūrų su 0–90 º sluoksnių orientacija. 0–0 º orientacijos struktūrų savasis dažnis palaipsniui didėja nuo PLA iki PLA-SCF ir PLA-CGF, o PLA-CCF pasižymi didžiausiu dažniu. 0–90 º orientuotose struktūrose jis didėja nuo PLA-CGF iki PLA-CCF, nuo PLA-CCF iki PLA ir galiausiai iki PLA-SCF.

5.7.3. Straipsnis [A3]. Virpesių valdymo gerinimas kinematiškai sužadintose skirtingos orientacijos adityviai pagamintose, ištisiniu pluoštu armuotose kompozitinėse struktūrose [58]

Šiame poskyryje pateikiamos nuorodos į mokslinį straipsnį, paskelbtą žurnale „Engineering Structures“ (Elsevier, 2024, Vol. 321). Jame nagrinėjami pirmasis, antrasis ir trečiasis disertacijos tikslai. Iki šiol šis straipsnis iš viso cituotas 1 kartą.

Šiame poskyryje, atlikus išsamią esamos literatūros apžvalgą nustatyta, kad šis tyrimas yra novatoriškas bandymas ištirti, kaip AM kompozitinės struktūros su dviem skirtingomis sluoksnių orientacijomis – 0–0 º ir 0–90 º – daro įtaką dinaminėms charakteristikoms ir virpesių slopinimui taikant MFC (M8507-P2). Šios kompozitinės struktūros buvo pagamintos iš PLA-CCF ir PLA armuoto ištisiniais stiklo pluoštais (PLA-CGF). Pagrindinis tyrimo tikslas – nustatyti sluoksnių orientaciją, kuri yra svarbi slopinant virpesius.

Be to, šiame poskyryje nagrinėjamos PLA ir PLA-SCF su 0–0 º ir 0–90 º orientacijomis dinaminės charakteristikos ir virpesių slopinimas. PLA ir PLA-SCF su 0–0 º orientacija dinaminės charakteristikos ir virpesių slopinimas buvo paskelbti straipsnyje [A1]. Tačiau reikia paminėti, kad su 0–90 º orientacijomis susijusios išvados anksčiau nebuvo skelbtos, todėl dabar jos įtrauktos į šį poskyrį. Šios informacijos pridėjimas yra labai svarbus skirtingų sluoksnių orientacijų PLA, PLA-SCF, PLA-CCF ir PLA-CGF pluoštų struktūrų įtakos dinaminėms savybėms ir virpesių slopinimo lyginamajam tyrimui.

1 pav. pavaizduotas eksperimentinis projektas buvo naudojamas stebėti ir tirti virpesių slopinimą kompozitinėse struktūrose. Sistemą sudaro 120 mm x 20 mm x 1,35 mm matmenų kompozitinė struktūra, integruota su MFC (M8507-P2).

Siekiant nustatyti kiekvieno bandinio savituosius dažnius, lenkimo virpesių formas ir amplitudės spektrus, naudotas „Polytec“ 3D lazerinis vibrometras (PSV-W-500).

Kiekvienos struktūros deformacija buvo matuojama lazeriniu poslinkio jutikliu (LK-G82). Rezultatai rodo, kad 0–90 º pluoštų struktūrų deformacijos yra didesnės, palyginti su atitinkamomis 0–0 º pluoštų struktūromis.

Antrajame eksperimento etape atlikta modalinė analizė, siekiant įvertinti pirmųjų keturių lenkimo virpesių būdingus dažnius, taip pat jų atitinkamas lenkimo virpesių formas ir amplitudės spektrus kiekvienai bandinio struktūrai su 0–0 º ir 0–90 º sluoksnių orientacija.

Didžiausia amplitudė kiekvienai bandinio struktūrai būdinga pirmajam dažniui, o mažiausia amplitudė – ketvirtajam dažniui.

Siekiant ištirti nevaldomą virpesių amplitudės elgseną, kiekviena bandinio struktūra buvo stimuliuojama pirmuoju rezonansiniu dažniu naudojant elektrodinaminį virpintuvą. Didžiausios nevaldomos virpesių amplitudės 0–0 º PLA-CCF, 0–90 º PLA-CCF, 0–0 º PLA-CGF ir 0–90 º PLA-CGF siekė maždaug nuo +210

μm iki –212 μm, kai dažnis 60 Hz, nuo +514 μm iki –545 μm, kai dažnis 26,6 Hz, nuo +244 μm iki –242 μm, kai dažnis 47,7 Hz, ir nuo +785 μm iki –810 μm.

0–0 º PLA ir 0–0 º PLA-SCF bandinių struktūrų atveju buvo stebimos atitinkamai maždaug ±400 μm esant 30 Hz ir ±370 μm esant 40,5 Hz nevaldomų virpesių amplitudės (paskelbti duomenys straipsnyje [A1]). 0–90 º PLA ir 0–90 º PLA-SCF nevaldomų virpesių amplitudės atitinkamai buvo maždaug ±526 μm, kai dažnis siekė 27,5 Hz, ir +492 μm iki –503 μm, kai dažnis 28,8 Hz.

Siekiant sumažinti kiekvienos struktūros virpesių amplitudę, MFC buvo žadinama įtampos signalu sukuriant priešpriešinę jėgą, mažinančią virpesių amplitudę. Norint maksimaliai sumažinti virpesių amplitudę, būtina tiksliai sureguliuoti tiek valdymo įtampos amplitudę, tiek fazę. Kontrolinė įtampa ir fazė 0–0 ° PLA-CCF, 0–90 ° PLA-CCF, 0–0 ° PLA-CGF ir 0–90 ° PLA-CGF buvo nustatyta taip: 10,52 V su 351° faze, 29,4 V su 45° faze, 17,68 V su 4° faze ir 43 V su 79° faze.

0–0 º PLA ir 0–0 º PLA-SCF valdymo įtampos su optimaliomis fazėmis buvo nustatytos atitinkamai 22,4 V su 29 º faze ir 13,92 V su 10 º faze (pateikta straipsnyje [A1]). Tuo tarpu 0–90 º PLA ir 0–90 º PLA-SCF nustatymai buvo tokie: 30,1 V su 37 º faze ir 27 V su 32 º faze.

Parinkta fazė ir valdymo įtampa lėmė amplitudės sumažėjimą daugiau nei 120 kartų, 80 kartų, 90 kartų ir 75 kartus atitinkamai 0–0 º PLA-CCF, 0–90 º PLA-CCF, 0–0 º PLA-CGF ir 0–90 º PLA-CGF. Panašiai, daugiau nei 80, 70, 110 ir 95 kartų sumažėjo atitinkamai 0–0 º PLA, 0–90 º PLA, 0–0 º PLA-SCF ir 0–90 º PLA-SCF. Rezultatai parodė, kad 0–0 º orientacijos sluoksnių pluoštų struktūros pasižymėjo didesniu virpesių amplitudžių sumažėjimu esant mažesnei valdymo įtampai, palyginti su atitinkamomis 0–90 º orientacijos struktūromis.

5.7.4. Straipsnis [A4]. Dinaminė analizė ir adityviuoju būdu pagamintų plonasienių polilaktino rūgšties polimero (PLAP) ir PLAP kompozitinių struktūrų, armuotų pluoštu virpesių valdymas: skaitinis tyrimas ir eksperimentinis patvirtinimas [59]

Šiame poskyryje pateikiama nuoroda į mokslinį straipsnį, paskelbtą žurnale „Materials“ (MDPI, 2024 m., 17 tomas). Jame nagrinėjamas ketvirtasis disertacijos tikslas.

Šiuo skaitiniu tyrimu siekiama patvirtinti anksčiau paskelbtus eksperimentinius tyrimus [57]. Ankstesniuose tyrimuose išsamiai nagrinėtos kinematiškai sužadintų, adityviai pagamintų pluoštais armuotų struktūrų dinaminės charakteristikos, įskaitant modalinį apibūdinimą, nuo dažnio priklausomus amplitudžių spektrus ir virpesių valdymą, kuriam įtakos turi MFC (M8507-P2).

Šiame skaitinio modeliavimo tyrime buvo modeliuojamos 0–0º orientuotos PLAP, PLAP-SCF ir PLAP-CCF struktūros, siekiant ištirti tokias dinamines charakteristikas, kaip modalinio (formų) apibūdinimo vertinimas ir dažninio atsako analizė (FRA), siekiant slopinti struktūrų, armuotų pluoštais, integruotų su MFC virpesius, įdiegiant atviro kontūro aktyvųjį virpesių valdymą.

Be to, panašūs tyrimai buvo išsamiai atlikti ir su kitomis struktūromis, tokiomis kaip 0–0 º PLAP-CGF, 0–90 º PLAP, 0–90 º PLAP-SCF, 0–90 º PLAP-CCF ir 0–90 º

PLAP-CGF. Tačiau šios struktūros nebuvo nagrinėtos ir straipsnyje jos neaptartos [59]. Labai svarbu įtraukti lyginamąją 0–0 º ir 0–90 º konfigūracijų analizę, kad būtų galima įvertinti jų dinamines charakteristikas ir virpesių slopinimą. Todėl šios papildomos struktūros nagrinėjamos ir aptariamos šiame poskyryje.

Armuotų pluoštais bandinių struktūrų, integruotų su MFC vykdikliais, baigtinių elementų modeliavimas (BEM) atliktas naudojant „Abaqus CAE 2024“ programinę įrangą.

Lanczos metodika taikyta bandinių struktūrų modaliniams saviesiems dažniams ir atitinkamoms virpesių formoms, nenaudojant išorinių jėgų, apskaičiuoti. 0–0 º orientuotų pluoštų struktūrų savieji dažniai yra didesni, palyginti su atitinkamomis 0–90 º orientuotomis pluoštų struktūromis. Nustatyta, kad 0–0 º orientuotų skaitinių modelių pirmieji savieji dažniai yra 30,45 Hz PLAP atveju, 39,95 Hz PLAP-SCF atveju, 60,50 Hz PLAP-CCF atveju ir 45,03 Hz PLAP-CGF atveju. Šios skaitinės vertės atitinka eksperimentinius dažnius, atitinkamai 30,00 Hz; 40,50 Hz; 60,00 Hz ir 47,70 Hz. Skaitinių modelių, orientuotų 0–90 º kampu, pirmieji savieji dažniai yra 28,63 Hz PLAP atveju, 29,47 Hz PLAP-SCF atveju, 27,89 Hz PLAP-CCF atveju ir 22,27 Hz PLAP-CGF atveju, o tai atitinka eksperimentines vertes, atitinkamai: 27,50 Hz; 28,80 Hz; 26,60 Hz ir 21,30 Hz.

Dažninio atsako analizė (FRA) nustato harmoninės jėgos veikiamos struktūros atsaką į dažnių spektrą. Kiekvienos struktūros dinaminis atsakas (amplitudės spektras), priklausantis nuo dažnio, buvo vertinamas dažnių spektre. Vėliau buvo kruopščiai ištirtas kiekvieno bandinio virpesių slopinimas ir palygintas su eksperimentiniais duomenimis, atkreipiant dėmesį į skaitinio modeliavimo apribojimus.

FRA rezultatai atskleidžia, kad tarp skaitinių ir eksperimentinių duomenų buvo didelis absoliučių virpesių amplitudžių verčių skirtumas. Abiejuose rezultatų rinkiniuose buvo stebima pastovi amplitudės kitimo tendencija rezonansiniuose dažniuose.

Nustatyta, kad 0–0 º orientacijos skaitinių rezultatų atveju virpesių amplitudės ties pirmuoju savuoju dažniu buvo didžiausios, kaip nurodyta toliau: PLAP atveju – 7,0870 µm, kai dažnis 30,45 Hz, PLAP-SCF atveju – 3,9240 µm, kai dažnis 40,00 Hz, PLAP-CCF atveju – 1,8980 µm, kai dažnis 60,5 Hz, PLAP-CCF atveju – 3,1702 µm, kai dažnis 45,03 Hz. Nustatytos atitinkamos eksperimentinės virpesių amplitudės pirmuoju savuoju dažniu: PLAP atveju – 9,295 µm, kai dažnis 30 Hz, PLAP-SCF atveju – 6,831 µm, kai dažnis 40,5 Hz, PLAP-CCF atveju – 4,139 µm, kai dažnis 60,0 Hz, PLAP-CCF atveju – 4,400 µm, kai dažnis 47,7 Hz. Skaitinių tyrimų rezultatuose, orientuotuose 0–90 º kampu, didžiausios virpesių amplitudės esant pirmajam savajam dažniui buvo tokios: PLAP atveju – 7,9860 µm, kai dažnis 28,63 Hz; PLAP-SCF atveju – 7,1110 µm, kai dažnis 29,47 Hz; PLAP-CCF atveju – 8,0267 µm, kai dažnis 27,89 Hz; PLAP-CCF atveju – 12,2230 µm, kai dažnis 22,27 Hz. Nustatytos atitinkamos eksperimentinės virpesių amplitudės pirmuoju savuoju dažniu: PLAP atveju – 10,9240 µm, kai dažnis 27,5 Hz; PLAP-SCF atveju – 9,7330 µm, kai dažnis

28,8 Hz; PLAP-CCF atveju – 10,1100 μm, kai dažnis 26,6 Hz; PLAP-CCF atveju – 9,2600 μm, kai dažnis 21,3 Hz.

Tiek skaitinio, tiek eksperimentinio scenarijaus atveju ketvirtajame savajame dažnyje buvo mažiausios virpesių amplitudės, o rezultatai atitiko tą pačią tendenciją.

Galiausiai buvo atlikta išsami skaitiniu būdu sumodeliuotų struktūrų armuotų pluoštais virpesių amplitudžių slopinimo analizė, o rezultatai palyginti ir patvirtinti pagal eksperimentinius duomenis. PLAP, PLAP-SCF, PLAP-CCF ir PLAP-CGF skaitiniai modeliai su 0–0 º ir 0–90 º sluoksnių orientacijomis buvo išoriškai sužadinti atitinkamais pirmaisiais rezonansiniais dažniais. Skaitiniai modeliai su 0–0 º orientacija atskleidė nevaldomų virpesių amplitudes atitinkamai nuo +435 μm iki –408 μm, ±395 μm, nuo +220 μm iki –224 μm ir nuo +252 μm iki –251 μm. Eksperimento atveju nevaldomų virpesių amplitudės buvo atitinkamai ±400 μm, ±370 μm, ±210 μm ir nuo +242 μm iki –240 μm.

Skaitinių modelių, orientuotų 0–90 º kampu, nevaldomų virpesių amplitudės buvo tokios: +548 μm –540 μm, +515 μm –510 μm, +555 μm –540 μm ir +820 μm –815 μm, atitinkamai PLAP, PLAP-SCF, PLAP-CCF ir PLAP-CGF. Atitinkamos eksperimentinės nevaldomos amplitudės buvo nuo +526 μm iki –525 μm, nuo +492 μm iki –503 μm, nuo +514 μm iki –545 μm ir nuo +785 μm iki –810 μm. Tiek skaitinės, tiek nevaldomos amplitudės.

Pritaikius priešpriešinę jėgą su MFC vykdikliu, PLAP, PLAP-SCF, PLAP-CCF ir PLAP-CGF, valdomų virpesių amplitudės 0–0 º orientuotose PLAP, PLAP-SCF, PLAP-CCF ir PLAP-CGF skaitmeniniuose modeliuose buvo atitinkamai maždaug ±19 μm, ±16 μm ir ±13 μm, ±14,3 μm. Eksperimentiškai nustatyta, kad atitinkamų modelių valdomų virpesių amplitudės buvo maždaug ±5 μm, ±3 μm, ±1,7 μm ir nuo +2,9 μm iki –2,4 μm. Ir skaitiniai, ir eksperimentiniai rezultatai rodo tą pačią amplitudės mažėjimo tendenciją nuo PLAP iki PLAP-SCF, PLAP-CGF ir galiausiai iki PLAP-CCF.

0–90 º orientuotų PLAP, PLAP-SCF, PLAP-CCF ir PLAP-CGF skaitinių modelių valdomos virpesių amplitudės atitinkamai buvo maždaug nuo +21,5 μm iki –21,7 μm, nuo +19,9 μm iki –20,4 μm, nuo +23,3 μm iki –21,5 μm ir nuo +25,5 μm iki –24,7 μm. Eksperimentiniu būdu atitinkamiems modeliams buvo nustatytos maždaug nuo +7,8 μm iki –6,4 μm, nuo +4,5 μm iki –5,8 μm, nuo +6,15 μm iki –6,4 μm ir nuo +8,5 μm iki –12,2 μm valdomos virpesių amplitudės. Tiek skaitiniai, tiek eksperimentiniai rezultatai rodo tą pačią amplitudės mažėjimo tendenciją nuo PLAP-CGF iki PLAP-CCF, PLAP ir galiausiai PLAP-SCF.

Bendros skaitinės ir eksperimentinės analizės išvados rodo, kad 0–0 º orientacijos sluoksnių struktūros pasižymėjo didesniu virpesių slopinimu, palyginti su atitinkamomis 0–90 º orientacijos sluoksnių struktūromis.

5.8. IŠVADOS

1. Atliktas adityviai pagamintų AM struktūrų dinamikos charakteristikų tyrimas ir gautos šios pagrindinės išvados:

- AM struktūros su 0–0 º sluoksnių orientacija pasižymėjo aukštesniais savaisiais dažniais nei tos, kurių atitinkama 0–90 º orientacija. Esant 0–0 º konfigūracijai sluoksniai turi vienodą kryptį, todėl padidėja konstrukcijos standumas, o tai lemia aukštesnius savuosius dažnius. Priešingai, 0–90 º orientacijos atveju sluoksniai yra statmeni vieni kitiems, todėl sumažėja standumas ir padidėja lankstumas, o tai lemia žemesnius savuosius dažnius. 0–0 º orientuotų sluoksnių struktūrų PLA, PLA-SCF, PLA-CCF ir PLA-CGF pirmieji savieji dažniai buvo atitinkamai: 30,0 Hz, 40,5 Hz, 60,0 Hz ir 47,7 Hz. Palyginimui, atitinkamos 0–90 º konfigūracijos vertės buvo 27,5 Hz, 28,8 Hz, 26,6 Hz ir 21,3 Hz.
- AM struktūrų su 0–0 º sluoksnių orientacija mažinimo koeficiento vertės buvo didesnės nei su atitinkama 0–90 º orientacija, o tai rodo didesnį slopinimą. Esant 0–0 º orientacijai, PLA, PLA-SCF, PLA-CCF ir PLA-CGF koeficientų vertės buvo atitinkamai: 0,043; 0,081; 0,214 ir 0,063, o PLA-CCF pasižymėjo didžiausiu slopinimu, o PLA – mažiausiu. Esant 0–90 º, atitinkamos koeficiento vertės buvo atitinkamai: 0,041, 0,052, 0,040 ir 0,038. PLA-SCF pasižymėjo didžiausiu slopinamuoju poveikiu, o PLA-CGF – mažiausiu.

2. Virpesių slopinimas buvo kruopščiai ištirtas ir palygintas kinematiškai sužadintose AM struktūrose, pagamintose iš PLA, PLA-SCF, PLA-CCF ir PLA-CGF, kurių sluoksnių orientacija 0–0 º ir 0–90 º. Gautos šios pagrindinės išvados:

- nustatyta, kad MFC vykdiklis efektyviau slopina virpesius standesnių AM struktūrų konstrukcijose. 0–0 º sluoksnių orientacijos struktūrose virpesių slopinimas yra didesnis, palyginti su atitinkamomis 0–90 º orientuotomis struktūromis.
- nustatyta, kad 0–0 º orientacijos struktūrose virpesiai sumažėja daugiau kaip 80 kartų PLA atveju, 110 kartų PLA-SCF atveju, 120 kartų PLA-CCF atveju ir 90 kartų PLA-CGF atveju. Esant 0–0 º orientacijai nustatyti reikšmingi, daugiau kaip 70 kartų sumažėję PLA virpesiai, 95 kartus – PLA-SCF, 80 kartų – PLA-CCF ir 75 kartus – PLA-CGF.

3. MFC vykdikliams teikiamo signalo fazės (nuo 0º iki 360º) daro didelę įtaką kinematiškai sužadintų AM struktūrų virpesių amplitudei.

- Tiksliai nustatant optimalias fazes PLA, PLA-SCF, PLA-CCF ir PLA-CGF su 0–0 º ir 0–90 º sluoksnių orientacijomis nustatyti tam tikri fazių intervalai, kuriuose nevaldomų virpesių amplitudė mažėjo, o už šių intervalų ribų amplitudė didėjo. 0–0 ° orientacijoje MFC vykdiklis slopina platesniame fazės intervale iki 130°, o 0–90 ° orientacijoje MFC apima fazės intervalą iki 120°. 0–0 º orientuotų struktūrų atveju specifiniai fazių intervalai buvo šie: PLA – nuo 330 º iki 90 º; PLA-SCF – nuo 310 º iki 70 º; PLA-CCF – nuo 290 º iki 50 º. PLA-CGF – nuo 300 º iki 70 º optimalios fazės, užtikrinančios didžiausią virpesių sumažėjimą, buvo 29 º PLA, 10 º PLA-SCF, 351º PLA-

CCF ir 4 º PLA-CCG. 0–90 º diapazonas buvo nuo 335 º iki 95 º PLA, nuo 330 º iki 90 º PLA-SCF, nuo 350 º iki 100 º PLA-CCF ir nuo 15 º iki 135 º PLA-CGF, o optimalios fazės buvo 37 º PLA, 32 º PLA-SCF, 45 º PLA-CCF ir 79 º PLA-CCG.

4. PLA, PLA-SCF, PLA-CCF ir PLA-CGF AM struktūrų su 0–0 º ir 0–90 º sluoksnių orientacijomis skaitiniai modeliai buvo sukurti naudojant „Abaqus 2024“ programinę įrangą. Siekiant ištirti jų dinamines charakteristikas ir virpesių slopinimą naudojant MFC vykdiklius, buvo atliktas modeliavimas, o rezultatai palyginti su eksperimentiniais duomenimis.

- Sukurtas skaitinis metodas veiksmingai perteikia realių AM struktūrų dinamines charakteristikas ir rodo, kad jis labai atitinka eksperimentinius duomenis. Atliekant modalinę analizę, 0–0 º ir 0–90 º orientuotų sluoksnių skaitinių modelių pirmųjų lenkimo virpesių savieji dažniai glaudžiai sutapo su eksperimentinėmis vertėmis, o jų skirtumai tesiekė apie 5 %. Aukštesniųjų lenkimo virpesių (antrojo, trečiojo ir ketvirtojo) savieji dažniai skyrėsi maždaug 10 % ir 16 % nuo eksperimentinių verčių atitinkamai: 0–0 º ir 0–90 º orientuotoms struktūroms.
- Atliekant virpesių valdymo analizę, 0–0 º orientuotų modelių PLA, PLA-SCF, PLA-CCF ir PLA-CGF valdomų virpesių amplitudės atitinkamai buvo maždaug ±19 µm, ±16 µm ir ±13 µm, ±14,3 µm, o eksperimentinės vertės buvo maždaug ±5 µm, ±3 µm, ±1,7 µm ir nuo +2,9 µm iki –2,4 µm. Ir skaitiniai, ir eksperimentiniai rezultatai rodo tą pačią amplitudės mažėjimo tendenciją nuo PLA iki PLA-SCF, PLA-CGF ir galiausiai iki PLA-CCF. 0–90 º modeliuose valdomų virpesių amplitudės buvo maždaug nuo +21,5 µm iki –21,7 µm, nuo +19,9 µm iki –20,4 µm, nuo +23,3 µm iki –21,5 µm ir nuo +25,5 µm iki –24,7 µm, o eksperimentinės vertės svyravo nuo +7,8 µm iki –6,4 µm, nuo +4,5 µm iki –5,8 µm, nuo +6,15 µm iki –6,4 µm ir nuo +8,5 µm iki –12,2 µm. Abiejų rinkinių amplitudės mažėjimo tendencija nuo PLA-CGF iki PLA-CCF, PLA ir galiausiai PLA-SCF buvo tokia pati.

REFERENCES

1. Al-Hababi, T. Cao, M. Saleh, B. Alkayem, NF. Xu, H. A critical review of nonlinear damping identification in structural dynamics: Methods, applications, and challenges. Sensors (Switzerland). 2020,20, 1–41. ISSN 14248220.
2. Awada, A. Younes, R. Optimized Active Control of a Smart Cantilever Beam Using Genetic Algorithm. Designs. 2022,6, 36.
3. Li, J. Xue, Y. Li, F. Narita, Y. Active vibration control of functionally graded piezoelectric material plate. Composite Structures. 2019,207, 509–18. ISSN 0263-8223.
4. Kapsalas, CN. Sakellariou, JS. Koustoumpardis, PN. Aspragathos, NA. An ARX-based method for the vibration control of flexible beams manipulated by industrial robots. Robotics and Computer-Integrated Manufacturing. 2018,52, 76–91. ISSN 07365845.
5. Song, ZG. Li, FM. Active aeroelastic flutter analysis and vibration control of supersonic composite laminated plate. Composite Structures. 2012,94, 702–13. ISSN 02638223.
6. Vadiraja, DN. Sahasrabudhe, AD. Vibration analysis and optimal control of rotating pre-twisted thin-walled beams using MFC actuators and sensors. Thin-Walled Structures. 2009,47, 555–67. ISSN 02638231.
7. Rimašauskienė, R. Jūrėnas, V. Radzienski, M. Rimašauskas, M. Ostachowicz, W. Experimental analysis of active–passive vibration control on thin-walled composite beam. Composite Structures. 2019,223, 110975. ISSN 02638223.
8. Ma, R. Bi, K. Hao, H. Inerter-based structural vibration control: A state-of-the-art review. Engineering Structures. 2021,243, 112655. ISSN 18737323.
9. Kamila, S. Introduction, Classification and Applications of Smart Materials: An Overview. American Journal of Applied Sciences. 2013,10, 876–80. ISSN 1554-3641.
10. Gopi Krishna, J. Thirumal, JR. Application of Smart Materials in Smart Structures. International Journal of Innovative Research in Science, Engineering and Technology. 2015,4, 5018–23.
11. Kim, HS. Kim, JH. Kim, J. A review of piezoelectric energy harvesting based on vibration. International Journal of Precision Engineering and Manufacturing. 2011,12, 1129–41. ISSN 2005-4602.
12. Konka, HP. Wahab, MA. Lian, K. Piezoelectric fiber composite transducers for health monitoring in composite structures. Sensors and Actuators A: Physical. 2013,194, 84–94. ISSN 0924-4247.
13. Nagendra Kumar, D. Raja, S. Ikeda, T. Active vibration control of smart plates with partially debonded multilayered PZT actuators. Smart Materials and Structures. 2007,16, 1584–94. ISSN 09641726.
14. Smith, R. Smart Material Applications. Smart Material Systems: Model Development, vol. 1, North Carolina, USA: Society for Industrial and Applied Mathematics; 2005, p. 1–41. ISSN 978-0-89871-747-1.
15. Deraemaeker, A. Nasser, H. Numerical evaluation of the equivalent properties of Macro Fiber Composite (MFC) transducers using periodic homogenization.

International Journal of Solids and Structures. 2010,47, 3272–85. ISSN 0020-7683.
16. Park, S. Inman, DJ. Yun, CB. An outlier analysis of MFC-based impedance sensing data for wireless structural health monitoring of railroad tracks. Engineering Structures. 2008,30, 2792–9. ISSN 0141-0296.
17. Betts, DN. Kim, HA. Bowen, CR. Inman, DJ. Optimal configurations of bistable piezo-composites for energy harvesting. Applied Physics Letters. 2012,100, 114104. ISSN 00036951.
18. Sreenivasa Prasath, S. Arockiarajan, A. Effective electromechanical response of macro-fiber composite (MFC): Analytical and numerical models. International Journal of Mechanical Sciences. 2013,77, 98–106. ISSN 0020-7403.
19. Friswell, MI. Ali, SF. Bilgen, O. Adhikari, S. Lees, AW. Litak, G. Non-linear piezoelectric vibration energy harvesting from a vertical cantilever beam with tip mass. Journal of Intelligent Material Systems and Structures. 2012,23, 1505–21. ISSN 1045389X.
20. Smart Materialn.d. https://www.smart-material.com/ (accessed March 6, 2022).
21. Ngo, TD. Kashani, A. Imbalzano, G. Nguyen, KTQ. Hui, D. Additive manufacturing (3D printing): A review of materials, methods, applications and challenges. Composites Part B: Engineering. 2018,143, 172–96. ISSN 1359-8368.
22. Turner, BN. Strong, R. Gold, SA. A review of melt extrusion additive manufacturing processes: I. Process design and modeling. Rapid Prototyping Journal. 2014,20, 192–204. ISSN 13552546.
23. Turner, BN. Gold, SA. A review of melt extrusion additive manufacturing processes: II. Materials, dimensional accuracy, and surface roughness. Rapid Prototyping Journal. 2015,21, 250–61. ISSN 13552546.
24. Mohamed, OA. Masood, SH. Bhowmik, JL. Optimization of fused deposition modeling process parameters: a review of current research and future prospects. Advances in Manufacturing. 2015,3, 42–53. ISSN 21953597.
25. He, F. Ning, H. Khan, M. Effect of 3D Printing Process Parameters on Damping Characteristic of Cantilever Beams Fabricated Using Material Extrusion. Polymers . 2023,15, 257. ISSN 2073-4360.
26. Maqsood, N. Rimašauskas, M. Influence of printing process parameters and controlled cooling effect on the quality and mechanical properties of additively manufactured CCFRPC. Composites Communications. 2022,35, 101338. ISSN 24522139.
27. Maqsood, N. Rimašauskas, M. Development and fabrication of continuous carbon fiber reinforced thermoplastic porous composite structures with different infill patterns by using additive manufacturing. Journal of Thermoplastic Composite Materials. 2023,36, 2050–75. ISSN 0892-7057.
28. Chacón, JM. Caminero, MA. García-Plaza, EP. Núñez, PJ. Additive manufacturing of PLA structures using fused deposition modelling: Effect of process parameters on mechanical properties and their optimal selection. Materials and Design. 2017,124, 143–57. ISSN 1873-4197.

29. Medel, F. Esteban, V. Abad, J. On the use of laser-scanning vibrometry for mechanical performance evaluation of 3D printed specimens. Materials & Design. 2021,205, 109719.
30. Yashavantha Kumar, GA. Sathish Kumar, KM. Free vibration analysis of smart composite beam. Materials Today: Proceedings. 2017,4, 2487–91. ISSN 22147853.
31. Zhang, WX. Zhang, W. Yang, DS. Luo, Z. Guo, XY. Vibration suppression of nonlinear laminated composite plates using internal oscillator-enhanced nonlinear energy sinks. Engineering Structures. 2023,279, 115579. ISSN 0141-0296.
32. Fang, X. Hao, H. Bi, K. An innovative pendulum-type column-in-column (PCIC) system for structural vibration control induced by seismic ground excitations. Engineering Structures. 2022,256, 113990. ISSN 18737323.
33. Wani, ZR. Tantray, M. Noroozinejad Farsangi, E. Nikitas, N. Noori, M. Samali, B. et al. A Critical Review on Control Strategies for Structural Vibration Control. Annual Reviews in Control. 2022,54, 103–24. ISSN 13675788.
34. Wu, D. Huang, L. Pan, B. Wang, Y. Wu, S. Experimental study and numerical simulation of active vibration control of a highly flexible beam using piezoelectric intelligent material. Aerospace Science and Technology. 2014,37, 10–9. ISSN 12709638.
35. Xie, C. Wu, Y. Liu, Z. Modeling and active vibration control of lattice grid beam with piezoelectric fiber composite using fractional order PDμ algorithm. Composite Structures. 2018,198, 126–34. ISSN 02638223.
36. Mayer, D. Herold, S. Passive, Adaptive, Active Vibration Control, and Integrated Approaches. Vibration Analysis and Control in Mechanical Structures and Wind Energy Conversion Systems, IntechOpen; 2017, p. 1–23.
37. Rezaei, M. Talebitooti, R. Liao, WH. Friswell, MI. Integrating PZT layer with tuned mass damper for simultaneous vibration suppression and energy harvesting considering exciter dynamics: An analytical and experimental study. Journal of Sound and Vibration. 2023,546, 117413. ISSN 0022-460X.
38. Przybylski, J. Gasiorski, G. Nonlinear vibrations of elastic beam with piezoelectric actuators. Journal of Sound and Vibration. 2018,437, 150–65. ISSN 0022-460X.
39. Miao, WK. Xu, ML. Wu, CS. Active vibration control of cantilever beam using MFC sensor and actuator. Recent Advances in Structural Integrity Analysis - Proceedings of the International Congress (APCF/SIF-2014). 2014, 447–52.
40. Gawryluk, J. Mitura, A. Teter, A. Dynamic control of kinematically excited laminated, thin-walled beam using macro fibre composite actuator. Composite Structures. 2020,236, 111898. ISSN 02638223.
41. Zippo, A. Ferrari, G. Amabili, M. Barbieri, M. Pellicano, F. Active vibration control of a composite sandwich plate. Composite Structures. 2015,128, 100–14. ISSN 02638223.
42. Lee, AJ. Xie, A. Inman, DJ. Suppression of cross-well oscillations for bistable composites through potential well elimination. Journal of Vibration and Acoustics, Transactions of the ASME. 2020,142, 031003. ISSN 15288927.

43. Hao, YX. Bai, CP. Zhang, W. Liu, LT. Yang, SW. Intrawell and interwell oscillations for bi-stable cross-ply laminates actuated by MFC under oscillating impulse voltages. International Journal of Non-Linear Mechanics. 2022,143, 104025. ISSN 00207462.
44. Li, C. Shen, L. Shao, J. Fang, J. Simulation and Experiment of Active Vibration Control Based on Flexible Piezoelectric MFC Composed of PZT and PI Layer. Polymers. 2023,15. ISSN 20734360.
45. Lu, Q. Wang, P. Liu, C. An analytical and experimental study on adaptive active vibration control of sandwich beam. International Journal of Mechanical Sciences. 2022,232, 107634. ISSN 0020-7403.
46. Wang, X. Morandini, M. Masarati, P. Velocity feedback damping of piezo-actuated wings. Composite Structures. 2017,174, 221–32. ISSN 0263-8223.
47. Chai, YY. Song, ZG. Li, FM. Active aerothermoelastic flutter suppression of composite laminated panels with time-dependent boundaries. Composite Structures. 2017,179, 61–76. ISSN 02638223.
48. Mitura, A. Gawryluk, J. Experimental and finite element analysis of PPF controller effectiveness in composite beam vibration suppression. Eksploatacja i Niezawodność – Maintenance and Reliability. 2022,24, 468–77. ISSN 1507-2711.
49. Kamel, MA. Ibrahim, K. El-Makarem Ahmed, A. Vibration control of smart cantilever beam using finite element method. Alexandria Engineering Journal. 2019,58, 591–601. ISSN 11100168.
50. Byeon, JH. Kim, SH. Extraction of the damping ratio of a beat wave using envelope logarithmic decrement. Journal of Mechanical Science and Technology. 2022,36, 2729–37. ISSN 19763824.
51. Lashin, MMA. Saleh, WS. Alrowais, F. Determination of Different Structures' Materials Natural Frequencies using Fuzzy Logic System. International Journal of Engineering and Advanced Technology. 2020,9, 723–7.
52. Miyashiro, D. Taira, H. Hamano, R. Reserva, RL. Umemura, K. Mechanical vibration of single-walled carbon nanotubes at different lengths and carbon nanobelts by modal analysis method. Composites Part C: Open Access. 2020,2, 100028. ISSN 2666-6820.
53. Raza, A. MAHATO, S. Rimašauskienė, R. Actuation Performance of Macro Fibre Composite (MFC) as Actuator in Vibration Reduction of Cantilever Beams. Mechanics. 2023,29, 42–50. ISSN 2029-6983.
54. Evci, C. Gülgeç, M. An experimental investigation on the impact response of composite materials. International Journal of Impact Engineering. 2012,43, 40–51. ISSN 0734743X.
55. Rimašauskas, M. Kuncius, T. Rimašauskienė, R. Processing of carbon fiber for 3D printed continuous composite structures. Materials and Manufacturing Processes. 2019,34, 1528–36. ISSN 15322475.
56. Raza, A. Rimašauskienė, R. Jūrėnas, V. Rimašauskas, M. An Experimental Study on the Dynamic Properties of 3D-Printed Structures with Different Layer Orientations. Journal of Vibration Engineering and Technologies. 2024. ISSN 25233939.
57. Raza, A. Rimašauskienė, R. Jūrėnas, V. Mahato, S. Experimental investigation of vibration amplitude control in additive manufactured PLA and PLA

composite structures with MFC actuator. Engineering Structures. 2023,294, 116802. ISSN 18737323.
58. Raza, A. Rimašauskienė, R. Jūrėnas, V. Kuncius, T. Enhancing vibration control in kinematically excited additively manufactured continuous fiber composite structures with distinct orientations. Engineering Structures. 2024,321. ISSN 18737323.
59. Raza, A. Mieloszyk, M. Rimašauskienė, R. Jūrėnas, V. Dynamic Analysis and Vibration Control of Additively Manufactured Thin-Walled Polylactic Acid Polymer (PLAP) and PLAP Composite Beam Structures: Numerical Investigation and Experimental Validation. Materials. 2024,17, 5478. ISSN 1996-1944.

COPIES OF PUBLICATIONS

Title [A1]: Experimental investigation of vibration amplitude control in additive manufactured PLA and PLA composite structures with MFC actuator
Authors: Ali Raza, Rūta Rimašauskienė, Vytautas Jūrėnas, Swarup Mahato

Engineering Structures 294 (2023) 116802

Contents lists available at ScienceDirect

Engineering Structures

journal homepage: www.elsevier.com/locate/engstruct

Experimental investigation of vibration amplitude control in additive manufactured PLA and PLA composite structures with MFC actuator

A. Raza [a], R. Rimašauskienė [a,*], V. Jūrėnas [b], S. Mahato [a]

[a] Kaunas University of Technology, Faculty of Mechanical Engineering and Design, Studentų str. 56, LT-51424 Kaunas, Lithuania
[b] Kaunas University of Technology, Institute of Mechatronics, Studentų str. 56, LT-51424 Kaunas, Lithuania

ARTICLE INFO

Keywords:
PLA composites
Macro Fiber Composite (MFC)
Additive manufacturing
Vibration suppression
Natural frequency
Optimal phase angle

ABSTRACT

In this study, Macro Fiber Composite (MFC) as actuator has been used for open-loop active vibration control (AVC) in additive manufactured structures made of polylactic acid (PLA) and PLA composites, such as PLA with short carbon fibers (PLA-SCF composite) and PLA with continuous carbon fibers (PLA-CCF composite), when subjected to forced vibrations. The laser vibrometer has been used to find the natural frequencies and bending mode shapes of each beam structure. The MFC patch (M8507-P2), used here as an actuator, is very sensitive to supplied voltages. Thus, it is very crucial to find out the optimum phase and amplitude of the input voltage. The optimal phase angle and voltage for each structure (PLA, PLA-SCF, PLA-CCF) are estimated by a domain search in an incremental manner. Once tuned with the optimal input voltage values, the proposed technique shows exceptional performance in vibration suppression. The results confirmed that this technique can be used in a wide range of composite materials.

1. Introduction

In recent times, vibration control in structural dynamics has been one of the most concerning issues in the research community. The structure starts vibrations when subjected to dynamic loading circumstances such as the external environment, machine vibrations, noise, and human activities. The structure is harmed by mechanical vibrations, which create premature fatigue and subsequently the structure collapses. Therefore, it is critical to maintain vibration in structures within the permissible limit to reduce the risk of failure [1–3]. Composite structures are extensively utilized in many engineering fields due to their exceptional properties, such as significant stiffness, low density, and high strength-to-weight ratio.

However, low-frequency resonance occurrences have a detrimental effect on these structures and raise significant concerns about structural integrity. These aspects inspire researchers to examine the vibration amplitude suppression approaches [4].

Several vibration control technologies, including active control (AC) which comprises both open loop and closed loop control approaches as well as semi-active control (SAC), passive control (PC), and hybrid control (HC), have been introduced in recent years to ensure system safety. A PC control system often consists of numerous materials and devices that provide a control force depending on the system's motion, whereas sensors and the control system are frequently used in AC, SAC, and HC. The PC technique is frequently implemented due to its low cost and ease of installation. [5,6]. It is also worth mentioning that active control approaches are becoming popular in scientific fields due to the availability of a variety of smart materials, such as piezoelectric type, shape memory alloys and others in the market [7,8]. Piezoelectric materials are extensively used as smart materials in various fields due to their rapid response and high efficiency.

Furthermore, due to the converse and direct piezoelectric effects, piezoelectric materials may be used as actuators and sensors, respectively. However, they have some limitations, such as high brittleness, low deformation, and low integration ability with curved structures due to their brittle nature, which have adverse effects on the stability and efficiency of piezoelectric materials [3]. These restrictions have encouraged researchers to work on alternative techniques for the development of advanced piezoelectric materials. To address the limitations of piezoelectric material for practical applications, extensive research has been conducted on the incorporation of piezoceramic fibers into polymeric matrix [9,10]. NASA invented Macro Fiber Composites (MFCs) in 1999 to address above mentioned limitations, the rectangular piezoceramic fibers had been incorporated into polymer matrix and

* Corresponding author.
E-mail address: ruta.rimasauskiene@ktu.lt (R. Rimašauskienė).

https://doi.org/10.1016/j.engstruct.2023.116802
Received 17 April 2023; Received in revised form 12 July 2023; Accepted 21 August 2023
Available online 30 August 2023

sandwiched between the protective and electrode layers [11–15]. Smart Material began commercializing this invention as NASA's licensed manufacturer and supplier in 2002 [16]. Wang et al. reported a numerical approach to develop a geometric nonlinear fiber-reinforced thin-walled composite beam integrated with piezo-composite actuators to create a smart structure for the aircraft wing. The simple negative velocity feedback approach was applied, and it was shown that the damping performance can be improved and the total cost of the system can also be decreased by selecting the suitable size and position of the piezo-actuator [17]. Dafang et al. conducted an experimental study on a flexible beam to examine the control of vibrations with piezoelectric patches. The independent modal space control technique was applied to specifically control and investigate the first three modes of the beam. A comparison between the vibration responses of the flexible beam before and after applying the control approach revealed a significant vibration suppression. Furthermore, a numerical simulation was performed to simulate the first three modes, and the results from the simulation and experiment were quite comparable. The findings indicate that proposed control method is quite effective in suppressing vibrations [18]. Li et al. presented a comprehensive numerical study on the AVC of a piezoelectric plate integrated with a piezoelectric patch, aiming to suppress vibrations. The velocity feedback approach was applied on the plate to observe the significant effect of AVC on the plate. The findings from the study reveal that a substantial vibration suppression is achieved. [1]. Kumar et al. investigated a finite element model (FEM) of a cantilever beam integrated with PZT patches to suppress the vibrations. Modal analysis is carried out on the ANSYS platform to determine the natural frequencies and mode shapes of the beam. The results from the modal analysis confirmed the effectiveness of this investigation for the SHM of beam structures [2]. Przybylski et al. did theoretical and experimental studies on nonlinear flexural vibration of uniform aluminum beams that were symmetrically integrated with smart piezoelectric actuators on their top and bottom sides. Theoretical and experimental findings prove that the piezoelectric actuators play a significant role important role in suppressing vibrations across various applications [19]. Xie et al. studied on the AVC of the beam using piezoelectric material as an actuator. The numerical dynamic model of the beam is developed and a new AVC technique (fractional-order PDμ algorithm) was applied to suppress vibrations in the beam under various external dynamic loading conditions. The results confirm that by applying this technique, the vibration amplitude can be suppressed more dramatically and quickly [20]. Several research have been conducted to examine the effectiveness of piezoelectric materials in vibration control applications, including AVC in space truss, column structures, and smart beam structures [21]. Mayer et al. worked on active, passive, adaptive, and integrated vibration control techniques and compared their respective design challenges and advantages. The study employed a design arrangement to demonstrate different ways of implementing a vibration control system, as well as the integration of various vibration control approaches [22]. Chai et al. reported the numerical simulation and theoretical investigation on the aero-thermoelastic behavior of the laminated structure. Two MFC patches were integrated with the structure; one as a sensor to measure strain and the other creates a control force to suppress vibrations in the structure. The findings confirm that MFC patch effectively reduces the vibration amplitude in the structure [23]. Miao et al. investigated the suppression of vibrations in the cantilever beam using MFCs as actuators and sensor. Two MFC patches were used for AVC in the cantilever beam, and the third was used as a sensor. The AVC for the first two modes of vibration was executed using the proportional derivative (PD) control and fuzzy control algorithms. The results confirm that vibrations in the first two modes are significantly suppressed, and this scheme can be implemented in different industrial applications to control vibrations [24]. Rimasauskiene et al. conducted an experimental study to observe the influence of active and passive control schemes on the vibration control of a composite structure by using MFC patch. The findings show that active and passive control schemes efficiently suppress vibrations of the beam structure [25]. Gawryluk et al. conducted an extensive study of various algorithms to suppress vibrations in the composite beam, and an MFC patch (MFC-8528 P1 type) was integrated with the beam. Simulation and experiment studies were carried out to suppress vibrations in the beam structure. The results of the simulation and the experiment confirm that the vibration amplitude can be significantly reduced by applying these control algorithms [26].Zippo et al. reported an experimental investigation on the AVC of a honeycomb carbon fiber sandwich composite plate bonded with MFCs as actuator and sensor. The first four modes were effectively controlled using a control algorithm (PPF). The control algorithm was found reliable and effective in suppressing the vibration amplitude in linear and nonlinear systems. It was concluded that more tests are needed to investigate the non-linear behavior of the system and the electromechanical interconnection between different components [27]. Danish et al. proposed a solution to suppress unwanted vibrations in a cross-ply lamination (bistable square) structure by integrating an extra composite strip. The investigation employs a parametric approach to examine how the potential energy (P.E) terrain and related dynamic properties vary with changes in the width and the thickness of the composite strip. Based on the findings from the analytical and numerical simulations, the article presents the optimal design specifications of the integrated strip for minimizing unwanted vibrations in the structure induced by periodic stimulation [28]. Rezaei et al. investigated the possibility of embedding a piezoelectric layer within a tuned mass damper system (TMDS) to achieve both power harvesting (PH) and vibration reduction concurrently. The investigation revealed that the TMDS proved effective in both vibration suppression within the host structure and enabling PH. Consequently, the investigation concludes that TMDS represents a potential approach for achieving both vibration suppression and PH [29]. Lee et al. conducted an investigation on a unique dual control approach to mitigate unwanted oscillations in bistable composites structure. The approach includes two MFCs and one Positive Position Feedback (PPF) controller. The approach entails applying a certain voltage to a single MFC to suppress one of the potential wells and push the structure towards a stable position. This is achieved by using a PPF controller to mitigate the resulting single-well vibrations in the structure through the second MFC. Both mathematical and experimental methods have been employed to demonstrate the effectiveness of the dual control approach in reducing the vibration amplitude under various oscillation scenarios [30]. Hao et al. conducted a study on the intra-well as well as inter-well vibrations of an asymmetric bi-stable rectangular-shaped laminate structure with a cross ply configuration stimulated by a MFC (d33 type). According to the findings, it is easier to achieve the snap-through response in laminate structure when excited by pulsating impulse voltages rather than constant (static) voltages. In addition, snap-through response can be enhanced by varying the frequency as well as amplitude of the supplied voltage to MFC within a specific range. The supplied voltage applies an external force to the system, thereby, altering its characteristics such as stiffness, damping, and others [31]. Li et al. utilized an active vibration control (AVC) approach to suppress vibration in a flexible beam. Two MFCs (P2 type) were integrated with the flexible beam; one as an actuator and the second as a sensor. The numerical simulation and experiment were performed on beam structure, applying both LQR and fuzzy control algorithm under diverse external dynamic conditions. The findings confirm that the LQR control approach is more effective in reducing vibration in beam structures than the fuzzy control [32].Lu et al. employed an adaptive feedback loop to suppress the vibration amplitude at low frequencies in a sandwich structure composite. A modified analytical model is presented that incorporates the impacts of MFC patches to investigate the vibration properties of the sandwich structure. Numerical simulations and experiments were carried out to validate the accuracy of the modified analytical model. The adaptive feedback loop scheme was employed analytically as well as experimentally, and the findings confirm that vibrations in sandwich structure can be suppressed effectively by applying this scheme [33]. Raza et al.

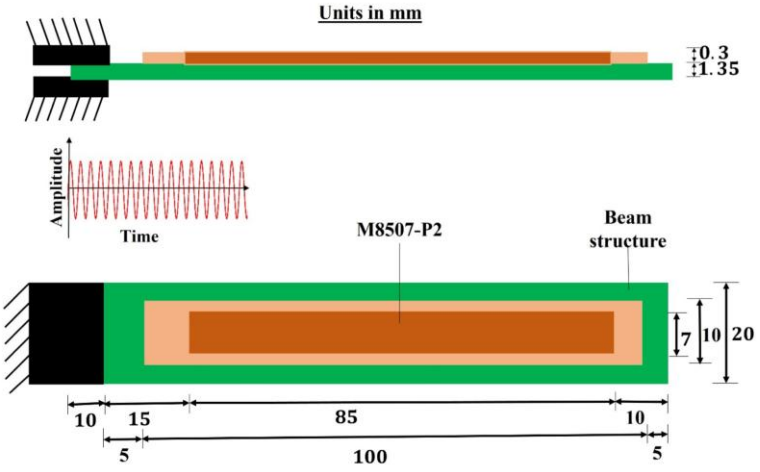

Fig. 1. Schematic view of the cantilever beam structure with the bonded MFC patch.

performed an investigation on the vibration suppression technique in beam structures made of various materials, using MFC (M8507, P2 type) as actuator vibration suppression technique. The ANSYS platform was used to create the FEA models of each beam integrated with the MFC. Each beam was subjected to an external force, causing it to vibrate, while MFC produced a counter-control force to reduce the vibration when a control voltage was provided to the MFC. The numerical simulation findings confirm that the MFC effectively reduces the vibration amplitude in each beam [34].

In order to conduct research on 3D structures, additive manufacturing (AM) technology has been widely used. AM technology creates 3D objects by adding layers on top of each other until the final object is manufactured [35,36].Over the years, AM technology has expanded significantly and is expected to continue growing in the future. Its versatility and affordability make it suitable for applications such as rapid prototyping and manufacturing. This technology can process various thermoplastic polymers, including polylactic acid (PLA) [37–39], acrylonitrile butadiene styrene (ABS) [38,39], polyamide (PA) and polycarbonate (PC) [40,41] as well as thermosetting polymers like epoxy resins. Depending on material selection, 3D printing of polymers holds potential applications in various sectors such as in the aviation sector for the manufacturing of complicated structures, in the architectural sectors for creating building models, and in the medical technology for creating organs [40–42]. Unfortunately, due to their lack of mechanical strength, the majority of 3D-printed models are primarily presented as speculative rather than functional. This limitation has been alleviated by incorporating nanoparticles or fibers into the polymer matrix to enhance mechanical strength [41]. Researchers have conducted extensive studies on the reinforcement of short or continuous carbon fibers in the polymer matrix such as PLA, ABS, nylon, PC, PETG and others, using AM technology [42–47].

After an extensive literature review, the authors conclude that a quantitative comparative study is needed on the use of Macro Fiber Composite (MFC) as actuator over various materials, especially additive manufactured (AM) fiber reinforced composite in the field of vibration control. This inspired the authors to utilize MFC (M8507-P2) as an actuator to control vibrations in AM cantilever beam structures with a 0°-0° layer orientation, which were made of polylactic acid (PLA) and PLA composites. The PLA composites include PLA with short carbon fibers (PLA-SCF composite) and PLA with continuous carbon fibers (PLA-CCF composite). The primary objectives of this study are to find out the dynamic properties (natural frequencies, bending mode shapes and vibration suppression with effect of MFC) of the additive-manufactured structures and identify the structure in which the MFC is most effective in limiting vibration amplitudes. Additionally, an open-loop active vibration control (AVC) approach with incremental domain searching has been employed to determine the optimal voltage and phase of the signal provided to MFC actuator at which maximal amplitude suppression is obtained for each structure. The modal analysis of each AM structure is performed to determine bending mode shapes, natural frequencies, and vibrating amplitudes at corresponding natural frequencies. Subsequently, the experimental results of vibration amplitude suppression, achieved by applying the MFC actuator at the first resonant frequencies, are thoroughly discussed. Furthermore, the approach and data provided in this research study could be useful for vibration control in various composite structures.

2. Materials and methods

In this experimental research, the transverse vibrations of additive manufactured cantilever beam structures manufactured from PLA and PLA composites were individually studied and reported. Transverse vibrations in the cantilever beam were produced by the influence of an electrodynamic shaker. To control vibrations, an open-loop active vibration control (AVC) experimental setup was created using the MFC (M8507-P2) as an actuator to provide forces for controlling the beam vibrations. The first resonant frequency of each structure is determined by model analysis, representing the frequency at which AVC exhibits the maximum damping effect.

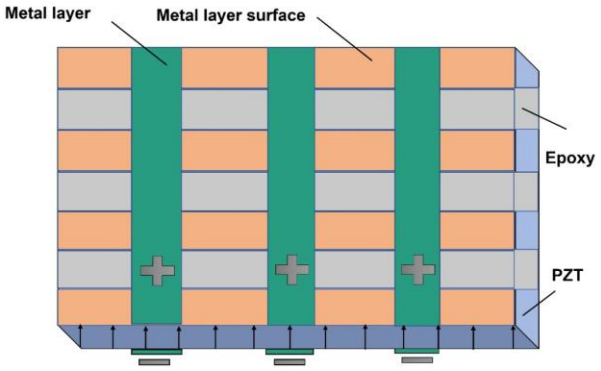

Fig. 2. Configuration of P2 type Macro Fiber Composite (MFC).

2.1. Design of the experiment

The vibration control system created consists of a beam structure (parameters 120 mm × 20 mm × 1.35 mm), and an MFC (M8507-P2) as actuator (active size 85 mm × 07 mm × 0.3 mm with an overall size 100 mm × 10 mm × 0.3 mm) produced by Smart Materials [16]. The beams are manufactured individually using additive manufacturing (AM) technology with PLA, PLA-SCF and PLA-CCF. A cantilever beam-type structure was used to simulate and investigate open-loop active vibration control (AVC) in materials (PLA, PLA-SCF and PLA-CCF). An electrodynamic shaker (DDR-11077) made by the German company VEB Robotron-Messelektronik "Otto Schon" Dresden was used to individually introduce vibrations from the clamped side of the beam structure, as shown in Fig. 1. The MFC (M8507-P2) as actuator, (Fig. 2) was bonded with epoxy to the surface, 5 mm from the clamped side of the cantilever beam. The schematic view of the cantilever beam structure with the MFC patch is presented in Fig. 1. In the MFC, rectangular piezo ceramic rods are sandwiched between polyimide film, electrodes, and adhesive layers. The ribbon-shaped rods receive and transmit the applied voltage through interdigitated arrangement of electrodes affixed to the film. This arrangement provides sealed, reliable, and ready-to-use in-plane poling, actuation, and sensing. The P2 type MFCs use the d31 effect to operate, and can contract up to 750 ppm at maximum voltage rate (-60 V to + 360 V) [16,25].

2.2. Fabrication of beam structures

For the preparation of PLA-based beam structures, a 1.75 mm diameter filament with a density of 1.24 g/cm^3, was used. It was supplied by Polymaker, China [48]. For the fabrication of PLA-SCF-based structures, a 1.75 mm diameter filament (XT-CF20) with a density of 1.35 g/cm^3 has been used. This material (XT-CF20) is manufactured by ColorFabb, The Netherlands [49]. Furthermore, for the preparation of PLA-CCF structures, Polymaker PLA (1.75 mm-diameter) by Polymaker was used as a matrix and T300B-3000 tow (7 μm-diameter of one fibre) purchased from Toray Composite Materials America, Inc. was used as a reinforcement material. The T300B-3000 tow is high performance carbon fibers with a density of 1.76 g/cm^3 [50].

PLA and PLA-SCF specimens were fabricated using an original Prusa i3 MK 3S & MK3S + 3D printer. The spool of PLA or PLA-SCF filament is placed on the printer's filament holder, and the filament is inserted through the extruder following the instructions from the Original Prusa i3 MK 3S & MK3S +. The printer bed and extruder are heated up to the required temperature before starting the process. This 3D printer operates based on FDM techniques, in which 3D geometry is created by placing layers on layers until the final part is manufactured. The controlled extrusion of thermoplastic filaments through a nozzle is the foundation of this technique. Once the printing process is completed, the object is allowed to cool down on the bed. The printing parameters have been reported in Table 1 [51].

Table 1
3D printing parameters for PLA, PLA-SCF, and PLA-CCF [51].

Parameters	Original Prusa i3 MK 3S & MK3S+		MeCreator 2
	PLA	PLA-SCR	PLA-CCF
Nozzle Diameter (mm)	0.4	0.4	1.5
Extrusion Multiplier	1	1	0.7
Extrusion Width (mm)	0.45	0.45	1.2
Layer Height (mm)	0.15	0.15	0.5
Printing Speed (mm/s)	25	25	3.0
Extruder Temperature (℃)	215	260	210
Bed Temperature (℃)	60	75	90
Fan Speed	50%	30%	60%
Infill Percentage	100%	100%	100%
Layer orientations	0°- 0°	0°-0°	0°-0°

The creation of a PLA-CCF composite specimen was performed using a modified MeCreator 2 FDM 3D printer. Two input paths were created: one for the PLA filament and the other for the impregnated CCF. The impregnation process of CCF has been thoroughly discussed by authors [52]. The drive wheel carried plastic material to the extrusion head, whereas the impregnated CCF was introduced directly into the printing nozzle through the extrusion head. The thermoplastic filament melted and formed a composite connection with the CCF before being extruded through a printing nozzle and printed on a bed platform made of borosilicate glass. Throughout the preparation of the PLA-CCF samples, the extrusion width, extruder temperature, and printing speed remained consistent at 1.2 mm, 210° and 3 mm/s, respectively [53]. The fabrication process of samples has been presented in Fig. 3.

In PLA-SCF, the reinforcement content was 20% (wt.)[49], while in the case of PLA-CCF, the reinforcement content was estimated using tool length path by knowing the number of layers and lines of the 3D printed sample and it was estimated about 45.93% (wt.). Furthermore, the mechanical properties of the materials used for the fabrication of the beam structure are reported in Table 2 [54].

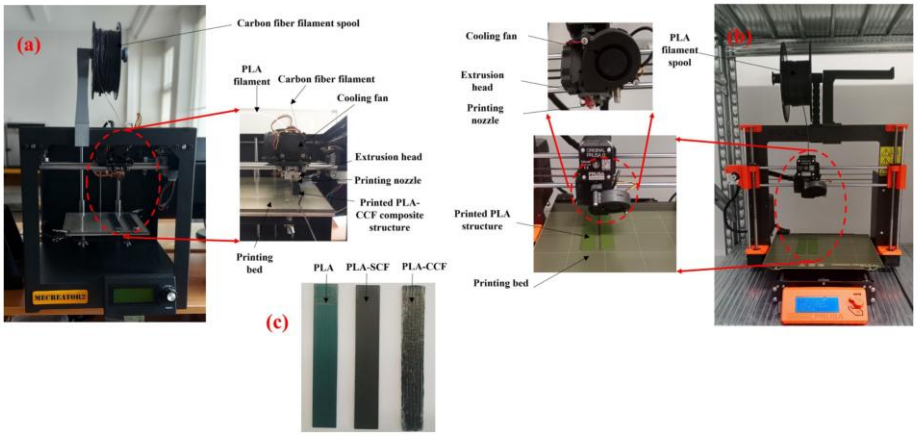

Fig. 3. Fabrication of beam structures: a) preparation of pla-ccf structures, b) preparation of pla and pla-scf structures, c) pla, pla-scf and pla-ccf samples.

Table 2
Properties of 3D Printed Material [54].

Material	Average Tensile strength (GPa)	Average Young's modulus (GPa)	Average Flexural stress (GPa)	AverageFlexural modulus (GPa)
PLA	0.0438	3.0	0.0832	3.1
PLA-SCF	0.0437	4.8	0.0763	4.5
PLA-CCF	0.2454	25.9	0.1689	10.6

2.3. Force equilibrium in the beam structure

The force equilibrium for the structures can be described as follows [25]:

$$F_{ext} + F + F_{piezo} = 0 \tag{1}$$

F_{ext} represents the external force that the electrodynamic shaker produces, and according to Ampere's force law it can be presented as [55,56]:

$$F_{ext} = BIL \tag{2}$$

where:

B = magnetic flux density.
I = current flowing across a wire.
L = overall length of wire within field.

Where $I = I \cdot sin\omega t$ and $F = k_{beam}\delta$ represents the bending force that is proportion to the beam flexure δ, and F_{piezo} is the force produced by the MFC actuator that has a reverse piezoelectric effect.

2.4. Experimental arrangement

The experimental arrangement presented in Fig. 4, was used to obtain experimental observations at the free end (one point) of each cantilever beam structure. The arrangement was specifically designed to

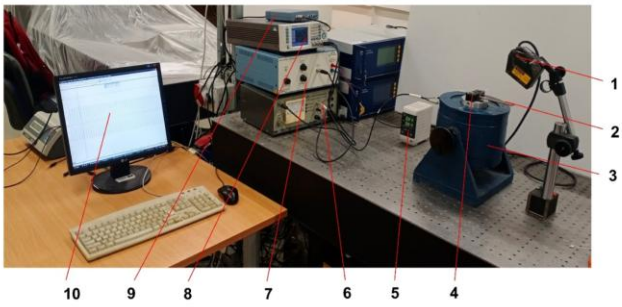

Fig. 4. Laser displacement sensor (LK-G82); 2- cantilever beam with MFC actuator; 3- electrodynamic shaker (DDR-11077); 4- clamper; 5- laser displacement sensor controller LK-G3001PV; 6- voltage amplifier (LV-103); 7- voltage amplifier (EPA-104); 8- function generator WW5064; 9- analogue/digital signal converter (ADC) Pico-Scope- 3424; 10- computer.

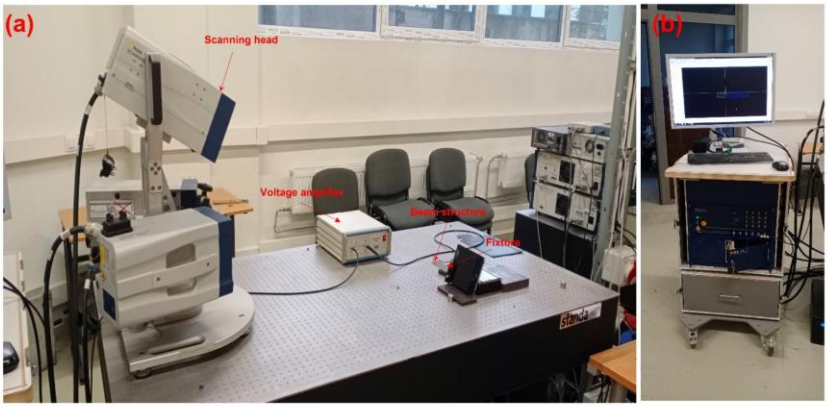

Fig. 5. Polytec 3D laser vibrometer (PSV-500): a) three scanning heads for 3D vibration measurement; b) data management system (control unit).

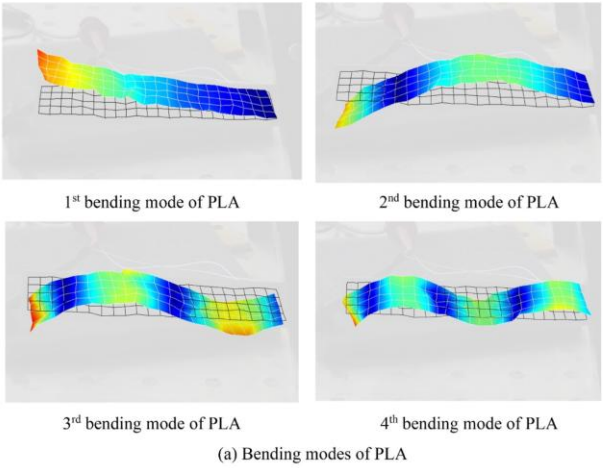

Fig. 6. The first four bending mode shapes of cantilever beam structures with M8507-P2: a) bending modes of PLA; b) bending modes of PLA-SCF and c) bending modes of PLA-CCF.

observe and investigate vibrations in each cantilever beam induced by an electrodynamic shaker. The purpose of the experiment was to observe the influence of MFC (M8507-P2) actuator to control the vibration amplitude of each beam structure (PLA, PLA-SCF, PLA-CCF).

The Polytec 3D laser vibrometer (PSV-W-500) manufactured by Polytech GmbH, Germany, shown in Fig. 5, was used to measure, natural frequencies, bending mode shapes, and the amplitudes of bending modes. This experimental setup consists of three scanning heads (for 3D vibration measurement), voltage amplifier (F10A) made by FLC electronics, Sweden, and data management system (PSV-500-3D-HV).

3. Results and discussions

To investigate each additive manufactured structure, the natural frequencies and the bending mode shapes are determined. Subsequently, the vibration amplitude reduction in each beam is performed with the effect of the MFC patch. The experimental results, along with detailed analysis are presented thoroughly in the article.

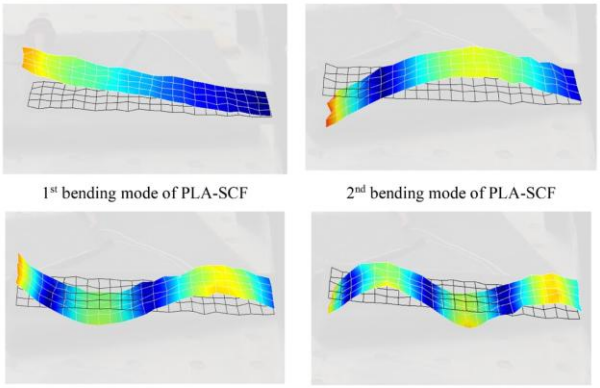

1st bending mode of PLA-SCF 2nd bending mode of PLA-SCF

3rd bending mode of PLA-SCF 4th bending mode of PLA-SCF

(b) Bending modes of PLA-SCF

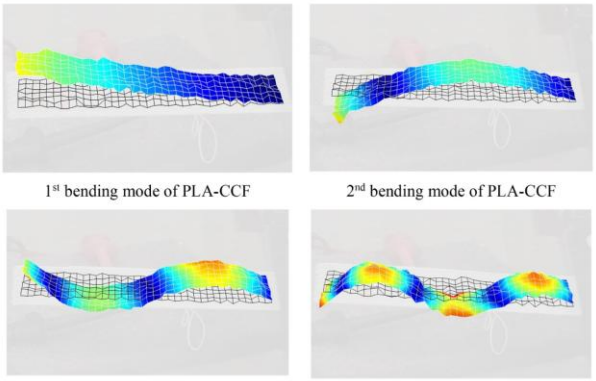

1st bending mode of PLA-CCF 2nd bending mode of PLA-CCF

3rd bending mode of PLA-CCF 4th bending mode of PLA-CCF

(c) Bending modes of PLA-CCF

Fig. 6. (*continued*).

Table 3
Natural frequency and displacement amplitude of cantilever beam structure made of PLA, PLA-SCF, and PLACCF with MFC patch.

Modes	PLA		PLA-SCF		PLA-CCF	
	Frequency (Hz)	Amplitude (μm)	Frequency (Hz)	Amplitude (μm)	Frequency (Hz)	Amplitude (μm)
1st Bending Mode	30	9.295	40.5	6.831	60	4.139
2nd Bending Mode	215	3.602	280.5	1.911	410	1.131
3rd Bending Mode	626.5	0.349	802	0.136	1153	0.110
4th Bending Mode	1207.5	0.129	1546	0.049	2192	0.022

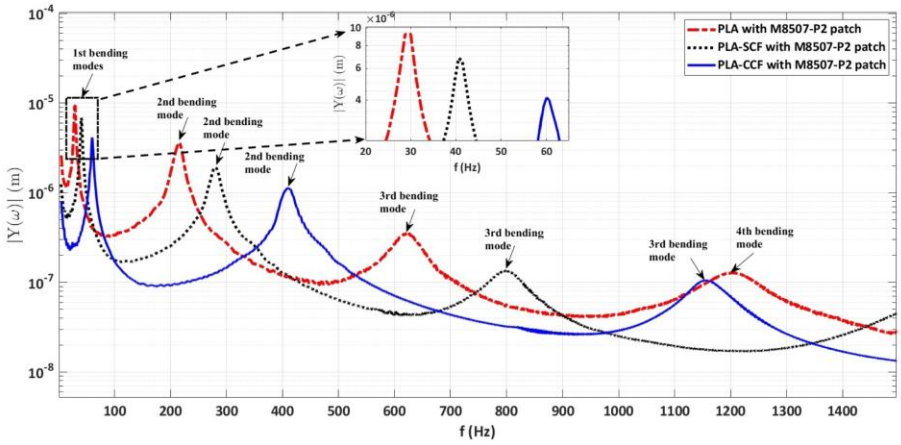

Fig. 7. Amplitude spectrum of the beam structure, made of PLA, PLA-SCF and PLA-CCF with MFC patch.

3.1. Estimation of natural frequencies and bending mode shapes

The first stage of the experimental investigation was focused on determining the natural frequencies and bending mode (BM) shapes of a structure made of PLA, PLA-SCF, and CCF individually. Vibrations were introduced in each structure, caused by the MFC actuator (M8507-P2) to determine the natural frequencies and mode shapes. The MFC patch was excited by a periodic chirp signal of 100 V. The integration of the MFC patch moderately increases the mass and stiffness of each material, causing the natural frequencies of each structure to vary from the actual cantilever beam.

The first four bending mode shapes of each beam structure are presented in Fig. 6. The natural frequencies and respective amplitudes of the first four bending modes are listed in Table 3. The mechanical properties of a material, particularly its mass and stiffness, determine its natural frequencies. Materials with higher stiffness and lower mass are commonly associated with higher natural frequencies [34,57,58].According to the researcher [54], PLA-CCF exhibits the highest Young's modulus of 25.9 GPa, followed by PLA-SCF with 4.8GPa and PLA with 3 GPa. The Young's modulus is directly associated with stiffness of the material, with higher values indicating increased stiffness. Consequently, when the Young's modulus of the material increases, the corresponding natural frequency also increases. The relationship is evident in Table 3, which demonstrates the increasing trend in natural frequencies from PLA (30 Hz) to PLA-SCF (40.5 Hz) to PLA-CCF (60 Hz).

It is reported in Table 3 that the vibration amplitudes are significantly reduced from the first BM to the fourth BM. The highest vibration amplitudes are found at the first natural frequencies, which are 9.295 μm at 30 Hz for PLA, 6.831 μm at 40.5 Hz for PLA-SCF, and 4.139 μm at 60 Hz for PLA-CCF. For PLA, PLA-SCF, and PLA-CCF, the second bending modes have amplitudes of 3.602 μm at 215 Hz, 1.911 μm at 280.5 Hz, and 1.131 μm at 410 Hz, respectively. The third bending modes for PLA, PLA-SCF, and PLA-CCF have amplitudes of 0.349 μm at 626.5 Hz, 0.136 μm at 802 Hz, and 0.110 μm at 1153 Hz, respectively. The lowest vibration amplitudes are obtained at the fourth natural frequencies of PLA, PLA-SCF, and PLA-CCF structures, which are 0.129 μm, 0.049 μm, and 0.022 μm at 1207.5 Hz, 1546 Hz, and 2192 Hz, respectively. The average amplitude spectrum of each structure is shown in Fig. 7. The inset portion in Fig. 7, presents the maximum vibration amplitude values of PLA, PLA-SCF, and PLA-CCF at the corresponding first natural frequency. Table 3 shows that the amplitude values of second mode of PLA, PLA-SCF, and PLA-CCF are 38.75%, 27.97%, and 27.32% of their respective first mode amplitudes. The third mode amplitude values of PLA, PLA-SCF, and PLA-CCF are only 3.75%, 1.99%, and 2.6% of their corresponding first mode amplitudes. Similarly, the fourth mode amplitudes of PLA, PLA-SCF, and PLA-CCF structures are determined as1.38%, 0.717%, and 0.53%, of their corresponding first mode amplitudes. It can be concluded from the above experimental results as well as from the literature study that the highest vibration amplitude consistently occurs at the first natural frequency and has a dominant impact on the overall vibration response [25]. Therefore, it was decided that only the first bending mode of each beam structure should be investigated as it is the dominant mode (with the largest amplitude) and offers the most potential for reducing vibration amplitude.

3.2. Tuning the optimal phase of the control voltage

Initially, the structure made of PLA, PLA-SCF, and PLA-CCF was individually excited by an electrodynamic shaker (subjected to harmonic signal) with the corresponding resonant frequencies, i.e., 30 Hz, 40.5 Hz, and 60 Hz, respectively (see Fig. 4) to get the uncontrolled displacement response.

The MFC actuator uses an alternating current (AC). Amplitude and phase are the two parameters that determine it. Although increasing the voltage amplitude will result in a greater force, as stated in the MFC patch's material specification, this will not result in the best possible control. This is true for both the amplitude and phase regulating parameters. Finding out the precise amplitude and phase at which the voltage will be applied provides incentive.

For a comparison study, the displacement-amplitude reduction is represented by.

$$rf = \left(\frac{Y_u - Y_c}{Y_u}\right) \times 100\% \tag{3}$$

Here, rf is reduction factor; Y_u and Y_c are uncontrolled and controlled amplitude in time domain, respectively. For the beam made

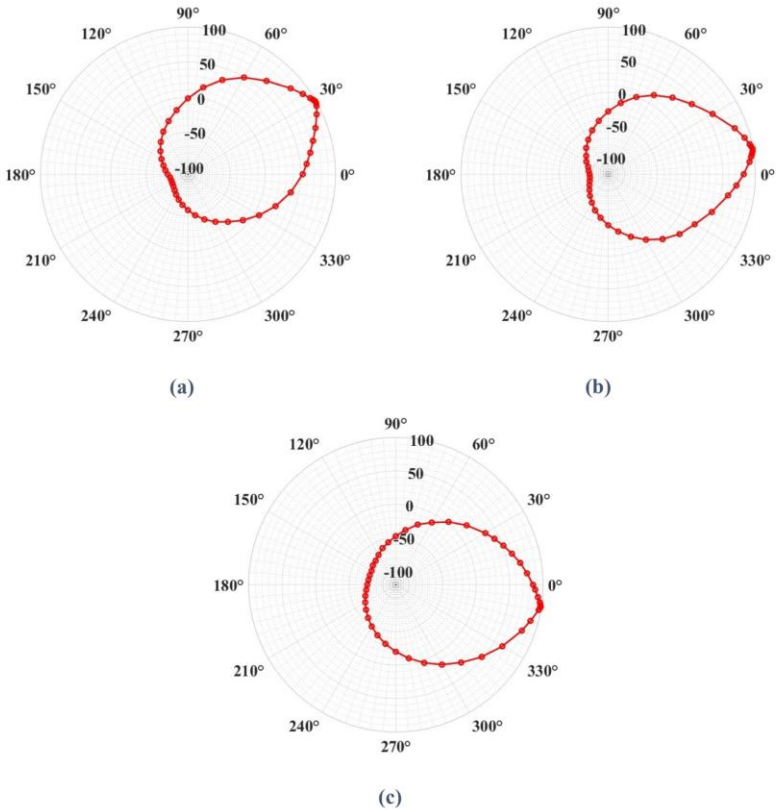

Fig. 8. Phase influence on amplitude reduction for (a) PLA, (b) PLA-SCF, and (c) PLA-CCF.

of PLA, the control voltage is increased by 2 mV step with a random phase between 0° and 360°. Once it shows a significant reduction in displacement around 1.12 V, changes in voltage amplitude are stopped. With that amplitude, the phase angle of the voltage is changed by steps of 5°. During this experiment, it is observed that it gives a maximum reduction near 30°. To locate the exact required phase, the increment of steps is set to 0.5°. When searching for this sub-step, it is found that the 29° phase angle gives the highest reduction in vibration amplitude. Setting this phase and the 1.12 V voltage, the MFC patch generate a force which makes Y_c near zero. Thus, the *rf* comes as 98.66% and shown in Fig. 8(a). An intriguing finding from this experiment is that when the phase value falls within a certain range, the amplitude of vibrations is reduced. However, when it is outside that range, the amplitude of vibration increases, and the dynamic system becomes unstable. For PLA beam, the stable domain spans from approximately 330° to 90° (including values from 330° to 360° and 0° to 90°). In this stable phase domain of 120°, Y_c grows turning *rf* positive, that indicates reduction in vibration amplitude. It is observed that the vibration amplitude starts to decrease within the stable phase domain (330° to 90°) and the maximum reduction is seen at 29° with a voltage of 1.12 V, as depicted in Fig. 8(a). The range between 90° to 330° constitutes the unstable domain here. In this approximately 240° phase range, the Y_c grows turning *rf* negative. In this unstable region (90° to 360°), an increase in vibration amplitude is recorded rather than a reduction. Therefore, the assessment of the unstable phase is also highly crucial for the secure operation of this control system.

The same steps are repeated for the beam made of PLA-SCF and it is found that 13.92 V gives a significant amplitude reduction. Once the voltage amplitude is set, the process is repeated to find the optimal phase angle by increasing the phase by 5° in each step. The *rf* is found near the 10° phase and, to be more exact, small steps are taken near this phase, as previously mentioned. In this case, the voltage with 13.92 V amplitude and 10° phase is found to produce the *rf* of 99.16%. In PLA-SCF, the stable domain spans from approximately 310° to 70° (including values from 310° to 360° and 0° to 70°), as presented in Fig. 8(b). In this stable phase range of 120°, Y_c grows turning *rf* positive. The vibration amplitude begins to decrease within the stable domain, and the maximum reduction in vibration amplitude is observed at the 10° phase

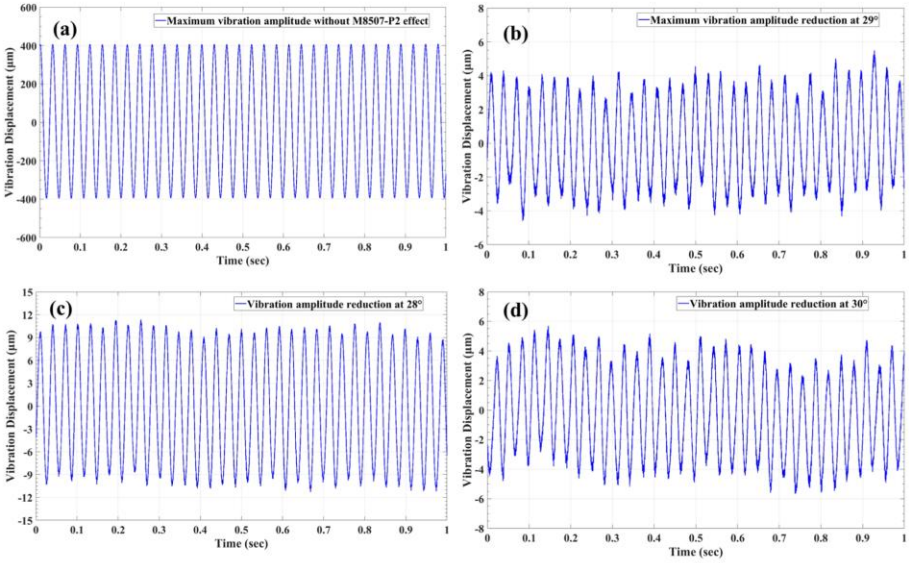

Fig. 9. Vibration amplitude in beam structure made of PLA with MFC actuator excited by electrodynamic shaker: (a) vibration amplitude without effect of MFC actuator (b) vibration amplitude with effect of MFC actuator at 29°(c) vibration amplitude with effect of MFC actuator at 28° (d) vibration amplitude with effect of MFC actuator at 30°.

with a voltage of 13.92 V. The unstable domain spans between 70° to 310° and the Y_c grows turning *rf* negative. Within the about 240° unstable phase region, the vibration amplitude begins to increase instead of decrease (see Fig. 8(b)).

A similar procedure is followed for PLA-CCF material beam, and it is found that the optimal voltage amplitude and phase are 10.52 V and 351°, respectively. With this input, the MFC patch generates force to give the reduction factor to 98.62%. The stable domain phase of a PLA-CCF beam ranges from 290° to 50° (containing values from 290° to 360° and 0° to 50°), as shown in Fig. 8 (c). The vibration amplitude decreases in this stable phase range of 120°, and the maximum vibration amplitude is found at 351° with voltage of 10.52 V. While the unstable phase domain ranges from 50° to 290° (Fig. 8 (c)), the vibration amplitude increases rather than decreases across this approximately 240° phase range. The experiments show that the stable operating range of the phase is around 120°, even if the optimal phase varies across materials.

3.3. Calculation of the amplitude reduction

The maximum amplitude in the PLA structure i.e.,- ±400 μm peak to peak, can be seen in Fig. 9 (a) when it was excited by an electrodynamic shaker near its first resonant frequency (30 Hz). The PLA structure experienced the highest level of amplitude reduction when the MFC patch was subjected to a control voltage of 22.4 V with an optimal phase angle of 29°, as depicted in Fig. 9 (b). After the maximum amplitude reduction, the peak-to-peak vibration amplitude of PLA was found to be from + 5.5 μm to −4.5 μm, and the amplitude reduction was observed more than 80 times. It has been presented in Fig. 9(c) and 9(d) when the MFC was supplied with the control voltage 22.4 V and phases close to the optimal phase, such as 28° and 29°, the peak-to-peak vibration amplitude was observed as + 11 μm to −11 μm and + 5.7 μm to −5.7 μm respectively. For the 28° and 29° phases, the amplitude reduction in the PLA structure was observed approximately 36 times and 70 times, respectively.

Fig. 10 (a) shows that the highest level of vibration amplitude was observed in the PLA-SCF structure i.e.,- ±370 μm peak to peak, when it was excited by an electrodynamic shaker close to the first resonant frequency (40.5 Hz). The highest level of vibration amplitude reduction was observed in the PLA-SCF structure, when the MFC patch was subjected to a control voltage of 13.92 V with an optimal phase of 10°. After the maximum amplitude reduction, the peak-to-peak vibration amplitude was noted to be from + 3.2 μm to −2.9 μm as provided in Fig. 10 (b). More than 110 times the amplitude reduction was achieved. Fig. 10 (c) and 10 (d) show that when the MFC patch was subjected to13.92 V with phases close to the optimal phase such as 9° and 11°, the peak-to-peak vibration amplitude was observed as + 6 μm to −6 μm and + 9 μm to −10 μm respectively. The vibration amplitude was reduced by approximately 60 and 40 times at 9° and 11° phases, respectively.

In case of PLA-CCF structure, the maximum vibration amplitude was observed i.e.,- ±210 μm peak to peak at the first resonant frequency (60 Hz), as given in the Fig. 11(a). The highest level of amplitude damping level was observed at 351°a phase with a voltage of 10.52 V. The maximum peak-to-peak vibration amplitude was measured from + 1.7 μm to −1.7 μm, as depicted in Fig. 11(b). with a vibration amplitude reduction more than 120 times. Fig. 11 (c) and 11 (d) illustrate that when the MFC actuator was subjected to phases such as 350° and 352°, the peak-to-peak vibration amplitude was observed + 6 μm to −6 μm and + 3 μm to −3.4 μm respectively. The amplitude reduction was approximately 35 and 65 times, at 350° and 352° phase, respectively.

Maximum amplitude reduction was achieved at phase angles of 29°, 9°, and 351°, with corresponding voltages of 22.4 V, 13.92 V, and 10.52 V for PLA, PLA-SCF, and PLA-CCF, respectively.

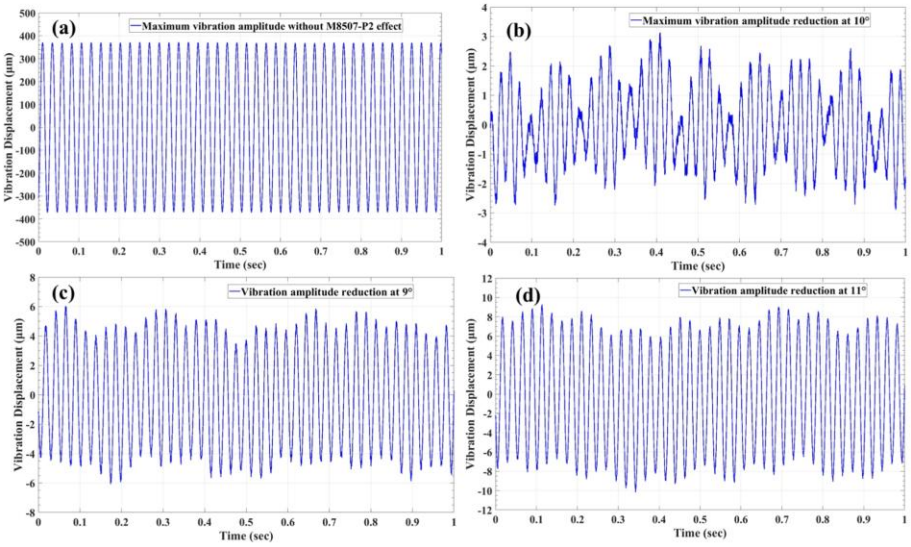

Fig. 10. Vibration amplitude in cantilever beam structure made of PLA-SCF with MFC actuator excited by electrodynamic shaker: (a) vibration amplitude without effect of MFC actuator (b) vibration amplitude with effect of MFC actuator at 10° (c) vibration amplitude with effect of MFC actuator at 9° (d) vibration amplitude with effect of MFC actuator at 11°.

PLA exhibited the highest peak-to-peak vibration amplitude, followed by PLA-SCF and PLA-CCF without the MFC effect. Cosequently, PLA required the highest voltages to achieve maximum vibration reduction, followed by PLA-SCF and PLA-CCF. Furthermore, according to the literature study, it is claimed that the location and type of MFC patch can be altered to observe the phenomenon of amplitude damping in various types of composite materials.

4. Conclusions

The aim of this article was to experimentally validate the open-loop AVC of the additive manufactured beam structures made of PLA, PLA-SCF and PLA-CCF using an MFC actuator. The significant reduction in amplitude demonstrated in the previous section provides evidence of its effectiveness. In view of the findings obtained in this article, the following conclusions have been deduced.

1. After conducting the first part of the experiment, it was observed that the natural frequencies showed an increasing trend from PLA (30 Hz) to PLA-SCF (40.5 Hz) to PLA-CCF (60 Hz) as beam structure was subjected to vibrations induced by a MFC patch (M8507-P2) with a periodic chirp signal of 100 V. Remarkably, the maximum vibration amplitudes were consistently observed at the first natural frequencies, such as 9.295 μm at 30 Hz for PLA, 6.831 μm at 40.5 Hz for PLA-SCF, and 4.139 μm at 60 Hz for PLA-CCF. In contrast, the PLA, PLA-SCF and PLA-CCF beam structures exhibited the lowest vibration amplitudes at their fourth natural frequencies such as 0.129 μm, 0.049 μm, and 0.022 μm at 1207.5 Hz, 1546 Hz, and 2192 Hz, respectively.
2. In the second phase, structures made of PLA, PLA-SCF, and PLA-CCF were individually excited at their respective first resonant frequencies (30 Hz,40.5 Hz and 60 Hz) using an electrodynamic shaker with harmonic signal of 0.16 V to obtain the uncontrolled displacement response. The maximum peak to peak displacement values were observed as ± 400 μm, ±370 μm and ± 210 μm for PLA, PLA-SCF and PLA-CCF structures, respectively.
3. An open-loop AVC approach with incremental domain searching was employed to determine stable phase domain of the signal provided to MFC actuator, achieving vibration amplitude suppression for each structure. The stable phase domains for PLA, PLA-SCF and PLA-CCF ranged from approximately 330° to 90°, 310° to 70° and 290° to 50° respectively. Notably, outside of these phase ranges, the vibration amplitude exhibited an increase rather than a decrease.
4. After meticulous fine tuning of stable phase region, the optimal phase and control voltage for maximum vibration amplitude reduction were determined. PLA exhibited the maximum reduction at a phase of 29° phase with control voltage of 22.4 V, while PLA-SCF demonstrated the optimal results at a phase of 10° with a control voltage of 13.92 Similarly, for PLA-CCF the maximum reduction was obtained at a phase of 351° with a control voltage of 10.52 V.
5. Finally, after implementing these optimizations (optimal phase with control voltage), the peak-to-peak vibration amplitude of PLA, PLA-SCF and PLA-CCFF ranged from + 5.5 μm to −4.5 μm, +3.2 μm to −2.9 μm and + 1.7 μm to −1.7, respectively. These optimizations led to impressive vibration reductions of more than 80 times, 110 times and 120 times for PLA, PLA-SCF and PLA-CCF, respectively.
6. Moreover, the findings confirmed that the MFC actuator was found to be more effective in containing the vibration amplitude of structures with highest first resonant frequency. Therefore, the maximum vibration amplitude reduction was observed in PLA-CCF, followed by PLA-SCF and PLA, respectively, in a controlled environment.

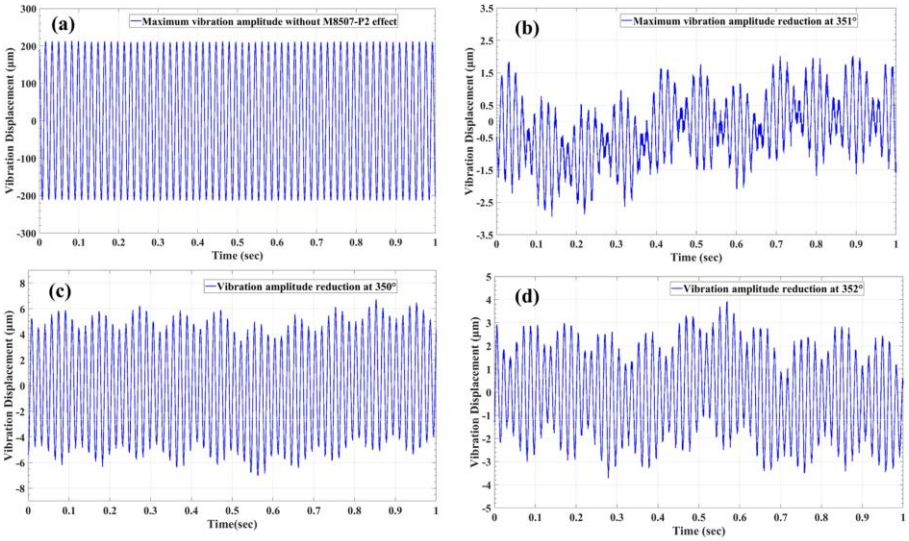

Fig. 11. Vibration amplitude in cantilever beam made of PLA-CCF with MFC actuator excited by electrodynamic shaker: (a) vibration amplitude without effect of MFC actuator (b) vibration amplitude with effect of M8507-P2 at 351° (c) vibration amplitude with effect of MFC actuator at 350° (d) vibration amplitude with effect of MFC actuator at 352°.

CRediT authorship contribution statement

A. Raza: Methodology, Software, Formal analysis, Validation, Investigation, Writing – original draft, Visualization. **R. Rimašauskienė:** Conceptualization, Writing – review & editing, Supervision. **V. Jūrėnas:** Methodology, Investigation, Writing – review & editing, Supervision. **S. Mahato:** Formal analysis.

Declaration of Competing Interest

The authors declare the following financial interests/personal relationships which may be considered as potential competing interests: Ruta Rimasauskiene reports financial support and equipment, drugs, or supplies were provided by Kaunas University of Technology. Ruta Rimasauskiene reports a relationship with Kaunas University of Technology that includes: employment and funding grants. Nothing.

Data availability

No data was used for the research described in the article.

Acknowledgement

Research was funded by a grant (No. S-M-ERA.NET-20-1) (project: "Additive Manufactured Composite Smart Structures with Embedded Fibre Bragg Grating Sensors", acronym: "AMCSS") from the Research Council of Lithuania.

References

[1] Li J, Xue Y, Li F, Narita Y. Active vibration control of functionally graded piezoelectric material plate. Compos Struct 2019;207:509–18. https://doi.org/10.1016/J.COMPSTRUCT.2018.09.053.
[2] Yashavantha Kumar GA, Sathish Kumar KM. Free vibration analysis of smart composite beam. Mater Today: Proc 2017;4:2487–91. https://doi.org/10.1016/j.matpr.2017.02.101.
[3] Awada A, Younes R, Ilinca A. Optimized Active Control of a Smart Cantilever Beam Using Genetic Algorithm. Designs (Basel) 2022;6(2):36.
[4] Zhang WX, Zhang W, Yang DS, Luo Z, Guo XY. Vibration suppression of nonlinear laminated composite plates using internal oscillator-enhanced nonlinear energy sinks. Eng Struct 2023;279:115579. https://doi.org/10.1016/J.ENGSTRUCT.2022.115579.
[5] Ma R, Bi K, Hao H. Inerter-based structural vibration control: A state-of-the-art review. Eng Struct 2021;243:112655. https://doi.org/10.1016/j.engstruct.2021.112655.
[6] Fang X, Hao H, Bi K. An innovative pendulum-type column-in-column (PCIC) system for structural vibration control induced by seismic ground excitations. Eng Struct 2022;256:113990. https://doi.org/10.1016/j.engstruct.2022.113990.
[7] Kamila S. Introduction, Classification and Applications of Smart Materials: An Overview. Am J Appl Sci 2013;10:876–80. https://doi.org/10.3844/AJASSP.2013.876.880.
[8] Gopi Krishna J, Thirumal JR. Application of Smart Materials in Smart Structures. International Journal of Innovative Research in Science. Eng Technol 2015;4(5018–23). https://doi.org/10.15680/IJIRSET.2015.0407206.
[9] Deraemaeker A, Nasser H. Numerical evaluation of the equivalent properties of Macro Fiber Composite (MFC) transducers using periodic homogenization. Int J Solids Struct 2010;47:3272–85. https://doi.org/10.1016/J.IJSOLSTR.2010.08.006.
[10] Park S, Inman DJ, Yun CB. An outlier analysis of MFC-based impedance sensing data for wireless structural health monitoring of railroad tracks. Eng Struct 2008;30:2792–9. https://doi.org/10.1016/J.ENGSTRUCT.2008.02.019.
[11] D.N. Betts University of Bath 1 Department of Mechanical Engineering, , Bath BA2 7AY, United Kingdom H.A. Kim University of Bath 1 Department of Mechanical Engineering, , Bath BA2 7AY, United Kingdom C.R. Bowen University of Bath 1 Department of Mechanical Engineering, , Bath BA2 7AY, United Kingdom D.J. Inman University of Michigan 2 Department of Aerospace Engineering, , Ann Arbor, Michigan 48109, USA Optimal configurations of bistable piezo-composites for energy harvesting Appl Phys Lett 100 11 2012 114104 10.1063/1.3693523.

[12] Konka HP, Wahab MA, Lian K. Piezoelectric fiber composite transducers for health monitoring in composite structures. Sens Actuators A Phys 2013;194:84–94. https://doi.org/10.1016/J.SNA.2012.12.039.
[13] Sreenivasa Prasath S, Arockiarajan A. Effective electromechanical response of macro-fiber composite (MFC): Analytical and numerical models. Int J Mech Sci 2013;77:98–106. https://doi.org/10.1016/J.IJMECSCI.2013.09.031.
[14] Nagendra Kumar D, Raja S, Ikeda T. Active vibration control of smart plates with partially debonded multilayered PZT actuators. Smart Mater Struct 2007;16:1584–94. https://doi.org/10.1088/0964-1726/16/5/012.
[15] Friswell MI, Ali SF, Bilgen O, Adhikari S, Lees AW, Litak G. Non-linear piezoelectric vibration energy harvesting from a vertical cantilever beam with tip mass. J Intell Mater Syst Struct 2012;23:1505–21. https://doi.org/10.1177/1045389X12455722.
[16] Smart Material n.d. https://www.smart-material.com/ (accessed March 6, 2022).
[17] Wang X, Morandini M, Masarati P. Velocity feedback damping of piezo-actuated wings. Compos Struct 2017;174:221–32. https://doi.org/10.1016/J.COMPSTRUCT.2017.04.016.
[18] Wu D, Huang L, Pan B, Wang Y, Wu S. Experimental study and numerical simulation of active vibration control of a highly flexible beam using piezoelectric intelligent material. Aerosp Sci Technol 2014;37:10–9. https://doi.org/10.1016/j.ast.2014.04.008.
[19] Przybylski J, Gasiorski G. Nonlinear vibrations of elastic beam with piezoelectric actuators. J Sound Vib 2018;437:150–65. https://doi.org/10.1016/J.JSV.2018.09.005.
[20] Xie C, Wu Y, Liu Z. Modeling and active vibration control of lattice grid beam with piezoelectric fiber composite using fractional order PDμ algorithm. Compos Struct 2018;198:126–34. https://doi.org/10.1016/j.compstruct.2018.05.060.
[21] Fallah N, Ebrahimnejad M. Active control of building structures using piezoelectric actuators. Appl Soft Comput 2013;13:449–61. https://doi.org/10.1016/J.ASOC.2012.08.010.
[22] Mayer D, Passive HS. Adaptive, Active Vibration Control, and Integrated Approaches. Vibration Analysis and Control in Mechanical Structures and Wind Energy Conversion Systems. IntechOpen 2017:1–23. https://doi.org/10.5772/INTECHOPEN.71838.
[23] Chai YY, Song ZG, Li FM. Active aerothermoelastic flutter suppression of composite laminated panels with time-dependent boundaries. Compos Struct 2017;179:61–76. https://doi.org/10.1016/j.compstruct.2017.07.053.
[24] Miao WK, Xu ML, Wu CS. In: Recent Advances in Structural Integrity Analysis - Proceedings of the International Congress (APCF/SIF-2014). Elsevier; 2014. p. 447–52.
[25] Rimašauskienė R, Jūrėnas V, Radzienski M, Rimašauskas M, Ostachowicz W. Experimental analysis of active–passive vibration control on thin-walled composite beam. Compos Struct 2019;223:110975. https://doi.org/10.1016/j.compstruct.2019.110975.
[26] Gawryluk J, Mitura A, Teter A. Dynamic control of kinematically excited laminated, thin-walled beam using macro fibre composite actuator. Compos Struct 2020;236:111898. https://doi.org/10.1016/j.compstruct.2020.111898.
[27] Zippo A, Ferrari G, Amabili M, Barbieri M, Pellicano F. Active vibration control of a composite sandwich plate. Compos Struct 2015;128:100–14. https://doi.org/10.1016/j.compstruct.2015.03.037.
[28] Danish B, Anilkumar PM, Rao BN. Suppression of cross-well vibrations of a bistable square cross-ply laminate using an additional composite strip. Int. J Dyn Control 2023;11. https://doi.org/10.1007/s40435-023-01153-1.
[29] Rezaei M, Talebitooti R, Liao WH, Friswell MI. Integrating PZT layer with tuned mass damper for simultaneous vibration suppression and energy harvesting considering exciter dynamics: An analytical and experimental study. J Sound Vib 2023;546:117413. https://doi.org/10.1016/J.JSV.2022.117413.
[30] Lee AJ, Xie A, Inman DJ. Suppression of cross-well oscillations for bistable composites through potential well elimination. J Vibr Acoust Trans ASME 2020;142:031003. https://doi.org/10.1115/1.4046123.
[31] Hao YX, Bai CP, Zhang W, Liu LT, Yang SW. Intrawell and interwell oscillations for bi-stable cross-ply laminates actuated by MFC under oscillating impulse voltages. Int J Non Linear Mech 2022;143:104025. https://doi.org/10.1016/j.ijnonlinmec.2022.104025.
[32] C. Li School of Mechanical Engineering, Jiangsu University of Science and Technology, Zhenjiang 212100, China L. Shen School of Mechanical Engineering, Jiangsu University of Science and Technology, Zhenjiang 212100, China J. Shao School of Mechanical Engineering, Jiangsu University of Science and Technology, Zhenjiang 212100, China J. Fang School of Mechanical Engineering, Jiangsu University of Science and Technology, Zhenjiang 212100, China Simulation and Experiment of Active Vibration Control Based on Flexible Piezoelectric MFC Composed of PZT and PI Layer Polymers (Basel) 15 8 2023 10.3390/polym15081819 1819.
[33] Lu Q, Wang P, Liu C. An analytical and experimental study on adaptive active vibration control of sandwich beam. Int J Mech Sci 2022;232:107634. https://doi.org/10.1016/J.IJMECSCI.2022.107634.
[34] Rimašauskienė R, Raza A, Mahato S. Actuation Performance of Macro Fibre Composite (MFC) as Actuator in Vibration Reduction of Cantilever Beams. Mechanics 2023;29(1):42–50.
[35] Savolainen J, Collan M. How Additive Manufacturing Technology Changes Business Models? – Review of Literature. Addit Manuf 2020;32:101070. https://doi.org/10.1016/J.ADDMA.2020.101070.
[36] Lazorenko G, Kasprzhitskii A. Geopolymer additive manufacturing: A review. Addit Manuf 2022;55:102782. https://doi.org/10.1016/J.ADDMA.2022.102782.
[37] Melnikova R, Ehrmann A, Finsterbusch K. 3D printing of textile-based structures by Fused Deposition Modelling (FDM) with different polymer materials. IOP Conf Ser Mater Sci Eng 2014;62:012018. https://doi.org/10.1088/1757-899X/62/1/012018.
[38] Tran P, Ngo TD, Ghazlan A, Hui D. Bimaterial 3D printing and numerical analysis of bio-inspired composite structures under in-plane and transverse loadings. Compos B Eng 2017;108:210–23. https://doi.org/10.1016/J.COMPOSITESB.2016.09.083.
[39] Tymrak BM, Kreiger M, Pearce JM. Mechanical properties of components fabricated with open-source 3-D printers under realistic environmental conditions. Mater Des 2014;58:242–6. https://doi.org/10.1016/J.MATDES.2014.02.038.
[40] García CR, Correa J, Espalin D, Barton JH, Rumpf RC, Wicker R, et al. 3D printing of anisotropic metamaterials. Prog Electromagn Res Lett 2012;34:75–82.
[41] Wang X, Jiang M, Zhou Z, Gou J, Hui D. 3D printing of polymer matrix composites: A review and prospective. Compos B Eng 2017;110:442–58. https://doi.org/10.1016/j.compositesb.2016.11.034.
[42] van de Werken N, Tekinalp H, Khanbolouki P, Ozcan S, Williams A, Tehrani M. Additively manufactured carbon fiber-reinforced composites: State of the art and perspective. Addit Manuf 2020;31:100962. https://doi.org/10.1016/J.ADDMA.2019.100962.
[43] Somireddy M, Singh CV, Czekanski A. Mechanical behaviour of 3D printed composite parts with short carbon fiber reinforcements. Eng Fail Anal 2020;107:104232. https://doi.org/10.1016/J.ENGFAILANAL.2019.104232.
[44] Ferreira RTL, Amatte IC, Dutra TA, Bürger D. Experimental characterization and micrography of 3D printed PLA and PLA reinforced with short carbon fibers. Compos B Eng 2017;124:88–100. https://doi.org/10.1016/J.COMPOSITESB.2017.05.013.
[45] Al Abadi H, Thai H-T, Paton-Cole V, Patel VI. Elastic properties of 3D printed fibre-reinforced structures. Compos Struct 2018;193:8–18.
[46] Oztan C, Karkkainen R, Fittipaldi M, Nygren G, Roberson L, Lane M, et al. Microstructure and mechanical properties of three dimensional-printed continuous fiber composites. J Compos Mater 2019;53(2):271–80.
[47] Naranjo-Lozada J, Ahuett-Garza H, Orta-Castañón P, Verbeeten WMH, Sáiz-González D. Tensile properties and failure behavior of chopped and continuous carbon fiber composites produced by additive manufacturing. Addit Manuf 2019;26:227–41. https://doi.org/10.1016/J.ADDMA.2018.12.020.
[48] Polymaker. PolyLite™ PLA technical data sheet 2017. https://c-3d.niceshops.com/upload/file/PolyLite_PLA_TDS_V3.pdf (accessed March 9, 2023).
[49] ColorFabb. ColorFabb (XT-CF20) technical datasheet 2022. https://colorfabb.com/media/datasheets/tds/colorfabb/TDS_E_ColorFabb_XT_CF20.pdf (accessed March 9, 2023).
[50] Toray composite materials America. T300 standard modulus carbon fiber technical data sheet 2018. https://www.rockwestcomposites.com/media/wysiwyg/T300DataSheet_1.pdf (accessed March 9, 2023).
[51] Maqsood N, Rimašauskas M. Tensile and flexural response of 3D printed solid and porous CCFRPC structures and fracture interface study using image processing technique. J Mater Res Technol 2021;14:731–42. https://doi.org/10.1016/J.JMRT.2021.06.095.
[52] Rimašauskas M, Kuncius T, Rimašauskienė R. Processing of carbon fiber for 3D printed continuous composite structures. Mater Manuf Process 2019;34:1528–36. https://doi.org/10.1080/10426914.2019.1655152.
[53] Maqsood N, Rimašauskas M. Development and fabrication of continuous carbon fiber reinforced thermoplastic porous composite structures with different infill patterns by using additive manufacturing. J Thermoplast Compos Mater 2022:1–26. https://doi.org/10.1177/08927057221088468/ASSET/IMAGES/LARGE/10.1177_08927057221088468-FIG12.JPEG.
[54] Maqsood N, Rimašauskas M. Characterization of carbon fiber reinforced PLA composites manufactured by fused deposition modeling. Composites Part C: Open Access 2021;4:100112. https://doi.org/10.1016/j.jcomc.2021.100112.
[55] Yao T, Wang Y, Wang Z, Qin C. Design and performance analysis of wave linear generator with parallel mechanism. Mech Sci 2021;12:405–17. https://doi.org/10.5194/MS-12-405-2021.
[56] Wu Q, Li W, Li J, Feng G, Zhang B. Electromagnetic-Thermal Analysis of High-Temperature Direct Drive Electric-Actuated Valve Canned Permanent Magnet Synchronous Motor. IEEJ Trans Electr Electron Eng 2023;18:105–19. https://doi.org/10.1002/tee.23703.
[57] Lashin MMA, Saleh WS, Alrowais F. Determination of Different Structures' Materials Natural Frequencies using Fuzzy Logic System. Int J Eng Adv Technol 2020;9(3):723–7.
[58] Miyashiro D, Taira H, Hamano R, Reserva RL, Umemura K. Mechanical vibration of single-walled carbon nanotubes at different lengths and carbon nanobelts by modal analysis method. Compos Part C: Open Access 2020;2:100028. https://doi.org/10.1016/J.JCOMC.2020.100028.

Title [A2]: An experimental study on the dynamic properties of 3D-printed structures with different layer orientations
Authors: Ali Raza, Rūta Rimašauskienė, Vytautas Jūrėnas, Marius Rimašauskas

Journal of Vibration Engineering & Technologies
https://doi.org/10.1007/s42417-024-01417-w

ORIGINAL PAPER

An Experimental Study on the Dynamic Properties of 3D-Printed Structures with Different Layer Orientations

Ali Raza[1] · Rūta Rimašauskienė[1] · Vytautas Jūrėnas[2] · Marius Rimašauskas[1]

Received: 6 July 2023 / Revised: 2 May 2024 / Accepted: 6 May 2024

Abstract
Purpose The PLA and PLA composites beam structures were manufactured using FDM technology to investigate the effect of layer orientations on the dynamic properties of the structure. The PLA composites consisted of PLA with short carbon fiber (PLA_SCF), and PLA with continuous carbon fiber (PLA_CCF).
Methods The deformation in each structure was obtained with a laser displacement sensor to estimate stiffness. The logarithmic decrement coefficient of each structure was calculated with laser displacement sensor, to examine the amplitude damping phenomena in structures. The Polytec 3D laser vibrometer was used to find out the amplitude spectrum and mode shapes, under dynamic loading conditions induced by the MFC patch. Moreover, the impact test was performed to measure the first natural frequency of each beam structure.
Results The results showed that structures with a 0°\0° layer orientation exhibited higher natural frequencies and stiffness compared to corresponding structures with a 0°\90° layer orientation. In the structures oriented at 0°\0°, both natural frequency and stiffness increased from PLA to PLA_SCF to PLA_CCF. While, when layers were oriented at 0°\90°, they increased from PLA_CCF to PLA to PLA_SCF.
Conclusion This research reveals how the dynamic properties of 3D-printed beam structures are influenced by two alternative layer orientations, 0°/0° and 0°/90°. The approaches employed in this study can be implemented in various types of 3D printed materials to investigate their dynamic characteristics.

Keywords FDM technology · PLA composites · Layer orientations · Dynamic properties · Stiffness · Natural frequency

Introduction

The creation of complicated structures with intricate geometries has been modified by 3D printing, which is also referred to as additive manufacturing technology [1]. Compared to traditional subtractive manufacturing techniques, additive manufacturing (AM) techniques create components layer-by-layer addition of material, some of which may be melted or cured. The key benefits of additive manufacturing (AM) technologies include their ability to fabricate components with complicated geometries and allow reduction of material waste. Fused Deposition Modelling (FDM) is one of the AM technologies that has received a lot of attention from the industrial, academic, and home sectors [2, 3]. 3D printers utilizing FDM, fabricate items by depositing filaments made of thermoplastic polymers that have been heated up to their melting point and extruded through nozzle [4]. This methodology makes it possible to design various structures with a variety of configurable features, making it a desirable option for several engineering applications [5]. Concerning the mechanical properties of 3D printed specimens, it should be noted that the mechanical characteristics of additively manufactured components are affected not only by the thermoplastic material but also by the printing settings such as layer height, layer orientations, filling density, temperature, and printing speed [6–8]. To maximize the performance and utility of AM structures in applications including vibration, resonance, and dynamic loading, it is essential to understand these factors [9]. Medel

✉ Ali Raza
ali.raza@ktu.edu

[1] Faculty of Mechanical Engineering and Design, Kaunas University of Technology, Studentų str. 56, Kaunas LT-51424, Lithuania

[2] Institute of Mechatronics, Kaunas University of Technology, Studentų str. 56, Kaunas LT-51424, Lithuania

Published online: 14 May 2024

et al. [10] used Laser Doppler Vibrometry (LDV) to assess the stiffness and damping behavior of 3D printed PLA rectangular prisms. The researchers investigated how printing parameters affected the dynamic and mechanical behavior of specimens made with various AM methods. The findings of the research can be used to identify optimal printing parameters for low damping ratios, resulting in improved inter-filament bonding. He et al. [5] investigated the influence of process variables (nozzle dimension, infill density, and layer orientation) on the damping characteristics of beam structure manufactured by material extrusion technique. The authors derived a mathematical model to illustrate how modal damping ratios and structural stiffness relate to one another. The findings indicate that a stiffer structure has a lower damping ratio. Overall, the study clarifies how 3D printing process variables affect the damping characteristics of cantilever beams made with MEX technology. Geng et al. [11] examined how printing variables influence the mechanical properties of 3D printed Polyphenylene Sulphide (PPS) specimens. The results showed that by changing the melt extrusion settings, PPS specimens' tensile and bending strengths are increased, and the inner gaps between neighboring filaments are also eliminated. Moreover, lowering the angle between the filament and load direction increases the tensile and bending strengths of PPS specimens with different filament orientations. Domingo-Espin et al. [12] studied the relationship between process parameters and the overall performance of FDM approach while manufacturing components for machinery and transport uses. The authors investigated the mechanical characteristics of polycarbonate using a dynamic mechanical setup, as well as a Taguchi technique and a statistical analysis of variance to determine the effect of factors on such mechanical characteristics. Maqsood et al. [6] reported a study how the controlled cooling and printing parameters affect the integrity and mechanical characteristics of CCFRPC. It emphasizes the critical need to select optimal printing parameters to achieve the maximum levels of tensile and flexural strength in composite structures. The findings of this study provide useful information for professionals engaged in additive manufacturing of composite structures, allowing them to enhance both the overall integrity and mechanical characteristics of the final product. Raza et al. [13] using FEM analysis in the ANSYS platform, the dynamic properties of the different composite beams were studied separately. The Macro fiber composite (MFC-8507 P2 type) was embedded with each beam structure to calculate the percentage amplitude reduction and RMS in each beam structure. Baqasah et al. [14] investigated 3D printed beam specimens made of ABS, examining their characteristics and response under dynamic loading conditions combined with temperature effects. The study involved the analysis of dynamic behavior, including natural frequencies and their respective amplitudes, as well as crack growth and crack penetration assessment. These aspects were studied through a combination of experimental, theoretical, and numerical approaches. The results of the study demonstrated that these approaches can be effectively employed as in-situ damage analysis tools to estimate crack penetration depth in ABS when subjected to dynamic loading conditions in conjunction with temperature variations. Afonso et al. [15] studied how the extrusion temperature and the printing speed affect the mechanical characteristics and weight of PLA products. The authors were successful in formulating mathematical models that accurately predicted the observed results. This study demonstrates the efficacy of using a systematic experimental design technique to develop mathematical equations-based predictive models that can be employed across several responses while keeping a consistent specimen structure Renganathan et al. [16] examined the friction characteristics of PLA samples printed using two distinct rates, 20 mm/s and 50 mm/s and three distinct fill patterns concentric, linear, and Hilbert. According to the study, printing configurations have an influence on the wear rate and friction coefficient. The findings indicate that a fill pattern printed at an optimal speed result in strong bonding between the layers and raster as well increases crystallinity for higher wear resistance. Wang et al. [17] carried out various experiments to examine the impact of diverse printing configurations such as printing temperature, speed, and layer thickness, on the mechanical characteristics, microstructure, and surface quality of 3D printed PEEK samples. The findings reveal that 3D printing with appropriate printing settings results in enhanced adhesion between layers and infill filaments, reduced surface roughness, decreased internal defects, and increased density of PEEK parts. Raza et al. [18] conducted a comprehensive study on 3D printed beam structures made from various materials. The study aimed to explore the dynamic characteristics of these structures and assess their ability to suppress vibrations. Specifically, the vibration suppression effect, with the integration of MFC actuator in the structures, has been thoroughly investigated. The results demonstrated that substantial vibration suppression was observed in the 3D printed structures. Taşcıoğlu et al. [19] conducted research on optimizing the printing factors and post-treatment techniques, to enhance the surface and structural quality of 3D manufactured PLA specimens. Layer thickness was found to be the most critical factor in influencing surface and structural (dimensional) quality in both 3D printed and post-treated PLA specimens. The printing temperature and the duration of the post-treatment procedure both have a considerable impact on the structural accuracy and surface quality of the fabricated specimen, respectively. He et al. [20] carried out

an experimental study on 3D printed beams fabricated using ABS material to examine their bending fatigue response under thermos-mechanical loading conditions. The specimens were manufactured with three distinct layer patterns: 0°, +45°/-45°, and 90°, as well as various printing settings, including nozzle sizes and layer thicknesses. The objective of the investigation was to determine the optimal layer pattern and printing settings that would result in exceptional fatigue resistance for the ABS beams. Kumar et al. [21] investigated the dynamic mechanical characteristics of PC/ABS composite specimens manufactured using the FFF technique. The study examines how the dynamic mechanical characteristics are affected by modifying the FFF process parameters as well as introducing TBBA and MCC substances into the PC/ABS material. Compared to undiluted PC /ABS material, the inclusion of TBBA and MCC substances considerably enhances the dynamic mechanical characteristics of the PC / ABS composite. Almutairie et al. [22] carried out a comparative investigation on 3D printed beams made from two distinct materials: ABS and PETG. This investigation examines the dynamic fatigue behavior of ABS and PETG beams when exposed to diverse thermal loading criteria. The beams were fabricated using customized layer angles of 45°, 60°, and 90° between the layers, using numerous printing settings. Additionally, the findings revealed that both the customized layer angles and temperature significantly influence the characteristics of ABS and PETG.

After a detailed examination of the available literature, the authors have concluded that most researchers have only investigated the impact of 3D printing process settings on the mechanical response of structures. Consequently, it is necessary to examine the impact of printing settings on dynamic characteristics (natural frequencies, bending mode shapes, decrement coefficient, damping and deformation). In this current work, beam structures made of PLA, PLA-SCF, and PLA_CCF are created using fused deposition modeling (FDM) with two distinct layer orientations (0°\0° and 0°\90°). The impact of these orientations on the dynamic features of the structures is investigated through various experiments.

Table 1 Printing settings for beam structures

Settings	Original Prusa		MeCreator-2
	PLA	PLA_SCF	PLA_CCF
Nozzle size	0.4 mm	0.4 mm	1.5 mm
Extrusion multiplier	1	1	0.7
Layer height	0.15 mm	0.15 mm	0.5 mm
Extrusion width	0.45 mm	0.45 mm	1.2 mm
Extruder temperature	215	260 ˚C	210 ˚C
Printing speed	25 mm/s	25 mm/s	3.0 mm/s
Bed temperature	60 ˚C	75 ˚C	90 ˚C
Fan speed	50%	30%	60%
filling density	100%	100%	100%
Printing orientation	0°/0° & 0°/90°	0°/0° & 0°/90°	0°/0° & 0°/90°

Materials and Methods

The dynamic characterizations of 3D printed beam structures such as PLA and PLA composites (PLA-SCF and PLA_CCF) with layer orientations 0°\0° and 0°\90° are studied separately. The following tests were carried out to investigate dynamic characterizations: modal analysis, impact test, calculation of decrement coefficient and deformation in each structure with the effect of applied weight.

Materials

To fabricate PLA beam structures, a filament with a size of 1.75 mm and a density of 1.24 g/cm³, produced by Polymaker, was utilized [23]. For PLA-SCF, a filament with a size of 1.75 mm and a density of 1.35 g/cm³, produced by ColorFabb, was employed [24]. Additionally, for PLA-CCF structures, PLA from Polymaker served as the matrix material, while T300B-3000 tow of carbon fibers, with a density of 1.76 g/cm³ and individual fiber diameter of 7 µm, produced by Toray Composite Materials, was used [25]. The CCF tow cannot be used directly for 3D printing. Thus, CCF tow must be impregnated before printing. Researchers comprehensively described this process in the article [26].

Preparation of Samples

In the current investigation, PLA, PLA_SCF, and PLA_CCF beam structures of size 120 mm×20 mm×1.35 mm were manufactured using fused deposition modelling (FDM) technology. The beam structures with layer orientations of 0°\0° and 0°\90° were prepared separately to investigate the influence of these layer orientations on dynamic characteristics of beam structures. The specific printing settings for the beam structures have been summarized in Table 1. The fabrication of PLA and PLA_SCF samples involved the use of an Original Prusa 3D printer (Model: MK 3 S & i3 MK3S+). This procedure includes loading the PLA or PLA/SCF filament onto the holder of the printer and feeding it through the extruder as per the manufacturer's guidelines. Prior to commencing the printing process, both the bed and extruder of the printer are preheated to the necessary degrees Celsius. This 3D printer operates on the principles of FDM, where layers are deposited one over the other to construct a 3D object. Central to this technique is the moderated thermoplastic extrusion from the nozzle. Upon completion of the printing task, the specimen remained on the bed to cool. The development of a PLA_CCF specimen was conducted

with a customized MeCreator-2 printer. Two separate paths were established for the PLA filament and the impregnated CCF tow. The drive wheel facilitated the transportation of the PLA to the extrusion head, whereas the CCF was fed directly to the printing nozzle through it. PLA underwent melting to create bonding with CCF before it was extruded through the nozzle onto a borosilicate glass bed [18, 27]. The process of fabricating samples is depicted in Fig. 1.

Deformation Under Point Load

The experimental setup shown in Fig. 2 was used to observe the deformation in beam structures with 0°\0° and 0°\90° layer orientations individually. The beam structure was fixed from one end and various static point laods were applied on the free end side of each structure, as presented in Fig. 3. The deformation in each structure was measured with a laser displacement sensor (LK-G82).

Logarithmic Decrement Coefficient Measurement

A new experimental approach, as shown in Fig. 4, has been used to determine the logarithmic decrement coefficient of each structure with layer orientations of 0°\0° and 0°\90°. The arrangement was especially created for observing the exponential damped response in each structure caused by an electrodynamic shaker (DDR-11,077), manufactured by VEB Robotron-Messelektronik Otto Schon, German and the response was measured at the one point from free end by a laser displacement sensor (LK-G82) made by Keyence Corporation, Japan. The structure was fixed from one side and vibrations in the structure were introduced by electro-dynamic shaker from fixed side as indicated schematically in Fig. 5. The burst signal of 50mV amplitude as input was provided to the electromagnetic shaker by the function / arbitrary waveform generator (33,220 A) built in Agilent, Malaysia. The decrement coefficient in each structure has been calculated using the following expression [28].

$$\delta = \ln\left(\frac{U_n}{U_{n+m}}\right)/m \tag{1}$$

Where:

U_n = amplitude at time t_n
U_{n+m} = amplitude at time t_{n+m}
m= number of cycles

Modal Analysis Testing

The setup shown in Fig. 6 has been utilized to obtain the natural frequencies, mode shapes, and amplitude of respective mode shapes of beam structures with 0°\0° and 0°\90° infill pattern separately. The MFC (M8507-P2) actuator

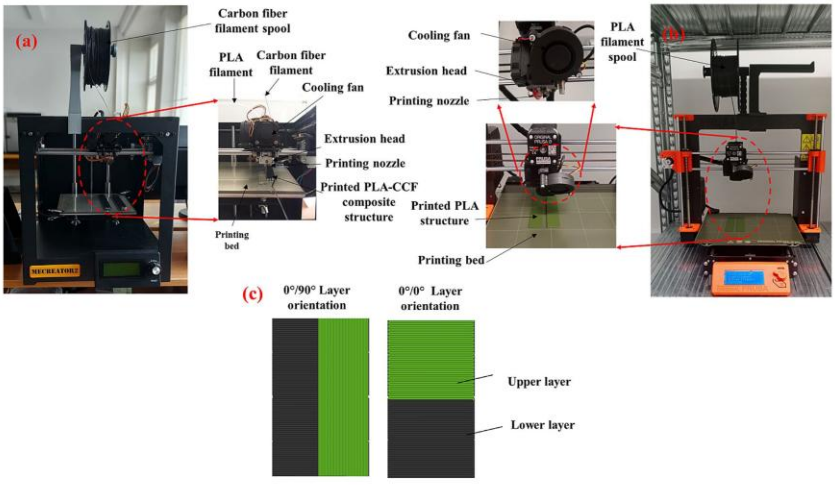

Fig. 1 Fabrication process of beam structures: **a**) fabrication of PLA_CCF, **b**) fabrication of PLA and PLA_SCF, **c**) 0°\ 0° and 0°\90° layer orientations

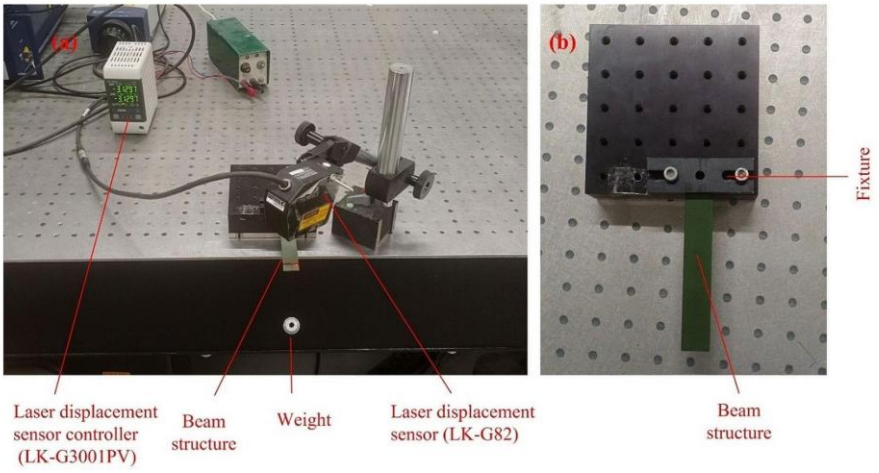

Fig. 2 Deformation measurement in beam structures: (**a**) experimental setup; (**b**) fixation of beam structure

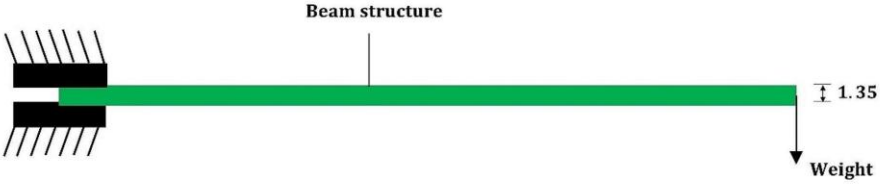

Fig. 3 Schematic of beam structure with point weight at free end

with beam structure at 5 mm from the fixed end of the structure, has been schematically shown in Fig. 7. The vibrations in each beam were generated by an MFC patch by providing 100 V chirp signal, and a Polytec 3D laser vibrometer (PSV-500, GmbH, Germany) was used to measure observations at the single point (free side) of the structure.

Impact Testing

An impact test is a quick and easy method for estimating the first natural frequencies in structures. The beam structure was fixed in a fixture and the vibrations in the structure were caused by impacting the free end of the structure with a relatively small object, as shown in Fig. 8. The exciting response of each structure was measured by a laser displacement sensor (LK-G82).

Result and Discussion

To thoroughly examine each beam structure, deformation in beam structures under point load, the logarithmic decrement coefficient to estimate amplitude damping of beam structures, the impact test to estimate the initial natural frequencies and the modal analysis test to identify natural frequencies and mode shapes at respective frequencies, have all been thoroughly discussed in this article.

Calculation of Deformation Under Point Load

Table 2 summarizes the deformation in structures with 0°\0° and 0°\90° layer orientations, subjected to point load. Deformation in structures increases linearly with increasing point load, as shown in Fig. 9. The maximum deformation is observed in PLA_CCF structure with 0°\90° layer

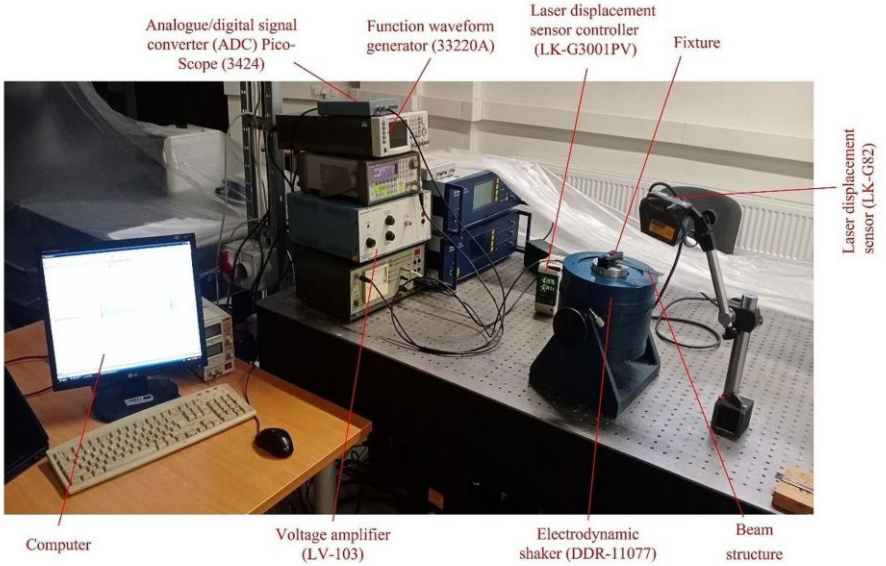

Fig. 4 Logarithmic decrement coefficient measurement

Fig. 5 Schematic view of vibration in beam structure by electromagnetic shaker

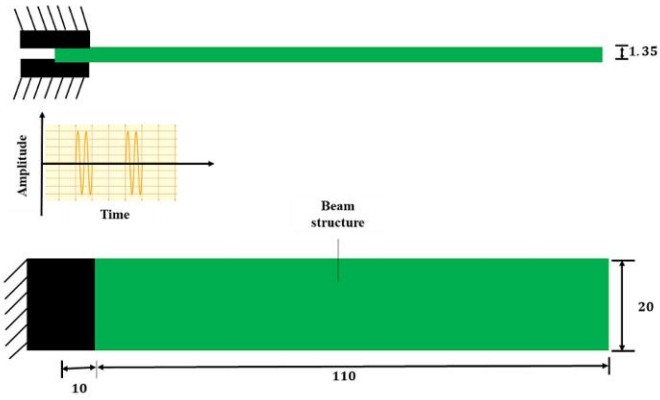

orientation, 5.02 mm, and the minimum deformation is found in PLA_CCF structure with 0°\0° layer orientation, 0.78 mm under the point load of 8 g. The deformations in beam structures with 0°\90° layer orientation have been found more compared to their corresponding structures with 0°\0° orientation. PLA structures oriented with 0°\0° and 0°\90° exhibit nearly similar deformations, measuring 2.72 mm and 2.79 mm, respectively, under 8 g load, as presented in Fig. 9. It appears that with a further increase in load, the deformation in both structures will be similar.

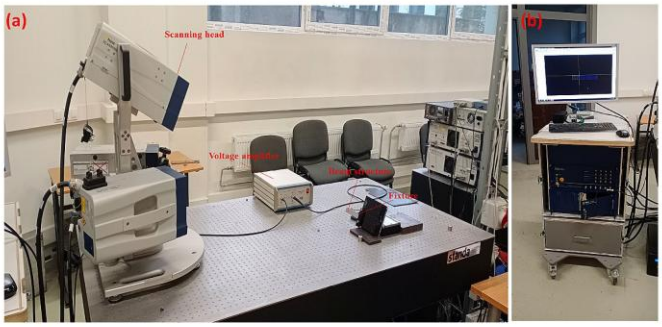

Fig. 6 Polytec 3D laser vibrometer: **a**) Scanning heads for modal analysis; **b**) data organizing system

Fig. 7 Diagram illustrating a beam structure incorporating MFC

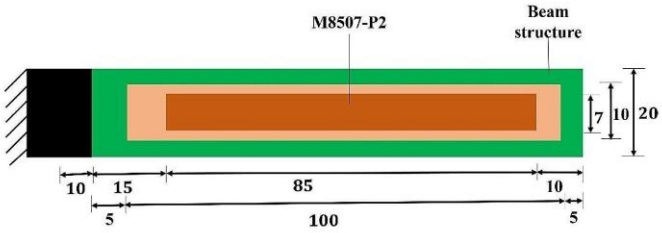

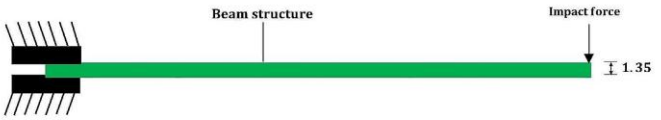

Fig. 8 Schematic view of impact force at free end of beam structure

Table 2 Deformation with weight in beam structures with 0°\0° and 0°\90° layer orientations

Weight (g)	0°\0° PLA (mm)	0°\90° PLA (mm)	0°\0° PLA_SCF (mm)	0°\90° PLA_SCF (mm)	0°\0° PLA_CCF (mm)	0°-90° PLA_CCF (mm)
2	0.72	0.80	0.33	0.59	0.20	1.27
4	1.37	1.44	0.67	1.06	0.39	2.52
6	2.05	2.11	1.00	1.57	0.59	3.77
8	2.72	2.79	1.34	2.08	0.78	5.02

The amount of deflection produced by the load on the material is generally described as the stiffness of the material. The experimental results (see Fig. 9) indicate that with a layer orientation of 0°/0°, the stiffness increases from PLA to PLA_SCF to PLA_CCF, while with a 0°\90° layer orientation, it increases from PLA_CCF to PLA to PLA_SCF.

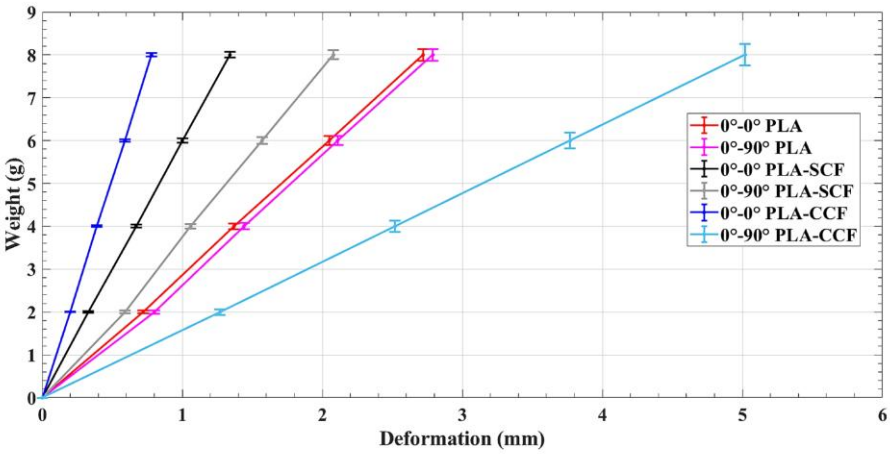

Fig. 9 Deformation in beam structures under point load

Table 3 Decrement coefficients of beam structures with 0°\0°and 0°\90° layer orientations

Beam structures	0°\0° layer orientation	0°\90° layer orientation
PLA	0.043	0.041
PLA-SCF	0.081	0.052
PLA_CCF	0.214	0.040

Calculation of Log Decrement Coefficient

The logarithmic decrement indicates how quickly the amplitude of a free damped vibration decreases, which generally represents the damping properties. It is described as the natural logarithmic ratio of the preceding amplitudes.

In the current study, the decrement coefficient of each structure was determined by taking the first five successive peak amplitudes i.e., U_n to U_{n+4} (4 cycles), as represented in Fig. 10(a). The vibrating periodic amplitudes of beam structures were recorded by a laser displacement sensor, as given in Fig. 10(b) through 10(g). In scenario of 0°\0° layer orientation, the vibrating amplitude of PLA_CCF (see Fig. 10(f)) abruptly drops and begins to fluctuate between −90 nm and +90 nm at 2 s, then continues to decline. The vibrating amplitudes of PLA (see Fig. 10(b)) and PLA_SCF (see Fig. 10(d)) progressively decline and begin to oscillate between −230 µm and +220 µm and −49 µm to +48 µm at 2 s, respectively and further decrease with time. Table 3 describes the decrement coefficient values for each beam structure. According to Eq. (1), the decrement coefficient values for PLA, PLA_SCF and PLA_CCF are 0.043,0.081 and 0.214, respectively. As a result of 0°\0° layer orientation, the vibration amplitude damping effect was observed maximum in PLA_CCF followed by PLA_SCF and PLA structures.

Whereas, in case of 0°\90° layer orientation, the vibrating amplitudes of PLA (see Fig. 10(c)), PLA-SCF (see Fig. 10(e)) and PLA_CCF (see Fig. 10(g)) progressively decline and start fluctuating between −273 µm and +280 µm, -150 µm to +149 µm and −207 µm to +197 µm respectively and further reduce over time. Based on Eq. 1, the decrement coefficients for the PLA, PLA-SCF, and PLA_CCF are 0.041, 0.052, and 0.040, respectively. Consequently, PLA_SCF had maximum amplitude damping effect, whereas PLA and PLA_CCF structures had amplitude damping effects that were quite close to one another. In structures oriented at 0°\0°, the layers are stacked immediately on top of each other in the vertical direction, resulting in strong interlayer bonding. Conversely, in 0°\90° oriented structures, the layers are stacked such that they are perpendicular to each other, leading to comparatively weaker layer bonding. Additionally, previous research has demonstrated that 0°\0° oriented structures are stiffer compared to their 0°\90° counterparts and proven stiffer materials exhibit more damping characteristics [13, 18]. Therefore, 0°\0° structures exhibit greater damping properties compared to corresponding 0°\90° beam structures.

Calculation of Natural Frequencies and Mode Shapes

This section of the article is focused on determining the natural frequencies and mode shapes of beam structures with

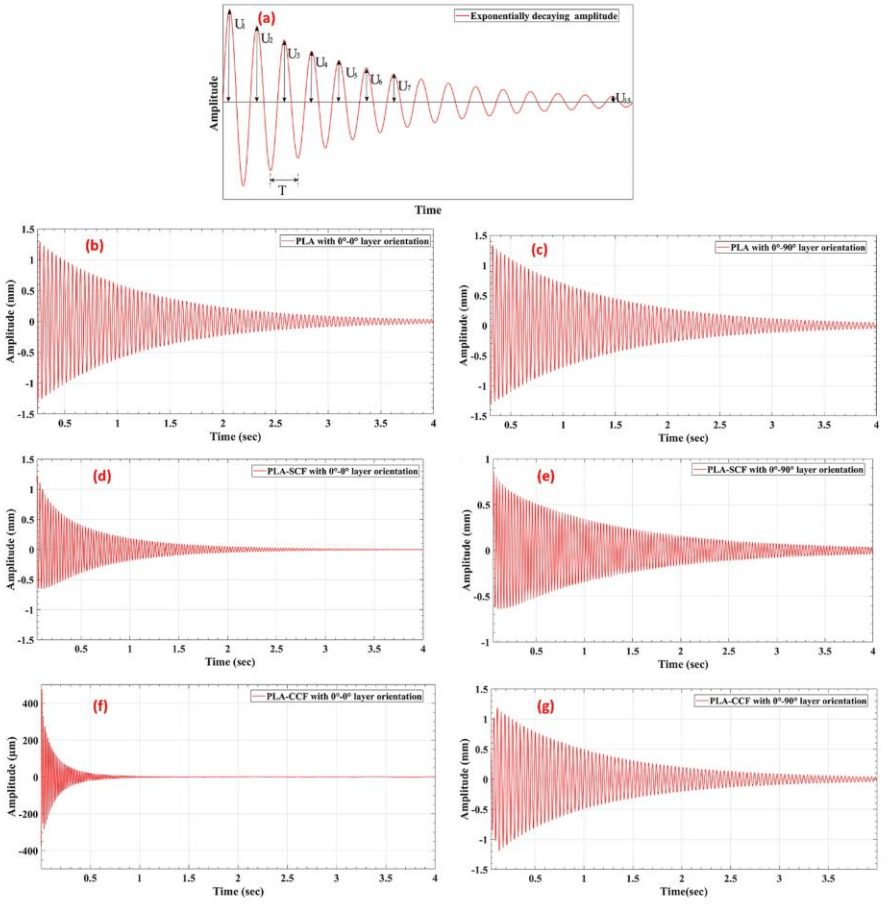

Fig. 10 Amplitude damping of PLA, PLA_SCF and PLA_CCF beam structures: (**a**) exponentially decaying amplitude trend; (**b**) 0°\0° PLA; (**c**) 0°\90° PLA; (**d**) 0°\0 PLA_SCF; (**e**) 0°\90° PLA_SCF; (**f**) 0°\0° PLA_CCF; (**g**) 0°\90° PLA_CCF

0\0°and 0°\90° layer orientations. The first four natural frequencies of the bending modes are summarized in Table 4. The weight and stiffness of each beam structure increases dramatically with the M8507-P2 patch, which causes the natural frequencies of the beam to differ from the real beam structure. Table 4 indicates that the natural frequencies of beam structures with 0°\0° layer orientation are comparatively higher than the respective structures with 0°\90° layer orientation. The mechanical characteristics of the material, such as its weight and stiffness, assess its natural frequencies. High natural frequencies (f) are believed to be present in structures with high stiffness (k) and light mass (m), according to Eq. (2) [13, 29, 30].

$$f = \frac{\sqrt{k/m}}{2\pi} \tag{2}$$

Moreover, the initial four bending mode shapes of the beam structures at their respective frequencies are presented in Fig. 11. According to modal testing findings (see Table 4), the 0°\0° oriented structures exhibited higher natural frequency values than their corresponding 0°\90° oriented structures. Researchers have experimentally validated that natural (inherent) frequency of the stiffer materials is always greater than that of low stiffness materials [13, 18]. Among 0°\0° oriented structures, PLA_CCF has the highest frequency, PLA_SCF has the intermediate, and PLA has the lowest frequency, whereas for 0°\90°oriented structures, PLA_SCF has the highest frequency, PLA, and PLA_CCF have the intermediate and lowest frequency, respectively.

Figure 12 (a) and 12 (b) show the average amplitude spectrum of beam structures with 0°\0° and 0°\90° layer orientations, respectively. Table 4 illustrates the vibration amplitudes of structures at respective frequencies. According to the findings, the vibration amplitude is highest at the first natural frequency and lowest at the fourth natural frequency. For PLA, PLA_SCF, and PLA_CCF with a 0°\0° layer orientation, the vibration amplitudes are observed 9.295 µm at 30 Hz, 6.831 µm at 40.5 Hz, 4.139 µm at 60 Hz and at fourth natural frequencies, they are 0.129 µm at 1207.5 Hz,0.049 µm at 1545.8 Hz, 0.022 µm at 2190 Hz, respectively.

However, with 0°\90° layer orientation, at first natural frequencies the amplitudes of PLA, PLA_SCF, and PLA_CCF are 10.924 µm at 27.5 Hz, 9.733 µm at 28.8 Hz, 10.110 µm at 26.6 Hz and, at fourth natural frequencies, 0.152 µm at 1157.5 Hz, 0.111 µm at 1193.8 Hz, and 0.121 µm at 1114.1 Hz are noted respectively.

Estimation of First Natural Frequency by Impact Test

The purpose of this testing was to find out the first natural frequency of each structure without MFC patch (only actual beam). Applying the impact force to the free end of the beam structure caused vibrations, which were then monitored using a laser displacement sensor (LK-G82). To determine the average value of each structure, the experiment was repeated three times and findings are reported in Table 5. Impact responses of structures made from various materials depend on several aspects, such as material properties (both the matrix and reinforcing elements), structure layout, the number of layers in structures, and the impact force [31]. It has been proven that 0°/0° layout structures are stiffer than corresponding 0°/90° layout structures, and stiffer structures have a higher initial natural frequency [13, 18]. Thus, the findings demonstrate that specimens with 0°\0° layout have substantially higher first natural frequency than 0°\90° layout specimens. Additionally, the increase in the first natural frequency for the 0°\0° and layer orientation specimens exhibit a trend like that found in the modal analysis test. However, the values of the first natural frequency obtained by the modal testing are significantly higher than the impact test, except for the PLA_SCF with the 0°\90° layer orientation, where the modal testing value (28.8 Hz) is lower than the impact test value (30.62 Hz). The beam structure with the MFC patch exhibits a different frequency than the actual beam due to the change in stiffness caused by the addition of the MFC patch.

Conclusion

In this article PLA, PLA_SCF and PLA_CCF specimens were manufactured using FDM technology. Each specimen was prepared with two distinct orientations: 0°\0° and 0°\90° separately. Calculation of the decrement coefficient, modal testing, and deformation in structures under various point loads are carried out to investigate the influence of distinct orientations on dynamical characteristics of beam structures. The following conclusions were derived from this investigation.

1. Under various static point loads, the structures oriented at 0°\90° show higher deformations than corresponding 0°\0° oriented structures. However, deformation in PLA specimens oriented at 0°\0° and 0°\90° is almost equal, measuring 2.72 mm and 2.79 mm, respectively, under a maximum point load of 8 g.
2. 2.In case of 0°\0° oriented beam structures, the decrement coefficients for the PLA, PLA_SCF, and PLA_CCF are 0.043, 0.081, and 0.214, respectively. Thus, the vibration damping effect was observed maximum in PLA_CCF followed by PLA_SCF and PLA. While in 0°\90° oriented structures, the PLA, PLA_SCF, and PLA_CCF have corresponding decrement coefficients of 0.041, 0.052, and 0.040. PLA_SCF showed maximum damping effect, whereas PLA and PLA_CCF structures had amplitude damping effects that were quite close to each other.
3. The initial four frequencies of the bending mode are recorded during the modal testing, and it is noted that the beam structures with 0°\0° orientation have higher natural frequencies than the corresponding 0°\90° oriented structures. The initial four bending mode frequencies of PLA, PLA_SCF and PLA_CCF vary from 30 Hz to 1207.5 Hz, 40.5 Hz to 1545.8 Hz, and 60 Hz to 2190 Hz in 0°\0° oriented structures respectively. While in 0°\90° oriented structures, the values range from 27.5 Hz to 1157.5 Hz, 28.8 Hz to 1193.8 Hz, and 26.6 Hz to 1114.1 Hz, respectively.

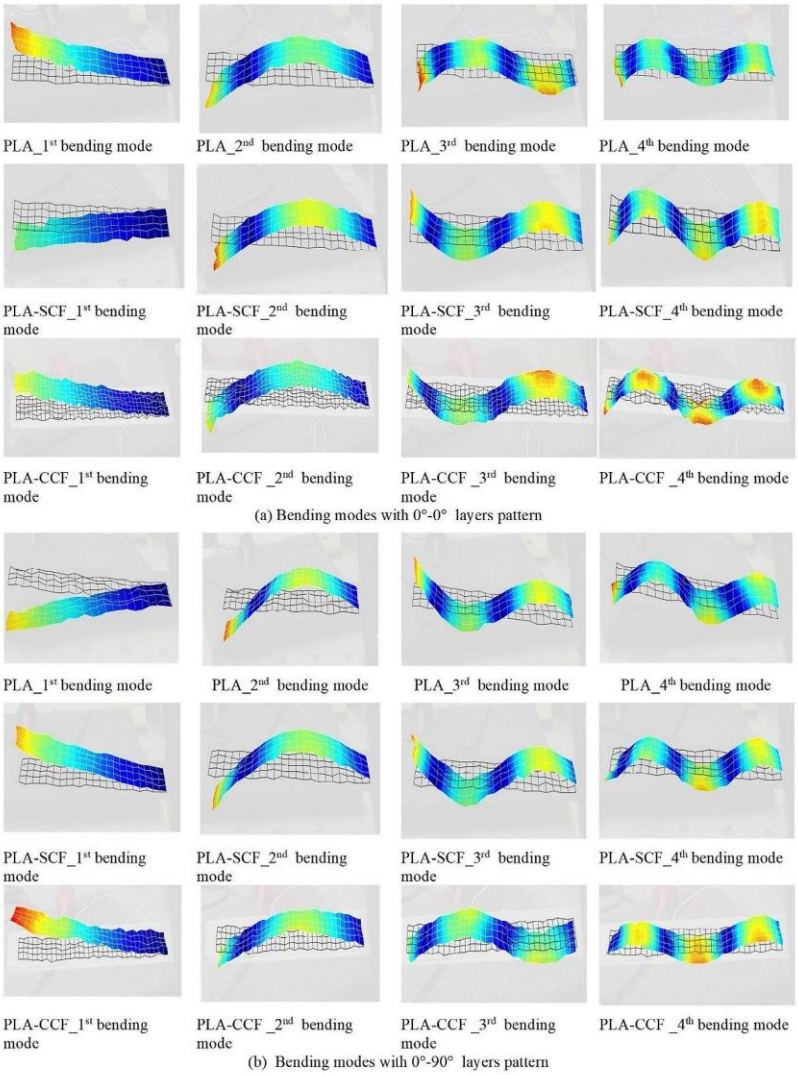

Fig. 11 Initial four bending mode shapes of PLA, PLA_SCF and PLA_CCF beam structures : **a**) bending mode shapes with 0°\0° orientation ; **b**) bending mode shapes with 0°\90° orientation

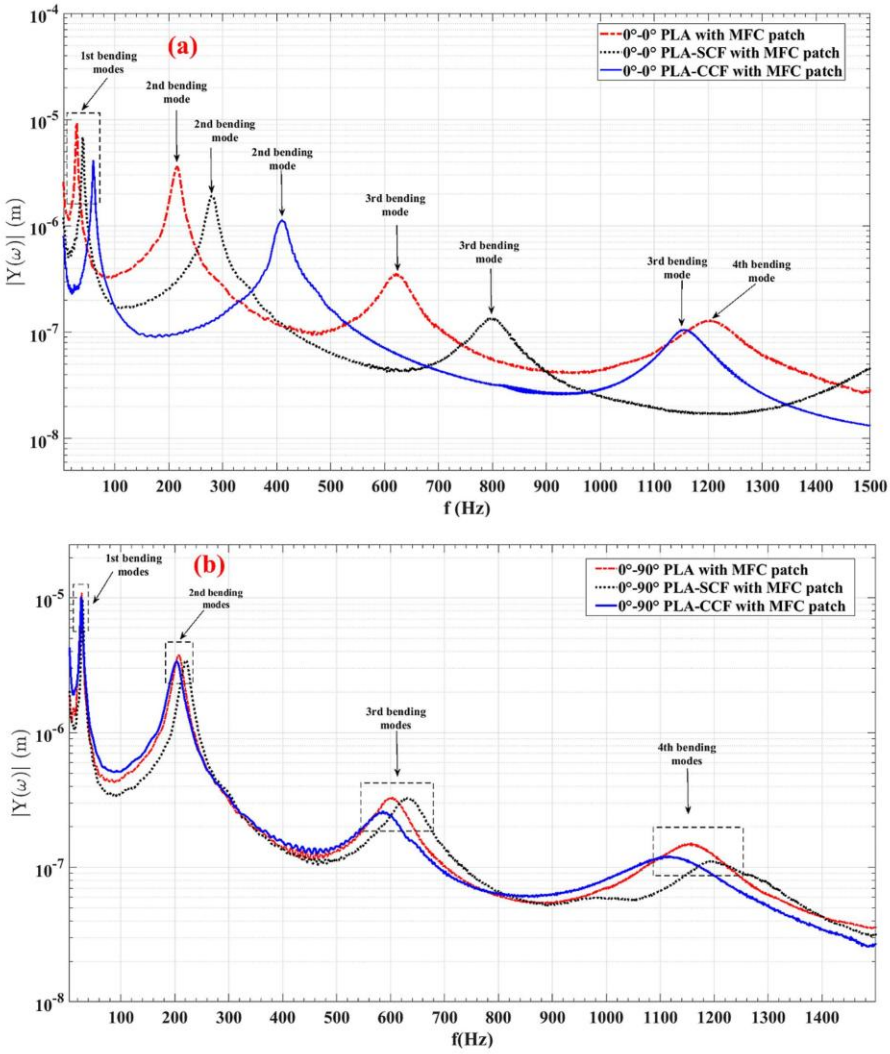

Fig. 12 Average amplitude spectrum of PLA, PLA_SCF and PLA_CCF beam structures: (**a**) 0°\0° oriented (**b**) 0°\90° oriented

Table 4 Natural frequency and amplitude of additive manufactured beam structures

Modes	PLA				PLA_SCF				PLA_CCF			
	0°\0° layer orientations		0°\90° layer orientations		0°\0° layer orientations		0°\90° layer orientations		0°\0° layer orientations		0°\90° layer orientations	
	Frequency (Hz)	Amplitude (µm)	Frequency (Hz)	Amplitude (µm)	Frequency (Hz)	Amplitude (µm)	Frequency (Hz)	Amplitude (µm)	Frequency (Hz)	Amplitude (µm)	Frequency (Hz)	Amplitude (µm)
1st Bending Mode	30.0	9.295	27.5	10.924	40.5	6.831	28.8	9.733	60.0	4.139	26.6	10.110
2nd Bending Mode	215.0	3.602	207.5	3.753	280.5	1.911	221.3	3.437	410.0	1.131	203.1	3.375
3rd Bending Mode	626.3	0.349	603.8	0.330	802.3	0.136	635.0	0.327	1153.1	0.110	592.2	0.255
4th Bending Mode	1207.5	0.129	1157.5	0.152	1545.8	0.049	1193.8	0.111	2190.0	0.022	1114.1	0.121

Table 5 Natural frequencies of beam structures by impact test

Beam structures	frequency of 0°\0° oriented structures (Hz)	frequency of 0°\90° oriented structures (Hz)
PLA	26.54	25.95
PLA_SCF	39.31	30.62
PLA_CCF	58.87	25.65

4. The first natural frequencies of actual beams (without patch) with 0°\0° and 0°\90° layer orientations were measured by impact test and noted that the values of first natural frequencies of beam structures (with patch) obtained by modal testing are significantly higher than those of the impact test, except for the PLA_SCF with the 0°\90° layer orientation.
5. The article's findings confirm that a structure with a high natural frequency and low deformation under point load exhibits high stiffness. In a 0°\0° oriented structures, the stiffness increases from PLA to PLA_SCF to PLA_CCF, whereas in 0°\90° oriented structures, it increases from PLA_CCF to PLA to PLA_SCF.

Declarations

Conflict of Interest The authors declare no conflicts of interest.

References

1. Ngo TD, Kashani A, Imbalzano G et al (2018) Additive manufacturing (3D printing): a review of materials, methods, applications and challenges. Compos B Eng 143:172–196. https://doi.org/10.1016/J.COMPOSITESB.2018.02.012
2. Turner BN, Strong R, Gold SA (2014) A review of melt extrusion additive manufacturing processes: I. process design and modeling. Rapid Prototyp J 20:192–204. https://doi.org/10.1108/RPJ-01-2013-0012
3. Turner BN, Gold SA (2015) A review of melt extrusion additive manufacturing processes: II. Materials, dimensional accuracy, and surface roughness. Rapid Prototyp J 21:250–261. https://doi.org/10.1108/RPJ-02-2013-0017
4. Mohamed OA, Masood SH, Bhowmik JL (2015) Optimization of fused deposition modeling process parameters: a review of current research and future prospects. Adv Manuf 3:42–53. https://doi.org/10.1007/S40436-014-0097-7
5. He F, Ning H, Khan M (2023) Effect of 3D Printing process parameters on damping characteristic of Cantilever beams fabricated using material extrusion. Polymers 15:257. https://doi.org/10.3390/POLYM15020257
6. Maqsood N, Rimašauskas M (2022) Influence of printing process parameters and controlled cooling effect on the quality and mechanical properties of additively manufactured CCFRPC. Compos Commun 35:101338. https://doi.org/10.1016/J.COCO.2022.101338
7. Maqsood N, Rimašauskas M (2023) Development and fabrication of continuous carbon fiber reinforced thermoplastic porous composite structures with different infill patterns by using additive

manufacturing. J Thermoplast Compos Mater 36:2050–2075. https://doi.org/10.1177/08927057221088468
8. Chacón J, Caminero M, García-Plaza E et al (2017) Additive manufacturing of PLA structures using fused deposition modelling: Effect of process parameters on mechanical properties and their optimal selection. Mater Des 124:143–157. https://doi.org/10.1016/j.matdes.2017.03.065
9. Medel F, Esteban V, Abad J (2021) On the use of laser-scanning vibrometry for mechanical performance evaluation of 3D printed specimens. Mater Des 205:109719. https://doi.org/10.1016/j.matdes.2021.109719
10. Medel F, Abad J, Esteban V (2022) Stiffness and damping behavior of 3D printed specimens. Polym Test 109:107529. https://doi.org/10.1016/J.POLYMERTESTING.2022.107529
11. Geng P, Zhao J, Gao Z et al (2021) Effects of Printing parameters on the Mechanical properties of High-Performance Polyphenylene Sulfide Three-Dimensional Printing. 3D Print Addit Manuf 8:33–41. https://doi.org/10.1089/3dp.2020.0052
12. Domingo-Espin M, Borros S, Agullo N et al (2014) Influence of Building parameters on the Dynamic Mechanical properties of Polycarbonate fused deposition modeling parts. 3D print. Addit Manuf 1:70–77. https://doi.org/10.1089/3dp.2013.0007
13. Raza A, MAHATO S, Rimašauskienė R (2023) Actuation performance of Macro Fibre Composite (MFC) as actuator in vibration reduction of Cantilever beams. Mechanics 29:42–50. https://doi.org/10.5755/j02.mech.31732
14. Baqasah H, He F, Zai BA et al (2019) In-situ dynamic response measurement for damage quantification of 3D printed ABS cantilever beam under thermomechanical load. Polym (Basel) 11. https://doi.org/10.3390/polym11122079
15. Afonso JA, Alves JL, Caldas G et al (2021) Influence of 3D printing process parameters on the mechanical properties and mass of PLA parts and predictive models. Rapid Prototyp J 27:487–495. https://doi.org/10.1108/RPJ-03-2020-0043
16. Renganathan S, D S (2022) Effect of fill pattern and printing speed on friction characteristics of FDM printed polylactic acid polymer. Adv Mater Process Technol 8:1583–1592. https://doi.org/10.1080/2374068X.2021.1948707
17. Wang P, Zou B, Xiao H et al (2019) Effects of printing parameters of fused deposition modeling on mechanical properties, surface quality, and microstructure of PEEK. J Mater Process Technol 271:62–74. https://doi.org/10.1016/j.jmatprotec.2019.03.016
18. Raza A, Rimašauskienė R, Jūrėnas V, Mahato S (2023) Experimental investigation of vibration amplitude control in additive manufactured PLA and PLA composite structures with MFC actuator. Eng Struct 294:116802. https://doi.org/10.1016/j.engstruct.2023.116802
19. Taşcıoğlu E, Kıtay Ö, Keskin AÖ, Kaynak Y (2022) Effect of printing parameters and post-process on surface roughness and dimensional deviation of PLA parts fabricated by extrusion-based 3D printing. J Brazilian Soc Mech Sci Eng 44. https://doi.org/10.1007/s40430-022-03429-7
20. He F, Khan M (2021) Effects of printing parameters on the fatigue behaviour of 3d-printed abs under dynamic thermo-mechanical loads. Polym (Basel) 13. https://doi.org/10.3390/polym13142362
21. Kumar M, Ramakrishnan R (2023) Effect of fused filament fabrication parameters and Tetrabromobisphenol-A/Microcrystalline Cellulose Additives on the dynamic mechanical behavior of Polycarbonate/Acrylonitrile–Butadiene–styrene blends for Precision structures. J Mater Eng Perform 32:886–894. https://doi.org/10.1007/s11665-022-07143-2
22. Almutairi MD, Mascarenhas TA, Alnahdi SS et al (2023) Modal response of hybrid raster orientation on material extrusion printed acrylonitrile butadiene styrene and polyethylene terephthalate glycol under thermo-mechanical loads. Polym Test 120:107953. https://doi.org/10.1016/j.polymertesting.2023.107953
23. Polymaker (2017) PolyLite™ PLA technical data sheet. https://c-3d.niceshops.com/upload/file/PolyLite_PLA_TDS_V3.pdf. Accessed 9 Mar 2023
24. ColorFabb (2022) ColorFabb (XT-CF20) technical datasheet. https://colorfabb.com/media/datasheets/tds/colorfabb/TDS_E_ColorFabb_XT_CF20.pdf. Accessed 9 Mar 2023
25. Toray composite materials America (2018) T300 standard modulus carbon fiber technical data sheet. https://www.rockwestcomposites.com/media/wysiwyg/T300DataSheet_1.pdf. Accessed 9 Mar 2023
26. Rimašauskas M, Kuncius T, Rimašauskienė R (2019) Processing of carbon fiber for 3D printed continuous composite structures. Mater Manuf Processes 34:1528–1536. https://doi.org/10.1080/10426914.2019.1655152
27. Maqsood N, Rimašauskas M (2021) Characterization of carbon fiber reinforced PLA composites manufactured by fused deposition modeling. Compos Part C: Open Access 4:100112. https://doi.org/10.1016/j.jcomc.2021.100112
28. Byeon JH, Kim SH (2022) Extraction of the damping ratio of a beat wave using envelope logarithmic decrement. J Mech Sci Technol 36:2729–2737. https://doi.org/10.1007/s12206-022-0506-y
29. Lashin MMA, Saleh WS, Alrowais F (2020) Determination of different structures' materials natural frequencies using fuzzy Logic System. Int J Eng Adv Technol 9:723–727. https://doi.org/10.35940/ijeat.b3641.029320
30. Miyashiro D, Taira H, Hamano R et al (2020) Mechanical vibration of single-walled carbon nanotubes at different lengths and carbon nanobelts by modal analysis method. Compos Part C: Open Access 2:100028. https://doi.org/10.1016/J.JCOMC.2020.100028
31. Evci C, Gülgeç M (2012) An experimental investigation on the impact response of composite materials. Int J Impact Eng 43:40–51. https://doi.org/10.1016/j.ijimpeng.2011.11.009

Title [A3]: Enhancing vibration control in kinematically excited additively manufactured continuous fiber composite structures with distinct orientations
Authors: Ali Raza, Rūta Rimašauskienė, Vytautas Jūrėnas, Tomas Kuncius

Engineering Structures 321 (2024) 118933

Contents lists available at ScienceDirect

Engineering Structures

journal homepage: www.elsevier.com/locate/engstruct

Enhancing vibration control in kinematically excited additively manufactured continuous fiber composite structures with distinct orientations

A. Raza [a], R. Rimašauskienė [a,*], V. Jūrėnas [b], T. Kuncius [a]

[a] Kaunas University of Technology, Faculty of Mechanical Engineering and Design, Studentų str. 56, LT-51424 Kaunas, Lithuania
[b] Kaunas University of Technology, Institute of Mechatronics, Studentų str. 56, LT-51424 Kaunas, Lithuania

ARTICLE INFO

Keywords:
Glass fiber
3D printing
Carbon fiber
MFC
Vibration damping
Layer orientations

ABSTRACT

The article is primarily focused on investigating vibration control in 3D printed composite beam structures. It specifically examines the impact of Macro Fiber Composite (MFC) on two distinct composite materials: polylactic acid (PLA) with continuous carbon fiber (PLA/CCF) and PLA with continuous glass fiber (PLA/CGF) under kinematical excitation. An essential aspect of the research is that both types of composites were manufactured with two distinct layer orientations: 0°/0° and 0°/90°. The modal analysis was performed to find out inherent frequencies and amplitude spectrum for composite beam using 3D laser vibrometer. To maximize vibration damping, an optimization process was implemented to fine-tune the voltage and phase of the signal delivered to the MFC (M8507-P2) for each structure. Following this, the article identified stable and unstable phase regions for each structure and extensively explored the vibration amplitude response within these regions. The study exposes that MFC is more successful in mitigating vibration in structures with 0°/0° orientations, exhibiting significantly greater vibration suppression compared to their corresponding 0°/90° structures.

1. Introduction

In this age of automation, smart materials have gained significant attention among researchers in the engineering domain. These materials provide novel solutions to significant engineering challenges, including the mitigation of vibration amplitudes, the minimization of noise levels and their potential applications in health monitoring [1–4]. Furthermore, smart materials are increasingly being employed in structural dynamics to dampen vibration amplitudes. These vibrations can pose substantial risks to structures, and it is imperative to mitigate them to prevent structural failures [5–7]. Composite structures, especially those reinforced with continuous carbon and glass fibers within polymer matrix, are widely used in various industries such as aviation, automobiles, construction, and more. This popularity is attributed to their high strength, elastic modulus, impressive strength-to-mass ratio, and minimal risk of failure [8–10]. But the presence of structural vibrations at low frequencies instigates concerns regarding the integrity of such structures, motivating the researchers to explore techniques for mitigating vibration amplitudes [11]. In pursuit of significant vibration suppression, the researchers have investigated several active control (AC) approaches encompassing open-loop, closed-loop, and semi-active control, in addition to passive control (PC) and hybrid approaches. The PC approaches are frequently implemented through the application of damping isolators. Meanwhile, the AC approaches are realized by integrating smart materials as sensors and actuators within the system [1,12,13]. Among smart materials, piezoelectric materials find extensive application as both sensors and actuators owing to their direct and converse piezo electric phenomena, respectively. However, they do have certain constraints, such as being highly brittle, exhibiting limited flexibility, and facing challenges in effectively integrating with surfaces that possess intricate designs. To alleviate these constraints, piezoceramic fibers were incorporated into polymer matrix [14–16]. In 1999, NASA introduced Macro Fiber Composites (MFCs), developed by incorporating rectangular-shaped piezoceramic fibers into a polymer matrix, as a solution to the constraints discussed earlier. These MFCs offer enhanced flexibility, facilitating their seamless integration with curved surfaces. Moreover, they produce greater actuation forces compared to piezoelectric patches [3,17–20]. By 2002, the Smart Material company commenced the supply of this innovation under the license granted by NASA [21,22].

* Corresponding author.
E-mail address: ruta.rimasauskiene@ktu.lt (R. Rimašauskienė).

https://doi.org/10.1016/j.engstruct.2024.118933
Received 22 December 2023; Received in revised form 30 July 2024; Accepted 3 September 2024
Available online 7 September 2024

Xie et al. conducted an investigation on the dampening of active vibrations in a lattice grid beam by utilizing piezoelectric material as actuation elements. They employed a novel approach by utilizing the fractional-order proportional-derivative (PD) approach to mitigate vibrations. Furthermore, the researchers conducted simulations involving the beam under diverse dynamic loads. These dynamic loads comprised of harmonic excitation, step excitation, and initial disturbance scenarios. The findings demonstrate that the applied control approach exhibited a significant and rapid decrease in vibration amplitudes, in comparison to the conventional integer-order PD control approach [23]. Dafang et al. did an experimental investigation involving a beam, with the aim of investigating vibration control through the utilization of piezoelectric patches. They employed the independent modal space control technique to focus on controlling and analyzing the initial three modes of the beam. An assessment of vibration behavior of the beam prior to and after implementing the control scheme indicated substantial vibration reduction. Furthermore, a simulation was carried out for the initial three modes, and the outcomes from both the simulation and the experiment showed significant comparability. The results strongly indicate that the implemented control method is highly effective in mitigating vibrations [24]. Li et al. conducted a thorough numerical investigation on Active Vibration Control (AVC) involving a piezoelectric plate coupled to a piezoelectric element. The primary objective was to mitigate vibrations effectively. The velocity-feedback method was implemented to assess the substantial impact of Active Vibration Control on the plate's behavior result. The study's results demonstrate the successful realization of substantial vibration reduction [5]. Kumar et al. investigated the integration of Lead Zirconate Titanate (PZT) patches with a cantilever beam, aiming to suppress vibrations. They developed a finite element model (FEM) and conducted modal analysis using the ANSYS software to find out the beam's inherent frequencies and corresponding mode shapes. The investigation's findings validated the efficacy of the SHM of beams [6]. Przybylski et al. performed nonlinear transverse vibration analysis on aluminum beam structures using both analytical and experimental approaches. The beams were constrained from both ends, and piezoelectric actuators were integrated at designated position. In analytical modelling, Euler-Bernoulli approach was utilized to formulate the influences of external force and piezo actuation on transverse vibration. While, the Lindstedt-Poincaré method was employed to determine solutions to nonlinear vibration issues. In addition, two different experimental setups were created to confirm analytical findings. This study concentrated on the impact of electric fields on piezo-actuator forces, as well as on the inherent frequencies of both systems. Furthermore, it was revealed that any instabilities in the structure due to external force could be lessened by implementing the piezo force. The findings from both analytical and experimental analyses demonstrate the suitability of piezoelectric actuators for control applications in smart structures [25]. Mayer et al. explored active, passive, adaptive, and combined vibration control approaches, analyzing the distinct design aspects and benefits associated with each. The study utilized a designed configuration to present diverse approaches for executing vibration control systems, including the integration of diverse methods for controlling vibrations [26]. Chai et al. conducted a study that encompassed both computational modeling and theoretical analysis of the aero-thermoelastic response exhibited by a laminated structure. The structure incorporated two MFC patches, with one functioning as a strain sensor and the second generating a control force to mitigate vibrations within the structure. The results validate the efficacy of the MFC patch in significantly decreasing vibration amplitudes within the structure [27] Gawryluk et al. carried out a comprehensive investigation focused on mitigating vibrations within a composite beam by incorporating an MFC patch (M8528-P1). Their study involved both simulations and experiments, with the goal of effectively reducing vibrations in the beam by employing various control algorithms. The results from both the simulations and experiments validate the effectiveness of these control algorithms in reducing vibrations [28]. Zippo et al. carried out an experiment focusing on the AVC of a composite plate made of honeycomb carbon fiber structure, utilizing MFCs for both actuation and sensing purposes. The study successfully employed a control algorithm (PPF) to effectively control the first four modes. The reliability and efficacy of the control algorithm were demonstrated in dampening vibration amplitudes across both linear and nonlinear systems [29]. Mitura et al. developed FEM for a beam structure composed of glass-epoxy with multi layers using the Abaqus platform. The purpose was to mitigate undesired vibrations through the application of embedded MFC actuators (M8528-P1). The PPF control was employed to manage vibration, and a dedicated subroutine was developed to incorporate PPF within the Abaqus platform. The study involved a comparison of the beam structure's behaviors with and without the implementation of the PPF controller. Subsequently, the numerical simulations associated with the efficacy of the PPF controller were validated through experimental verification [30]. Miao et al. aimed to mitigate active vibrations (AV) in a beam by utilizing MFC patches, which were employed as both actuators and sensor. The experimental setup consisted of integrating two of these patches as actuators onto the beam, while the third patch served as a sensor. The study employed proportional derivative and fuzzy control approaches, leading to significant suppression of vibration amplitudes observed in the first two modes [31]. Danish et al. introduced a method to mitigate undesired vibrations within a cross-ply lamination structure through the incorporation of an additional composite layer. The study employs parametric methodology to analyze how changes in the dimensions (width and thickness) of the composite layer impact the potential energy landscape and associated dynamic characteristics. Through theoretical and numerical simulations, the study demonstrates the suitable design parameters of the embedded layer. These specifications effectively work to minimize the undesired vibrations that arise due to cyclic excitation within the structure [32]. Rimasauskiene et al. did an investigation focused on observing the impact of an MFC patch on the vibration control of a beam by employing active and passive control schemes. The results demonstrate the effective reduction of vibrations within the beam through the implementation of both active and passive control schemes [33]. Raza et al. designed a numerical model of beams composed of various materials in the ANSYS platform embedded with MFC (M8507-P2) to suppress the vibrations. Every beam was kinematically excited to produce vibrations, while MFC patch generates a compensatory control force to mitigate the vibration. The results demonstrate that the MFC patch significantly decreased the vibration amplitudes in every beam [34]. Lee et al. conducted a study involving a distinct dual control methodology designed to attenuate oscillations within bistable composite structures. The approach comprised of two MFCs and one PPF controller. In this approach, one of the potential wells was suppressed and the structure was directed towards the stable side when one of the MFCs experienced voltage. While the second MFC was used to suppress vibrations that occurred due to single-well scenario, with the support of PPF controller. This unique dual control approach was confirmed through mathematical and experimental study [35].

The current investigation is an extension of our previous work [36], the previous study was that primarily centered on vibration amplitude control using MFC patch (M8507-P2) in additively manufactured (AM) beam structures with 0°/0° layer orientation. These AM beams were fabricated from polylactic acid (PLA), PLA reinforced with short carbon fiber (PLA/SCF) and PLA reinforced with continuous carbon fibers (PLA/CCF). An incremental parameter tuning scheme was used to determine optimal voltage and phase settings for each beam to achieve maximum vibration damping. Thus, a significant vibration amplitude control was identified in each AM beam.

After conducting an in-depth review of the existing literature, the authors identified that the current study represents a pioneering effort in exploring how AM composite structures with two distinct layer orientations, 0°/0° and 0°/90°, influence dynamic characteristics, especially vibration damping, with the application of MFC (M8507-P2). These

composite structures were made from PLA/CCF and PLA reinforced with continuous glass fibers (PLA/CGF). The primary aim of the study is to identify a distinct layer orientation that contributes a significant role in vibration damping. The dynamic characteristics comprised of natural frequencies, bending mode (BM) shapes, and vibration damping in kinematically excited beams. The deformation response of each composite structure was measured under various static loads. Modal analysis was conducted to evaluate inherent frequencies, corresponding bending mode shapes, and amplitude spectrum for each composite structure. Additionally, an incremental parameter tuning methodology was implemented to optimize control voltage and phase signals supplied to the MFC, achieving maximum vibration damping. The vibration amplitude behaviors in both stable and unstable phase regions were identified and analyzed. Ultimately, a thorough analysis was performed on the vibration amplitude responses of each kinematically composite structure with influence of MFC to identify the most effective layer orientation for vibration control.

2. Methodology

In this investigation, vibration amplitude control in AM composite structures with two distinct layer orientations such as 0°/0° and 0°/90°, were thoroughly examined and reported. These structures were fabricated from PLA/CCF and PLA/CGF. Each composite structure was stimulated by an electrodynamic shaker, and to control amplitude vibration amplitude, an open-loop active vibration control (OLAVC) arrangement was created, employing the MFC (M8507-P2). The vibration amplitude control of each composite structure has been determined at its first resonant frequency.

2.1. Additive manufacturing of composite structures

For creating composite structures involving PLA/CCF and PLA/CGF, Polymaker PLA filament served as the matrix material, which has a diameter of 1.75 mm [37]. As for reinforcement, TORAYCA T300 [38], with a single-fiber diameter of 7 μm, was used for PLA/CCF, while VETROTEX EC11300, featuring a single-fiber diameter of 11 μm, was chosen for PLA/CGF.

Composite specimens reinforced with continuous carbon fiber and glass fiber were produced using the MeCreator 2 printer with a modified printing head. The printing method employed is based on Co-Extrusion with Towpreg technology. In other words, the modified printing head has two input channels: one for PLA thermoplastic matrix and another for impregnated continuous carbon fiber or glass fiber. The authors have exhaustively examined the impregnation process for continuous fiber [39]. These materials are mixed in the heating element, resulting in a homogeneous composite filament that is deposited on the printing platform through the 1.5 mm nozzle. To enhance adhesion between the specimen and the glass platform, 3D LAC was used. The printing settings are presented in Table 1. The fabrication process of composite structures is depicted in Fig. 1, whereas schematic description of fabrication process with modified printing head is illustrated in Fig. 2.

Table 1
Printing settings for fabricating of PLA/CCF and PLA/CGF.

Settings	Composite structures	
	PLA/CCF	PLA/CGF
Nozzle diameter (mm)	1.5	1.5
Extrusion multiplier	0.7	0.7
Extrusion width (mm)	1.2	1.2
Layer height (mm)	0.5	0.5
Printing speed (mm/s)	3.0	3.0
Extruder temperature (°C)	210	220
Bed temperature (°C)	90	95
Fan speed (%)	60	100
Infill percentage	100	100
Layer orientations	0°/0°, 0°/90°	0°/0°,0°/90°

As depicted in Table 1, three parameters: extruder temperature, bed temperature and fan speed, vary while printing PLA thermoplastic composite structures with CCF and CGF reinforcements. During printing process of PLA/CGF composite structures, the extruder temperature was risen by 10 degrees Celsius to enhance the secondary impregnation between the reinforcement and the matrix, as the single-fiber diameter of the CGF is 57.14 % larger than the CCF. This adjustment increases the printability and stability of the printing process. The differences in fan speed and bed temperature are associated with adhesion between printed composite line and printing bed during changes in the printing direction. The optimal adjustments of these parameters minimize the line end pull and ensure specimen length stability during printing, as the matrix material cools quickly and adheres better to the printing bed. Moreover, the cooling rate (fan speed) and bed temperature are kept higher for CGF because after impregnation, it becomes less flexible and stiffer than the CCF, requiring higher adhesion during printing.

Moreover, it is important to highlight that the width of the specimen does not align as an integer multiple of the extrusion width due to the intricacy in printing continuous fiber reinforced composite structures using the Co-Extrusion with Towpreg process and limitations in the fused deposition modeling (FDM) technology itself. In FDM technology, it is impossible to fully eliminate air voids; that occur between the printing lines or layers. To minimize this air voids percentage, the printing lines should overlap. While, during printing process, any variations in the fiber extrusion multiplier of the matrix material have a direct impact on the printing line width. The line width should be optimally adjusted according to the diameter of the fiber reinforcement.

2.2. Experimental configuration

The experimental design shown in Fig. 3 was utilized to observe and examine the vibration damping in composite structures. The system comprises a composite structure with dimensions of 120 mm × 20 mm× 1.35 mm, integrated with an MFC (M8507-P2) made by Smart Material [21]. The MFC actuator was integrated with epoxy, 5 mm from the fixed edge of the composite structure, as illustrated in Fig. 4. The OLAVC approach has been used to measure vibration damping; experimental approach layout is schematically depicted in Fig. 5. Vibrations were introduced into each composite structure from the fixed edge side using an 'Electrodynamic Shaker (DDR-11077)', with the input signal supplied through a function generator (WW5064). Vibration amplitudes were monitored and measured 4 mm from the free end of each beam, with the impact of the MFC patch assessed using a Laser Displacement Sensor (LDS). The voltage signal with the optimal phase was supplied to the MFC through the function generator (WW5064) to achieve maximum reduction in amplitude. The LDS (LK-G82) captured the deformation in the composite beam and transferred signal to the LDS control unit (LK-GD500) for processing. This data in analogue format was further processed through a Pico-Scope 3424 device, which functioned as analog to digital converter (ADC). The data was then analyzed using Pico-Scope 6 software which then displayed the results on the computer screen.

2.3. Experimental modal analysis (EMA)

The experimental design depicted in Fig. 6 was utilized to ascertain the inherent frequencies, bending mode shapes, and amplitude spectra for each beam. The MFC actuator was affixed to each composite structure mounted 5 mm from the fixed edge, as depicted in Fig. 4. The composite structures started vibration when a chirp signal of 100 V was supplied to MFC actuator. To examine the responses at the free end, a Polytec 3D laser vibrometer (PSV-500) was utilized.

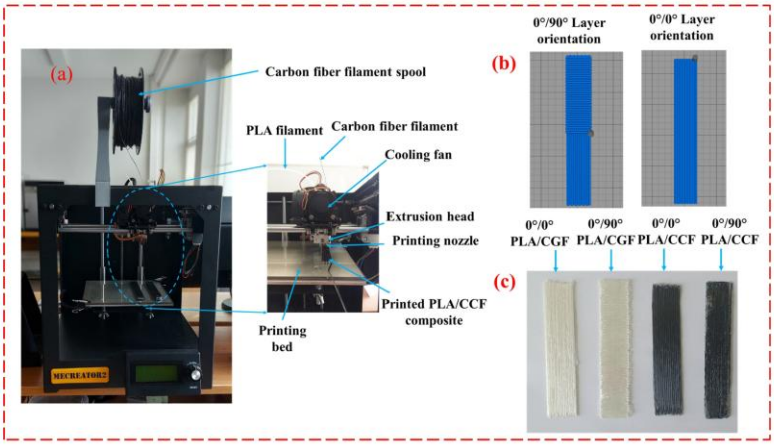

Fig. 1. Fabrication scheme of composite structures: a) preparation process of composite structures; b) depiction of 0°/0° and 0°/90° layer patterns; c) 3D printed composite structures.

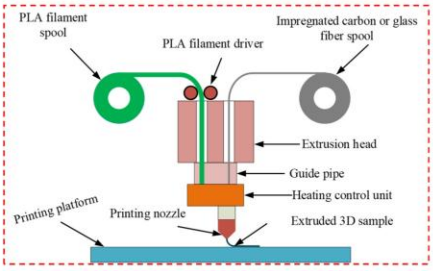

Fig. 2. Schematic description of fabrication process with modified printing head.

2.4. Structure response to a static concentrated load

The experimental design, as illustrated in Fig. 7, was utilized to assess the deformation in PLA/CCF and PLA/CGF composite structures. Both structures were comprised with 0°/0° and 0°/90° layer orientations. The deformation assessment in each structure was carried out by fixing one side and subjecting the free end to various static concentrated loads, as shown in Fig. 8. The response in each composite structure was examined using an LDS (LK-G82).

3. Results and discussions

This article extensively examines and discusses the impact of MFC on reducing vibration amplitudes in composite structures made of PLA/CCF and PLA/CGF, which are oriented with 0°/0° and 0°/90° layer configurations.

3.1. Determination of deformation under a point load

Table 2 presents a summary of the deformation observed in PLA/CCF and PLA/CGF composite structures.These structures have 0°/0° and 0°/90° layer orientations, and the deformation was examined under a static load applied at free side beam. The masses of the composite structures, as determined by the weight cell, have been reported in Table 3. It is illustrated in Fig. 9, the deformation in PLA/CCF and PLA/CGF composite structures shows a linear progression as the load varies from 2 g to 8 g. The deformation in PLA/CCF with 0°/0° and 0°/90° orientations varies between 0.20 mm to 0.78 mm and 1.27 mm to 5.02 mm, correspondingly, as the load changes from 2 g to 8 g. Conversely, in PLA/CGF with 0°/0° and 0°/90° orientations, the deformation changes between 0.41 mm to 1.47 mm and 1.85 mm to 6.69 mm, correspondingly, across the load range of 2 g to 8 g.The PLA/CCF and PLA/CGF structures with 0°/0° layer orientations exhibit less deformation as compare to their corresponding 0°/90° layer orietation structures. The structures with minimal deformation are generally associated with enhanced stiffness [40]. Moreover,the findings highlight that the PLA/CCF structures demonstrate greater stiffness compared to their corresponding PLA/CGF structures with 0°/0° and 0°/90° layer orientations. Among the examined structures, the PLA/CCF structures with 0°/0° layers exhibit the highest stiffness, while the PLA/CGF structures with 0°/90° layers demonstarte the lowest stiffness.

3.2. Modal analysis

In the second phase of the experimentation, modal analysis was conducted to evaluate the inherent frequencies and corresponding bending mode (BM) shapes and amplitude spectra of PLA/CCF and PLA/CGF composite structures with 0°/0° and 0°/90° layer orientations. Vibrations were induced in each structure using an integrated MFC (M8507-P2). The integrated MFC patch was stimulated with a chirp signal of 100 V, generated by a function generator, is an integral part of the 3D laser vibrometer. The initial four BM shapes of composite structures have been depicted in Fig. 10. The inherent frequencies, along with their corresponding amplitude have been provided in Table 4. The frequencies sequentially increase from 0°/90° PLA/CGF (21.3 Hz) to 0°/

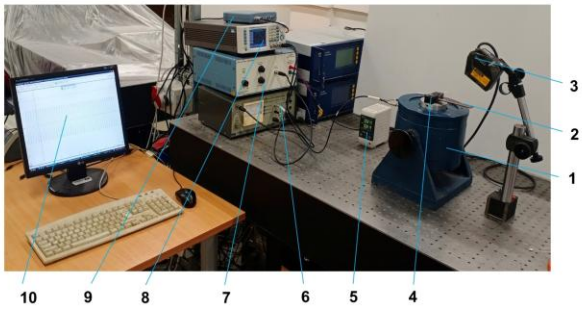

Fig. 3. Experimental design configuration for vibration damping evaluation: 1- electrodynamic shaker; 2- Composite structure integrated with MFC; 3- Laser displacement sensor (LDS); 4-Fixture; 5- LDS control unit 6- voltage amplifier (LV-103); 7- voltage amplifier (EPA-104); 8- function generator 9- ADC Pico Scope-; 10- computer system.

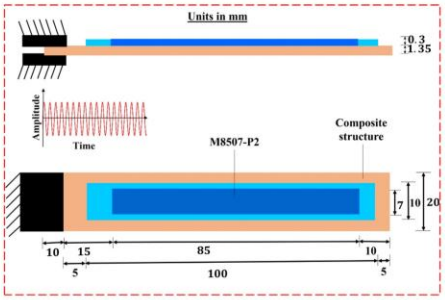

Fig. 4. Visual depiction of composite structure with MFC.

90° PLA/CCF (26.6 Hz), followed by 0°/0° PLA/CGF (47.7 Hz) and ultimately 0°/0° PLA/CCF (60 Hz). Structures with high stiffness and low weight are thought to demonstrate enhanced inherent frequencies, as described by the equation.

$$\hat{f} = \sqrt{\hat{k}/\hat{m}} \quad /2\pi \tag{1}$$

Where $\hat{f}$, $\hat{k}$ and $\hat{m}$ correspond to frequency, stiffness, and weight, respectively [34,41,42]. In the preceding section, it has been experimentally demonstrated that the stiffness increases sequentially from 0°/90° PLA/CGF to 0°/90° PLA/CCF to 0°/0° PLA/CGF to 0°/0° PLA/CCF, with corresponding weights of 3.26 g, 2.86 g, 3.24 g, and 2.82 g respectively. Moreover, the reported experimental results (refer to Table 4) indicate a significant reduction in vibration amplitudes as the BM proceeds from the first to the fourth for each composite structure In Table 4, vibration amplitudes were measured through Polytec 3D laser vibrometer. The laser vibrometer scans the entire surface of composite structure, scanning each point on surface three times to ensure the reliability of data. It then measures the vibration amplitude of each point, which is processed by Polytec PSV software (control unit). This software calculates the final amplitude by averaging the amplitudes of all points on the surface [43]. The maximum amplitude for each composite structure is noted at the first frequencies: 9.26 μm for 0°/90° PLA/CGF at 21.3 Hz, 10.11 μm for 0°/90° PLA/CCF at 26.6 Hz,4.40 μm for 0°/0° PLA/CGF at 47.7 Hz and 4.14 μm for 0°/0° PLA/CCF at 60 Hz. Conversely, the lowest amplitudes are observed at fourth frequencies: 0.10 μm for 0°/90° PLA/CGF at 918 Hz, 0.12 μm for 0°/90° PLA/CCF at 1114 Hz,0.05 μm for 0°/0° PLA/CGF at 1707 Hz and 0.02 μm for 0°/0° PLA/CCF at 2190 Hz. Furthermore, Fig. 11, illustrates the amplitude

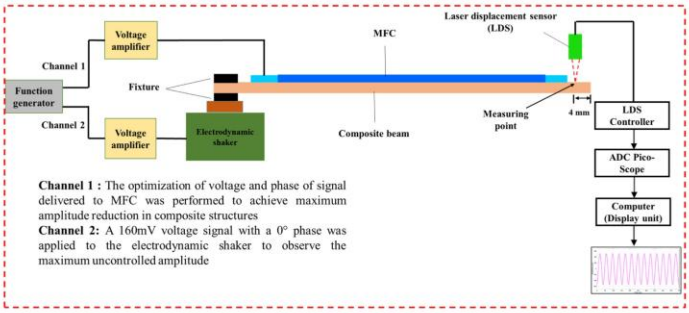

Fig. 5. Schema of experimental approach layout.

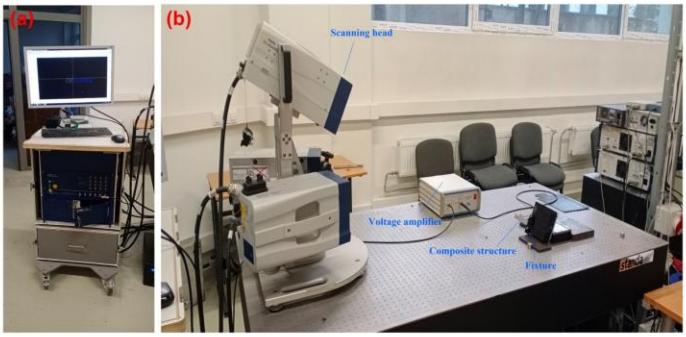

Fig. 6. Polytec 3D laser vibrometer: a) data management system; b) experimental setup for modal analysis.

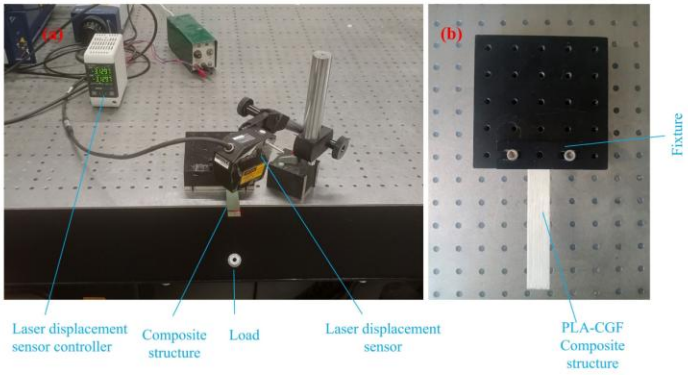

Fig. 7. Estimation of deformation in composite structures: a) experimental setup b) clamping of composite structure.

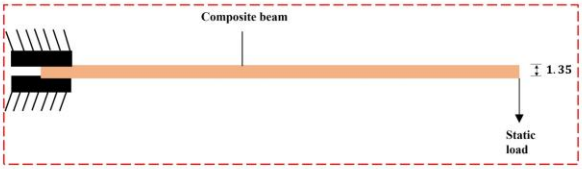

Fig. 8. Depiction of composite structure with concentrated static load at free end.

Table 2
Deformation in composite structures under applied load.

Weight (g)	0°/0° PLA/ CCF (mm)	0°/90° PLA/ CCF (mm)	0°/0° PLA/ CGF (mm)	0°/90° PLA/ CGF (mm)
2	0.20	1.27	0.41	1.85
4	0.39	2.52	0.78	3.55
6	0.59	3.77	1.12	5.06
8	0.78	5.02	1.47	6.69

Table 3
Masses of composite structures.

Layer configuration	Masses of samples in grams	
	PLA/CCF (g)	PLA/CGF (g)
0°/0°	2.82	3.24
0°/90°	2.86	3.26

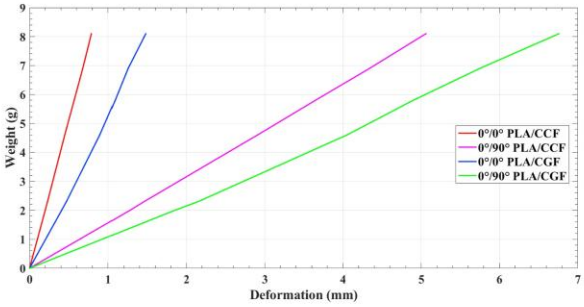

Fig. 9. Deformation progression in composite structures as load varies.

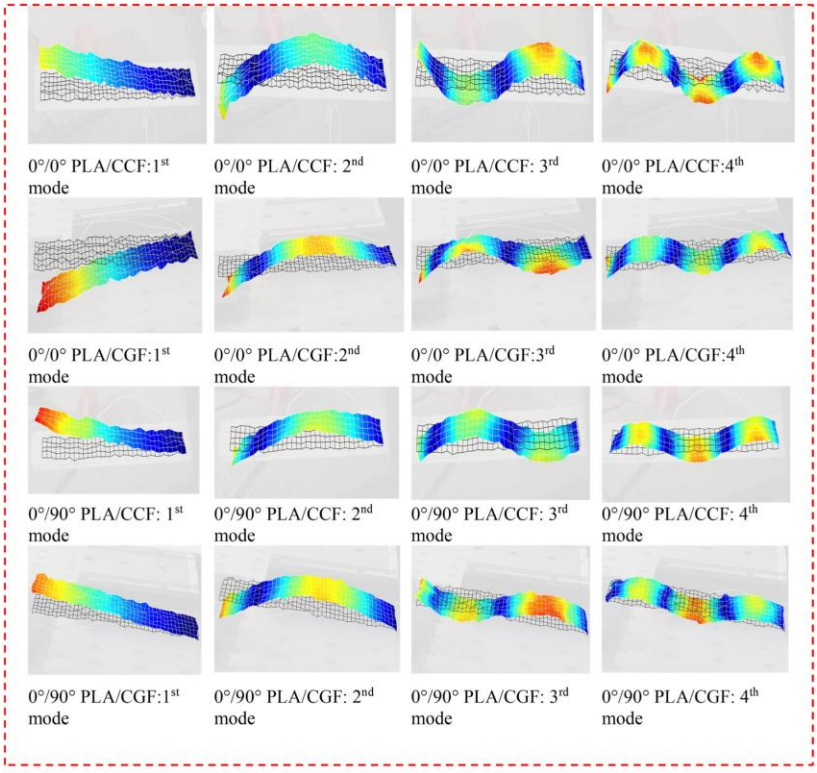

Fig. 10. Initial four bending modes of PLA/CCF and PLA/CGF with 0°/0° and 0°/90° orientations.

Table 4
Inherent frequencies and corresponding amplitudes for PLA/CCF and PLA/CGF composite structures.

Bending modes	0°/0° PLA/CCF		0°/90° PLA/CCF		0°/0° PLA/CGF		0°/90° PLA/CGF	
	frequency (Hz)	amplitude (μm)	frequency (Hz)	amplitude (μm)	frequency (Hz)	amplitude (μm)	frequency (Hz)	amplitude (μm)
1st	60	4.14	26.6	10.11	47.7	4.40	21.3	9.26
2nd	410	1.13	203	3.38	315.6	1.45	165	3.33
3rd	1153	0.11	592	0.26	895.3	0.12	480	0.25
4th	2190	0.02	1114	0.12	1707	0.05	918	0.10

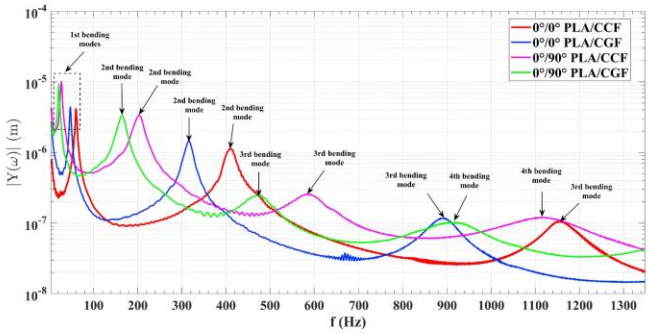

Fig. 11. Amplitude spectra of PLA/CCF and PLA/CGF with 0°/0° and 0°/90° orientations.

spectra of PLA/CC and PLA/CGF, oriented with 0°/0° and 0°/90° layer arrangements. The amplitudes for second BM for 0°/90° PLA/CGF, 0°/90° PLA/CCF, 0°/0° PLA/CGF and 0°/0° PLA/CCF, are approximately only 36.0 %, 33.4 %,33.0 % and 27.3 % respectively of their respective first BM amplitudes. Similarly, third BM amplitudes for these orientations are about 2.7 %,2.6 %,2.7 % and 2.6 % of their respective first BM amplitudes. Furthermore, the fourth BM amplitudes exhibit values of around 1 %, 1.2 %,1.1 % and 0.5 % compared to their respective first BM amplitude. The values for BM from second to fourth for each composite structure are determined as less than 40 % of their respective first BM amplitudes. Therefore, based on the reported experimental findings and the literature study, it can be deduced that the first BM always exhibits the maximum vibration amplitude and dominance in the entire vibrational behavior [33,34,44]. Thus, this article focuses on further investigating the reduction in vibration amplitude at the first BM due to its dominance.

3.3. Optimizing the control voltage phase

At the start, the 0°/0° PLA/CCF, 0°/90° PLA/CCF, 0°/0° PLA/CGF, and 0°/90° PLA/CGF composite structures were individually subjected to vibration using an electrodynamic shaker. Each structure was exposed to its corresponding resonant frequency: 60 Hz, 26.6 Hz, 47.7 Hz, and 21.3 Hz, to attain maximum uncontrolled amplitudes.

To achieve vibration amplitude reduction in beams, a voltage signal was introduced to MFC, generating a counter force that decreases the vibration amplitude. As the voltage amplitude increased, the MFC produced more force, as specified by the manufacturer [21]. However, this approach does not yield optimal control, applicable to both amplitude and phase regulation. Accurate tuning of both the control voltage amplitude and phase is imperative for achieving maximum reduction in vibration amplitude.

For a comparative analysis, vibration amplitude reduction can be quantified using the equation:

$$R = \left(\frac{W_u - W_c}{W_u}\right) \times 100\% \quad (2)$$

In this equation, R, W_u, W_c correspond to the reduction factor, uncontrolled amplitude, and controlled amplitude in the time series.

In the 0°/0° PLA/CCF composite structure, the control voltage was raised in 2 mV steps using a function generator (WW5064), while maintaining a random phase spanning the entire 360° range. A substantial decrease in amplitude was observed at approximately 10.52 V. Consequently, further voltage adjustment was halted, and instead, phase adjustments were made in increments of 2°. During phase adjustment, significant amplitude reduction was noted at 30°. To identify the optimal phase, the voltage amplitude was fine-tuned in sub-steps of 0.5° around 30°, and the maximum decrease in vibration amplitude was detected at 29°. Upon implementing a control voltage of 10.52 V with 29° phase, the MFC produced an optimal force that effectively minimized W_c to nearly zero. The resulted in an R value of 99.19 %, as depicted in Fig. 12 (a). An interesting insight derived from this investigation is that the vibration amplitude of the dynamic system only decreases when voltage phase exists within specific range. The stable phase range for 0°/0° PLA/CCF spans from 290° to 50° (comprising both intervals 290° to 360° and 0° to 50°) as illustrated in Fig. 12 (a). Within this stable range, the W_c value remains lower compared to W_u,yielding a positive R value indicative of a decrease in vibration magnitude. Conversely, in the unstable range falling between 50° to 290°, the W_c value exhibits a higher value compared to W_u, and resulting in a negative R value negative that signifies an increase in vibration amplitude within this region instead of a reduction.

The corresponding steps were carried out for the 0°/90° PLA/CCF composite structure, resulting in a significant amplitude reduction noted at 29.4 V. The optimal phase was then determined by increasing the phase in 2° increments, and significat vibration reduction was observe at phase of 44°. Further fine-tuning was done using sub-steps of 0.5° centered around 44°. The optimal phase was found to be 45°, at which

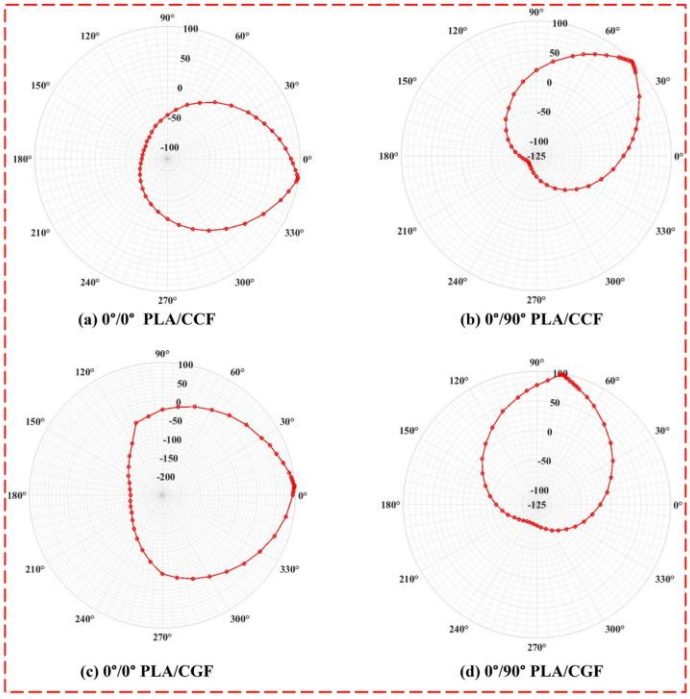

Fig. 12. Influence of phase on the vibration amplitude: (a) 0°/0° PLA/CCF, (b) 0°/90° PLA/CCF (c) 0°/0° PLA/CGF (d) 0°/90° PLA/CG.

maximum reduction was noted. Applying a control voltage of 29.4 V along with phase of 45° resulted in an R value of 98.18 %, as depicted in Fig. 12 (b). The stable region ranges from 350° to 100° (encompassing both intervals 350° to 360° and 0° to 100°). Within the stable region, the value of W_c remains lower than W_u,resulting in a positive R value indicating vibration amplitude reduction. However, in the unstable range spanning between 100° to 350°, the value of W_c exceeds W_u, and leading to a negative R value. The negative value suggests an increase in vibration amplitude within this region instead of a reduction.

A similar approach was adopted for 0°/0° PLA/CGF composite structure and determining optimal voltage and phase settings of 17.68 V and 4° respectively. Employing these inputs with the MFC resulted in an R value of 98.90 %. The stable phase region spans approximately 300° to 70° (encompassing both intervals 300° to 360° and 0° to 70°), as illustrated in Fig. 12(c). Within stable region 300° to 70°, the of W_c remains lower compared to W_u, resulting in a positive R value that indicates a significant amplitude reduction. Conversely, in the unstable region falling between 300° to 70°, a negative R value indicates an increase in vibration amplitude instead of a decrease. In case of 0°/90° PLA/CGF composite structure, the optimal voltage and phase are found to be 43 V and 79°, respectively. With these inputs, an R value of 98.70 % is achieved. The stable phase region comprises approximately 15° to 135°, revealing the amplitude reduction, as depicted in Fig. 12 (d). While, in the unstable region falling between 135° to 15° (encompassing both intervals 135° to 360° and 0° to 15°) in which vibration amplitude increases. The findings indicate that the stable operational span for the 0°/0° PLA/CCF and 0°/90° PLA/CGF is approximately 120° and while for 0°/0° PLA/CGF and 0°/90° PLA/CCF, it is approximately 110°.

3.4. Assessment of amplitude reduction in composite structure

This section provides a detailed examination on the effectiveness of MFC in vibration damping of composite structures, specifically PLA/CCF and PLA/CGF, with 0°/0° and 0°/90° orientations.

The PLA/CCF composite structure with a 0°/0° orientation exhibited its highest amplitude, ranging approximately from + 210 μm to −212 μm, as illustrated in Fig. 13 (a). This occurred when the composite structure was subjected to stimulation from an electrodynamic shaker operating in close to its initial resonant frequency of 60 Hz, with a phase of 0°and an amplitude of 160 mV. Significantly, the 0°/0° PLA/CCF composite structure showed the most substantial reduction in maximum amplitude when a 10.52 V control voltage was applied to MFC, accompanied by an optimal phase angle of 351°, as depicted in Fig. 13 (b). The range of vibration amplitude from the maximum to minimum extended from + 1.7 μm to −1.7 μm, indicating a remarkable reduction in amplitude by over 120 times. This remarkable reduction highlights the efficacy of MFC in vibration damping of 0°/0° PLA/CCF. The 351° phase difference demonstrates that the electrodynamic shaker and MFC signals are approximately out of phase, resulting in effective vibration cancellation and producing maximum damping. The 351° phase

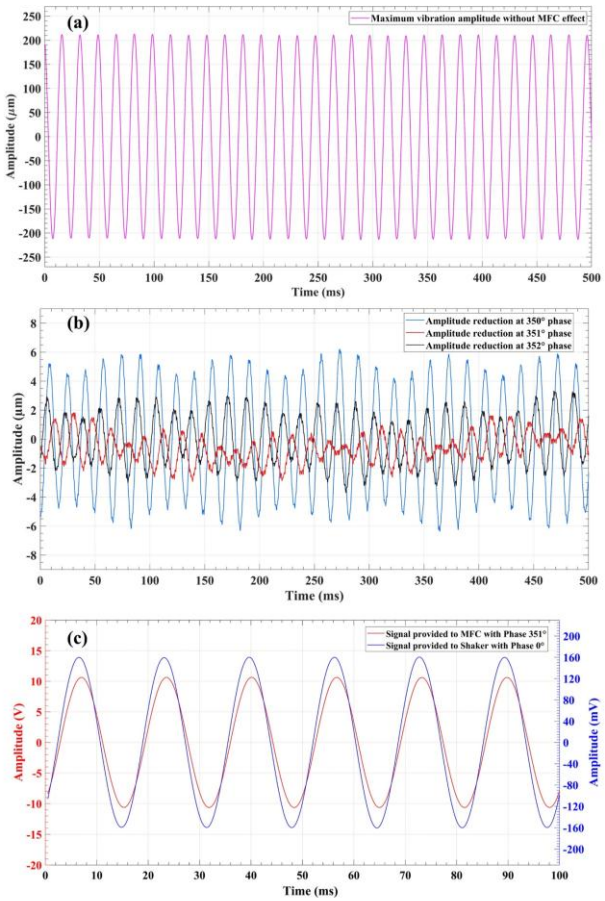

Fig. 13. Vibration amplitude behavior in composite structure comprising 0°/0° PLA/CCF: (a) Uncontrolled vibration amplitude (b) Controlled vibration amplitude at 350°, 351° and 352°, with influence of MFC (c) 351° phase difference between the electrodynamic shaker signal and MFC signal, realizing maximum vibration reduction.

difference between the electrodynamic shaker and the MFC signals can be seen in Fig. 13 (c). Additionally, Fig. 13(b) demonstrated that when applying a 10.52 V control voltage with phases of 350° and 352° to the MFC, corresponding maximum to minimum vibration amplitudes of + 6 μm to −6 μm and + 3 μm to −3.4 μm were recorded, respectively. The resulting decrease in amplitude at phases 350° and 352° was approximately 35 and 65 times, respectively. The comparatively lower vibration damping at 350° and 352° adjacent phases, relative to the optimal phase of 351°, exhibits the sensitivity of the 0°/0° PLA/CCF composite structure to phase angle. Even a slight variation in phases adjacent to optimal phase leads to substantially lower vibration damping.

The PLA/CCF composite structure, with a 0°/90° orientation as shown in Fig. 14(a), demonstrated its highest vibration amplitude, ranging approximately from + 514 μm to −545 μm. This happened when the composite structure was exposed to excitation from a shaker operating close to its initial resonant frequency of 26.6 Hz, with a phase of 0°and an amplitude of 160 mV. The 0°/90° orientation exhibits higher vibration amplitude than the 0°/0° orientation, demonstrating the distinct dynamic vibration response associated with the 0°/90° orientation. The most significant vibration amplitude reduction in 0°/90° PLA/CCF was noted at a 29.4 V control voltage with optimal phase of 45°. Following the substantial vibration reduction, the maximum to minimum vibration amplitude was recorded + 6.15 μm to −6.4 μm, representing a remarkable amplitude reduction of over 80 times. The need of a higher control voltage with optimal phase to assess maximum

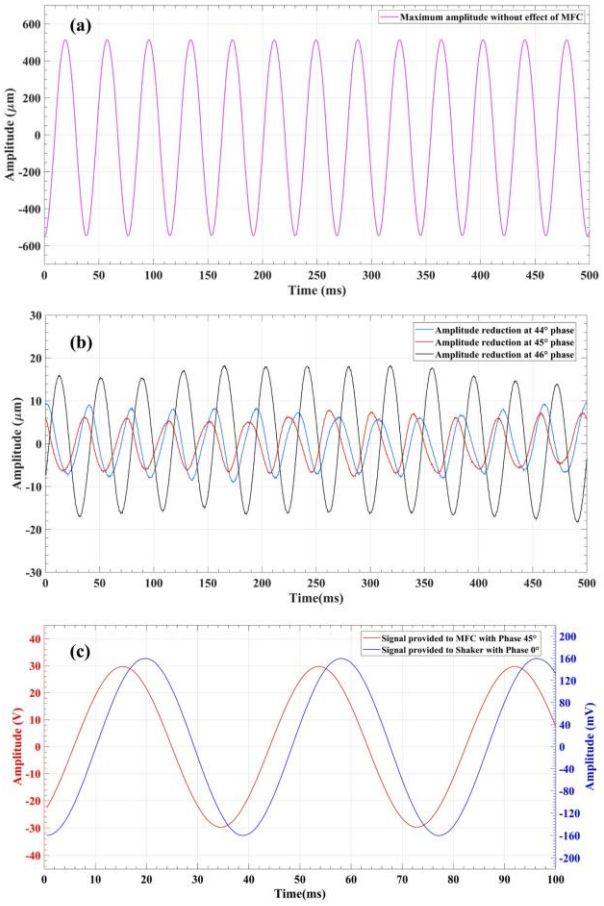

Fig. 14. Vibration amplitude behavior in composite structure comprising 0°/90° PLA/CCF: (a) Uncontrolled vibration amplitude (b) Controlled vibration amplitude at 44°, 45° and 46°, with influence of MFC (c) 45° phase difference between the electrodynamic shaker signal and MFC signal, realizing maximum vibration reduction.

damping in the 0°/90° orientation, compared to 0°/0° orientation, indicates that layer orientations significantly influence the interaction between MFC actuation and vibration dynamics of composite structures. This demonstrates the crucial role of layer orientations in vibration damping. The 45° phase difference between the electrodynamic shaker and the MFC signals has been depicted in Fig. 14(c). Moreover, amplitude reductions exceeding 30 times and 60 times were achieved when the MFC was exposed to a 29.4 V control voltage of at phases of 44° and 46° respectively, as presented in Fig. 14 (b). The beam's vibration amplitude ranged around from + 16 μm to −16.19 μm and + 8 μm to −8.9 μm, respectively. The results indicate that the optimal phase (45°) produces the maximum vibration damping, while adjacent phases (44° and 46°) also provide significant vibration damping.

A similar approach was adopted for PLA/CGF composite structure with a 0°/0° orientation, which exhibited its highest vibration amplitude, ranging approximately from + 244 μm to −242 μm (see Fig. 15 (a)) at its initial resonant frequency of 47.7 Hz. This amplitude was observed slightly higher than 0°/0° PLA/CCF, indicating differing vibration dynamic response characteristics between two composite structures. The highest vibration damping, exceeding 90 times, was achieved when the MFC was exposed to 17.68 V control voltage with phase angle of 4°, resulting in a vibration amplitude that ranged around from + 2.9 μm to −2.4 μm was observed. The 4° phase indicates that shaker signal and MFC signals are approximately in phase alignment,

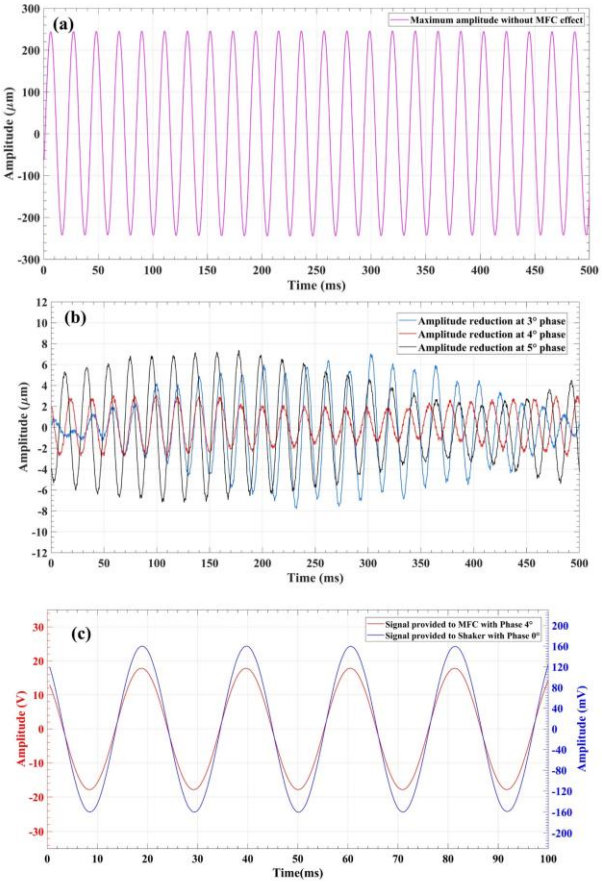

Fig. 15. Vibration amplitude behavior in composite structure comprising 0°/0° PLA/CGF: (a) Uncontrolled vibration amplitude (b) Controlled vibration amplitude at 3°, 4° and 5°, with influence of MFC (c) 4° phase difference between the electrodynamic shaker signal and MFC signal, realizing maximum vibration reduction.

effectively canceling out the vibration effects and thus producing maximum vibration damping. The 4° phase difference between the electrodynamic shaker signal and the MFC signal has been revealed in Fig. 15 (c). Vibration amplitude damping of over 35 times and 30 times were realized when the PLA/CGF (0°/90°) structure was subjected to phase angles of 3° and 5°, respectively, as illustrated in Fig. 15 (b). The beam's vibration amplitude ranged approximately from + 6.4 μm to −6.8 μm and μm 7.1 μm to −7 μm, respectively. The results indicate that the phases around the optimal phase still provide significant vibration damping. In case of PLA/CGF with 0°/90° orientation, the highest vibration amplitude was approximately in the range of + 785 μm to −810 μm at its initial resonant frequency of 21.3 Hz (see Fig. 16(a)). This 0°/90° PLA/CGF indicates the highest vibration amplitudes among all the examined composite structures. The most substantial vibration reduction, exceeding 75 times, was observed when the MFC received a 43 V voltage at a 79° phase angle, as illustrated in Fig. 16(b), resulting in a vibration amplitude ranging from around + 8.5 μm to −12.2 μm. The requirement of high control voltage with an optimal phase indicates an intricate interaction between MFC actuation and vibration dynamics of 0°/90° PLA/CGF structure. Moreover, the high phase difference of 79° demonstrates a substantial lag in the dynamic behavior of 0°/90° PLA/CGF structure relative to the control signal provided to the MFC. Fig. 16 (c) illustrates a 79° phase difference between the electrodynamic shaker and the MFC signals. At phase angles of 78° and 80°, corresponding vibration amplitude damping, over 60 times and 25 times was achieved, respectively, as depicted in Fig. 16 (b). The vibration amplitude ranged approximately from + 17.4 μm to −12.4 μm and + 24.5 μm to −30.7 μm, respectively. Additionally, the adjacent phases (78° and 80°)

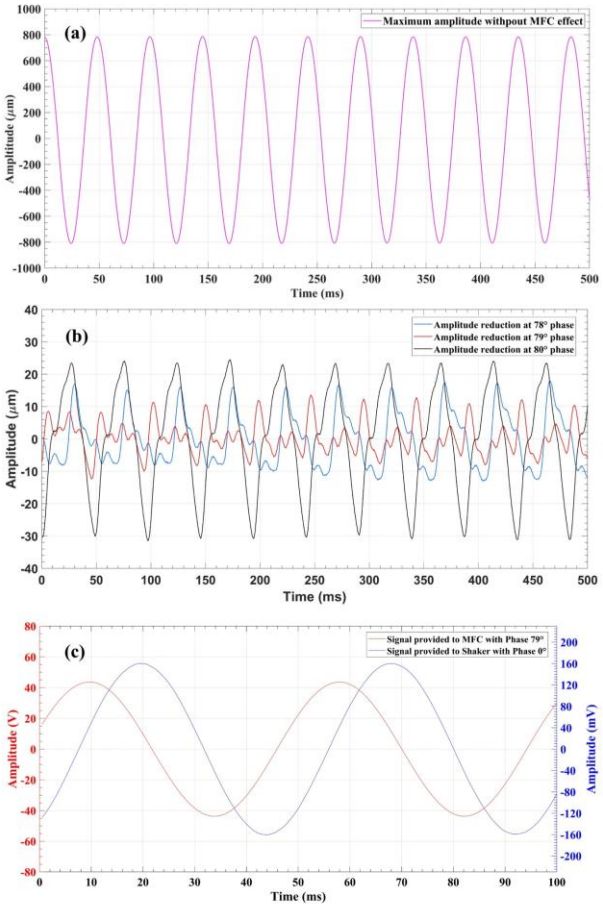

Fig. 16. Vibration amplitude behavior in composite structure comprising 0°/0° PLA/CGF: (a) Uncontrolled vibration amplitude (b) Controlled vibration amplitude at 78°, 79° and 80°, with influence of MFC (c) 79° phase difference between the electrodynamic shaker signal and MFC signal, realizing maximum vibration reduction.

to the optimal phase (79°) also offer considerable vibration damping.

Overall, the highest uncontrolled vibration amplitude was measured in 0°/90° PLA/CGF configuration, followed by 0°/90° PLA/CCF, 0°/0° PLA/CGF and 0°/0° PLA/CCF. It is worth noting that, to attain maximum vibration reduction, the 0°/90° PLA/CGF demanded the highest voltage at 43 V with 79° phase, followed by 0°/90° PLA/CCF at 29.4 V with a 45° phase, 0°/0° PLA/CCF at 17.68 V with a 4° phase and 0°/0° PLA/CCF at 10.52 V with a 351° phase. Furthermore, composite structures with 0°/0° layer configurations exhibited more effective vibration reduction compared to their corresponding 0°/90° layer configurations, influenced by MFC. The vibration damping analysis is also summarized in Table 5.

4. Conclusions

In this experimental study, the vibration amplitude reduction is thoroughly analyzed in AM composite structure fabricated with PLA/CCF and PLA/CGF. These structures have distinct 0°/0° and 0°/90° layer orientations. An OLAVC approach is applied to achieve substantial amplitude reduction. Considering the findings achieved in this study, the subsequent inferences are derived:

1. In the initial phase of experimentation, the stiffness of each beam was evaluated using deformation under the point load approach. The stiffness of the PLA/CCF and PLA/CGF composite structures with 0°/

Table 5
vibration damping analysis in composite structures.

Composite structures	A_1 = Uncontrolled peak-to-peak amplitude (μm)	Optimal voltage and phase for maximum damping	A_2= Controlled peak-to-peak amplitude (μm)	Reduction factor= A_1 / A_2
0°/0° PLA/ CCF	+ 210 to −212	10.52 V with 351° phase	+ 1.7 to −1.7	> 120 times
0°/ 90°PLA/ CCF	+ 514 to −545	29.4 V with 45° phase	+ 6.15 to −6.4	> 80 times
0°/0°PLA/ CGF	+ 244 to −242	17.68 V with 4° phase	+ 2.9 to −2.4	> 90 times
0°/90° PLA/CGF	+ 785 to −810	43 V with 79° phase	+ 8.5 to −12.2	> 75 times

0° layer patterns was identified higher than that of their corresponding 0°/90° layer patterns structures. While the overall stiffness follows a sequence from 0°/90° PLA/CGF to 0°/90° PLA/CCF to 0°/0° PLA/CGF, and ultimately to 0°/0° PLA/CCF.

2. In the second phase of experiments, the inherent frequencies of the first four BM for each composite structure were determined with a 3D laser vibrometer. The inherent frequencies progressively increase from 0°/90° PLA/CGF (21.3 Hz) to 0°/90° PLA/CCF (26.6 Hz) to 0°/0° PLA/CGF (47.7 Hz), and ultimately to 0°/0° PLA/CCF (60 Hz). Additionally, the amplitude spectrum showcased the maximum amplitude aligned with the first inherent frequencies, measuring 9.26 μm, 10.11 μm,4.40 μm and 4.14 μm respectively.
3. To investigate the uncontrolled vibration amplitude behavior, each composite structure was stimulated at first resonant frequency using electrodynamic shaker. The maximum amplitudes for 0°/0° PLA/ CCF, 0°/90° PLA/CCF, 0°/0° PLA/CGF and 0°/0° PLA/CCF exhibited a range approximately from + 210 μm to −212 μm at 60 Hz, + 514 μm to −545 μm at 26.6 Hz, + 244 μm to −242 μm at 47.7 Hz and + 785 μm to −810 μm, respectively.
4. Utilizing an OLAVC methodology with incremental parameter tuning, optimal control voltage and phase settings were determined to achieve maximum amplitude reduction. The control voltage along with phase for 0°/0° PLA/CCF, 0°/90° PLA/CCF, 0°/0° PLA/CGF and 0°/0° PLA/CCF were determined as follows:10.52 V with 351° phase,29.4 V with 45°phase, 17.68 V with 4° phase and 43 V with 79° phase.
5. Upon applying these optimizations, amplitude reduction of more than 120 times,80 times,90 times and 75 times was observed for 0°/0° PLA/CCF, 0°/90° PLA/CCF, 0°/0° PLA/CGF and 0°/0° PLA/CCF respectively.
6. Furthermore, the results indicated that 0°/0° layer orientations demonstrated higher vibration reduction with lower control voltage compared to 0°/90°. The overall sequence of amplitude reduction progressively increases from 0°/90° PLA/CGF to 0°/90° PLA/CCF to 0°/0° PLA/CGF, and finally to 0°/0° PLA/CCF.

Declaration of Competing Interest

The authors declare the following financial interests/personal relationships which may be considered as potential competing interests: Ruta Rimasauskiene reports financial support and equipment, drugs, or supplies were provided by Kaunas University of Technology. Ruta Rimasauskiene reports a relationship with Kaunas University of Technology that includes: employment and funding grants. Nothing.

Data availability

No data was used for the research described in the article.

References

[1] Gülbahçe E, Çelik M. Active vibration control of a smart beam by a tuner-based PID controller. J Low Freq Noise Vib Act Control 2018;37:1125–33. https://doi.org/10.1177/1461348418782169.
[2] Pandey A, Arockiarajan A. Actuation performance of macro-fiber composite (MFC): modeling and experimental studies (C) Sens Actuators A Phys 2016:114–29. https://doi.org/10.1016/J.SNA.2016.07.022.
[3] Konka HP, Wahab MA, Lian K. Piezoelectric fiber composite transducers for health monitoring in composite structures. Sens Actuators A Phys 2013;194:84–94. https://doi.org/10.1016/J.SNA.2012.12.039.
[4] Kim HS, Kim JH, Kim J. A review of piezoelectric energy harvesting based on vibration. 2011;12: Int J Precis Eng Manuf 2011;12(6):1129–41. https://doi.org/10.1007/S12541-011-0151-3.
[5] Li J, Xue Y, Li F, Narita Y. Active vibration control of functionally graded piezoelectric material plate. Compos Struct 2019;207:509–18. https://doi.org/10.1016/J.COMPSTRUCT.2018.09.053.
[6] Yashavantha Kumar GA, Sathish Kumar KM. Free vibration analysis of smart composite beam. Mater Today Proc 2017;4:2487–91. https://doi.org/10.1016/j.matpr.2017.02.101.
[7] Awada A, Younes R. Optimized active control of a smart cantilever beam using genetic algorithm. Des (Basel) 2022;6:36. https://doi.org/10.3390/designs6020036.
[8] Jia Y, Wei X, Xu L, Wang C, Lian P, Xue S, et al. Multiphysics vibration FE model of piezoelectric macro fibre composite on carbon fibre composite structures. Compos B Eng 2019;161:376–85. https://doi.org/10.1016/j.compositesb.2018.12.081.
[9] Liu Q, Xu X, Ma J, Wang J, Shi Y, Hui D. Lateral crushing and bending responses of CFRP square tube filled with aluminum honeycomb. Compos B Eng 2017;118:104–15. https://doi.org/10.1016/J.COMPOSITESB.2017.03.021.
[10] Shi Y, Swait T, Soutis C. Modelling damage evolution in composite laminates subjected to low velocity impact. Compos Struct 2012;94:2902–13. https://doi.org/10.1016/J.COMPSTRUCT.2012.03.039.
[11] Zhang WX, Zhang W, Yang DS, Luo Z, Guo XY. Vibration suppression of nonlinear laminated composite plates using internal oscillator-enhanced nonlinear energy sinks. Eng Struct 2023;279:115579. https://doi.org/10.1016/J.ENGSTRUCT.2022.115579.
[12] Ma R, Bi K, Hao H. Inerter-based structural vibration control: a state-of-the-art review. Eng Struct 2021;243:112655. https://doi.org/10.1016/j.engstruct.2021.112655.
[13] Fang X, Hao H, Bi K. An innovative pendulum-type column-in-column (PCIC) system for structural vibration control induced by seismic ground excitations. Eng Struct 2022;256:113990. https://doi.org/10.1016/j.engstruct.2022.113990.
[14] Deraemaeker A, Nasser H. Numerical evaluation of the equivalent properties of macro fiber composite (MFC) transducers using periodic homogenization. Int J Solids Struct 2010;47:3272–85. https://doi.org/10.1016/J.IJSOLSTR.2010.08.006.
[15] Park S, Inman DJ, Yun CB. An outlier analysis of MFC-based impedance sensing data for wireless structural health monitoring of railroad tracks. Eng Struct 2008;30:2792–9. https://doi.org/10.1016/J.ENGSTRUCT.2008.02.019.
[16] Topolov VY, Bisegna P, Bowen CR. Piezo-active composites: orientation effects and anisotropy factors. Springe Ser Mater Sci 2014:185. https://doi.org/10.1007/978-3-642-38354-0.
[17] Betts DN, Kim HA, Bowen CR, Inman DJ. Optimal configurations of bistable piezo-composites for energy harvesting. Appl Phys Lett 2012;100:114104. https://doi.org/10.1063/1.3693523.
[18] Sreenivasa Prasath S, Arockiarajan A. Effective electromechanical response of macro-fiber composite (MFC): Analytical and numerical models. Int J Mech Sci 2013;77:98–106. https://doi.org/10.1016/J.IJMECSCI.2013.09.031.
[19] Friswell MI, Ali SF, Bilgen O, Adhikari S, Lees AW, Litak G. Non-linear piezoelectric vibration energy harvesting from a vertical cantilever beam with tip mass. J Intell Mater Syst Struct 2012;23:1505–21. https://doi.org/10.1177/1045389×12455722.
[20] Zhang SQ, Li YX, Schmidt R. Modeling and simulation of macro-fiber composite layered smart structures. Compos Struct 2015;126:89–100. https://doi.org/10.1016/J.COMPSTRUCT.2015.02.051.
[21] Smart Material n.d. ⟨https://www.smart-material.com/⟩ (Accessed 6 March 2022).
[22] NASA n.d. ⟨https://www.nasa.gov/⟩ (Accessed 6 March 2022).
[23] Xie C, Wu Y, Liu Z. Modeling and active vibration control of lattice grid beam with piezoelectric fiber composite using fractional order PDμ algorithm. Compos Struct 2018;198:126–34. https://doi.org/10.1016/j.compstruct.2018.05.060.
[24] Wu D, Huang L, Pan B, Wang Y, Wu S. Experimental study and numerical simulation of active vibration control of a highly flexible beam using piezoelectric intelligent material. Aerosp Sci Technol 2014;37:10–9. https://doi.org/10.1016/j.ast.2014.04.008.
[25] Przybylski J, Gasiorski G. Nonlinear vibrations of elastic beam with piezoelectric actuators. J Sound Vib 2018;437:150–65. https://doi.org/10.1016/J.JSV.2018.09.005.
[26] Mayer D., Herold S. Passive, Adaptive, Active Vibration Control, and Integrated Approaches. Vibration Analysis and Control in Mechanical Structures and Wind Energy Conversion Systems, IntechOpen; 2017, p. 1–23. https://doi.org/10.5772/INTECHOPEN.71838.
[27] Chai YY, Song ZG, Li FM. Active aerothermoelastic flutter suppression of composite laminated panels with time-dependent boundaries. Compos Struct 2017;179:61–76. https://doi.org/10.1016/j.compstruct.2017.07.053.

[28] Gawryluk J, Mitura A, Teter A. Dynamic control of kinematically excited laminated, thin-walled beam using macro fibre composite actuator. Compos Struct 2020;236:111898. https://doi.org/10.1016/j.compstruct.2020.111898.
[29] Zippo A, Ferrari G, Amabili M, Barbieri M, Pellicano F. Active vibration control of a composite sandwich plate. Compos Struct 2015;128:100–14. https://doi.org/10.1016/j.compstruct.2015.03.037.
[30] Mitura A, Gawryluk J. Experimental and finite element analysis of PPF controller effectiveness in composite beam vibration suppression. Eksploat i Niezawodn – Maint Reliab 2022;24:468–77. https://doi.org/10.17531/ein.2022.3.8.
[31] Miao W.K., Xu M.L., Wu C.S. Active vibration control of cantilever beam using MFC sensor and actuator. Recent Advances in Structural Integrity Analysis - Proceedings of the International Congress (APCF/SIF-2014) 2014:447–452. https://doi.org/10.1533/9780081002254.447.
[32] Danish B, Anilkumar PM, Rao BN. Suppression of cross-well vibrations of a bistable square cross-ply laminate using an additional composite strip. Int J Dyn Control 2023;11. https://doi.org/10.1007/s40435-023-01153-1.
[33] Rimašauskienė R, Jūrėnas V, Radzienski M, Rimašauskas M, Ostachowicz W. Experimental analysis of active–passive vibration control on thin-walled composite beam. Compos Struct 2019;223:110975. https://doi.org/10.1016/j.compstruct.2019.110975.
[34] Raza A, MAHATO S, Rimašauskienė R. Actuation performance of macro fibre composite (MFC) as actuator in vibration reduction of cantilever beams. Mechanics 2023;29:42–50. https://doi.org/10.5755/j02.mech.31732.
[35] Lee AJ, Xie A, Inman DJ. Suppression of cross-well oscillations for bistable composites through potential well elimination. J Vib Acoust, Trans ASME 2020;142:031003. https://doi.org/10.1115/1.4046123.
[36] Raza A, Rimašauskienė R, Jūrėnas V, Mahato S. Experimental investigation of vibration amplitude control in additive manufactured PLA and PLA composite structures with MFC actuator. Eng Struct 2023;294:116802. https://doi.org/10.1016/j.engstruct.2023.116802.
[37] Polymaker. PolyLiteTM PLA technical data sheet 2017. ⟨https://c-3d.niceshops.com/upload/file/PolyLite_PLA_TDS_V3.pdf⟩ (Accessed 9 March 2023).
[38] Toray composite materials America. T300 standard modulus carbon fiber technical data sheet 2018. ⟨https://www.rockwestcomposites.com/media/wysiwyg/T300DataSheet_1.pdf⟩ (Accessed 9 March 2023).
[39] Rimašauskas M, Kuncius T, Rimašauskienė R. Processing of carbon fiber for 3D printed continuous composite structures. Mater Manuf Process 2019;34:1528–36. https://doi.org/10.1080/10426914.2019.1655152.
[40] Gopi Krishna J, Thirumal JR. Application of smart materials in smart structures. Int J Innov Res Sci, Eng Technol 2015;4:5018–23. https://doi.org/10.15680/IJIRSET.2015.0407206.
[41] Lashin MMA, Saleh WS, Alrowais F. Determination of different structures' materials natural frequencies using fuzzy logic system. Int J Eng Adv Technol 2020;9:723–7. https://doi.org/10.35940/ijeat.b3641.029320.
[42] Miyashiro D, Taira H, Hamano R, Reserva RL, Umemura K. Mechanical vibration of single-walled carbon nanotubes at different lengths and carbon nanobelts by modal analysis method. Compos Part C: Open Access 2020;2:100028. https://doi.org/10.1016/J.JCOMC.2020.100028.
[43] Scislo L. Single-point and surface quality assessment algorithm in continuous production with the use of 3D laser doppler scanning vibrometry system. Sensors 2023;23. https://doi.org/10.3390/s23031263.
[44] Raza A, Rimašauskienė R, Jūrėnas V, Rimašauskas M. An experimental study on the dynamic properties of 3D-printed structures with different layer orientations. J Vib Eng Technol 2024. https://doi.org/10.1007/s42417-024-01417-w.

Title [A4]: Dynamic analysis and vibration control of additively manufactured thin-walled polylactic acid polymer (PLAP) and PLAP composite beam structures: numerical investigation and experimental validation
Authors: Ali Raza, Magdalena Mieloszyk, Rūta Rimašauskienė, Vytautas Jūrėnas

materials

MDPI

Article

Dynamic Analysis and Vibration Control of Additively Manufactured Thin-Walled Polylactic Acid Polymer (PLAP) and PLAP Composite Beam Structures: Numerical Investigation and Experimental Validation

Ali Raza [1,*], Magdalena Mieloszyk [2], Rūta Rimašauskienė [1,*] and Vytautas Jūrėnas [3]

[1] Faculty of Mechanical Engineering and Design, Kaunas University of Technology, Studentų Str. 56, LT-51424 Kaunas, Lithuania
[2] Institute of Fluid-Flow Machinery, Polish Academy of Sciences, Fiszera 14 Str., 80-231 Gdansk, Poland; mmieloszyk@imp.gda.pl
[3] Institute of Mechatronics, Kaunas University of Technology, Studentų Str. 56, LT-51424 Kaunas, Lithuania
* Correspondence: ali.raza@ktu.edu (A.R.); ruta.rimasauskiene@ktu.lt (R.R.)

Abstract: This study primarily presents a numerical investigation of the dynamic behavior and vibration control in thin-walled, additively manufactured (AM) beam structures, validated through experimental results. Vibration control in thin-walled structures has gained significant attention recently because vibrations can severely affect structural integrity. Therefore, it is necessary to minimize these vibrations or keep them within acceptable limits to ensure the structure's integrity. In this study, the AM beam structures were made of polylactic acid polymer (PLAP), short carbon fiber reinforced in PLAP (SCFR|PLAP), and continuous carbon fiber reinforced in PLAP (CCFR|PLAP), with $0^{\circ}|0^{\circ}$ layer orientations. The finite element modeling (FEM) of the AM beam structures integrated with macro fiber composite (MFC) was carried out in Abaqus. The initial four modal frequencies of bending modes (BMs) and their respective modal shapes were acquired through numerical simulation. It is crucial to highlight the numerical findings that reveal discrepancies in the 1st modal frequencies of the beams, ranging up to 1.5% compared to their respective experimental values. For the 2nd, 3rd, and 4th modal frequencies, the discrepancies are within 10%. Subsequently, frequency response analysis (FRA) was carried out to observe the frequency-dependent vibration amplitude spectrum at the initial four BM frequencies. Despite discrepancy in the amplitude values between the numerical and experimental datasets, there was consistency in the overall amplitude behavior as frequency varied. THz spectroscopy was performed to identify voids or misalignment errors in the actual beam models. Finally, vibration amplitude control using MFC (M8507-P2) was examined in each kinematically excited numerical beam structure. After applying a counterforce with the MFC, the controlled vibration amplitudes for the PLAP, SCFR|PLAP, and CCFR|PLAP configurations were approximately ± 19 µm, ± 16 µm, and ± 13 µm, respectively. The trend in the controlled amplitudes observed in the numerical findings was consistent with the experimental results. The numerical findings of the study reveal valuable insights for estimating trends related to vibration control in AM beam structures.

Keywords: thin-walled beam; MFC; modal frequencies; THz spectroscopy; vibration control; amplitude spectrum

Citation: Raza, A.; Mieloszyk, M.; Rimašauskienė, R.; Jūrėnas, V. Dynamic Analysis and Vibration Control of Additively Manufactured Thin-Walled Polylactic Acid Polymer (PLAP) and PLAP Composite Beam Structures: Numerical Investigation and Experimental Validation. *Materials* **2024**, *17*, 5478. https://doi.org/10.3390/ma17225478

Academic Editor: Giovanni Garcea

Received: 7 October 2024
Revised: 28 October 2024
Accepted: 7 November 2024
Published: 9 November 2024

1. Introduction

Currently, vibration suppression in structural dynamics has emerged as a prominent domain of research. These structures, either with simple or intricate designs, are susceptible to vibrations caused by various sources such as machinery noise, wind loads, human activities, and others [1]. These vibrations can significantly compromise structural integrity,

leading to premature fatigue and eventual failure. Therefore, it is necessary to mitigate these vibrations or keep them within an acceptable limit to minimize the risk of structural failure [2,3]. It is noteworthy to describe that thin-walled composite beam structures have a considerable number of engineering applications. Structures such as helicopter blades, aircraft blades, robotic arms, [4] and wing turbine blades demonstrate the geometry of thin-walled beams. However, flutter is a challenging issue concerned with these kinds of structures and needs to be minimized or eliminated [5]. In recent times, structures are manufactured using various types of composite materials to obtain high specific stiffness as well as specific strength. On the other hand, vibration suppression has emerged as a crucial issue for the operational performance of the system due to the flexible properties of the composite structures [6,7].

Many vibration suppression technologies, such as active control, semi-active control, passive control, and integrative control, have been implemented recently to enhance system integrity. A passive control scheme includes incorporating various damping materials or devices (e.g., mass, spring, and damper), producing the control counter force in reaction to external disturbances and does not need any external electrical source for operation. However, other schemes generally require actuators, sensors, and controllers to function. These can provide control counter forces to the system based on the real-time data but need external electrical sources to activate these devices [8]. It is important to highlight that active control schemes are increasingly used in numerous engineering fields due to the easy market accessibility of a range of smart materials, particularly piezoelectric [9,10]. Piezoelectric materials are often used for energy harvesting [11], monitoring structural integrity [12], and vibration suppression applications [13], due to their effective electromechanical capabilities, substantial blocking force, excellent stiffness, and prompt response [14]. Piezoelectric materials, such as lead zirconium titanate (PZT), are commonly employed in numerous industrial applications due to their excellent stiffness and ability to generate high actuation force. Additionally, they may be implemented as sensors and actuators attributed to direct piezoelectric and converse phenomena, respectively. However, they have some constraints, such as brittle behavior, inadequate flexibility, and limited capability to adapt curved surfaces [2]. The polyvinylidene fluoride is an alternative piezoelectric material that is relatively more flexible than PZT but generates less actuation force.

To alleviate the challenges of piezoelectric materials for real-life application, thorough studies have been carried out on the polymeric matrix reinforced with piezoceramic fibers [15,16]. In 1999, NASA developed various types of macro fiber composites (MFCs) to overcome their limitations. The polymeric matrix was reinforced with rectangular-shaped piezoceramic fibers and positioned within protective and electrode wraps [17–19]. Afterwards, in 2002, the Smart Materials Corp. commenced the production and supply of the MFCs under a licensed manufacturer agreement for NASA-developed technology [20].

Dafang et al. carried out an experimental study on active vibration control of a flexible beam manufactured from epoxy resin and fiberglass, employing the independent mode control (IMC) technique to control the first three modes independently. Piezoelectric patches, used as actuators, were integrated with the beam at designated positions to damp vibrations. The findings demonstrate that the modal damping of the beam structures was significantly enhanced by using the IMC technique. To perform the numerical simulation, the dynamic equation governing the beam was formulated using Hamilton's principle. The simulation results were closely aligned with the experimental results. The findings from experiments and simulations illustrate that employing the piezoelectric actuators enabled the IMC technique to effectively suppress vibrations [21]. Raza et al. conducted numerical simulations on the vibration control of beam structures with distinct material properties integrated with MFC (M8507-P2) using the ANSYS R19.1 software. Modal analysis was thoroughly performed on each beam to assess the modal frequencies and modal shapes. Additionally, vibration control employing MFC was executed on each beam, with the maximum vibration reduction noted in the beam with the highest 1st resonant frequency. The findings confirm that this scheme could be effectively implemented across

various materials to control vibration [22]. Silva et al. conducted an experimental study on active vibration control in composite beams by applying electromagnetic actuators. A fuzzy logic methodology was employed to control the vibration amplitude of the beams. An identical mathematical model of the experimental setup was developed using the unique methodology, and numerical simulations were performed on the model using the MATLAB platform. Both numerical and experimental results for vibration suppression of the first mode in frequency and time aspects were compared and validated. The insights reveal the robustness of the control methodology applied to suppress vibration amplitude [23]. Rimašauskienė et al. accomplished an experimental investigation to evaluate the combined impact of a unique active–passive vibration control methodology on the beam structure with the application of an MFC patch. The results demonstrate that the suggested methodology effectively facilitates in the vibration suppression of the beam structure [7]. Raza et al. performed a comprehensive investigation on the dynamic characteristics of 3D-printed beam structures integrated with MFC (M8507-P2). The beams were developed using polylactic acid polymer (PLAP), short carbon fiber reinforced in PLAP (SCFR | PLAP), and continuous carbon fiber reinforced in PLAP (CCFR | PLAP) beam structures oriented at two distinct layer patterns: 0° | 0° and 0° | 90°. The deformation, decrement coefficient, and modal characteristics were assessed, and the impact test was conducted on each beam to observe the influence of distinct layer patterns on dynamic characteristics. The findings demonstrate that the two distinct orientations (0° | 0° and 0° | 90°) have a significant effect on the dynamic characteristics of the beam [24]. Moreover, Raza et al. presented a detailed study of vibration damping with the influence of MFCs in 3D-printed composite structures made of CCFR | PLAP and continuous glass fiber reinforced in PLAP (CGFR | PLAP) with two distinct orientations (0° | 0° and 0° | 90°). The findings illustrate that the structures with 0° | 0° orientation exhibit higher vibration damping compared to those with the 0° | 0° orientation [25]. Karimi et al. presented a comprehensive review of the fused deposition modeling (FDM) approaches employed in the 3D printing of continuous and short fiber-reinforced composites. Continuous fiber-reinforced composite parts are receiving greater interest in industries, compared to short fibers, due to their excellent strength. Moreover, various fiber reinforcement composite fabrication approaches were discussed, especially two approaches: in situ fusion and ex situ prepreg. However, voids and irregularities were found in the parts fabricated by these two approaches. To alleviate these problems, new approaches have been established by researchers through modifications to these two techniques, resulting in the filling of voids and irregularities and enhancing the mechanical properties of composites parts [26]. Wani et al. conducted a comprehensive review of various control methodologies, including active, passive, and hybrid control, for effectively controlling vibrations in structures. The adoption of a specific control technique is influenced by the complexity of the structural system. Furthermore, it was reported that more than one type of technique may be implemented to control vibrations effectively [27]. Ding et al. presented a novel vibration control methodology to manage vertical vibrations within the engineering framework. Traditional tuned fluid column dampers (TFCDs) are employed to mitigate vibrations in horizontal orientations. This study introduces a novel methodology based on TFCD, aimed at successfully suppressing vibrations in vertical orientations. Afterward, the motion equations of the proposed system were formulated using Lagrange equations and further validated through numerical simulations in the ANSYS suite. The outcomes provide valuable insights into the capabilities of the suggested TFCD methodology and illustrate its potential to suppress vibrations in the vertical direction [28]. Wang et al. proposed a practical technique, 'dynamic mode decomposition (DMD) approach', to formulate a low-order state-space model (SSM) for mitigating vibrations in a cable strut-based framework, relying on data regarding the framework's behavior and input control force. The data related to the input control force were determined by stimulating the framework with integrated actuators. A novel linear quadratic regulator (LQR)-based approach, DMD-LQR, was developed using the DMD-based SSM. This approach has been proven to be more computationally effective relative to the FEM-derived LQR approach.

The efficacy of the novel approach (DMD-LQR) was also demonstrated through numerical simulations. The findings illustrate the effectiveness of this novel approach in mitigating vibrations [29]. Zang et al. conducted analytical and experimental studies on the nonlinear vibration control in coupled carbon composite beam structures with secured ends under thermal influence. The modal characterization and mode frequencies of the coupled beams were determined using the 'Rayleigh–Ritz' approach and confirmed by FEM. Dynamic equations of motion were formulated using Lagrange's set of equations and the 'Galerkin' approach. Additionally, the frequency-dependent amplitude response was assessed through the harmonic balance technique and verified through the 'Runge–Kutta' approach. For the experimental study based on the analytical study, NiTiNOL-steel wires were placed on the coupled beams in accordance with a predefined layout. The experimental findings demonstrate that the steel wires effectively damp the vibrations in the coupled composite beams and align with the analytical results [30]. Guang Sun et al. presented a 'linear active disturbance rejection control (LADRC)' approach to mitigate vibrations in beam structures integrated with piezoelectric patches acting as actuators. The beam structures were externally stimulated by harmonic loads. Initially, the fundamental equations of the beam with actuators were formulated utilizing the Euler–Bernoulli beam model along with Lagrange's equations. The LADRC approach for the beam with piezoelectric patches was derived from these fundamental equations. To confirm the accuracy of the analytical study, the same analysis was performed using ANSYS and experimentally. The findings validate that the applied approach has a substantial effect on controlling vibrations in beam structures [31]. Soltani et al. carried out a thorough investigation of vibration control of multi-layer sandwich-based micro-beams manufactured from piezoelectric materials. To examine the effectiveness of control measures for the sandwich beam structure and to assess the relevant mechanical characterization, both Hamiltonian and 'generalized differential quadrature (GDQ)' methodologies were applied in determining the solution discretely. Moreover, the authors designed several controllers to investigate the tracking characterization and vibration dampening of the system. The findings of this investigation demonstrated that the Linear Quadratic Integral-based control technique performed considerably more effectively in controlling vibration and enhancing tracking characteristics [32]. Moreira et al. proposed a unique passive damping approach for light and elastic frameworks by introducing viscoelastic material (VM) to address vibration challenges and potential early failure under dynamic loading conditions. They incorporated indentations on the internal surfaces of the host structure (bottom layer), along with the confining layer (upper layer) sandwiching the VM layer, which adopted a wave-like configuration. The modeling of this sandwich structure was performed using the 'NX Nastran software' in association with the Siemens FEMAP software, with the facilitation of the MATLAB platform for mesh creation. The insights confirm that the VM layer significantly enhances passive damping treatment [33]. Kamel et al. developed a dynamic model of a carbon composite-based cantilever beam in ANSYS using FEM to control vibrations. Frequency analysis of the dynamic model was conducted in ANSYS considering four distinct scenarios. The state space model (SSM) of the smart beam for each scenario was created in the MATLAB platform using the results obtained from ANSYS. Subsequently, a PID controller was developed using the SSM derived from the first scenario in the MATLAB platform and confirmed against the other three scenarios. To enhance the performance of the system, three additional smart controllers based on fuzzy logic were studied. The findings reveal that fuzzy-based controllers contributed a significant role in the vibration control of the beam system [34].

This numerical study aims to validate previously published experimental investigations [35]. Prior research extensively explored the dynamic characteristics of kinematically stimulated, additively manufactured (AM) beam structures, including modal characterization, frequency-dependent amplitude spectra, and vibration control influenced by MFC (M8507-P2). The beam structures were fabricated using PLAP, SCFR|PLAP, and

CCFR | PLAP with 0° | 0° layer orientations, and their fabrication process has been thoroughly discussed in a published experimental work [35].

This is the first time the dynamic characteristics and vibration control in numerical models of PLAP, SCFR | PLAP, and CCFR | PLAP with [0° | 0°] layer sequences integrated with MFC (M8507-P2) have been comprehensively discussed and validated against previously published experimental results. However, challenges arose due to the general assumptions adopted in the numerical simulations compared to the experimental scenarios.

Initially, the finite element modeling (FEM) of PLAP, SCFR | PLAP, and CCFR | PLAP with MFC (M8507-P2) was performed in the Abaqus CAE 2024 platform. Following this, the modal characterization assessment of each numerical beam model was conducted to assess the modal frequencies and their respective modal shapes. The discrepancies in numerical and experimental modal frequencies for each beam have been reported separately. Additionally, frequency response analysis (FRA) was carried out to assess the frequency-dependent amplitude spectra of the numerical models, and comparisons were made with the experimental results. In the next section, THz spectroscopy was performed to reveal voids or misalignment errors in the 3D-printed layers of actual beam models. Finally, vibration control in each numerical model, utilizing MFC counterforces, was thoroughly examined and compared with experimental results. A detailed investigation of the discrepancies between the simulation and experimental results has also been presented. Based on the findings, the beam structure that exhibited the highest vibration suppression was identified.

2. Materials and Methodology

In this numerical simulation investigation, the 0° | 0°-oriented PLAP, SCFR | PLAP and CCFR | PLAP beam structures were modeled to study dynamic characteristics such as modal characterization assessment and FRA, with the goal of mitigating vibrations in beam structures integrated with MFCs by implementing open-loop active vibration control (OL-AVC). The numerical results were thoroughly compared and validated with previously published experimental study by the authors. The overview of the steps involved in the numerical simulation investigation has been demonstrated in Figure 1.

In Figure 1, three main steps involved in the numerical simulation are illustrated: pre-processing, solution, and post-processing. In the pre-processing step, the geometry of the beam structure with the MFC is created and defined. The material properties are assigned to the beam and MFC separately, interaction is established between them, element types are assigned, and meshing is performed. Then, boundary conditions are applied, followed by defining various analysis steps such as linear perturbation frequency (to assess natural frequencies and mode shapes), steady-state dynamics (to assess frequency-dependent amplitude), and dynamics implicit (to analyze vibration control with MFCs).

In the solution step, a job is created for each step and executed for analysis. The progress of each numerical simulation is monitored, and the convergence of the results is confirmed. If the results do not converge, mesh refinement is performed, and the analysis steps are repeated.

In the post-processing step, the results are visualized and examined, and the required data are extracted. The graphs are generated to describe the results. Finally, the simulation results are validated against the experimental results to confirm the accuracy of the numerical findings.

A thorough discussion of numerical modeling, simulation investigation, and validation with the experiment are discussed in subsequent sections.

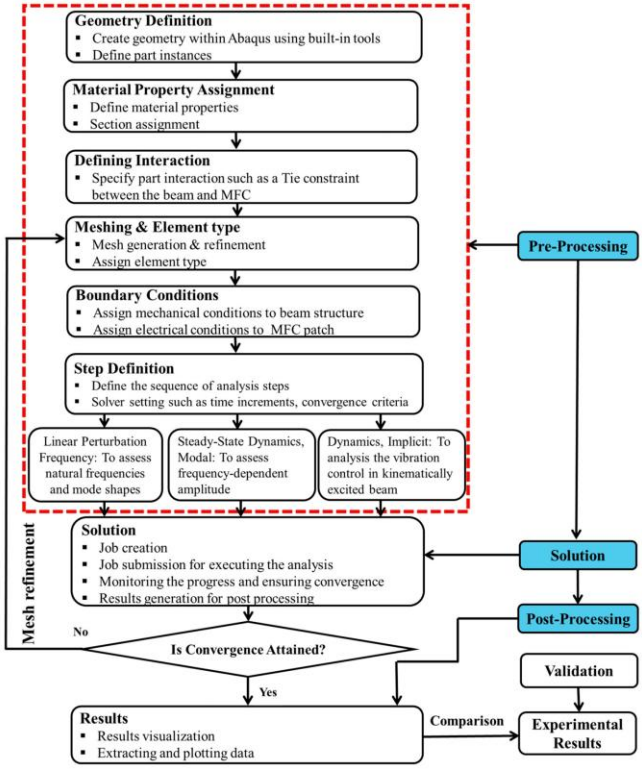

Figure 1. Overview of steps involved in numerical simulation.

2.1. Finite Element Modeling (FEM)

In this section, the FEM of laminated beam structures (length: 110 mm; width: 20 mm; thickness: 1.35 mm) with MFC patches is outlined. The overall effective dimensions of both numerical models and AM beam structures were considered similar. However, the actual length of the AM beam was 120 mm, as a 10 mm portion of the beam was placed within a support to firmly fix the beam from one side. Thus, the effective length of AM beams during the experiments was used 110 mm. Firstly, the PLAP and SCFR | PLAP laminated beams with [0° | 0°] layer sequences were individually modeled as continuum solid shells (CSS8). The layup-ply approach was adopted to describe the layer arrangement. The [0° | 0°] layer sequence indicates that all layers were aligned parallel (along the same axis) to each other without any angular deviation between them, as presented in Figure 2a. Conversely, the CCFR | PLAP beam composite with [0° | 0°] fiber layer sequences, was represented as continuum solid shells (CSS8) using a representative volume element (RVE) with an ~18% volume fraction of fibers (consistent with AM beam structures). Similarly, in the CCFR | PLAP model, [0° | 0°] fiber layer sequences showed that the direction of the fibers in both layers was parallel to each other (along the same axis), as illustrated in Figure 2b. The

material parameters for modeling beam structures are detailed in Table 1. Subsequently, the FEM of integrated MFC (M8507-P2) was performed using piezoelectric solid elements (C3D20RE). The active part of the MFC (length: 85 mm; width: 0.7 mm; thickness: 0.3 mm) was simplified as a homogeneous material rather than an intricate design. The material parameters of the MFC are listed in Table 2. The active portion of the MFC was affixed to each beam structure in accordance with AM samples, i.e., 15 mm from the fixed end. The Tie constraint was implemented to ensure interaction between the surfaces of the beam and the MFC. After numerically modeling the geometry, hexahedral (hex) meshing with refinement was performed on the MFC and each beam structure, resulting in no additional significant changes in the computed natural frequencies. The aim of the mesh refinement was to attain greater exactness; however, excessive refinement prolonged the computational time required to obtain the desired output, rendering it impractical for use. Further, mechanical boundary conditions involved fixing one side of the beam, with nodes restricted to displace in the X, Y, and Z direction, as depicted in Figure 3a. On the other side, a sinusoidal force was employed to kinematically excite the beam. However, due to limitations of the Abaqus, it was not possible to apply the excitation force through the fixed side as was carried out in the experiments exhibited in Figure 3b. The electrical boundary conditions, such as a sinusoidal signal (U_{MFC}), were applied from the upper side of the MFC, while the bottom side was grounded (0 V).

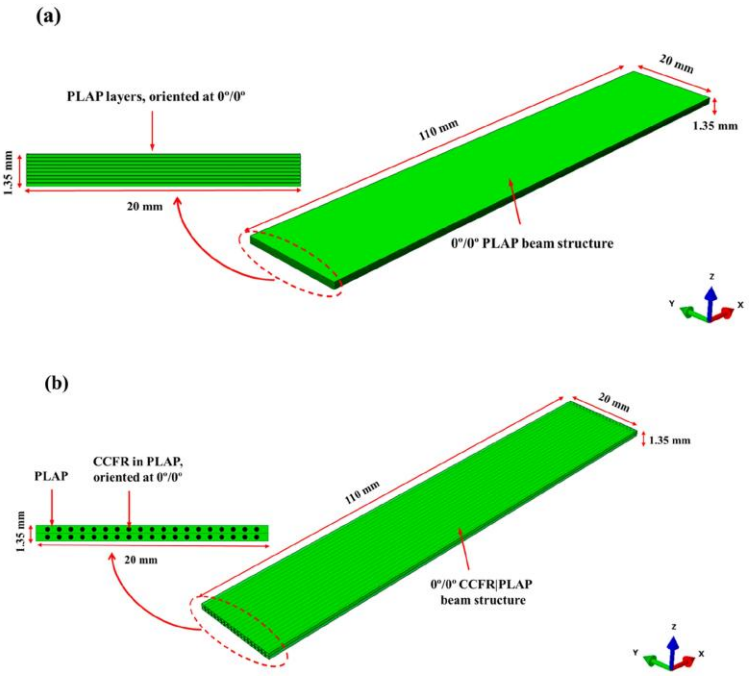

Figure 2. Modeling beam structures oriented at 0° | 0°: (**a**) approach for PLAP and SCFR | PLAP beam structures and (**b**) approach for CCFR | PLAP.

Table 1. Mechanical parameters of PLAP, SCFR | PLAP, and CCF [22,36–38].

Parameters	PLAP	PLAP | SCF	CCF
Young's Modulus (Y)	$(2636 \pm 330) \times 10^6$ Pa	5143×10^6 Pa	230×10^9 Pa
Poisson's Ratio (υ)	0.36	0.4	0.2
Tensile Strength	$(46.6 \pm 0.9) \times 10^6$ Pa	76×10^6 Pa	3530×10^6 Pa
Density	1.17 to 1.24 g/cm^3	1.35 g/cm^3	1.76 g/cm^3

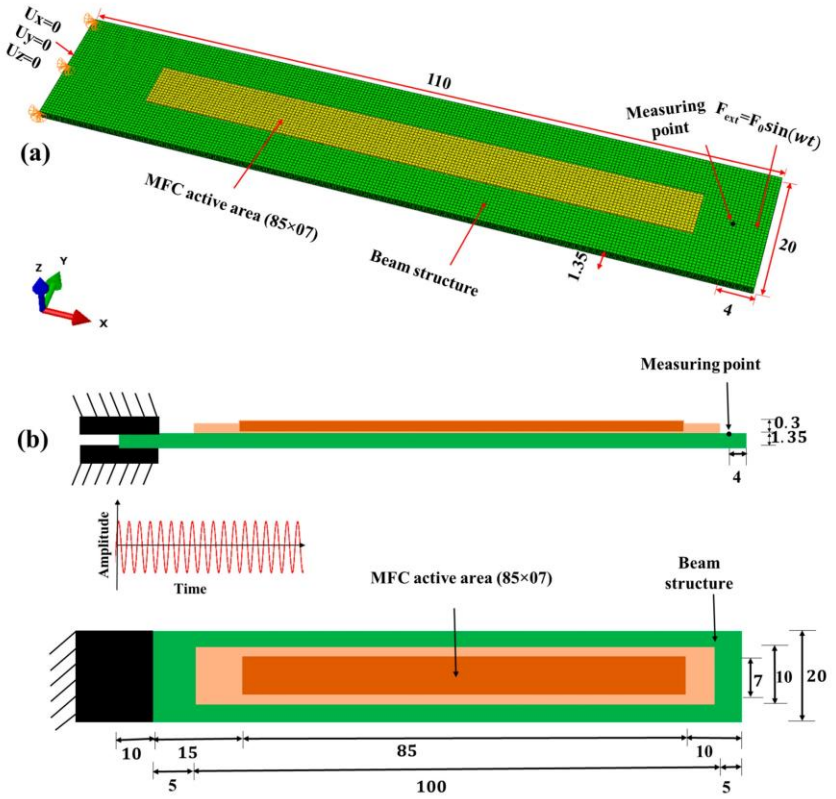

Figure 3. Beam structures integrated with MFC, illustrating boundary conditions (units in mm): (**a**) FEM model and (**b**) schematic view of experimental sample.

Table 2. Material Parameters of MFC (M8507-P2) [20,22,39,40].

Parameters	Values
Young's Modulus (Y)	$Y_1 = 30.336 \times 10^9$ Pa
	$Y_2 = Y_3 = 15.857 \times 10^9$ Pa
Shear Modulus	$G_{12} = G_{13} = G_{23} = 5.515 \times 10^9$ Pa
Poisson's Ratio (υ)	$\upsilon_{12} = \upsilon_{13} = 0.31$
	$\upsilon_{23} = 0.438$
Density	5.44 g/cm^3
Piezoelectric Coefficient	$d_{31} = -170$ pm/V
	$d_{32} = -100$ pm/V

2.2. Modal Analysis

The Lanczos methodology has been employed to compute the modal natural frequencies and corresponding mode shapes of beam structures without applying external forces. This process involves specifying the geometric configurations of the beam structures, material characteristics, and boundary conditions, such as fixing one side of the beam structure firmly.

The Abaqus employs the following fundamental governing equations to determine the modal frequencies and mode shapes, as explained in the Abaqus documentation [41]:

$$\boldsymbol{M}\ddot{\boldsymbol{z}}(t) + \boldsymbol{K}\boldsymbol{z}(t) = 0 \tag{1}$$

The above equation describes the motion of the undamped system with multiple degrees of freedom.

Where $\boldsymbol{M}$, $\ddot{\boldsymbol{z}}(t)$, $\boldsymbol{z}(t)$, $\boldsymbol{K}$ describe mass matrix, acceleration vector, displacement vector, and stiffness matrix.

Assuming harmonic motion of the dynamic system,

$$\boldsymbol{z}(t) = \boldsymbol{\Phi_n} \sin(w_n t) \tag{2}$$

By substituting Equation (2) into Equation (1),

$$\boldsymbol{M}\left(-w_n^2 \boldsymbol{\Phi_n} \sin(w_n t)\right) + \boldsymbol{K}(\boldsymbol{\Phi_n} \sin(w_n t)) = 0 \tag{3}$$

This simplifies to the following:

$$\left(\boldsymbol{K} - w_n^2 \boldsymbol{M}\right)\boldsymbol{\Phi_n} = 0 \tag{4}$$

Equation (4) represents equilibrium equation governing the dynamics of structure for undergoing free vibration that is formulated as an eigenvalue problem:

$$\lambda_n = w_n^2;\ (\boldsymbol{K} - \lambda_n \boldsymbol{M})\boldsymbol{\Phi_n} = 0 \tag{5}$$

where $\boldsymbol{K}$, $\boldsymbol{\Phi_n}$, λ_n, and $\boldsymbol{M}$ represent stiffness matrix, eigenvectors, eigenvalues, and mass matrix, respectively.

The eigenvalues λ_n yield the modal frequencies, while the eigenvectors, $\boldsymbol{\Phi_n}$, provide the mode shapes of structures. This is a general form of equation to compute modal frequencies and mode shapes. The relation between the eigenvalues λ_n and f_n is described as follows:

$$\lambda_n = w_n^2 \tag{6}$$

$$w_n = \sqrt{\lambda_n} \tag{7}$$

$$w_n = 2\pi f_n \tag{8}$$

where w_n and f_n represent the angular and linear natural frequencies, respectively.

The Lanczos methodology encompasses a set of Lanczos runs, with each run consisting of several iterations to refine the solution. The following spectral transformation is employed by Lanczos for each run.

$$\boldsymbol{M}\left(\boldsymbol{K} - \sigma\, \boldsymbol{M}\right)^{-1} \boldsymbol{M}\boldsymbol{\Phi_n} = \theta \boldsymbol{M}\boldsymbol{\Phi_n} \tag{9}$$

where σ and θ are the phase shift and eigenvalue, respectively. This transformation provides effective convergence to the expected eigenvalues. The eigenvectors of this equation (Equation (4)) and the spectral transform equation (Equation (9)) are the same, but the eigenvalues have the following relationship:

$$\lambda_n = \frac{1}{\theta} + \sigma \tag{10}$$

2.3. Frequency Response Analysis (FRA)

The frequency-dependent dynamic response (amplitude spectrum) of each beam structure (PLAP, SCFR | PLAP, and CCFR | PLAP) with layers oriented at 0° | 0° was assessed across a frequency spectrum and subjected to dynamic loading conditions. One side of the beam structure was firmly fixed, while the harmonic excitation force was applied to the free-end side, as exhibited in Figure 4.

Figure 4. Schematic depiction of beam structure with MFC to assess frequency-dependent dynamic behavior.

The FRA primarily depends on the previously performed modal analysis, as described in Equation (9). Modal analysis determines the modal frequencies (w'_n) and modal shapes of the beam structure, which are crucial for describing the dynamic behavior of the beam structure. FRA finds out the response of the structure subjected to harmonic force over a spectrum of frequencies. The displacement spectrum $\boldsymbol{z}(t)$ in response to the applied force can be stated as the cumulative total from each modal mode, as described in the Abaqus documentation [41]:

$$\boldsymbol{z}(t) = \sum_{n=1}^{\infty} \alpha_n \boldsymbol{\Phi_n} \tag{11}$$

where α_n and $\boldsymbol{\Phi_n}$ denote the modal amplitude and mode shape (mode coordinates) of nth mode, respectively. Where Equation (12) describes α_n:

$$\alpha_n = \left(\boldsymbol{\Phi_n}^{\mathrm{T}} \mathbf{F}_0\right) / \left(w_n^2 - w^2 + 2i\, \int_n w_n w\right) \tag{12}$$

In Equation (12), $\boldsymbol{F}_0$, w and $\int_n$ denote the force exertion, excitation frequency, and damping ratio, respectively.

2.4. THz Spectroscopy

The non-destructive C-scanning of beam structures was performed to identify internal defects using the THz spectrometer (TPSTM Spectra 300 THz Pulsed Imaging and Spectroscopy from TeraView), as presented in Figure 5a. This high-tech instrument employs terahertz (THz) radiation to analyze samples made from various materials. The unique characteristics of THz radiation enable it to penetrate samples, making it effective for non-destructive testing and imaging. The applicability of the NDT technique is primarily limited to the inspection of non-conductive materials, such as polymers [42] or glass fiber-reinforced polymers [43]. Its main advantage is the low power (below 1 µW [44]) generated by a THz wave that reduces the risk of destroying sensitive materials. THz waves are totally reflected by conductive materials. CCFR structures contain conductive carbon fibers reinforced in a non-conductive polymeric matrix. The applicability range of the NDT method for CCFR strongly depends on the carbon fiber content. For instance, CCFR laminates manufactured using infusion method have a high fiber content (typically 60–70% of total weight [45]). In such case, THz spectroscopy can be used to detect coatings (e.g., contaminations, thickness variation [46]) or surface damage (e.g., burn [47]). A comparative analysis of the influence of different carbon fiber alignments in CCFR laminates on THz wave penetration depth is thoroughly presented by authors [48]. In the analyzed CCFR | PLAP samples, the fiber content is significantly lower, approximately 18%. This lower amount of conductive material (carbon fiber) allows THz spectroscopy to inspect the whole structure.

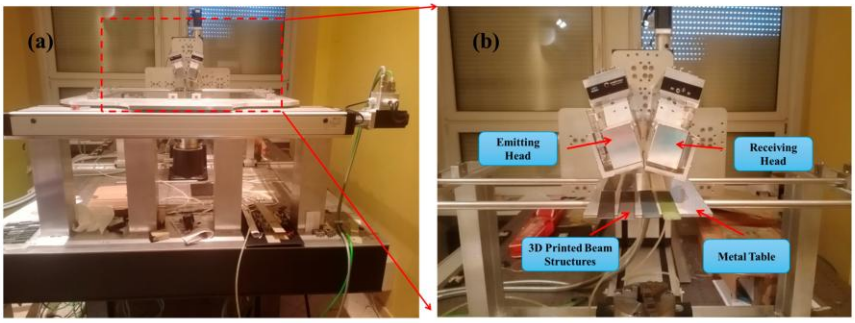

Figure 5. Non-destructive C-scanning of beam structures to identify the internal defects: (**a**) THz spectrometer setup for experiment and (**b**) illustration identifying internal defects.

The spectrometer facilitates the determination of sample parameters within the THz frequency range and is capable of scanning samples in either reflection or transmission mode. Its imaging capability allows for the measurement of samples up to 700 mm × 700 mm in size. For the investigation, each beam structure, with dimensions of 120 mm × 20 mm × 1.35 mm, was placed on a metal table and examined in reflection mode. The measuring heads were configured with a 22° angle between them, as presented in Figure 5b. Since THz radiation is significantly affected by moisture, the investigation was conducted using an air dryer to minimize moisture around the measuring heads and an air conditioner to maintain an ambient temperature of 20 °C. The scanning step was set to 0.2 mm in the xy plane, and THz signals were recorded with 10 averages.

2.5. Examination of Vibration Control with Influence of MFC

To analyze vibration damping, the dynamic response equation of the beam structure with MFC has been employed and is as follows:

$$\mathbf{M}\ddot{\mathbf{z}}(t) + \mathbf{C}\dot{\mathbf{z}}(t) + \mathbf{K}\mathbf{z}(t) = \mathbf{F}_{ext} - \mathbf{F}_{MFC} \tag{13}$$

Here, **C** represent the damping matrix, $\dot{z}(t)$ is the velocity vector, $\mathbf{F}_{ext}$ denotes the external force on the beam to generate vibrations, and $\mathbf{F}_{MFC}$ indicates the force provided by the MFC to damp vibration amplitude.

$$\text{Where } \mathbf{F}_{ext} = \mathbf{F}_0 sin(wt) \text{and } \mathbf{F}_{MFC} = d_{31} A V_0 sin(wt) \tag{14}$$

where A, V_0, and d_{31} indicate the active area of the MFC, amplitude of harmonic signal provided to MFC, and piezoelectric coefficient, respectively.

The force ($\mathbf{F}_{MFC}$) produced by the MFC operates in opposition to the external harmonic force and effectively reduces the vibration amplitude in the beam structure. The damping matrix $\mathbf{C}'$, incorporated in the Equation (13), inherently encompasses the internal friction and other energy dissipative effects that are crucial to damp vibration amplitude in the beam structure.

3. Results and Discussions

To examine the dynamic characteristics of beam structures (PLAP, SCFR | PLAP, and CCFR | PLAP), modal characteristics' assessment and FRA were carried out using the Abaqus. THz spectroscopy was carried out to identify defects in AM structures. Afterwards, vibration suppression in each beam was thoroughly studied and compared with the published experimental data [35], addressing the limitations of the numerical simulation.

3.1. Assessment of Modal Characteristics of Beam Structures

In the preliminary phase of the numerical simulation investigation, the emphasis is on identifying the modal frequencies and modal bending mode shapes of numerical beam structures. By incorporating the MFC (M8507-P2) patch within the beams, each beam experiences a slight enhancement in mass and stiffness, leading to deviations in natural frequencies compared to beams without the MFC patch [24,35]. The natural frequencies of the first four bending mode shapes have been presented in Table 3, and it can be clearly observed that the natural frequencies of beams with the MFC are higher than those of beams without the MFC. The average computational time to calculate the natural frequencies of the numerical beam models was approximately 26 min. The initial four bending mode shapes of each numerical beam model are presented in Figure 6. The first natural frequencies of the numerical models were found to be 30.45 Hz for PLAP, 39.95 Hz for SCFR | PLAP, and 60.50 Hz for CCFR | PLAP. These numerical values closely align with the experimental frequencies of 30.00 Hz, 40.50 Hz, and 60.00 Hz, respectively, resulting in differences of only 1.50%, 1.35%, and 0.83% for PLAP, SCFR | PLAP, and CCFR | PLAP, respectively. The fourth natural frequencies of the numerical models were found to be 1268.00 Hz for PLAP, 1580.70 Hz for SCFR | PLAP, and 2189.70 Hz for CCFR | PLAP. The corresponding experimental values were 1207.50 Hz, 1546.00 Hz, and 2192.00 Hz, with differences of approximately 5.01%, 2.24%, and 0.10% for PLAP, SCFR | PLAP, and CCFR | PLAP, respectively. The second and third natural frequencies of the numerical models deviate within 10% from the experimental values.

Several factors could contribute to discrepancies between the modal frequencies of the FEM and actual AM beam models. Firstly, the geometry of the AM beam could differ slightly from the idealized numerical model used in Abaqus. This difference might be due to internal irregularities such as defects that are not perfectly considered in the numerical model. Secondly, defining boundary conditions in the numerical model with simple assumptions could lead to inconsistencies with experimental results. For instance, in the numerical simulation, the beam structure is confirmedly fixed at one end, while in real

conditions (experiments), there is a possibility that the beam was not firmly fixed, leading to a lack of consistency with the numerical model. To further investigate this, the node locations of the first four bending modes of one of the AM beams and its corresponding numerical model, specifically CCFR | PLAP with MFC, have been determined and presented in Figure 7. In the AM model, the node locations were identified using the 3D laser vibrometer, while in the numerical, the Abaqus platform was used. It can be clearly noted from Figure 7 that the beams vibrate very close to the fixed side, especially in the 2nd, 3rd, and 4th bending modes of both the AM and numerical models. There is a possibility that the AM beam was not firmly fixed, and displacement from the fixed end occurred during vibrating conditions.

Table 3. Natural frequencies of 0° |0°-oriented beam structures with and without MFC: experiments and numerical simulation results.

Bending Modes	0° | 0° PLAP			0° | 0° SCFR | PLAP			0° | 0° CCFR | PLAP		
	Experiment with MFC (Hz)	Numerical Without MFC (Hz)	Numerical with MFC (Hz)	Experiment with MFC (Hz)	Numerical Without MFC (Hz)	Numerical with MFC (Hz)	Experiment with MFC (Hz)	Numerical Without MFC (Hz)	Numerical with MFC (Hz)
1st	30.00	26.89	30.45	40.50	34.70	39.95	60.00	61.47	60.5
2nd	215.00	168.23	236.33	280.50	216.96	289.47	410.00	384.71	392.83
3rd	626.50	471.76	671.73	802.00	608.53	825.02	1153.00	1076.10	1119.00
4th	1207.50	927.35	1268.00	1546.00	1196.50	1580.70	2192.00	2106.20	2189.70

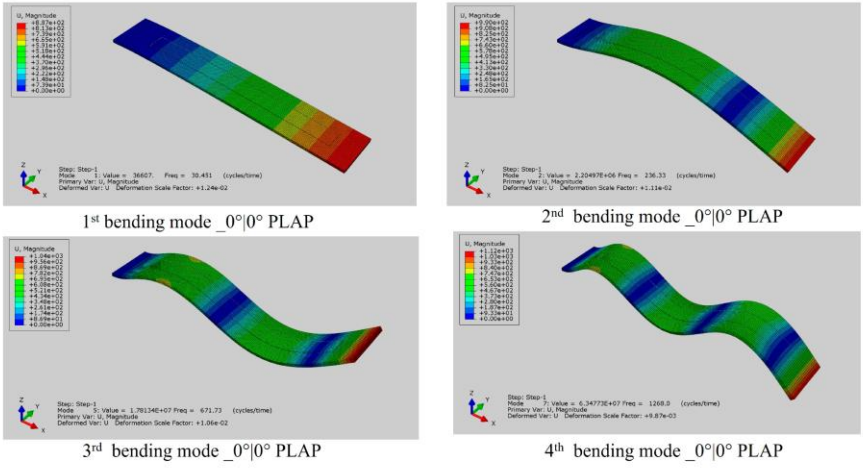

(a) Bending modes _0°|0° PLAP

Figure 6. *Cont.*

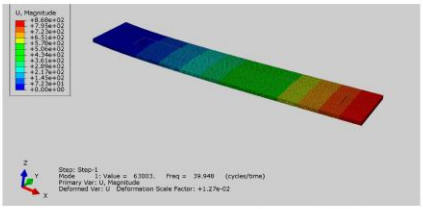

1st bending mode _0°|0° SCFR|PLAP

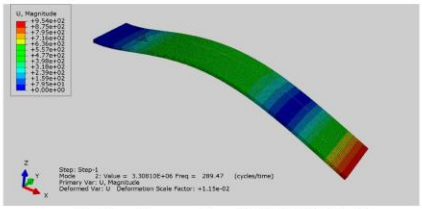

2nd bending mode _ 0°|0° SCFR|PLAP

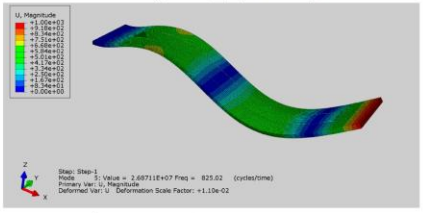

3rd bending mode _ 0°|0° SCFR|PLAP

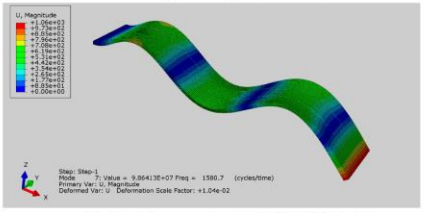

4th bending mode _0°|0° SCFR|PLAP

(b) Bending modes _0°|0° SCFR|PLAP

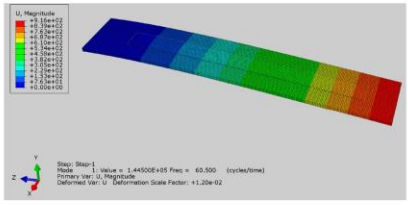

1st bending mode _0°|0° CCFR|PLAP

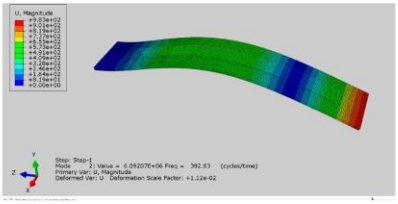

2nd bending mode _0°|0° CCFR|PLAP

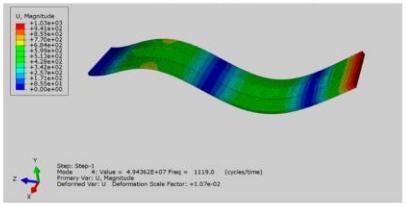

3rd bending mode _0°|0° CCFR|PLAP

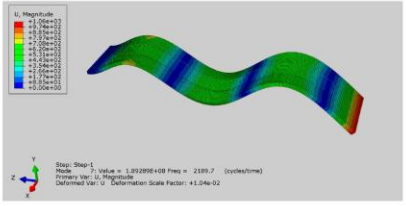

4th bending mode _0°|0° CCFR|PLAP

(c) Bending modes _0°|0° CCFR|PLAP

Figure 6. Initial four bending modes of MFC-integrated 0°|0°-oriented beam structures: (**a**) bending modes _0°|0° PLAP, (**b**) bending modes _0°|0° SCFR|PLAP, and (**c**) bending modes _0°|0° CCFR|PLAP.

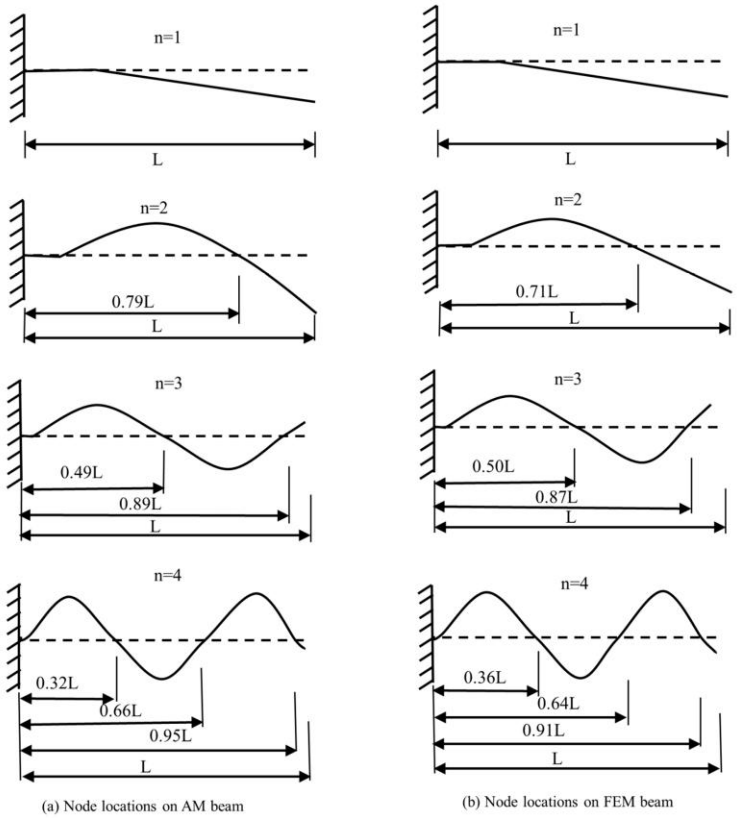

Figure 7. Node locations on beam structure integrated with MFC: (**a**) node locations on AM beam and (**b**) node locations on AM beam.

3.2. Frequency Response Analysis (FRA) of Beam Structures

In this section, a detailed discussion has been provided on the frequency-dependent dynamic behavior of the numerical beam models (PLAP, SCFR | PLAP, and CCFR | PLAP) integrated with the MFC under harmonic excitations. To assess the dynamic behavior, one side of numerical model was fixed, as depicted in Figure 4, while a sinusoidal force with an amplitude of $\pm 1 \times 10^{-8}$ N was applied to the other side. Figure 8 illustrates the amplitude spectrum of numerical and AM beam models at the first four resonant frequencies of bending modes. Table 4 presents the initial four bending mode numerical resonant frequencies of beam structures along with their amplitudes. The average computational time to compute the FRA response of beam structures was approximately 55 min.

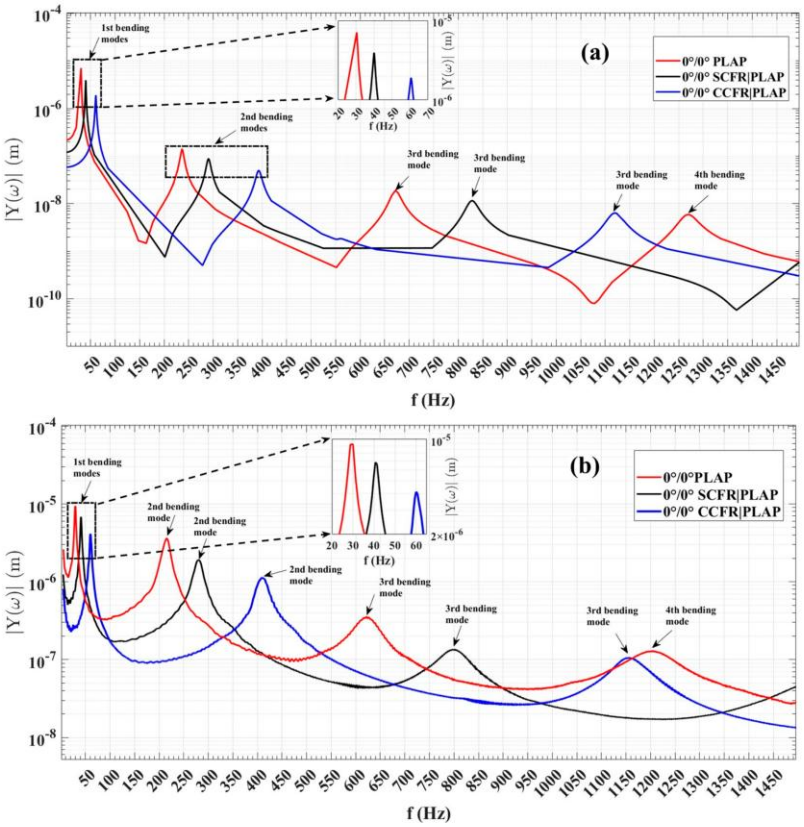

Figure 8. Frequency-dependent amplitude spectrum of 0°|0°-oriented beam structures: (**a**) numerical data and (**b**) experimental data.

Table 4. Numerical natural frequencies of 0°|0°-oriented beam structures with amplitudes.

Bending Modes	0°|0° PLAP		0°|0° SCFR|PLAP		0°|0° CCFR|PLAP	
	Numerical Frequency (Hz)	Amplitude (μm)	Numerical Frequency (Hz)	Amplitude (μm)	Numerical Frequency (Hz)	Amplitude (μm)
1st	30.45	7.0870	40.00	3.9240	60.50	1.898
2nd	236.33	0.1420	290.42	0.0874	392.83	0.0496
3rd	671.73	0.0189	827.70	0.0115	1119.00	0.00636
4th	1268.00	0.0059	1585.10	0.0034	2189.70	0.0016

These trends in numerical findings were confirmed with the early published experimental data [33]. The frequency-dependent dynamic response of the actual AM beam structures was measured by fixing one side of each beam structure in a fixture and applying a 100 V excitation signal to the MFC patch. The amplitude spectrum of each beam structure, illustrating the variation in vibration amplitudes with changing frequencies, was measured by a 3D laser vibrometer (PSV-W-500) manufactured by 'Polytec GmbH, Germany'. Notably, the amplitude spectrum revealed (Figure 8) that vibration amplitudes peaked at the first resonant frequencies of the bending mode and decreased towards the fourth resonance frequencies in both numerical and experimental data. Although there was a considerable difference in the absolute values of vibration amplitudes between the numerical and experimental data, a consistent trend in amplitude variation over the resonant frequencies was observed in both sets of results.

Moreover, the resonant frequencies of FEM and AM beams were noted to be near each other, as reported in Table 3. Despite the discrepancy in the vibration amplitude values between the two datasets, there was consistency in the overall behavior of vibration amplitudes as frequency varied. For instance, in the numerical results, the vibration amplitudes at the first resonance frequency were observed to be the highest as follows: 7.0870 µm at 30.45 Hz for PLAP, 3.9240 µm at 40.00 Hz for SCFR | PLAP, and 1.8980 µm at 60.5 Hz for CCFR | PLAP. The corresponding experimental vibration amplitudes at the first resonance frequency were as follows: 9.295 µm at 30 Hz for PLAP, 6.831 µm at 40.5 Hz for SCFR | PLAP, and 4.139 µm at 60 Hz for CCFR | PLAP.

In the numerical results, the lowest vibration amplitudes were noted at the fourth resonant frequency: 0.0059 µm at 1268.00 Hz for PLAP, 0.0034 µm at 1585.10 Hz for SCFR | PLAP, and 0.0016 µm at 2189.70 Hz for CCFR | PLAP. The corresponding experimental values were observed to be 0.1290 µm at 1207.50 Hz for PLAP, 0.0490 µm at 1546.00 Hz for SCFR | PLAP, and 0.0220 µm at 2192.00 Hz for CCFR | PLAP.

Both the numerical and experimental results follow the same trend. Similarly, the variation in the vibration amplitudes of the numerical model at the second and third resonant frequencies follows the same trend observed in the experimental model, as illustrated in Figure 8.

Overall, the numerical approach effectively captures the dynamic behavior of each AM beam structure, as evidenced by the consistency of numerical results with the experimental results. However, the observed differences in absolute amplitude values may be attributed to the limitations in boundary conditions: in experimental case, the excitation force was provided by the MFC patch, while in numerical case, the force was provided at the free-end side of each beam structure.

3.3. Analysis of THz Spectroscopy Findings

The aim of utilizing THz spectroscopy was to analyze the beam structures of real samples that were modeled using the Abaqus CAE 2024 software. The simulations were performed under the assumption that the real structures were ideal, without voids or fiber alignment errors in any 3D-printed layer or across consecutive layers.

C-scans were determined for three samples and presented in Figure 9a–c. In each case, three surfaces were determined: the upper surface of the sample, the bottom surface of the sample, and the image obtained from the metal table. In the case of PLAP (Figure 9), the image of the upper surface (Figure 9a) presents its periodic irregularity. The image of the bottom surface (Figure 9b) shows that the sample was manufactured from thin PLAP filament lines that were aligned so closely together they were not visible using the 'naked eye'. Such internal structure influences the vibration properties of the material. The image obtained from the metal plate (Figure 9c) contains information about both the material's periodic irregularity (probably due to the PLAP filaments in consecutive layers not being perfectly aligned) and the joint PLAP filaments creating the structure.

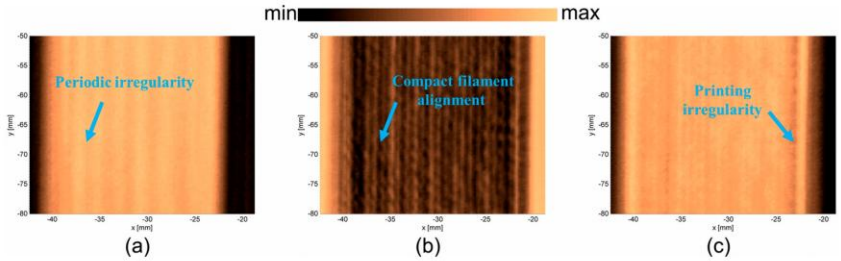

Figure 9. PLAP surfaces: (**a**) upper surface, (**b**) bottom surface, and (**c**) metal table.

In the case of SCFR | PLAP (Figure 10), determining the upper surface was more challenging than in the PLAP case (pure polymer), probably due to the irregular distribution of conductive short carbon fibers in the SCFR | PLAP composite. Therefore, the image for the upper surface (Figure 10a) appears blurred. However, it is still possible to observe the periodicity of the sample surface. The image of the bottom surface (Figure 10b) indicates the characteristics of manufacturing method, revealing the sample was manufactured from thin parallel SCFR | PLAP filaments. The structure contains some discontinuations, observed as circular objects randomly distributed in the structure. This may be an effect of locally higher or lower amounts of short carbon fibers in the SCFR | PLAP-printed filaments. Such inequality should not considerably influence the vibrational properties of the material. However, differences in the mechanical properties of carbon fiber and polymer could result in such areas to be an origin of structural damage. The image determined from the metal table (Figure 10c) indicates that, when considering the whole thickness of the sample, the short carbon fibers are equally distributed.

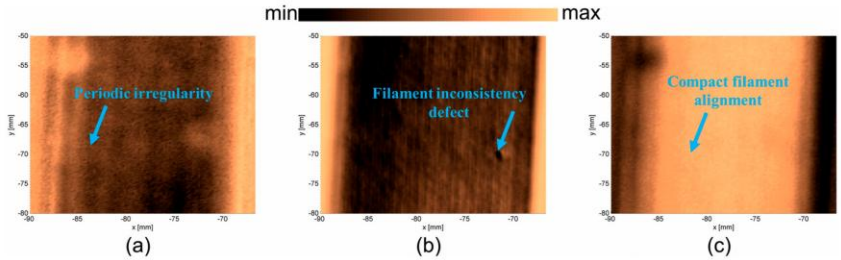

Figure 10. SCFR | PLAP surfaces: (**a**) upper surface, (**b**) bottom surface, and (**c**) metal table.

In the case of CCFR | PLAP (Figure 11), the upper surface image (Figure 11a) shows that it is not perfectly flat, and the carbon fibers are not perfectly aligned. The areas with darker colors can be described as voids and regions with a higher amount of PLAP (pure polymer). The images of the bottom surface (Figure 11b) and metal table (Figure 11c) confirm the presence of voids. These are visible as irregular light lines (Figure 11b) between the carbon fibers and as irregular dark lines (Figure 11c) between reflections from the metal table. Such voids and misalignments of carbon fibers influence the vibrational parameters of the analyzed CCFR | PLAP structure, indicating potential origins of structural damage.

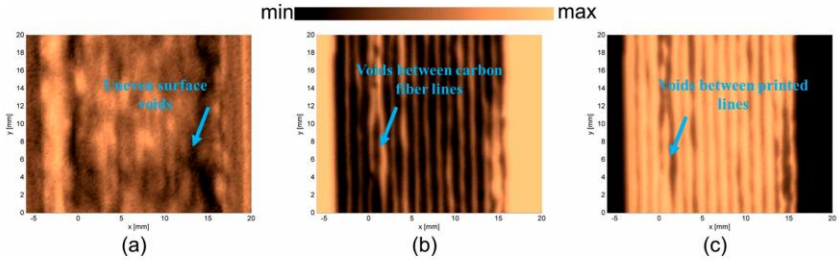

Figure 11. CCFR | PLAP surfaces: (**a**) upper surface, (**b**) bottom surface, and (**c**) metal plate.

3.4. Analysis of Vibration Amplitude Control in Beam Structures

This analysis provides a comprehensive discussion on vibration amplitude control in numerically modeled beam structures, comparing and validating the results obtained with experimental data. The damping characteristics of the numerical beam structures are adjusted to ensure that the numerical and experimental absolute uncontrolled vibration amplitudes are comparable. The average computational time to determine the controlled vibration amplitude in beam structures was around 97 min. The PLAP numerically modeled beam exhibited the highest uncontrolled vibration amplitude ranging from +435 µm to −408 µm when subjected to a harmonic force at its first resonant frequency of 30.45 Hz, as depicted in Figure 12a. To obtain an uncontrolled amplitude approximately identical to the experimental results, a specific force value for each beam was determined using the following expression [49]:

$$\mathbf{F_{ext}} = 3\mathrm{YID}/\mathrm{L}^3 \quad (15)$$

where $\mathbf{F}_{ext}$, Y, I, D, and L indicate the load at the free end, Young's Modulus, moment of inertia related to the cross-section, maximum peak-to-peak deflection, and length of each beam, respectively.

By applying a counter force through the MFC at the same resonant frequency (30.45 Hz), the maximum controlled vibration amplitude was observed to be approximately ±19 µm (see Figure 12b). This represents an overall reduction in controlled vibration amplitude of more than 22 times compared to the uncontrolled scenario. In the experimental scenario, the AM beam structure was stimulated at its first resonant frequency (30 Hz) with an electromagnetic shaker, resulting in an uncontrolled vibration amplitude of approximately ±410 µm. Applying a counterforce with the MFC at the same resonant frequency (30 Hz), the controlled amplitude was reduced to around ±5 µm. This demonstrates an overall reduction in controlled vibration amplitude of around 80 times.

For the SCFR | PLAP numerical model, the uncontrolled highest vibration amplitude was observed around ±395 µm when subjected to a harmonic force near its first resonant frequency of 40 Hz, as depicted in Figure 13a. In experiments with the AM model, the uncontrolled amplitude was noted around ±370 µm at its first resonant frequency of 40.5 Hz. Upon applying a counterforce through the MFC, the controlled numerical and experimental vibration amplitudes were observed around ±16 µm and ±3 µm, respectively, as presented in Figure 13b. This reflects an overall reduction in controlled vibration amplitudes of approximately 25 times and 110 times, respectively.

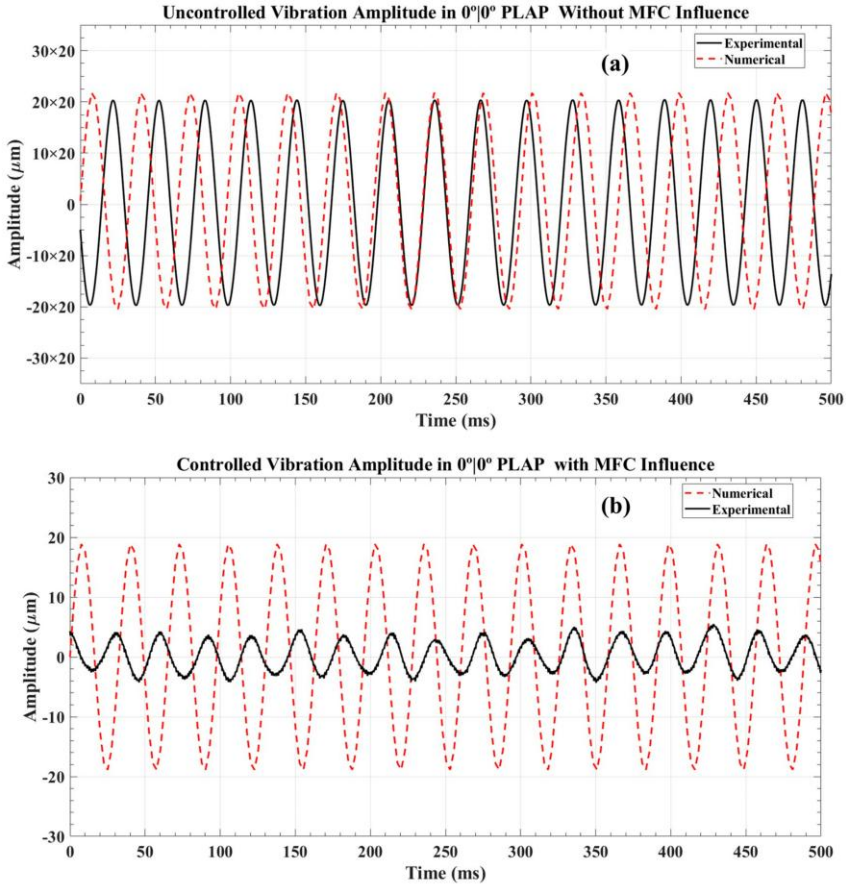

Figure 12. Vibration amplitude analysis in 0° | 0° PLAP beam structure: (**a**) uncontrolled vibration amplitude and (**b**) controlled vibration amplitude.

In both the numerical and AM models of the CCFR | PLAP, the numerical model exhibited uncontrolled amplitudes ranging from +220 µm to −224 µm, while the AM model showed an approximate amplitude of ±210 µm, as illustrated in Figure 14a. These measurements were taken at their respective first resonant frequencies, approximately 60.5 Hz for the numerical model and 60 Hz for the AM model. After the MFC applied a counterforce, the numerical and AM beams exhibited controlled amplitudes of ±13 µm and ±1.7 µm, respectively, as demonstrated in Figure 14b. This represents an overall reduction in controlled amplitudes of approximately 31 times for the numerical model and 120 times for the AM model.

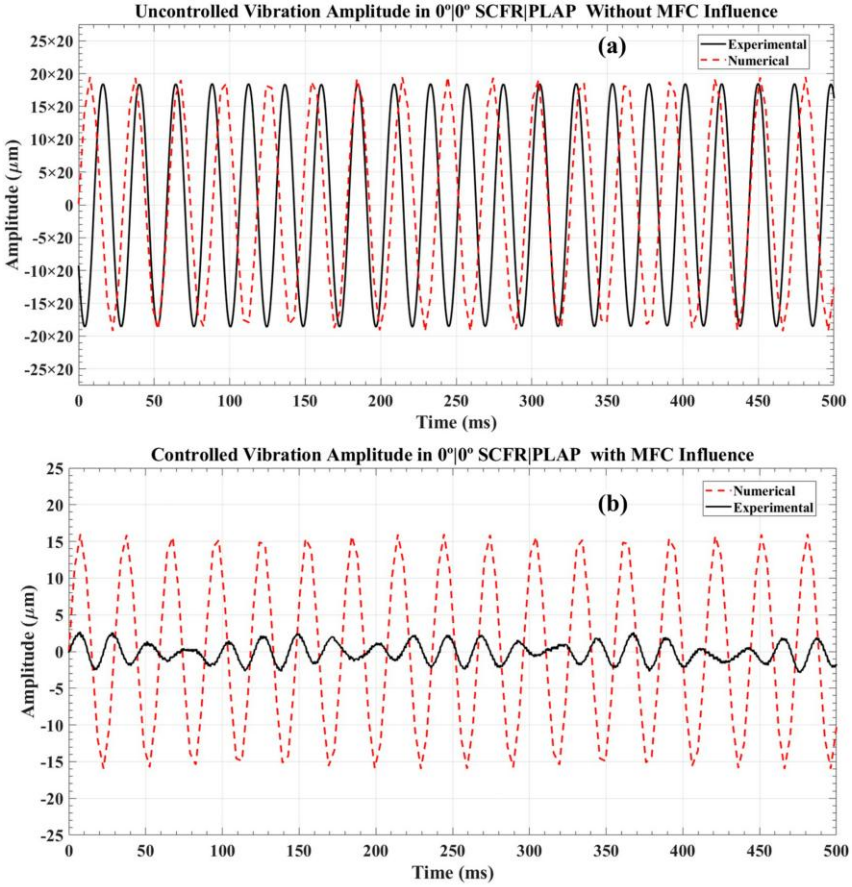

Figure 13. Vibration amplitude analysis in 0° | 0° SCFR | PLAP beam structure: (**a**) uncontrolled vibration amplitude and (**b**) controlled vibration amplitude.

The results demonstrate significant changes in the reduction ratios for PLAP, SCFR | PLAP, and CCFR | PLAP in experimental cases, with reductions of 80 times, 110 times, and 120 times, respectively. In contrast, numerical models exhibited reductions of 22 times, 25 times, and 31 times, respectively. However, the peak-to-peak controlled vibration amplitudes remain relatively consistent, such as ±5 μm, ±3 μm, and ±1.7 μm for PLAP, SCFR | PLAP, and CCFR | PLAP in experimental scenarios, and ±19 μm, ±16 μm, and ±13 μm in numerical scenarios, respectively. It indicates consistent effectiveness in controlling vibration amplitudes in both numerical and experimental scenarios.

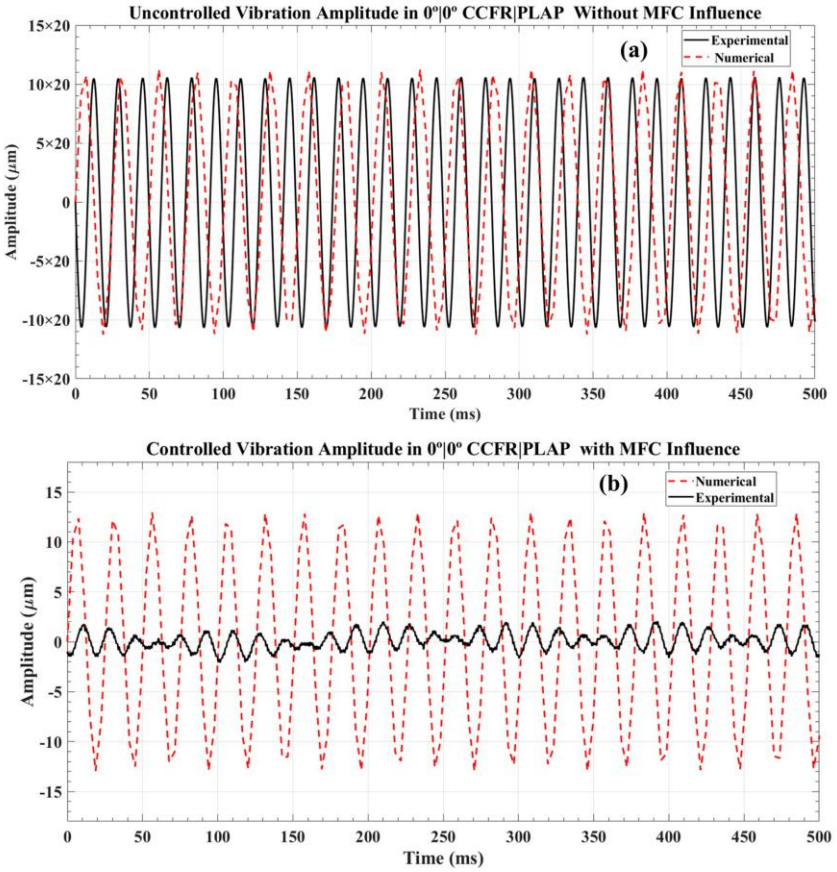

Figure 14. Vibration amplitude analysis in 0° | 0° CCFR | PLAP beam structure: (**a**) uncontrolled vibration amplitude and (**b**) controlled vibration amplitude.

The disparity in controlled vibration amplitudes between the numerical and experimental results is influenced by the inherent limitations of the numerical models, which do not fully capture the complexities of real experimental conditions. Numerical simulations typically rely on generalized assumptions and may not properly account for material imperfections such as voids, porosity, or any irregularities, which are present in the actual model. Additionally, environmental factors and intricate damping characteristics resulting from the fixture used to secure one side of the beam during experiments are not fully considered in the numerical simulation.

The numerical findings provide valuable insights for estimating trends related to vibration control in AM beam structures. However, the experimental data are crucial

for improving and optimizing vibration amplitude control methodologies to assure their efficacy in real-life applications. Despite the disparity in controlled vibration amplitudes between numerical and experimental models, the trend of reduction factor in both scenarios is similar. It increases from PLAP to SCFR | PLAP and then continues with CCFR | PLAP.

4. Conclusions

In this article, the numerical models of $0^\circ|0^\circ$ PLA, $0^\circ|0^\circ$ SCFR | PLA, and $0^\circ|0^\circ$ CCFR | PLA beam structures integrated with the MFC have been investigated to study their dynamic characteristics and control vibration amplitude under kinematically stimulated conditions. The numerical results are comprehensively compared and validated against previously published experimental results. In response to the findings from the results, the subsequent conclusions are formulated.

1. The 1st resonant frequencies were found to rise from 30.45 Hz for PLAP, to 39.95 Hz for SCFR | PLAP, and then to 60.5 Hz for CCFR | PLAP. The numerical values align with experimental values of 30 Hz, 40.5 Hz, and 60 Hz, with discrepancies of 1.50%, 1.35%, and 0.83%, respectively.
2. Numerical analysis of the frequency-dependent amplitudes of the initial four bending modes exhibited that the 1st resonant frequency had the highest amplitudes, while the lowest amplitudes were observed at the 4th resonant frequencies. A similar trend in frequency-dependent amplitudes was observed in the experimental scenario.
3. THz spectroscopy was performed to identify voids or misalignments in the real AM samples. The PLAP revealed periodic irregularities, SCFR | PLA showed random discontinuities, and CCFR | PLA showed a significant number of voids and misalignments in the continuous carbon fiber.
4. The numerically models of PLAP, SCFR | PLAP, and CCFR | PLAP were externally stimulated at their respective 1st resonant frequencies, revealing uncontrolled vibration amplitudes of +435 µm to −408 µm, ±395 µm, and +220 µm to −224 µm, respectively. In the experimental case, uncontrolled vibration amplitudes were ±400 µm, ±370 µm, and ±210 µm.
5. After applying a counterforce with the MFC, the controlled vibration amplitudes in the numerical models for PLAP, SCFR | PLAP, and CCFR | PLAP were approximately ±19 µm, ±16 µm, and ±13 µm, respectively. Experimentally, the controlled vibration amplitudes were observed to be around ±5 µm, ±3 µm, and ±1.7 µm for the respective models. Both numerical and experimental results exhibited the same trend in decreasing amplitude from PLAP to SCFR | PLAP and finally to CCFR | PLAP.
6. Numerical simulation provides valuable insights for estimating trends in controlling vibration amplitudes. However, experimental data are crucial for improving and optimizing vibration amplitude reduction methodologies to ensure their efficacy in real-life applications.

Author Contributions: Conceptualization: A.R., M.M. and R.R.; data curation, A.R.; formal analysis, A.R.; investigation, A.R., M.M., R.R. and V.J.; methodology, A.R.; resources, M.M. and R.R.; software, A.R. and M.M.; supervision, M.M. and R.R.; validation, A.R.; visualization, A.R.; writing—original draft, A.R.; writing—review and editing, M.M., R.R. and V.J. All authors have read and agreed to the published version of the manuscript.

Funding: This research received no external funding.

Institutional Review Board Statement: Not applicable.

Informed Consent Statement: Not applicable.

Data Availability Statement: The original contributions presented in the study are included in the article, further inquiries can be directed to the corresponding authors.

Acknowledgments: The numerical simulations were carried out using the computers of the Centre of Informatics, Tricity Academic Supercomputer & Network. Analyses related to THz spectroscopy were supported by the project: 'Additive manufactured composite smart structures with embedded FBG sensors (AMCSS)' funded by the National Science Centre, Poland, under M-ERA.NET 2 Call 2019, grant agreement 2019/01/Y/ST8/00075.

Conflicts of Interest: The authors declare no conflict of interest.

Abbreviations

Acronym	Full Term
MFC	Macro fiber composite
PLAP	Polylactic acid polymer
SCFR|PLAP	Short carbon fiber reinforced in PLAP
CCFR|PLAP	Continuous carbon fiber reinforced in PLAP
CGFR|PLAP	Continuous glass fiber reinforced in PLAP
FRA	Frequency response analysis
NDT	Non-destructive testing
BM	Bending mode
AM	Additively manufactured
FEM	Finite element modeling

References

1. Al-Hababi, T.; Cao, M.; Saleh, B.; Alkayem, N.F.; Xu, H. A Critical Review of Nonlinear Damping Identification in Structural Dynamics: Methods, Applications, and Challenges. *Sensors* **2020**, *20*, 7303. [CrossRef] [PubMed]
2. Awada, A.; Younes, R.; Ilinca, A. Optimized Active Control of a Smart Cantilever Beam Using Genetic Algorithm. *Designs* **2022**, *6*, 36. [CrossRef]
3. Li, J.; Xue, Y.; Li, F.; Narita, Y. Active Vibration Control of Functionally Graded Piezoelectric Material Plate. *Compos. Struct.* **2019**, *207*, 509–518. [CrossRef]
4. Kapsalas, C.N.; Sakellariou, J.S.; Koustoumpardis, P.N.; Aspragathos, N.A. An ARX-Based Method for the Vibration Control of Flexible Beams Manipulated by Industrial Robots. *Robot. Comput. Integr. Manuf.* **2018**, *52*, 76–91. [CrossRef]
5. Song, Z.-G.; Li, F.M. Active Aeroelastic Flutter Analysis and Vibration Control of Supersonic Composite Laminated Plate. *Compos. Struct.* **2012**, *94*, 702–713. [CrossRef]
6. Vadiraja, D.N.; Sahasrabudhe, A.D. Vibration Analysis and Optimal Control of Rotating Pre-Twisted Thin-Walled Beams Using MFC Actuators and Sensors. *Thin-Walled Struct.* **2009**, *47*, 555–567. [CrossRef]
7. Rimašauskienė, R.; Jūrėnas, V.; Radzienski, M.; Rimašauskas, M.; Ostachowicz, W. Experimental Analysis of Active–Passive Vibration Control on Thin-Walled Composite Beam. *Compos. Struct.* **2019**, *223*, 110975. [CrossRef]
8. Ma, R.; Bi, K.; Hao, H. Inerter-Based Structural Vibration Control: A State-of-the-Art Review. *Eng. Struct.* **2021**, *243*, 112655. [CrossRef]
9. Kamila, S. Introduction, Classification and Applications of Smart Materials: An Overview. *Am. J. Appl. Sci.* **2013**, *10*, 876–880. [CrossRef]
10. Gopi Krishna, J.; Thirumal, J.R. Application of Smart Materials in Smart Structures. *Int. J. Innov. Res. Sci. Eng. Technol.* **2015**, *4*, 5018–5023.
11. Kim, H.S.; Kim, J.-H.; Kim, J. A Review of Piezoelectric Energy Harvesting Based on Vibration. *Int. J. Precis. Eng. Manuf.* **2011**, *12*, 1129–1141. [CrossRef]
12. Konka, H.P.; Wahab, M.A.; Lian, K. Piezoelectric Fiber Composite Transducers for Health Monitoring in Composite Structures. *Sens. Actuators A Phys.* **2013**, *194*, 84–94. [CrossRef]
13. Kumar, D.N.; Raja, S.; Ikeda, T. Active Vibration Control of Smart Plates with Partially Debonded Multilayered PZT Actuators. *Smart Mater. Struct.* **2007**, *16*, 1584–1594. [CrossRef]
14. Smith, R. Smart Material Applications. In *Smart Material Systems: Model Development*; Society for Industrial and Applied Mathematics: Philadelphia, PA, USA, 2005; Volume 1, pp. 1–41, ISBN 978-0-89871-583-5.
15. Deraemaeker, A.; Nasser, H. Numerical Evaluation of the Equivalent Properties of Macro Fiber Composite (MFC) Transducers Using Periodic Homogenization. *Int. J. Solids Struct.* **2010**, *47*, 3272–3285. [CrossRef]
16. Park, S.; Inman, D.J.; Yun, C.-B. An Outlier Analysis of MFC-Based Impedance Sensing Data for Wireless Structural Health Monitoring of Railroad Tracks. *Eng Struct* **2008**, *30*, 2792–2799. [CrossRef]
17. Sreenivasa Prasath, S.; Arockiarajan, A. Effective Electromechanical Response of Macro-Fiber Composite (MFC): Analytical and Numerical Models. *Int. J. Mech. Sci.* **2013**, *77*, 98–106. [CrossRef]
18. Friswell, M.I.; Ali, S.F.; Bilgen, O.; Adhikari, S.; Lees, A.W.; Litak, G. Non-Linear Piezoelectric Vibration Energy Harvesting from a Vertical Cantilever Beam with Tip Mass. *J. Intell. Mater. Syst. Struct.* **2012**, *23*, 1505–1521. [CrossRef]

19. Betts, D.N.; Kim, H.A.; Bowen, C.R.; Inman, D.J. Optimal Configurations of Bistable Piezo-Composites for Energy Harvesting. *App.l Phys. Lett.* **2012**, *100*, 114104. [CrossRef]
20. Smart Material. Available online: https://www.smart-material.com/ (accessed on 6 March 2022).
21. Wu, D.; Huang, L.; Pan, B.; Wang, Y.; Wu, S. Experimental Study and Numerical Simulation of Active Vibration Control of a Highly Flexible Beam Using Piezoelectric Intelligent Material. *Aerosp. Sci. Technol.* **2014**, *37*, 10–19. [CrossRef]
22. Raza, A.; Mahato, S.; Rimašauskienė, R. Actuation Performance of Macro Fibre Composite (MFC) as Actuator in Vibration Reduction of Cantilever Beams. *Mechanics* **2023**, *29*, 42–50. [CrossRef]
23. da Silva, C.A.X.; Lara-Molina, F.A.; da Costa, R.R.C.; Koroishi, E.H.; Alves, M.T.S.; Palácios, R.H.C. Vibration Attenuation of a Composite Beam by Fuzzy Control. *J. Vib. Eng. Technol.* **2024**, *12*, 191–200. [CrossRef]
24. Raza, A.; Rimašauskienė, R.; Jūrėnas, V.; Rimašauskas, M. An Experimental Study on the Dynamic Properties of 3D-Printed Structures with Different Layer Orientations. *J. Vib. Eng. Technol.* **2024**, 1–14. [CrossRef]
25. Raza, A.; Rimašauskienė, R.; Jūrėnas, V.; Kuncius, T. Enhancing Vibration Control in Kinematically Excited Additively Manufactured Continuous Fiber Composite Structures with Distinct Orientations. *Eng. Struct.* **2024**, *321*, 118933. [CrossRef]
26. Karimi, A.; Rahmatabadi, D.; Baghani, M. Various FDM Mechanisms Used in the Fabrication of Continuous-Fiber Reinforced Composites: A Review. *Polymers* **2024**, *16*, 831. [CrossRef] [PubMed]
27. Wani, Z.R.; Tantray, M.; Farsangi, E.N.; Nikitas, N.; Noori, M.; Samali, B.; Yang, T.Y. A Critical Review on Control Strategies for Structural Vibration Control. *Annu. Rev. Control* **2022**, *54*, 103–124. [CrossRef]
28. Ding, H.; Bi, K.; Song, J.; Fang, X. Vertical Vibration Control of Structures with Tuned Liquid Column Dampers. *Int. J. Mech. Sci.* **2024**, *279*, 109502. [CrossRef]
29. Wan, H.-P.; Ma, Q.; Dong, G.-S.; Luo, Y.; Ni, Y.-Q. Data-Driven Model Reduction Approach for Active Vibration Control of Cable-Strut Structures. *Eng. Struct.* **2024**, *302*, 117434. [CrossRef]
30. Zang, J.; Ren, H.-M.; Song, X.-Y.; Zhang, Z.; Zhang, Y.-W.; Chen, L.-Q. Vibration Control of Interconnected Composite Beams: Dynamical Analysis and Experimental Validations. *Mech. Syst. Signal Process.* **2024**, *208*, 111008. [CrossRef]
31. Sun, X.G.; Chi, W.C.; Wang, Y.Q. Linear Active Disturbance Rejection Control Algorithm for Active Vibration Control of Piezo-Actuated Beams: Theoretical and Experimental Studies. *Thin-Walled Struct.* **2024**, *199*, 111782. [CrossRef]
32. Soltani, M.; Fesharaki, J.J.; Galehdari, S.A.; Esfahani, R.T.; Shahgholi, M. A Comprehensive Evaluation of the Vibration Control Approach of the Multi-Layer Sandwich Composite Piezoelectric Micro-Beam Using Higher-Order Elasticity Theory and Surface Energy. *Structures* **2024**, *60*, 105880. [CrossRef]
33. Moreira, R.A.S.; Marques, A.P. Simulation on Dynamic Passive Control of Structures Using Corrugated Viscoelastic Damping Treatments. *Simulation* **2024**, *100*, 683–694. [CrossRef]
34. Kamel, M.A.; Ibrahim, K.; Ahmed, A.E.-M. Vibration Control of Smart Cantilever Beam Using Finite Element Method. *Alex. Eng. J.* **2019**, *58*, 591–601. [CrossRef]
35. Raza, A.; Rimašauskienė, R.; Jūrėnas, V.; Mahato, S. Experimental Investigation of Vibration Amplitude Control in Additive Manufactured PLA and PLA Composite Structures with MFC Actuator. *Eng. Struct.* **2023**, *294*, 116802. [CrossRef]
36. Polymaker PolyLiteTM PLA Technical Data Sheet. Available online: https://ec3d.co.za/wp-content/uploads/2022/08/PolyLite%E2%84%A2-PLA_TDS_V3.pdf?srsltid=AfmBOopruFk5-qatnuWiZR6Q2I8dFuh4pnvGAUf08AiIStX_vD0KKD5a (accessed on 9 March 2023).
37. ColorFabb ColorFabb (XT-CF20) Technical Datasheet. Available online: https://colorfabb.com/media/datasheets/tds/colorfabb/TDS_E_ColorFabb_XT_CF20.pdf (accessed on 9 March 2023).
38. Toray Composite Materials America T300 Standard Modulus Carbon Fiber Technical Data Sheet. Available online: https://www.rockwestcomposites.com/media/wysiwyg/T300DataSheet_1.pdf (accessed on 9 March 2023).
39. Zhang, S.-Q.; Li, Y.-X.; Schmidt, R. Modeling and Simulation of Macro-Fiber Composite Layered Smart Structures. *Compos. Struct.* **2015**, *126*, 89–100. [CrossRef]
40. Pandey, A.; Arockiarajan, A. Actuation Performance of Macro-Fiber Composite (MFC): Modeling and Experimental Studies. *Sens. Actuators A Phys.* **2016**, *248*, 114–129. [CrossRef]
41. Abaqus CAE. Available online: https://docs.software.vt.edu/abaqusv2024/English/ (accessed on 23 June 2024).
42. Sommer, S.; Probst, T.; Kraus, E.; Baudrit, B.; Town, G.E.; Koch, M. Cure Monitoring of Two-Component Epoxy Adhesives by Terahertz Time-Domain Spectroscopy. *Polym. Sci. Ser. B* **2016**, *58*, 769–776. [CrossRef]
43. Lu, X.; Shen, Y.; Xu, T.; Sun, H.; Zhu, L.; Zhang, J.; Chang, T.; Cui, H.-L. Accurate Detection of Porosity in Glass Fiber Reinforced Polymers by Terahertz Spectroscopy. *Compos. Part B Eng.* **2022**, *242*, 110058. [CrossRef]
44. Mittleman, D. *Sensing with Terahertz Radiation*; Springer: Berlin/Heidelberg, Germany, 2013; Volume 85.
45. Gajjar, T.; Shah, D.B.; Joshi, S.J.; Patel, K.M. Analysis of Process Parameters for Composites Manufacturing Using Vacuum Infusion Process. *Mater. Today Proc.* **2020**, *21*, 1244–1249. [CrossRef]
46. Ospald, F.; Zouaghi, W.; Beigang, R.; Matheis, C.; Jonuscheit, J.; Recur, B.; Guillet, J.-P.; Mounaix, P.; Vleugels, W.; Bosom, P.V.; et al. Aeronautics Composite Material Inspection with a Terahertz Time-Domain Spectroscopy System. *Opt. Eng.* **2013**, *53*, 031208. [CrossRef]
47. Karpowicz, N.; Dawes, D.; Perry, M.J.; Zhang, X.-C. Fire Damage on Carbon Fiber Materials Characterized by THz Waves. In *Terahertz for Military and Security Applications IV*; SPIE: Bellingham, WA, USA, 2006; Volume 6212, pp. 124–131. [CrossRef]

48. Mieloszyk, M.; Majewska, K.; Ostachowicz, W. Studies of Fibre Reinforced Polymer Samples with Embedded FBG Sensors. In Proceedings of the 13th International Conference on Damage Assessment of Structures: DAMAS, Porto, Portugal, 9–10 July 2019; Springer: Singapore, 2020; pp. 926–936.
49. Mott, R.L.; Vavrek, E.M.; Wang, J. Stress and Deformation Analysis. In *Machine Elements in Mechanical Design*; Pearson Education, Inc.: New York City, NY, USA, 2018; Volume 6, pp. 87–141, ISBN 978-0-13-444118-4.

CURRICULUM VITAE

Name, Surname: Ali Raza
E-mail: alirazuet@gmail.com
LinkedIn: www.linkedin.com/in/ali-raza-9b00b127a
Google Scholar:
https://scholar.google.com/citations?user=&user=VqLyoIwAAAAJ

Education:

2021–2025 **PhD in Mechanical Engineering**
Kaunas University of Technology, Kaunas, Lithuania
2016–2018 **Master of Science in Mechanical Design Engineering**
University of Engineering and Technology, Lahore, Pakistan
2009–2013 **Bachelor of Science in Mechatronics & Control Engineering**
University of Engineering and Technology, Lahore, Pakistan

Work Experience:

2019-2021 **Lecturer**
National Textile University, Faisalabad, Pakistan
2014-2019 **Lab Engineer**
National Textile University, Faisalabad, Pakistan

Research Interests:

- ✓ 3D Printing: Fused Deposition Modeling (FDM)
- ✓ Dynamic Characterization of Composite Structures
- ✓ Vibration Control Analysis of Composite Structures
- ✓ Mechanical and Thermal Characterization of Materials
- ✓ Finite Element Modeling and Simulation

JOURNAL PUBLICATIONS AND CONFERENCES

List of scientific publications related to the dissertation:

1. **Raza, Ali**; Rimašauskienė, Rūta; Jūrėnas, Vytautas; Mahato, Swarup. Experimental investigation of vibration amplitude control in additive manufactured PLA and PLA composite structures with MFC actuator // Engineering structures. London: Elsevier. ISSN 0141-0296. eISSN 1873-7323. 2023, vol. 294, art. no. 116802, p. 1-13. DOI: 10.1016/j.engstruct.2023.116802. **[Q1]**

2. **Raza, Ali;** Rimašauskienė, Rūta; Jūrėnas, Vytautas; Rimašauskas, Marius. An experimental study on the dynamic properties of 3D-printed structures with different layer orientations // Journal of Vibration Engineering & Technologies: Springer Nature. ISSN 2523-3920. eISSN 2523-3939. 2024, vol. 12, p. 321-334. DOI: 10.1007/s42417-024-01417-w. **[Q2]**

3. **Raza, Ali;** Rimašauskienė, Rūta; Jūrėnas, Vytautas; Kuncius, Tomas. Enhancing vibration control in kinematically excited additively manufactured continuous fiber composite structures with distinct orientations // Engineering structures. London: Elsevier. ISSN 0141-0296. eISSN 1873-7323. 2024, vol. 321, art. no. 118933, p. 1-15. DOI: 10.1016/j.engstruct.2024.118933. **[Q1]**

4. **Raza, Ali;** Mieloszyk, Magdalena; Rimašauskienė, Rūta; Jūrėnas, Vytautas. Dynamic analysis and vibration control of additively manufactured thin-walled polylactic acid polymer (PLAP) and PLAP composite beam structures: numerical investigation and experimental validation // Materials. Basel: MDPI. ISSN 1996-1944. 2024, vol. 17, iss. 22, art. no. 5478, p. 1-26. DOI: 10.3390/ma17225478**. [Q1]**

List of international conferences related to dissertation:

1. **Raza, Ali**; Rimašauskienė, Rūta. Influence of distinct 3D printing layer patterns on the dynamic characteristics of composite structures // ICCS27: 27th international conference on composite structures, 3-6 September 2024, University of Bologna, Ravenna, Italy.

2. **Raza, Ali**; Rimašauskienė, Rūta. Measurements of vibration displacement reduction in glass fiber composite structures with laser and non-contact approaches // Materials engineering and modern manufacturing 2023: 30th international Baltic conference, 19-20 October 2023, Kaunas University of Technology, Kaunas, Lithuania.

3. **Raza, Ali**; Rimašauskienė, Rūta. Vibration control in additive manufactured cantilever beams made of PLA and PLA composites using macro fiber composite (MFC) // Joint event: ICCS26 - 26th international conference on composite structures & MECHCOMP8 - 8th international conference on mechanics of composites, 27-30 June 2023, Faculty of engineering, University of Porto, Porto, Portugal.

4. **Raza, Ali;** Rimašauskiene, Ruta; Mahato, Swarup. A study on effectiveness of macro fiber composite actuator in vibration reduction of composite beam // CMM-SolMech 2022: 24th international conference on computer methods in mechanics (CMM). 42nd solid mechanics conference (SolMech), 5-8 September 2022, Institute of fundamental technological research, Polish academy of sciences, Świnoujście, Poland.

5. **Raza, Ali**; Rimašauskienė, Rūta; Mahato, Swarup. Comparative study on the actuation performance of macro fiber composite (MFC, P2 Type) in vibration reduction among rectangular composite beams // Mechanika 2022: proceedings of the 26th international scientific conference, 20 May 2022, Kaunas university of technology, Kaunas, Lithuania.

6. **Raza, Ali;** Rimašauskienė, Rūta. Smart composite structures by 3D printing technology // 1st international conference on polymers and composites (ICPC 2021), 7-8 December 2021, National textile university, Faisalabad, Pakistan.

ACKNOWLEDGEMENTS

First and foremost, I would like to thank Almighty ALLAH, the Most Merciful and Benevolent, for granting me the strength to overcome and complete this challenging phase of my life.

I would like to express my heartfelt gratitude to my supervisor, Assoc. Prof. Dr. Rūta Rimašauskienė. Without her significant support, valuable suggestions, and guidance, this doctoral dissertation would not have been possible.

I also express my appreciation to Prof. Vytautas Jūrėnas from the Institute of Mechatronics, KTU for his help and guidance during experimentation,

Continuing, my gratitude also goes to Assoc. Prof. Dr. Magdalena Mieloszyk, under whose supervision I completed a five-month traineeship at the Institute of Fluid Flow Machinery, Polish Academy of Sciences, Gdansk, Poland. During this time, I learned and performed the numerical modeling and simulation portion of my PhD dissertation.

I express my deep appreciation to the reviewers of the dissertation, Prof. Dr. Regita Bendikienė, Prof. Dr. Saulius Baskutis and Prof. Dr. Giedrius Janušas, for their valuable remarks, recommendations and suggestions, which enhanced the quality of the dissertation.

I am highly thankful to Kaunas University of Technology, Lithuania for giving me the opportunity to join this esteemed institution as a doctoral student and for providing me with all the necessary support to fulfill my dream here. I am deeply grateful to have received funding from the Doctoral School of Kaunas University of Technology as a PhD student, which provided me with valuable opportunities to participate in reputable conferences, present my work, and engage with the research community in the technological field.

I sincerely acknowledge the Research Council of Lithuania for providing me with funding to attend reputable conferences during my doctoral studies at Kaunas University of Technology and for giving me the opportunity to expand my horizons.

I extend my sincere gratitude to Prof. Dr. Marius Rimašauskas, Dr. Nabeel Maqsood, and Dr. Tomas Kuncius for their assistance in 3D printing and for providing me with valuable data related to 3D printing during my PhD studies. I would also like to thank Dr. Swarup Mahato for his insightful guidance in the analysis of the experimental findings.

I would like to express my deepest gratitude to my parents, whose unwavering support and sacrifices have made this achievement possible. Words cannot fully express my appreciation for the hardships they endured to provide me with the education and guidance needed for a better future. Although they are no longer with us, I am confident that they are watching over me from heaven and would be proud of everything I have achieved.

I am deeply thankful to all my family members, especially my wife, brother, and sisters, as well as my friends in Pakistan, for their kind support, prayers, and the many

sacrifices they have made on my behalf. Their unwavering love, encouragement, good wishes, and prayers have always surrounded me.

During my PhD journey, I lost my beloved father and grandmother, and I never imagined that my last meeting with them before leaving for my studies would truly be our final moment together. This journey would never have been possible without their blessings and prayers. It was one of the most difficult times of my life, and words cannot fully express how hard it was. During my time in Lithuania, I made several great friends and spent wonderful moments with them. Without their support, this period might not have been as easy to get through. My sincere appreciation goes to all these friends.

Ali Raza

UDK 658.512.2+534.83](043.3)

SL344. 2025-07-08, 19 leidyb. apsk. l. Tiražas 14 egz. Užsakymas 115.
Išleido Kauno technologijos universitetas, K. Donelaičio g. 73, 44249 Kaunas
Spausdino leidyklos „Technologija“ spaustuvė, Studentų g. 54, 51424 Kaunas